VOLUME 36 MARCH 1958 NUMBER 3

Canadian Journal of Physics

Published by THE NATIONAL RESEARCH COUNCIL

OTTAWA CANADA

CANADIAN JOURNAL OF PHYSICS

(*Formerly Section A, Canadian Journal of Research*)

Under the authority of the Chairman of the Committee of the Privy Council on Scientific and Industrial Research, the National Research Council issues THE CANADIAN JOURNAL OF PHYSICS and five other journals devoted to the publication, in English or French, of the results of original scientific research. Matters of general policy concerning these journals are the responsibility of a joint Editorial Board consisting of: members representing the National Research Council of Canada; the Editors of the Journals; and members representing the Royal Society of Canada and four other scientific societies.

Manuscripts for publication should be submitted to Dr. H. E. Duckworth, Editor, Canadian Journal of Physics, Hamilton College, McMaster University, Hamilton, Ontario.

(For instructions on preparation of copy, see **Notes to Contributors** (inside back cover).)

Proof, correspondence concerning proof, and orders for reprints should be sent to the Manager, Editorial Office (Research Journals), Division of Administration and Awards, National Research Council, Ottawa 2, Canada.

Subscriptions, renewals, requests for single or back numbers, and all remittances should be sent to Division of Administration and Awards, National Research Council, Ottawa 2, Canada. Remittances should be made payable to the Receiver General of Canada, credit National Research Council.

The journals published, frequency of publication, and prices are:

Canadian Journal of Biochemistry and Physiology	Monthly	$3.00 a year
Canadian Journal of Botany	Bimonthly	$4.00 a year
Canadian Journal of Chemistry	Monthly	$5.00 a year
Canadian Journal of Microbiology	Bimonthly	$3.00 a year
Canadian Journal of Physics	Monthly	$4.00 a year
Canadian Journal of Zoology	Bimonthly	$3.00 a year

The price of regular single numbers of all journals is 75 cents.

CORRECTIONS

Canadian Journal of Physics, Vol. 35, 1957.

page 615	$3\nu_1+2\nu_2+\nu_3$	$R(32)$	read 6.595	instead of 6.495
618	$2\nu_1+\nu_2+\nu_3-\nu_2$	$R(15)$	4.784	4.769
620	Tableau VI	ω_1	1354.91	1354.94
		ω_2	673.00	673.02
		ω_3	2396.49	2396.40
		x_{12}	3.65	3.62
621	Equation (3)	W'	$-(W_0\ldots$	$(W_0\ldots$
623	Line 17	W_0	51.33	51.31
624	04^01	W_0	4958.64	4968.64
629	Line 13		B'^c, D'^c	B'^d, D'^d
	Line 14		B'^d, D'^d	B'^c, D'^c
648	Reference 6		**40**, 339	**40**, 1950

Canadian Journal of Physics

Issued by THE NATIONAL RESEARCH COUNCIL OF CANADA

VOLUME 36 MARCH 1958 NUMBER 3

THE TOWNSEND DISCHARGE IN A COAXIAL DIODE WITH AXIAL MAGNETIC FIELD[1]

P. A. REDHEAD

ABSTRACT

An approximate theory is developed of the breakdown characteristics of a coaxial diode in an axial magnetic field, taking into account the effects of elastic collisions. It is assumed that the electron moves in a constant electric field between collisions and thus the theory is valid only in the appropriate range of magnetic field and voltage. Estimates of transit time and of space-charge effects are also made. Measurements in the pressure range 10^{-3} to 10^{-9} mm. Hg are in general agreement with the theory.

1. INTRODUCTION

A self-sustained Townsend discharge in a coaxial diode with an axial magnetic field can be used very effectively as a means for measuring extremely low gas pressures. The theory of the striking characteristics of such discharges has been studied by Somerville (1952) and by Haefer (1953*a* and *b*, 1954), and the operation of vacuum gauges using this type of discharge has been described by Beck and Brisbane (1952) and Haefer (1953*b*, 1954).

This paper presents a theory of the striking characteristics of coaxial cylinders in an axial magnetic field which takes into account the effects of elastic collisions of the electrons. Measurements of the striking characteristics are also presented, which were made on a number of magnetron diodes designed for the measurement of extremely low pressures (below 10^{-10} mm. Hg). The operation of these diodes as pressure gauges is described in a companion paper (Hobson and Redhead 1958).

A schematic diagram of the electrode arrangement used for the measurements is shown in Fig. 1. The inner cylinder was used as the anode (radius r_a) and the outer cylinder as the cathode or ion-collector (radius r_k). The ends of the cathode cylinder were partially closed to prevent migration of electrons from the discharge in an axial direction. The auxiliary cathode is a box-like structure enclosing the ion-collector and acting as an electrostatic shield; for larity this is not shown in Fig. 1. Connected to the auxiliary cathode are

[1]Manuscript received September 24, 1957.
Contribution from the Radio and Electrical Engineering Division, National Research Council, Ottawa, Canada.
Issued as N.R.C. No. 4621.

two short cylindrical shields which project through holes in the end-plates of the cathode. These cylindrical shields reduce the electric field at the edges of the end-plates and suppress any field-emission from the cathode. The structure of this tube suggested that it be christened the "inverted-magnetron gauge" (abbreviated to I.M.G. hereafter).

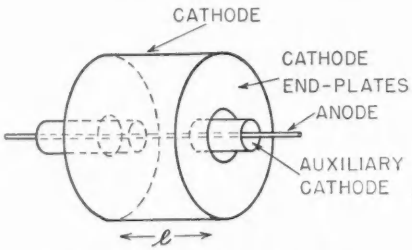

FIG. 1. Schematic diagram of diode.

The theory of the striking characteristics will be developed for infinitely long cylinders, i.e. neglecting the effects of the end-plates. This approximation is reasonable on the upper branch of the striking characteristic since, as will be seen later, the breakdown condition is first satisfied at the mid-point of the cathode cylinder where the probability of electron escape is greatest and the distortion of the electric field by the end-plates is least.

2. THEORY OF STRIKING CHARACTERISTICS

(*a*) *Electron and Ion Trajectories*

Fig. 2 shows a typical potential distribution measured with an analogue field plotter for I.M.G. No. 16 (see Table II for dimensions). It will be seen that an electron liberated within the ion-collector cylinder is trapped axially by the electric field. Provided the magnetic field is in excess of the cutoff field, which is the only case considered, the electron is trapped radially by the magnetic field. Electrons will follow a hypocycloidal path around the anode, while simultaneously oscillating back and forth in the axial (Z) direction. Approximate electron trajectories are indicated in Fig. 3 where the crosses indicate inelastic collisions. Electrons leaving the cylindrical portion of the cathode surface perform one arch of a cycloid before striking the cathode surface again; if they suffer an inelastic collision in this first arch they are assumed to return to thermal energy and to start their cycloidal motion once more from the point of collision, and thus to escape from the cathode. Electrons which have escaped from the cathode and which do not suffer further collisions will circle the anode in a hypocycloid generated by a circle of diameter D rolling on a circle of constant radius. The mean θ-directed velocity of the electrons is E/B (E, electric field; B, magnetic field). Thus electrons can only advance towards the anode by suffering ionizing collisions.

The trajectories of the positive ions formed by inelastic collisions of the electrons are relatively unaffected by the magnetic field because of the large

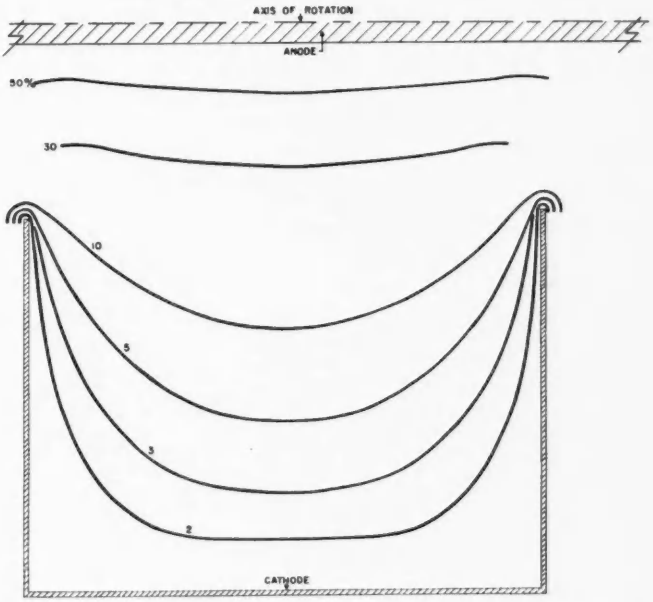

FIG. 2. Measured potential distribution in I.M.G. No. 16 with the dimensions indicated in Table II.

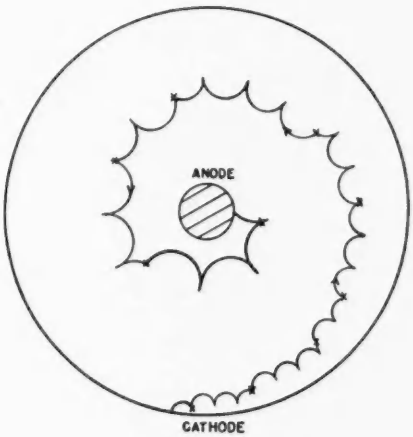

FIG. 3. Approximate electron trajectories.

ionic mass. The positive ions will move to the cathode with a transit time which is very much shorter than the electron transit time.

The above description of the trajectories is greatly simplified since the effects of space-charge and the distortion of the electric field by the end-plates have been ignored. The situation is further complicated by the presence of electronic oscillations in the gauge which are of considerable amplitude at higher pressures.

The theory of the striking characteristics will be developed on the assumption that the electric field is that which would exist in a cylindrical condenser of infinite length, and the effects of space-charge and of oscillations will be ignored.

(*b*) *Derivation of* α

Previous derivations of the first Townsend coefficient (α) in crossed electric and magnetic fields (Kugler *et al.* 1933; Haefer 1953*a* and *b*; Somerville 1952) have ignored the contribution to α made by those electrons which have been elastically scattered. The following analysis will take into account the elastically scattered electrons by an approximate method. We will first consider the case of crossed, uniform electric and magnetic fields. The electron trajectories in such a system are cycloidal, as indicated in Fig. 4. The diameter of the rolling circle generating the cycloid is

$$D = 2E/\eta B^2, \tag{1}$$

where η is the charge-to-mass ratio of the electron.

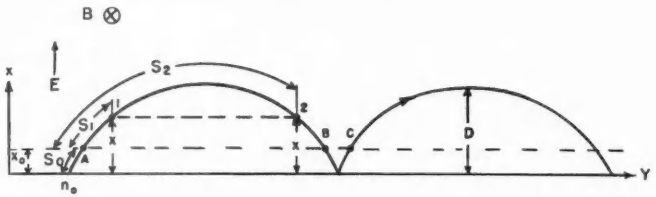

FIG. 4. Electron trajectories in crossed, uniform electric and magnetic fields.

The arc length of the cycloid from a point of height x_0 to a point of height x is given by

$$\begin{aligned} S_1 &= 2D[1-(1-x/D)^{1/2}]-S_0, \\ &= 2D[(1-x_0/D)^{1/2}-(1-x/D)^{1/2}], \end{aligned}$$

and similarly

$$S_2 = 2D[(1-x_0/D)^{1/2}+(1-x/D)^{1/2}],$$

where S_0 is the path length to a point of height x_0. x_0 is the value of x at which electrons have sufficient energy to enter into inelastic collisions; thus $x_0 = V_i/E$, where V_i is the ionization potential of the gas. It will be assumed that for $x < x_0$ only elastic collisions are possible, while for $x > x_0$ inelastic collisions can occur.

Electrons that are elastically scattered in the region $x < x_0$ will perform orbits that do not reintersect the plane $x = 0$, and will in almost all cases eventually pass through the plane $x = x_0$ and be capable of entering into inelastic collisions, thus contributing to the avalanche process. In previous treatments of this problem it was assumed that the elastically scattered electrons do not enter into the avalanche process, thus underestimating α. We shall assume that all the elastically scattered electrons are capable of suffering inelastic collisions, at some later time, and contributing to the avalanche process.

The contribution of the elastically scattered electrons will be taken into account in an approximate way by assuming that the number of electrons available at the plane $x = x_0$ is the same as that which would exist if no elastic collisions occurred in the region $x < x_0$. Thus, referring to Fig. 4, the number of electrons at point A is n_0, and all the electrons at point B are still available at point C. For this assumption to be valid, the average path length above x_0 of the electron elastically scattered below x_0 must approximate the path length above x_0 of the unscattered electron. Calculations have been made of the path length, above x_0, of the electron which is elastically scattered into the negative y-direction at $x = x_0$. This electron has the maximum path-length above x_0 of any electron and this path length can be approximated as

$$S = S_u\sqrt{(1+r)/(1-r)},$$

where

$$r = \sqrt{x_0/D},$$

and S_u is the path length, above x_0, of the unscattered electron.

For $x_0/D = 0.36$, $S/S_u = 2$. Thus for $x_0/D < \frac{1}{3}$, the maximum path-length of an elastically scattered electron is less than twice that of the unscattered electron. Thus the assumption that the average path-length, above x_0, of the elastically scattered electron approximates that of the unscattered electron is reasonable, provided that x_0/D is not large.

The number of electrons at A being n_0, then the number at point 1 is

$$n_{S_1} = n_0 \exp(-S_1/\lambda),$$

and, similarly, at point 2 is

$$n_{S_2} = n_0 \exp(-S_2/\lambda),$$

where λ is the electron mean-free-path for all collisions and is assumed independent of electron energy.

The number of electrons which have suffered inelastic collisions with energies greater than eEx (e, electronic charge) in the first cycloidal arch is

$$(2) \qquad n(x)_1 = n_{S_1} - n_{S_2} = 2n_0 \exp\left[-\frac{2D}{\lambda}\left(1-\frac{x_0}{D}\right)^{1/2}\right] \sinh\frac{2D}{\lambda}\left(1-\frac{x}{D}\right)^{1/2}.$$

The arc length from A to B is $4D(1-x_0/D)^{1/2}$ and thus the number of electrons at B is given by

$$(3) \qquad n_B = n_0 \exp[-(4D/\lambda)(1-x_0/D)^{1/2}].$$

Combining equations (2) and (3) we can show that the total number of electrons with energies greater than eEx which have suffered inelastic collisions is given by

$$\frac{n(x)}{n_0} = \frac{1}{n_0}\sum_{i=1}^{\infty} n(x)_i = \frac{\sinh[(2D/\lambda)(1-x/D)^{1/2}]}{\sinh[(2D/\lambda)(1-x_0/D)^{1/2}]}. \tag{4}$$

When $2D/\lambda \ll 1$, then

$$\frac{n(x)}{n_0} = \left[\frac{1-x/D}{1-x_0/D}\right]^{1/2}, \tag{5}$$

which is the ratio of the path length above x to the path length above x_0.

By differentiation of equation (4) we find that the number of electrons that have suffered inelastic collisions in the energy range eEx to $eE(x+\delta x)$ is

$$\frac{dn(x)}{dx} = -n_0 \frac{\cosh[(2D/\lambda)(1-x/D)^{1/2}](1-x/D)^{1/2}}{\lambda \sinh[(2D/\lambda)(1-x_0/D)^{1/2}]}.$$

Then the most probable value of x for an inelastic collision to occur is

$$\bar{x} = \int_{x_0}^{D} (x/n_0)dn(x)$$
$$= \frac{1}{\lambda \sinh[(2D/\lambda)(1-x_0/D)^{1/2}]} \int_{x_0}^{D} \frac{x \cosh[(2D/\lambda)(1-x/D)^{1/2}]}{(1-x/D)^{1/2}} dx.$$

Integration then leads to

$$\frac{\bar{x}}{\lambda} = \frac{x_0}{\lambda} + \left(1-\frac{x_0}{D}\right)^{1/2} \coth\left[\frac{2D}{\lambda}\left(1-\frac{x_0}{D}\right)^{1/2}\right] - \frac{\lambda}{2D}. \tag{6}$$

When $2D/\lambda$ is small, then

$$\bar{x} = \tfrac{1}{3}(x_0+2D); \tag{7}$$

Haefer (1953*a*) finds $\bar{x} = \frac{2}{3}D$, which is meaningless when $x_0 > \frac{2}{3}D$.

The first Townsend coefficient, α, defined as the number of ion pairs formed per unit distance of electron advance in the direction of the electric field, is given by

$$\alpha = \frac{1}{g\bar{x}} \frac{n(x_0)}{n_0} = \frac{1}{g\bar{x}}, \tag{8}$$

where g is a correction factor, greater than unity, to account for the fact that when the electron energy exceeds eV_i the probability of a collision causing ionization is not unity.

Combining equations (1), (7), and (8), we find that for $2D/\lambda \ll 1$,

$$\alpha = \frac{3E}{g(4E^2/\eta B^2 + V_i)}, \tag{9}$$

where we see that α is independent of the mean free path. This independency arises in the uniform field case because we have assumed the discharge to be of infinite extent in the lateral direction. In a coaxial system the electron

orbits are closed and the electron, being trapped in the system, will circle the anode indefinitely at a fixed mean radius until collision occurs; thus we would again expect α to be independent of λ.

This method of deriving $\bar{x}$ and α is only applicable to cylindrical geometry when the cycloid height $D(r)$ is sufficiently small that the electric field can be considered constant over the cycloid. When $D(r)$ becomes an appreciable fraction of the cathode radius, the uniform field assumption is no longer valid, and the above analysis is inapplicable.

(*c*) *The Breakdown Equation for Inhomogeneous Fields*

For a discharge in a cylindrical condenser with zero magnetic field the electron multiplication is not given by $\exp \int \alpha \, dr$ (Morton 1946) since the electron energy distribution is not the same as in a constant electric field where the distribution has had sufficient time to come to equilibrium with the field. However, when an axial magnetic field is applied, the electrons advance in a radial direction very slowly and the electron energy distribution can reach equilibrium with the field. Thus the Townsend breakdown relation for a coaxial diode in a magnetic field may be written

$$\Gamma\left[\exp\left(\int_{r_0}^{r_a}\alpha(r)dr\right)-1\right]=1, \tag{10}$$

where r_0 is the maximum radius at which ionization can occur, and Γ is the effective third Townsend coefficient for all secondary processes. Combining equations (9) and (10), we obtain

$$\log\left(1+\frac{1}{\Gamma}\right)=\int_{r_0}^{r_a}\alpha\,dr=\frac{3}{2}\frac{E_k r_k}{g V_i}\log\left[1+\frac{\eta V_i}{4}\left(\frac{Br_0}{E_k r_k}\right)^2\right] \tag{11}$$

when the upper limit of the integral is taken as zero (i.e., $r_0/r_a \gg 1$) and E_k is the field at the cathode surface.

The characteristic may be divided into two regions:

(*a*) where the maximum energy of the electron in a cycloidal arch originating at the cathode surface is greater than the ionizing energy,

$$V_k(\max) = E_k D_k = 2E_k^2/\eta B^2 > V_i;$$

and (*b*) where the maximum cycloidal energy at the cathode is less than the ionizing energy,

$$V_k(\max) < V_i.$$

In region (*a*) the secondary electrons emitted from the cylindrical surface of the cathode can cause ionization in their first cycloidal arch and enter the discharge directly. In region (*b*) electrons emitted from the curved surface of the cathode cannot cause ionization in their first cycloidal arch and thus most of these electrons will be recaptured at the cathode. Some electrons can escape by making elastic collisions but this number is extremely small at low pressures. In this region the effective gamma is essentially controlled by the end-plates of the cathode cylinder and by processes within the discharge volume.

In region (*a*), $r_0 = r_k$, and thus equation (11) becomes

$$\log\left(1+\frac{1}{\Gamma}\right) = \frac{3}{2}\frac{E_k r_k}{g V_i}\log\left[1+\frac{\eta V_i}{4}\left(\frac{B}{E_k}\right)^2\right]. \tag{12}$$

For $(B/E_k)^2$ small,

$$E_k r_k = \frac{\frac{3}{8}\eta(Br_k)^2}{g\log(1+1/\Gamma)}. \tag{13}$$

Equation (13) represents the upper parabolic branch of the striking characteristic shown in Fig. 5, and agrees with the limiting form found by Haefer (1953*b*, Eq. 16).

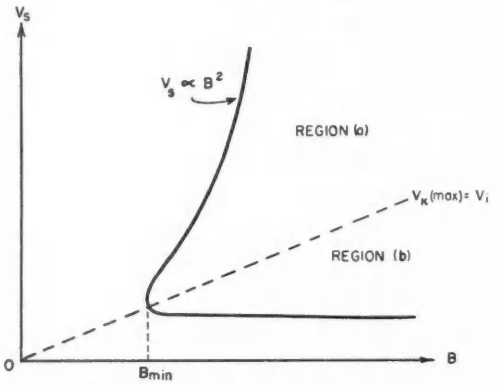

FIG. 5. Theoretical striking characteristic.

In region (*b*) $r_0 = r_1$, where r_1 is the maximum radius at which an electron can acquire ionizing energy in its cycloidal path; thus r_1 is the radius at which $V(\max) = V_i$ or

$$r_1^2 = \frac{2}{\eta V_i}\left(\frac{E_k r_k}{B}\right)^2. \tag{14}$$

Substituting this value of r_1 for r_0 in equation (11) leads to

$$E_k r_k = (5/3) g V_i \log(1+1/\Gamma). \tag{15}$$

Thus in region (*b*) the striking voltage will be independent of magnetic field provided that Γ remains constant.

The minimum anode striking voltage, on the lower branch, derived from equation (15) is

$$V_s(\min) = (5/3) g V_i \log(r_k/r_a)\log(1+1/\Gamma). \tag{16a}$$

The minimum magnetic field is found by substituting equation (14), with $r_1 = r_k$, in (15), which gives

$$Br_k(\min) = (5/3) g (2V_i/\eta)^{1/2}\log(1+1/\Gamma). \tag{16b}$$

(d) The Gamma Processes

In region (*a*) of the striking characteristic the electrons emitted from the curved surface of the cathode have a finite probability of escaping from the cathode and entering the discharge. An electron emitted from the curved surface which performs one complete cycloidal arch without suffering a collision is recaptured by the cathode and fails to enter the discharge. Electrons which suffer inelastic or elastic collisions follow orbits which do not intersect the cathode surface a second time. Thus the effective gamma of the curved surface (Γ_1) is the intrinsic gamma (γ_1) modified by the probability of escape of the electron from the curved surface. If n_0 electrons are emitted from the curved surface, only $n_0 \exp(-4D_k/\lambda)$ electrons will return to the cathode. Thus the effective gamma is given by

$$\Gamma_1 = \gamma_1[1-\exp(-4D_k/\lambda)],$$

which, for $4D_k/\lambda \ll 1$, reduces to

$$\Gamma_1 = 4\gamma_1 D_k/\lambda. \tag{17}$$

When the effective gamma of the curved surface is large compared to that of the end-plates, the upper branch of the characteristic is controlled by Γ_1, and by substituting equation (17) in (16*b*) we find that

$$Br_k(\min) = a_1 \log(b_1/p), \tag{18}$$

where p is the pressure, and a_1 and b_1 are constants.

When the cathode escape probability ($4D_k/\lambda$) is large, and thus the Γ_1 process is important on the upper branch of the characteristic, then D_k/r_k will also be large at low pressures (large λ). Under these conditions the assumption that the electric field is constant over the cycloid height is no longer valid and the foregoing analysis cannot be applied to the upper branch of the characteristic.

In region (*b*) of the striking characteristic, the cathode escape probability is essentially zero. Secondary electrons emitted from the end-plates can enter the discharge with their axial velocity component unaffected by the magnetic field. These electrons can contribute to the formation of a discharge, provided that they form ion pairs at a radius where the maximum cycloid energy exceeds the ionization potential ($V(\max) > V_i$), so that the slow electron from the ion pair is capable of causing further ionization. The orbits of the electrons emitted from the end-plates are extremely complex, and a complete formulation of the effective end-plate gamma, Γ_2, is not possible. However, an approximate calculation has been made of the longest path length of an electron emitted from an end-plate before it reaches the opposite end-plate. It was assumed that the electron remains at a constant mean radius during its transit of the gauge and that the cycloid heights were small in all cases. A maximum value of the θ-directed velocity was found as a function of the radius at which the electron was emitted by using the theoretical value of radial field. This velocity was compared with the minimum value of the mean axial velocity at the same radius obtained from the measured potential

distributions. For the standard operating conditions the path length of an electron which travels an axial distance l is given by

$$S_l \leqslant 1.22l.$$

Thus it is reasonable to assume that Γ_2 will vary in the same way as Γ_1, with the axial length of the gauge l replacing $4D_k$ as the characteristic length; thus

$$\Gamma_2 \doteq \gamma_2 l/\lambda, \qquad \text{for } l/\lambda \ll 1.$$

Substituting this value of Γ_2 in equation (16a) gives

$$V_s(\min) = a_2 \log(b_2/p), \tag{19}$$

where a_2 and b_2 are constants.

When Γ_2 is very small the effect of the end-plates on the discharge is negligible and the lower branch of the striking characteristic will rise and tend to follow the line $V_k(\max) = V_i$ (see Fig. 5). This rising characteristic of the lower branch has been observed by Penning (1936) in long discharge tubes at low pressures, where the influence of the end-plates on the discharge will be minimized.

3. TRANSIT TIMES AND SPACE CHARGE

The electron path length for one complete revolution of the electron around the anode is given by

$$L = 2\pi r \cdot \frac{\text{arc length of the cycloid}}{\text{circumference of the rolling circle}}$$

$$= 2\pi r \cdot 4D/\pi D = 8r.$$

The electron will then circle the anode $\lambda/8r$ times between collisions, and the time between collisions is given by

$$\tau_c = \frac{\lambda/8r.2\pi r}{v_t} = \lambda\pi/4v_t,$$

where v_t is the average tangential velocity of the electrons given by $v_t = E/B$.

The average radial distance moved between collisions is $\bar{x}$, which, for $2D/\lambda \ll 1$, can be approximated as (see equation (7))

$$\bar{x} = \tfrac{1}{3}(x_0+2D).$$

The radial velocity of the electrons is then given by

$$v_r = \frac{\bar{x}}{\tau_c} = \bar{x} \cdot \frac{4v_t}{\pi\lambda} = \frac{4V_i}{3B\pi\lambda}\left[1+\frac{4}{\eta V_i}\left(\frac{E_k r_k}{Br}\right)^2\right].$$

The maximum electron transit time is given by

$$\tau_- = \int_{r_0}^{r_a} \frac{dr}{v_r} = \frac{3B\pi\lambda}{4V_i}\left[r_0 - \frac{2E_k r_k}{B(V_i\eta)^{1/2}} \tan^{-1}\left(\frac{Br_0}{E_k r_k}\frac{(V_i\eta)^{1/2}}{2}\right)\right]$$

if the upper limit of the integral is taken as zero; i.e., $r_a \ll r_k$.

In region (*a*), $r_0 = r_k$, and when $B/E_k < 1$, we find that

$$\tau_-(a) \doteq \eta \frac{r_k \pi \lambda}{16} \cdot \frac{B^3}{E_k^2}. \tag{19a}$$

In region (*b*), $r_0 = r_1$, and substituting r_1 from equation (14), we find that

$$\tau_-(b) \doteq \frac{\pi \lambda E_k r_k}{5(2\eta)^{1/2} V_i^{3/2}}. \tag{19b}$$

For air, $V_i \doteq 15$ volts, $\lambda \doteq 5 \times 10^{-5}/p$ (p in mm. Hg), and taking $r_k/r_a = 30$, we find that

$$\tau_-(b) = 8.04 \times 10^{-13} V_A/p.$$

The trajectories of the positive ions are only slightly affected by the magnetic field because of the large mass of the ions. The ionic transit-time will be estimated as the transit-time of an ion in a cylindrical diode with zero magnetic field and no space-charge. The radius of the diode will be arbitrarily taken as $2r_k$. Using the data of Ferris (1936) we find the transit-time, as defined above, for ions of mass 29 to be

$$\tau_+ = \frac{1.27 \times 10^{-2} r_k}{\sqrt{V}}$$

for $r_k/r_a = 30$.

Values of the electron and ion transit-times are shown in Table I for the following conditions:

$$V_A = 6 \text{ kv.}, \quad r_k/r_a = 30, \quad r_k = 1.5 \text{ cm.}, \quad M = 29, \quad V_i = 15 \text{ volts,}$$

and

$$\lambda = 5 \times 10^{-3}/p \text{ cm.}$$

TABLE I

p (mm. Hg)	$\tau_-(b)$ (sec.)	$\tau_-(b)/\tau_+$	Space-charge
10^{-2}	4.8×10^{-7}	0.2	+
10^{-4}	4.8×10^{-5}	20	−
10^{-6}	4.8×10^{-3}	2×10^{3}	−
10^{-8}	4.8×10^{-1}	2×10^{5}	−
10^{-10}	48	2×10^{7}	−
10^{-12}	4.8×10^{3}	2×10^{9}	−

The tabulated values are very approximate since the distortion of the assumed electric fields by the end-plates will seriously affect the estimated transit-times. Also, at the higher pressures λ/r_k will approach unity and affect the estimate of τ_-/τ_+. However, these values may be used as a rough guide to indicate the order of magnitude of these parameters.

For a pressure of about 2×10^{-3} mm. Hg τ_-/τ_+ is unity; thus for pressures above this value the space-charge will be positive and for lower pressures the space-charge will be negative. Thus at pressures above 2×10^{-3} mm. Hg, the discharge current will decrease with applied voltage, and at lower pressures it will increase with voltage.

4. MEASURED STRIKING CHARACTERISTICS

Figs. 6 through 8 show the measured striking characteristics of tubes 19, 16, and 4, respectively, with dry air as the test gas. The salient dimensions

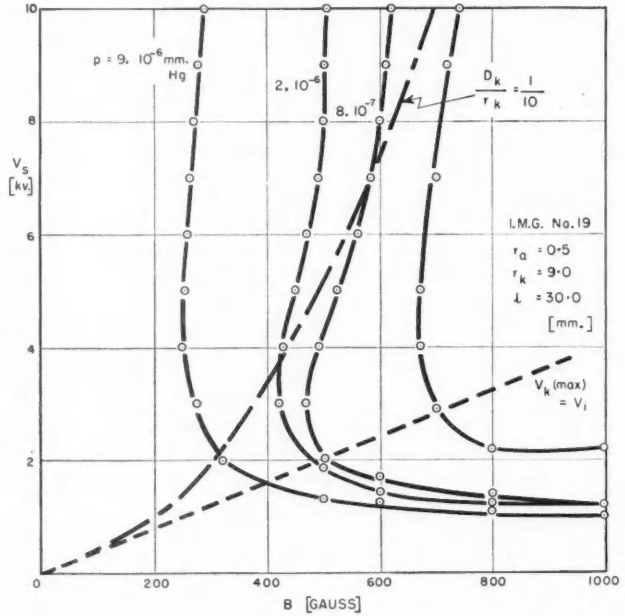

FIG. 6. Measured striking characteristics for I.M.G. No. 19.

of these tubes are given in Table II. The upper dashed parabola in these three figures is the locus of the condition $D_k/r_k = 1/10$. This value of D_k/r_k has been arbitrarily chosen as the maximum value for which the constant field assumption used in the foregoing analysis can be considered applicable. Thus we cannot expect the characteristics in the region above this line to be explainable on this simple theory. For I.M.G. Nos. 16 and 4 all the upper branch characteristics, in the pressure range used in the measurements, lie above the $D_k/r_k = 1/10$ line. These characteristics are almost lines of constant magnetic field with a slight negative slope at high pressures. The characteristics of I.M.G. No. 19 which lie below this line show the approximate parabolic form that the constant field theory predicts.

TABLE II

(All dimensions in millimeters)

	I.M.G. No.			
	19	16	4	3
r_a	0.5	0.5	0.125	0.5
r_k	9	15	15	15
l	30	13.5	15	15

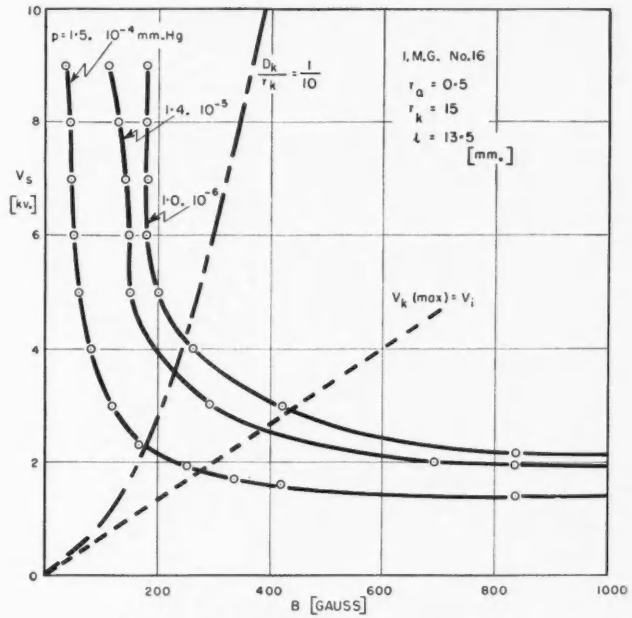

FIG. 7. Measured striking characteristics for I.M.G. No. 16.

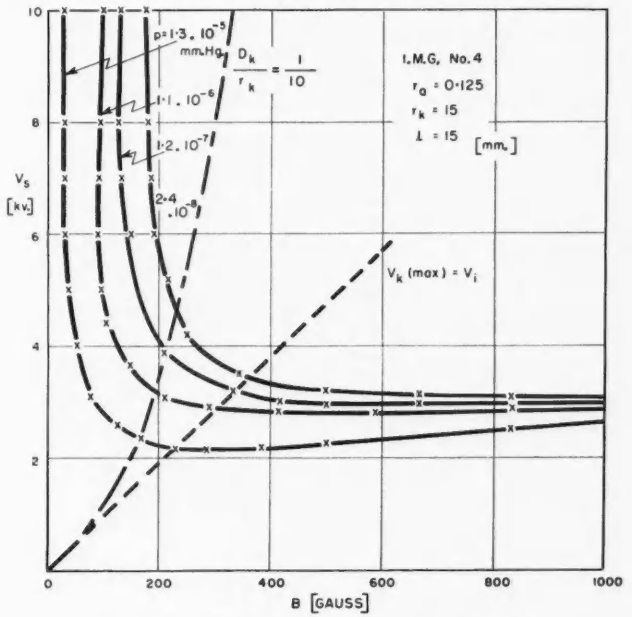

FIG. 8. Measured striking characteristics for I.M.G. No. 4.

The lower dashed line in the three figures is the locus of the condition that the maximum energy of an electron in a cycloid originating at the curved surface of the cathode is equal to the ionizing energy ($V_k(\max) = V_i$) for $V_i = 15$ volts.

The measurements for I.M.G. Nos. 4 and 16 were continued out to magnetic fields of 3×10^3 gauss. In both cases the lower branch from 10^3 to 3×10^3 gauss was exactly horizontal. For I.M.G. No. 19, the maximum field obtainable with the solenoid used with this tube was 10^3 gauss.

Measurement of the striking voltage below 10^{-8} mm. Hg was impossible to achieve with any accuracy because of the large and variable time-lag between the application of the voltage and the establishment of the discharge. This time-lag increased as pressure was decreased, and was as long as 10 minutes at pressures near 10^{-12} mm. Hg. However, no tubes failed to strike even at the lowest pressures obtainable.

Fig. 9 shows striking voltage as a function of pressure for a magnetic field well out on the lower branch of the characteristic (2060 gauss) for two

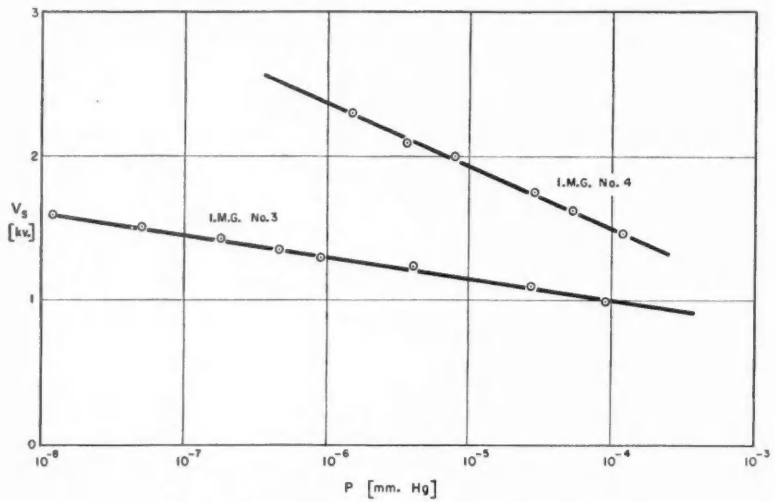

FIG. 9. Striking voltage vs. pressure for $B = 2060$ gauss.

tubes, differing only in their anode diameters (see Table II for dimensions). This value of magnetic field was used when operating the tubes at very low pressures. A linear relation between V_s and log p was observed, in accordance with equation (19); this linear relation was closely obeyed by all the tubes at high magnetic fields (*ca.* 2×10^3 gauss).

I.M.G. No. 3 closely approximated the dimensions of the gauges used for pressure measurements below 10^{-10} mm. Hg. Extrapolation of the curve of Fig. 9 to pressures of 10^{-12} mm. Hg indicates a striking voltage of 2.2 kv., which is in general agreement with rough estimates made at that pressure.

From the intercepts of the curves of Fig. 9 on the p-axis and assuming that $\Gamma_2 = \gamma_2 l/\lambda$, we can estimate the value of γ_2, the intrinsic gamma of the end-plates. For I.M.G. No. 3, $\gamma_2 \doteq 7\times10^{-4}$, and for I.M.G. No. 4, $\gamma_2 \doteq 1\times10^{-2}$.

Fig. 10 shows Br_k(min) as a function of pressure for three tubes whose dimensions are given in Table II. These data are a reasonable fit to a straight line on a Br_k(min) vs. log p plot, in agreement with equation (18). For I.M.G. No. 16 there is considerable deviation from the straight line for pressures above 10^{-4} mm. Hg.

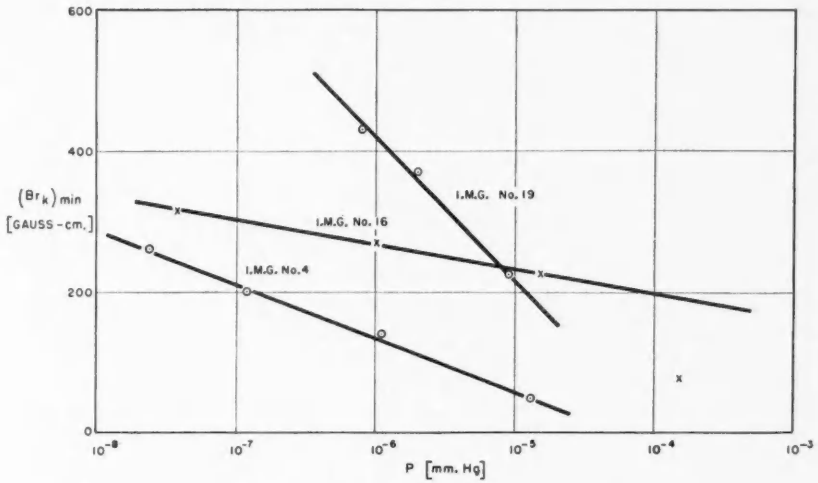

FIG. 10. Minimum magnetic field vs. pressure.

5. COMMENTS

The simple theory developed on the assumption that the electric field is constant over any one cycloidal arch is in agreement with the measured striking characteristics in region (b) and is in qualitative agreement with the observed striking characteristics in region (a) when D_k/r_k is sufficiently small. This theory cannot be applied in that part of region (a) where D_k/r_k is large and steeply rising characteristics are observed. An explanation of the characteristics when D_k/r_k is large awaits the development of a theory which takes account of the more complex electron paths that occur in this region.

The measured characteristics of this type of discharge are significantly affected by electronic oscillations in the discharge. Any theoretical treatment of the discharge characteristics that ignores these oscillatory effects can only give a first-order approximation to the measured characteristics; in particular, such a theory will be most in error at higher pressures.

ACKNOWLEDGMENTS

It is a pleasure to acknowledge the work of A. W. Pye and R. D. Cottee

in making the experimental tubes, and of L. E. Erickson in making some of the measurements. J. P. Hobson and E. V. Kornelsen contributed many useful suggestions and criticisms.

REFERENCES

BECK, A. H. and BRISBANE, A. D. 1952. Vacuum, **2**, 137.
FERRIS, W. R. 1936. Proc. I.R.E. **24**, 82.
HAEFER, R. 1953*a*. Acta Phys. Austriaca, **7**, 52.
——— 1953*b*. Acta Phys. Austriaca, **7**, 251.
——— 1954. Acta Phys. Austriaca, **8**, 213.
HOBSON, J. P. and REDHEAD, P. A. 1958. Can. J. Phys. **36**, 271.
KUGLER, G. A., OLLENDORFF, F., and ROGGENDORF, A. 1933. Z. Physik, **81**, 733.
MORTON, P. L. 1946. Phys. Rev. **70**, 358.
PENNING, F. M. 1936. Physica, **3**, 873.
SOMERVILLE, J. M. 1952. Proc. Phys. Soc. B, **65**, 620.

OPERATION OF AN INVERTED-MAGNETRON GAUGE IN THE PRESSURE RANGE 10^{-3} TO 10^{-12} MM. Hg[1]

J. P. Hobson and P. A. Redhead

ABSTRACT

A cold-cathode ionization gauge with axial magnetic field and radial electric field is described which is useful in the pressure range 10^{-3} to 10^{-12} mm. Hg and has a sensitivity of about 1 amp./mm. Hg. This gauge has the structure of an inverted magnetron with an auxiliary cathode which provides the initial field emission and allows the positive-ion current to be measured independently of the field-emission current. The operation and calibration of the gauge in a dynamic vacuum system is described for the pressure range 10^{-3} to 5×10^{-9} mm. Hg. Pressures ranging from 10^{-8} to 10^{-12} mm. Hg were obtained in sealed-off systems. Liquid-helium trapping was used for pressures below 10^{-10} mm. Hg. It is shown that the gauge gives a reliable indication of pressure below 10^{-10} mm. Hg when the pressure is determined by helium diffusion through the envelope.

1. INTRODUCTION

Measurement of extremely low pressures is normally performed with a triode ionization gauge. A lower limit to the pressure measurable with such a gauge is reached when the ion current becomes so small that it is masked by the pressure-independent photocurrent to the ion collector. This photocurrent is produced by X-rays released from the grid structure by the ionizing electron-current. The Bayard–Alpert gauge (Bayard and Alpert 1950) was designed to reduce this effect by decreasing the surface area of the ion collector to a minimum; the lowest measurable pressure with this type of gauge is about 10^{-10} mm. Hg.

The possibility of using a Penning type of cold-cathode gauge for the measurement of pressures below 10^{-10} mm. Hg was examined, since this type of gauge appeared to have two advantages: (*a*) there is no X-ray limit since the electron current producing the X-radiation is proportional to pressure; and (*b*) the lowest measurable pressure is not limited by the vapor pressure of a hot tungsten filament, which is 10^{-12} mm. Hg at 2300° K. (Alpert and Buritz 1954). Previous designs of Penning ionization-gauges suffered from two defects which made them unsuitable for the measurement of extremely low pressures: (*a*) most designs of Penning gauge fail to strike at pressures below about 10^{-5} mm. Hg; and (*b*) the ion-collecting electrode is exposed to high electric fields and the resultant field-emission from this electrode is indistinguishable in the measuring circuit from the positive-ion current. This field-emission current establishes a lower pressure limit analogous to the X-ray limit in the triode ionization gauge. The first defect can be overcome by a suitable geometric arrangement of electrodes which produces efficient electron trapping in the discharge region; such designs have been described by Beck

[1]Manuscript received September 23, 1957.
Contribution from the Radio and Electrical Engineering Division, National Research Council, Ottawa, Ontario.
Issued as N.R.C. No. 4622.

and Brisbane (1952) and Haefer (1953 and 1954). To overcome the second defect, previous designs have been modified by the addition of auxiliary-cathode electrodes which shield the ion collector from high electric fields and from which the field emission, required to start the discharge, is drawn.

This paper describes a gauge designed with the above factors in mind, which has proved useful in the range of pressures from 10^{-3} mm. Hg to the lowest pressures obtainable in this laboratory (about 10^{-12} mm. Hg). The structure of this gauge suggested that it be christened the "inverted-magnetron gauge" (I.M.G. hereafter).

The theory and measurement of the striking characteristics of this gauge are described in a companion paper (Redhead 1958).

2. DESCRIPTION OF GAUGE

Fig. 1 shows a cutaway view of the basic arrangement of electrodes in the I.M.G. The ion collector is a close-ended cylinder with holes in the center

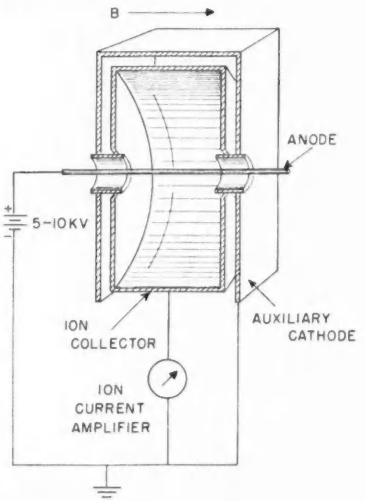

FIG. 1. Cutaway diagram of inverted magnetron gauge and associated circuit.

of the end plates through which the anode and the shielding tubes pass. The auxiliary cathode is a box-like structure enclosing the ion collector and acting as an electrostatic shield. Welded through the sides of the box are two short tubular shields which project into the ion collector and through which the anode passes. Dimensions which have proved to give satisfactory performance are given in Table I. The shield cylinders project 2 mm. inside the ion collector and protect the end plates of the ion collector from exposure to high electric fields; they also provide the field-emission current which initiates the discharge. The current to the auxiliary cathode, consisting partly of the field-emission current, does not flow through the ion-current amplifier.

The anode was made of tungsten, all other electrodes were made of Nichrome V. All parts were rigorously hydrogen-fired before assembly; in the later gauges the parts were also vacuum-fired before assembly.

TABLE I

DIMENSIONS OF I.M.G. NO. 16

Electrode	Symbol	Dimension (mm.)
Anode radius	r_a	0.5
Ion collector radius	r_k	15
Ion collector length		13.5
Shield cylinder radius		3

3. OPERATING CHARACTERISTICS ABOVE 5×10^{-9} MM. Hg

(a) Static Characteristics

Measurements in the pressure range 10^{-3} to 5×10^{-9} mm. Hg were made in a continuously pumped system by introducing dry air or helium through a variable leak. Pressure calibration was done with a Bayard–Alpert gauge (B.A.G. hereafter) of standard design. The B.A.G. was operated with the grid at +300 v., the filament at +45 v., the collector at ground, and a grid current of 8 ma. The sensitivity of the gauge under these conditions was such that the equivalent nitrogen pressure (in mm. Hg) was equal to five times the ion current (in amperes). Pressures quoted in this paper are equivalent nitrogen pressures.

A standard operating condition for the I.M.G. was chosen with a magnetic field of 2060 gauss and an anode voltage of 6 kv. Over a wide range of pressure the collector current obeys the relationship

$$i_k = cp^n, \tag{1}$$

where p is the pressure and c is a constant, and where n lies between 1.10 and 1.4 for various gauges. The value of the exponent n is essentially independent of the anode voltage, and approaches unity as the magnetic field is increased. The dimensions of the gauge have little effect on the value of n. Fig. 2 shows the current–pressure characteristic for I.M.G. No. 4 at a magnetic field of 2060 gauss, with dry air as the calibrating gas. The data of Fig. 2 are fitted by $n = 1.10$.

The measured current–voltage characteristics at a magnetic field of 2060 gauss are all of similar shape at pressures below 10^{-4} mm. Hg. At these pressures the voltage–current curve rises steeply and approaches a constant-current characteristic at high voltages. Above this pressure a radical change in shape occurs, and the curve approaches a constant-voltage characteristic. Calculations of the ratio of the transit-time of positive ions to that for electrons show that the net space-charge is negative for pressures below about 10^{-3} mm. Hg, and positive for higher pressures (see Redhead 1958, Table I). Thus the measured change in the behavior of the current–voltage characteristic occurs at a pressure where the approximate theory indicates that the space charge changes from negative to positive.

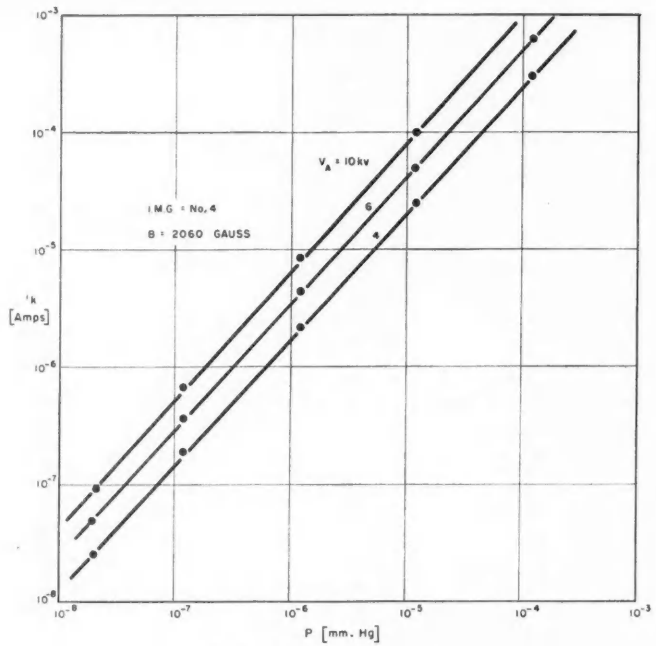

FIG. 2. Collector current versus pressure.

Measurements were made of the magnetic field and voltage necessary to give a particular collector current at a fixed pressure, and these constant-current characteristics plotted on the V_A–B plane. The shape of these curves followed the shape of the striking characteristic and suggested that the relation

$$i_k/p = k(V_A - V_s) \tag{2}$$

might be approximately correct. Here V_A is the anode voltage and V_s the striking voltage. Fig. 3 shows $V_A - V_s$ plotted against i_k/p for the standard magnetic field (2060 gauss). At high magnetic fields the above relationship is seen to hold over a pressure range of four decades. This relationship has been found to be approximately correct for all gauges over a very wide range of pressure. The non-linear relation between i_k and p for fixed V_A and B (equation (1)) occurs because V_s is a slowly varying function of pressure (Redhead 1958, equation (19)). Equation (2) indicates the importance of keeping V_s as low as possible in order to obtain a near-linear relationship between ion current and pressure.

The sensitivity ratio of the gauge to helium and air was measured in the pressure range 10^{-4} to 10^{-8} mm. Hg, and is shown in Fig. 4 for a magnetic field of 2350 gauss, and an anode voltage of 6 kv. This ratio decreases with pressure, and is a function of anode voltage.

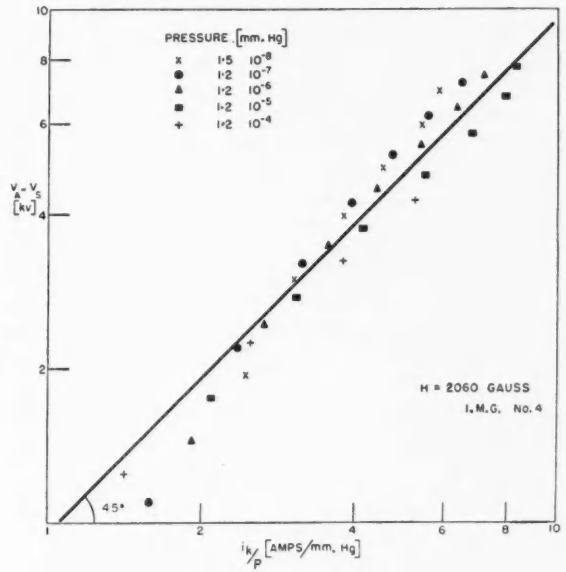

FIG. 3. $V_a - V_s$ versus i_k/p.

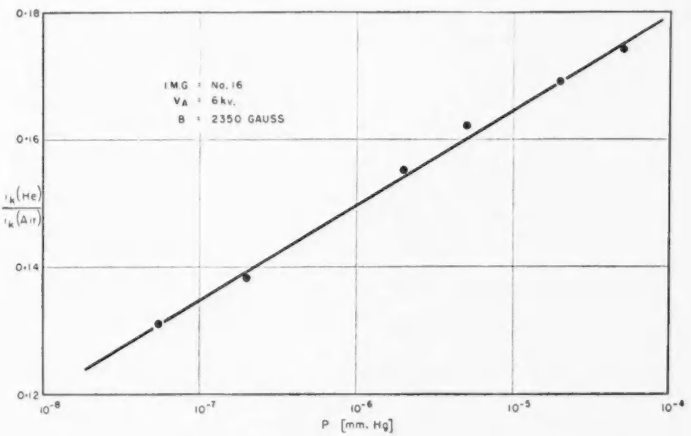

FIG. 4. Sensitivity ratio for helium and air as a function of pressure.

(b) Oscillatory Behavior

Oscillations were observable in the gauges under almost all conditions; over certain limited ranges of the parameters these oscillations were remarkably stable, both in frequency and amplitude. Some general comments can be

made about these oscillations in the regions where they were sufficiently stable to allow meaningful measurements to be made.

The observed frequencies of these oscillations (in I.M.G. No. 16) varied from 400 c.p.s. to 150 kc./s., in the pressure range 10^{-7} to 10^{-4} mm. Hg, and the frequency was independent of the impedance of the external circuit. Discontinuous jumps in frequency from one mode of oscillation to another were observed, which coincided with small changes in the collector current. These mode changes account for some of the small discontinuities in the pressure–current characteristics that were observed.

For fixed magnetic field and voltage the frequency increased linearly with collector current and was independent of the nature of the gas present. Measurements of frequency were made with helium and air at a pressure of about 5×10^{-6} mm. Hg as a function of collector current by varying anode voltage. For equal collector currents the frequencies observed for helium and air were equal to within the experimental error.

Fig. 5 shows frequency measured on I.M.G. No. 16 as a function of anode voltage, magnet current, and collector current. Magnetic field was related to

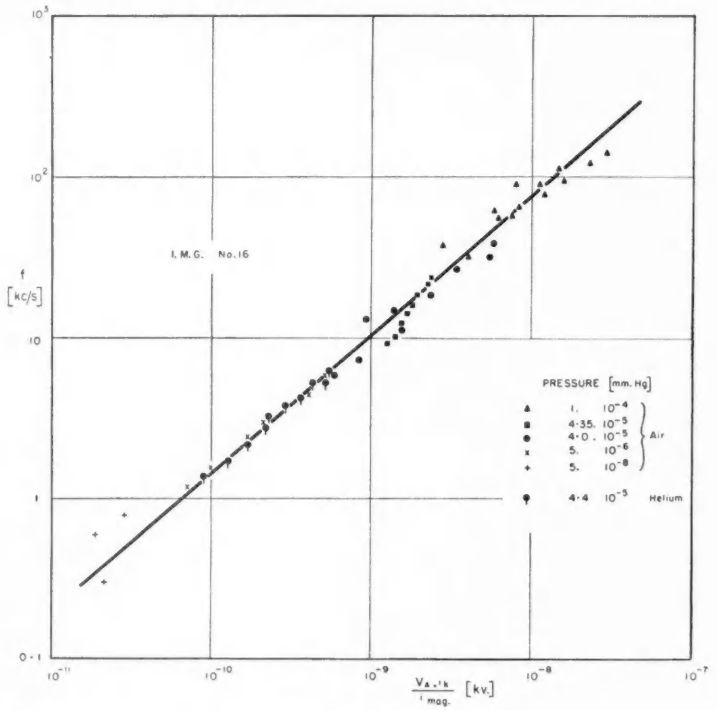

FIG. 5. Frequency of oscillations as a function of anode voltage, collector current, and magnet current for I.M.G. No. 16.

magnetic current in the following way: $B(\text{gauss}) = 10.8\, i_{\text{mag}}(\text{ma.})$. These data, taken in the pressure range 10^{-4} mm. Hg to 10^{-8} mm. Hg with both air and helium, are a reasonable fit to the relation

$$f = k(V_A i_k / B)^{0.85}. \tag{3}$$

When the amplitude of the oscillations was large, electrons could gain sufficient energy to reach the auxiliary cathode. The electron current to the auxiliary cathode was quite large at higher pressures, and changed discontinuously as the coherent oscillations started or stopped.

4. OPERATING CHARACTERISTICS BELOW 10^{-8} MM. Hg

(*a*) *Apparatus*

The apparatus (Fig. 6) used in this pressure range consisted of a sealed-off pyrex envelope containing an I.M.G., a standard B.A.G., a screen between

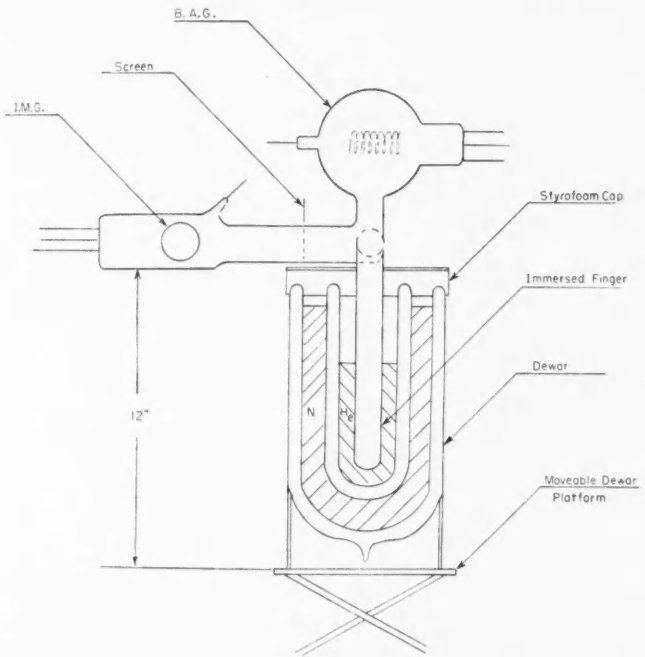

FIG. 6. Experimental apparatus for measurements below 10^{-8} mm. Hg.

the two gauges, and a finger extending down into a simple liquid helium dewar which could be raised or lowered on a movable platform. The enclosed volume was usually about 900 cc. and the inner diameter of the finger was 2.3 or 1.1 cm. The over-all finger length was 30 cm. Normally about 170 cc. of liquid helium were transferred. The screen was operated about 700 v. below

ground potential to prevent interaction between the two gauges, which was often found to be present even at the very low pressures used, in contrast to the results of Leck and Riddoch (1956). Ten sealed-off systems of this type, designated by the letters A, B, C, etc., were constructed and similar experiments performed on each. The system letter and corresponding I.M.G. design number are here given for future reference: A7, B10, C11, A′ = A repumped 7, D7, E11, F13, G15, H15, J15.

The systems were evacuated by a mercury diffusion pump with a solid-CO_2 trap in series with a liquid-nitrogen trap between pump and system. The systems were baked for about 15 hours at 475°–500° C. Pressures between 5×10^{-11} and 5×10^{-10} mm. Hg were obtained after seal-off as measured by the B.A.G.

(*b*) *Experimental Procedure and General Results*

The results obtained on all systems were not quantitatively the same but the procedures followed are described with reference to Fig. 7, which gives the results of a run on system A.

The gauges were switched off overnight to permit the pressure to rise in the system by diffusion of atmospheric helium through the pyrex walls. The gauges were then switched on simultaneously and their collector currents as a function of time recorded with the whole system at room temperature (i_k refers to collector current of I.M.G. or B.A.G.). The conductance of the tubing joining the gauges was approximately 37 liters/second for helium and the conductance of the I.M.G. end openings was greater than 12 liters/second, or about 500 times the I.M.G. electronic pumping speed for helium. Hence corrections for pressure drops between gauges could be neglected. It may be noted from Fig. 7 that the I.M.G. took a short time to strike. After subtraction of the B.A.G. X-ray limit (see Section 4(*d*)) the I.M.G. calibration curve

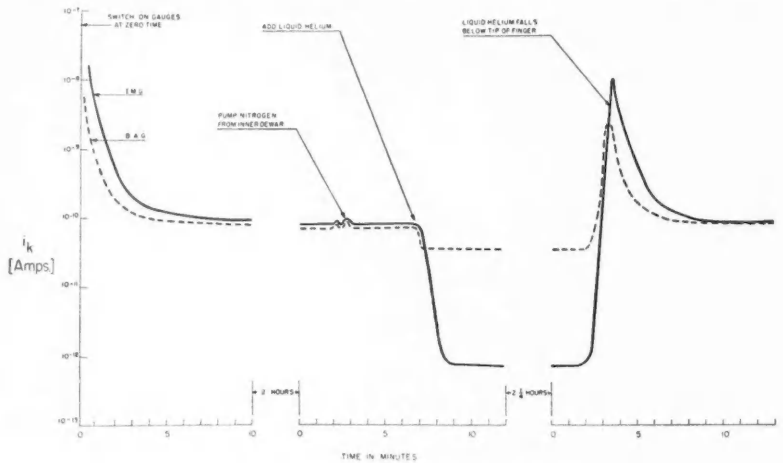

FIG. 7. Summarized record of experiment.

from 10^{-8} to 10^{-10} mm. Hg was obtained. The results of this calibration for three I.M.G. designs differing in detail are given in Fig. 8. I.M.G. pressures quoted later have been obtained from the observed currents by means of these curves.

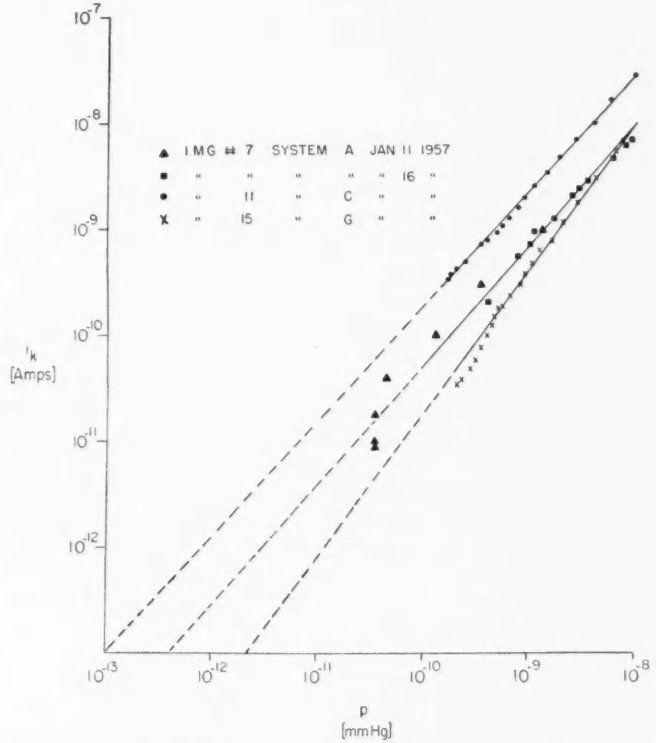

FIG. 8. I.M.G. calibration curves below 10^{-8} mm. Hg. Magnetic field, 2060 gauss. Anode volts, 6 kv.

Before any refrigerants were added, i.e., during the 2-hour period of Fig. 7, two measurements were made:

(i) The room-temperature leak-rate was found by measuring the increase in pressure in the system after the gauges had been switched off for a known time (usually about 15 minutes). A typical record of I.M.G. collected current after gauge turn-on is shown in Fig. 9(*a*). The leak-rate C is given by

$$C = (P_{\text{peak}} - P_{\text{eq}})/t, \tag{4}$$

where P_{peak} is the pressure corresponding to i_{peak} in Fig. 9(*a*), and P_{eq} is the equilibrium pressure corresponding to i_{eq}. t is the elapsed time the gauge was inoperative. With a new system the leak-rate was about 5×10^{-11} mm. Hg per

minute, which is greater than the 3×10^{-11} mm. Hg per minute obtained by Alpert and Buritz (1954), probably because of the higher surface area to volume ratio of the systems used in the present experiments. The observed C rose as much as a factor of 10 a few days after the first use of liquid helium, which

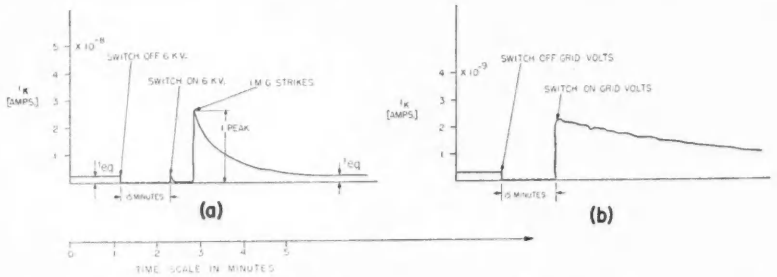

FIG. 9. (*a*) Leak-up transient of I.M.G. at room temperature. (*b*) Leak-up transient of B.A.G. at room temperature.

has been attributed to the increase of helium in solution in the envelope. For comparison, a similar leak-up record for a B.A.G. is shown in Fig. 9(*b*). It may be noted that there is no time delay between the application of voltages and the striking of the gauge, as there is with the I.M.G. This time delay, while often a disadvantage, permits a clear separation between the switching transient and the start of I.M.G. operation (see Fig. 9(*a*)). The characteristic electronic pumping time, τ_E, of either gauge could be measured from the decay of the pressure following the peak in Figs. 9(*a*) and 9(*b*). Typical values for τ_E obtained in these experiments were for the I.M.G., 0.7 minute, and for the B.A.G., 4 minutes; corresponding to electronic pumping speeds of 0.02 and 0.004 liter/second respectively for helium. The curves of currents versus time after gauge turn-on shown in Fig. 9 have been termed "leak-up transients at room temperature".

(ii) A collector-current versus grid-voltage characteristic for the B.A.G. was measured after the manner of Alpert and Buritz (1954). The results are discussed in Section 4(*d*).

Following these two measurements liquid nitrogen was added to both dewars (to precool the inner dewar), which caused a pressure drop of as much as 30% in some systems. An unknown portion of this drop may be assigned to the elimination of helium diffusion through the finger (Rogers, Buritz, and Alpert 1954). When the liquid nitrogen was removed from the inner dewar two peaks in collector current were generally observed and were assigned to adsorbed gases.

The transfer of liquid helium caused both collector currents to drop sharply. In the case shown in Fig. 7 the B.A.G. current fell to 3×10^{-11} amp., corresponding to 1.5×10^{-10} mm. Hg, and taken as the X-ray limit of the B.A.G. (see Section 4(*d*)), while the I.M.G. (No. 7) current fell to 8×10^{-13} amp., corresponding to a pressure of 2.6×10^{-12} mm. Hg (from Fig. 8). At I.M.G.

currents less than 10^{-12} amp. the signal-to-noise ratio was about 2:1. Frequently, but not in Fig. 7, the I.M.G. current with liquid helium present fell by about a factor of two during a $2\frac{1}{2}$ hour immersion period with no change in B.A.G. current.

While liquid helium was present the leak-rate measured by switching off either gauge for a known time was always zero, demonstrating that the pumping action of the gauges was not sensibly influencing equilibrium pressures and that all gases, in particular helium, were being continuously adsorbed on the cold finger.

A repetition of (ii) above with liquid helium present gave results discussed in Section 4(*d*). When the liquid helium level fell below the tip of the finger a rise in currents, usually fast, was observed (Fig. 7). This pressure rise was caused by gas, mainly helium, desorbing from the finger, followed by electronic pumping of the desorbed gas. This desorption transient, termed the "*d*-transient", could be produced at will by lowering the dewar at any time during immersion. For a *d*-transient with a steep leading edge a *d* leak-rate could be found from the peak height less the equilibrium pressure divided by the elapsed time the finger had been immersed in liquid helium, in a manner analogous to equation (4).

(*c*) *Lack of Reproducibility of I.M.G. Collector Currents with Liquid Helium Present*

The collector currents with liquid helium present showed essential reproducibility in B.A.G. currents, but large divergencies in I.M.G. currents. Fig. 10 shows the equilibrium values of I.M.G. and B.A.G. currents, measured simultaneously, first at room temperature and a short time later with liquid helium in the dewar, for all immersions for which these four currents were

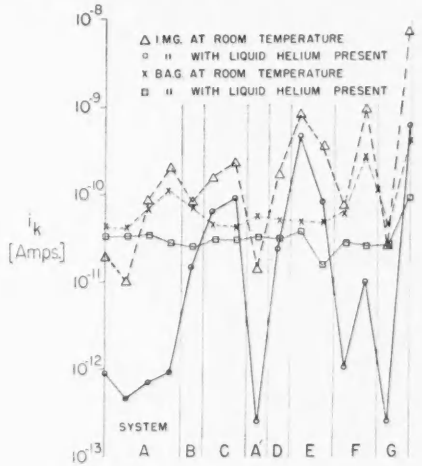

FIG. 10. Equilibrium I.M.G. collector currents at room temperature, and later with liquid helium present, for systems A–G.

measured. Conversion of currents to pressures with the data of Fig. 8 reduces but does not remove the essential scatter. The 15 immersions shown were performed with eight different systems. The ratio of pressure at room temperature as measured by the I.M.G. ranged from 1.5 to 150 over all experiments performed, both these two extremes being obtained with the same system.

Most of these scattered results were in the pressure range below the B.A.G. X-ray limit and hence the B.A.G. could not be used as an independent measure of pressure. The question naturally arises whether the I.M.G. provides a reliable measure of pressure in this range. An investigation was therefore undertaken to provide more details about the observed variations in I.M.G. currents with liquid helium present.

It was found that high I.M.G. currents with liquid helium present resulted when an immersion followed a heavy outgassing of the B.A.G. or severe heating of the system. Low I.M.G. currents with liquid helium present were observed after the gauges had been turned off or had operated normally for many hours. For example, the two immersions with system G shown in Fig. 10 were performed on the same day and differed only in that a heavy outgassing of the B.A.G. (250 ma. d-c. bombardment current at 800 v. a-c.) for $\frac{1}{2}$ hour was carried out between the two immersions. The second immersion took place 1.3 hours after the return of the B.A.G. to normal operation. In Fig. 11 are given results illustrating the same point.

Further detailed information on the processes involved in these experiments was provided by the three immersions labelled E1, E2, E3, of Fig. 11, and

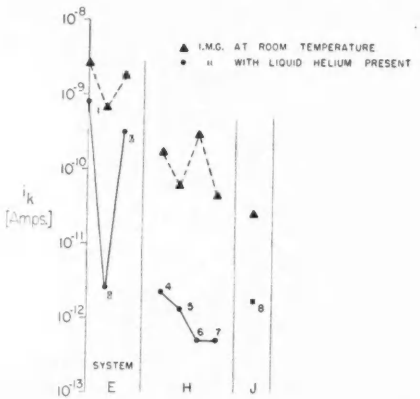

FIG. 11. Equilibrium collector currents at room temperature, and later with liquid helium present, for systems E, H, J.

1. 46 hours after heavy B.A.G. outgas.
2. 7 days after 1 but with no B.A.G. outgas in the interim, but with B.A.G. operating intermittently.
3. 4 hours after 2 with 1 hour heavy outgas of B.A.G. in interim.
4. 22 hours after seal-off, no B.A.G. operation.
5. 45 hours after seal-off, no B.A.G. operation.
6. 5 days after seal-off, no B.A.G. operation.
7. 47 days after seal-off, no B.A.G. operation.
8. 23 hours after seal-off, no B.A.G. operation.

by a fourth immersion with the B.A.G. operated alone in the same system a few hours before E2. In particular the results of E1 and E3, which yielded high I.M.G. currents with liquid helium, are to be contrasted with those of E2, which yielded a low I.M.G. current in the presence of liquid helium.

It has been shown by Alpert and Buritz (1954) that if the equilibrium between helium diffusion through pyrex and electronic pumping determines the equilibrium pressure P'_{eq} (mm. Hg), then

$$P'_{eq}/\tau_E' C' = 1, \tag{5}$$

where τ_E' is the characteristic electronic pumping time for He (minutes) $= V/S_E'$ (here V is the volume of the system in liters, S_E' is the electronic pumping speed for helium in liters/minute), and C' is the leak-rate of helium into the system in mm. Hg/minute. For the runs mentioned above P_{eq}, τ_E, and C were measured as described in Section 4(b)(i) and equation (5) checked with the results shown in Table II.

TABLE II

RESULTS ON SYSTEM E

Gauge	P_{eq} (mm. Hg)	τ_E (minutes)	C (mm. Hg/minute)	$P_{eq}/\tau_E C$
I.M.G.(E1)	1.1×10^{-9}	0.70	2.7×10^{-10}	15
B.A.G.	2.4×10^{-9}	4.4	4.6×10^{-10}	1.2
I.M.G.(E2)	3.1×10^{-10}	0.80	4.2×10^{-10}	0.91
I.M.G.(E3)	7.8×10^{-10}	0.77	5.5×10^{-10}	1.9

For runs E1 and E3, equation (5) is not satisfied, while for the other two runs it is satisfied for both gauges within experimental error. It may be noted that C does not vary much from run to run.

A comparison was also made between the room-temperature leak-up transients and the d-desorption transients. For each run one leak-up transient at room temperature and four d leak-up transients were observed. These five transients are arranged in horizontal rows across Figs. 12(a) and 12(b), those of Fig. 12(a) being room-temperature transients and those of Fig. 12(b) being d-transients. Each row corresponds to a different run, the top row with the B.A.G. operating alone and the second and third rows with the I.M.G. operating alone during runs E2 and E3 respectively. In Fig. 12(a) the bracketed figures represent the time in minutes the gauge was not operating. In the first and third d-transients of any run the gauge was operating when the dewar was lowered, while in the second and fourth d-transients the gauge was off when the dewar was lowered and was turned on a short time later. For the d-transients the first figure in brackets represents the time the finger was cold, and the second the time between the lowering of the dewar and the start of operation of the gauge (both in minutes). For either gauge all transients have a characteristic shape except for two desorption peaks during run E3 when the dewar was lowered with the I.M.G. operating. In these cases a sharp spike is superimposed on the normal background. If the spikes are disregarded (dotted line in Fig. 12(b)) the results become the same as

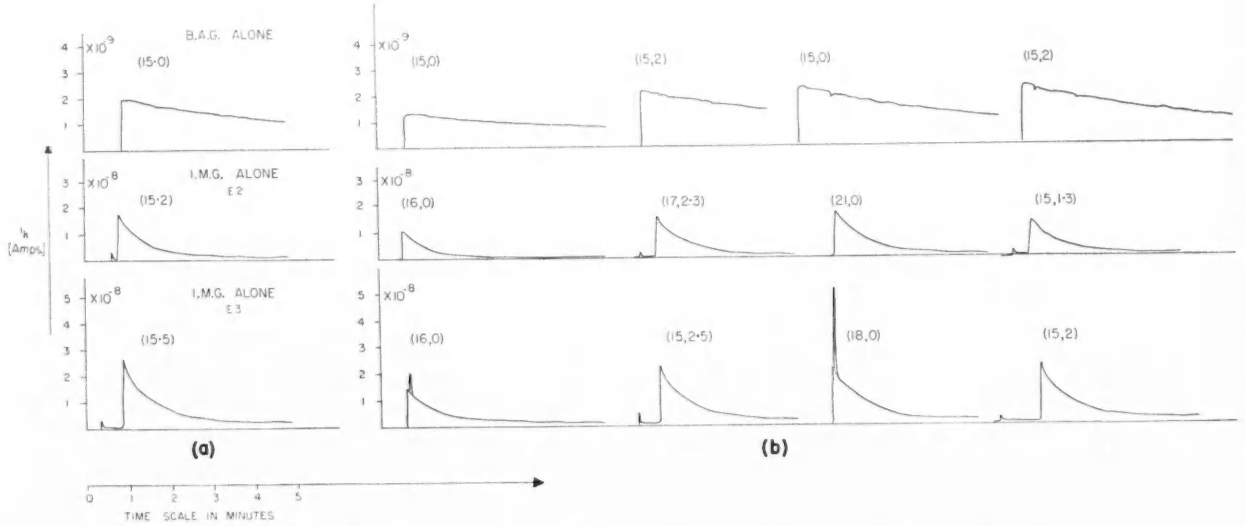

FIG. 12. (*a*) Room-temperature leak-up transients (system E). (*b*) *d*-Desorption transients (system E).

those of E2. The tendency for the first d-transient to be lower than the others may be due to an initial irreversible adsorption of gas (Armbruster and Austin 1944). If the spikes and the smaller desorption transients are disregarded, then the room-temperature and d leak-up transients are essentially the same. The presence of the spike causes the d leak-rate to exceed the room-temperature leak-rate, a result observed many times on other systems on both the I.M.G. and B.A.G. In particular, during run E1 the ratio of d leak-rate to room-temperature leak-rate was a factor of four. An interesting feature of the spike is that it is not seen if there is a delay of 2 minutes between the lowering of the dewar and the start of operation of the gauge, suggesting pumping of the gas in the spike by other than electronic means.

The results of the B.A.G. run and E2 have been adopted as characteristic of a system with equilibrium pressures determined by helium diffusion (termed "process I"), and those of E1 and E3 as indicating the presence of a second and essentially different process (termed "process II"). Process I has the properties: (1) that $P_{eq} = \tau_E C$, and (2) that d-desorption transients are identical to room-temperature leak-up transients; while process II has the properties: (1) that $P_{eq} > \tau_E C$, and (2) that d-desorption transients can have a sharp spike superimposed on the room-temperature leak-up transient. Process II gives high I.M.G. currents with liquid-helium trapping and the presence of this process in varying degree is taken to account for the scattered results of Fig. 10. Further investigation is being carried out on process II, and it is hoped that results will soon be available.

In the present paper discussion will henceforth be limited to those cases where no evidence of process II was observed. Such cases are now discussed.

(*d*) *Results for Systems with Equilibrium Pressures Determined by Helium Diffusion*

Fig. 13 shows two plots of the type described by Alpert and Buritz (1954) for B.A.G. collected current versus voltage between grid and filament. The upper curve was taken at room temperature and the lower with liquid helium present, a short time later. There is no doubt that the addition of the liquid-helium trap reduces the pressure, and the question arises whether any estimate of pressure with liquid helium present may be made from the B.A.G. Accordingly the dashed straight line was taken as the X-ray contribution, which was subtracted from the observed results to yield the dashed curves. The upper dashed curve has the familiar shape of an ionization-probability curve and the lower dashed curve does not. While the detailed shape of the lower dashed curve was not quantitatively reproducible either in the same gauge or in different gauges, its general shape was always different from the ionization-probability curve. It was concluded that no quantitative estimate of pressure in the presence of liquid-helium trapping could be made with the B.A.G. The current at the normal operating grid voltage of 255 appeared to be exactly on the X-ray line and was taken as the X-ray limit of the B.A.G. This corresponded to a pressure between 1.0×10^{-10} and 1.5×10^{-10} mm. Hg for the gauges used, and the results of Fig. 13 indicate that the true pressure with

liquid helium present is at least an order of magnitude below this, placing an approximate upper bound on the true pressure at 10^{-11} mm. Hg.

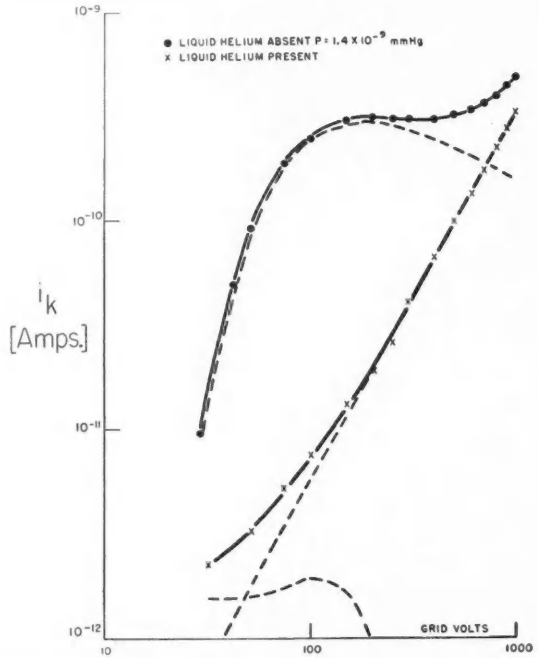

FIG. 13. Collected current versus grid voltage for Bayard–Alpert gauge, with grid current held constant.

A lower bound may be found by comparison between an ideally calculated pumping speed of the liquid-helium trap (S_T) and a measured electronic pumping speed of the I.M.G. for helium (S_E). The expected pressure with liquid helium present (P_{He}) may then be obtained from the measured pressure with liquid nitrogen in the trap (P_N) from:

$$P_{He} = P_N S_E/(S_T+S_E). \tag{6}$$

In the calculation of S_T it has been assumed that the pressure inside the finger immersed in liquid helium is zero and hence S_T is just the conductance of the trap tubing. Seventeen centimeters of tubing were taken at room temperature, and 8 cm. inside the dewar above the liquid helium level at liquid nitrogen temperature, with the remaining 5 cm. immersed in helium and hence not contributing to the conductance. For A, A′, G, H, the tubing inner diameter was 2.3 cm., while for E it was 1.1 cm.

The values of P_{He} obtained from (6) with S_T calculated as indicated above are shown in Fig. 14 along with the observed pressures as given by the I.M.G.

for nine immersions. With one exception, where the deviation is not serious, the I.M.G. observed pressure lies between the approximate upper bound of 10^{-11} mm. Hg and the calculated lower bound.

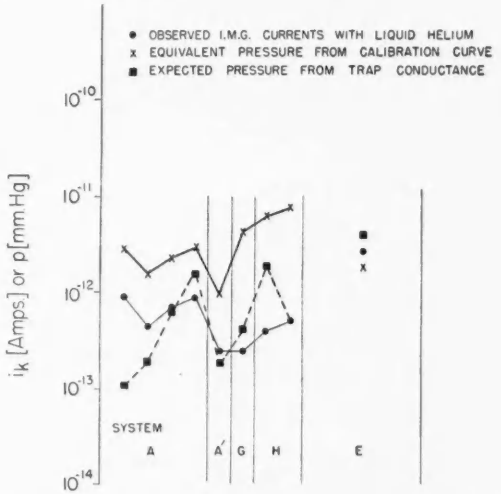

FIG. 14. I.M.G. results with liquid helium trapping in the absence of process II.

It is possible that the true pressure approaches the lower bound, and a residual current in the I.M.G. analogous to the X-ray current of the B.A.G. limits the use of the I.M.G. to a range above 10^{-12} mm. Hg. Measurements rule out the possibillty that an ohmic leakage is responsible for this residual current.

It is also possible that a true pressure of about 10^{-12} mm. Hg exists above 10^{-6} to 10^{-5} monolayers of helium adsorbed on pyrex at 4.2° K., and that the I.M.G. is giving a true measure of this equilibrium pressure. The thermomolecular pressure correction of 0.12 tends to be compensated by a factor of about 0.12 (Fig. 4, and see also Alpert 1953) for the ionization probability of helium as compared to nitrogen, and hence equivalent nitrogen pressures in the gauge at room temperature are numerically almost equivalent to true helium pressures in the finger at 4.2° K. While the helium adsorption isotherm has not been measured at coverages as low as those found in these experiments it is suggested by Meyer (1956) that more helium is adsorbed at low pressures than is predicted by an extrapolation of the Brunauer–Emmett–Teller theory. Garfunkel and Wexler (1954) place an upper bound of 10^{-10} mm. Hg for helium on brass at approximately 1.4° K., probably with higher coverages than those used here. Thus a true helium equilibrium pressure of 10^{-12} mm. Hg in the finger at liquid-helium temperature does not appear impossible.

Thus the I.M.G. appears to give a valid measure of helium pressure down to 10^{-12} mm. Hg. Experiments with liquid-helium trapping in pyrex apparatus

of the size used cannot be expected to produce pressures below 10^{-13} mm. Hg. Whether the lower gauge limit is instrumental or a true pressure is still to be decided.

5. CONCLUSION

The inverted-magnetron gauge has been shown to be useful in the pressure range 10^{-3} to 10^{-12} mm. Hg. The upper limit is set by the radical change in characteristics that occurs when space charge becomes positive. The lower limit has not been determined with certainty and may extend below 10^{-12} mm. Hg. The sensitivity of this type of gauge is an order of magnitude greater than that of the Bayard–Alpert gauge.

ACKNOWLEDGMENTS

It is a pleasure to acknowledge the work of A. W. Pye and R. D. Cottee in making the experimental gauges, and of L. E. Erickson in making some of the measurements. Liquid helium was kindly supplied by the Low Temperature Group of the Pure Physics Division of these laboratories. The authors wish to acknowledge fruitful discussion with Dr. D. Manchester of the above group concerning the adsorption of helium at low temperatures.

REFERENCES

ALPERT, D. 1953. J. Appl. Phys. **24**, 860.
ALPERT, D. and BURITZ, R. S. 1954. J. Appl. Phys. **25**, 202.
ARMBRUSTER, M. H. and AUSTIN, J. B. 1944. J. Am. Chem. Soc. **66**, 159.
BAYARD, R. T. and ALPERT, D. 1950. Rev. Sci. Instr. **21**, 571.
BECK, A. H. and BRISBANE, A. D. 1952. Vacuum, **2**, 137.
GARFUNKEL, M. P. and WEXLER, A. 1954. Rev. Sci. Instr. **25**, 170.
HAEFER, R. 1953. Acta Phys. Austriaca, **7**, 251.
——— 1954. Acta Phys. Austriaca, **8**, 213.
LECK, J. H. and RIDDOCH, A. 1956. Brit. J. Appl. Phys. **7**, 153.
MEYER, L. 1956. Phys. Rev. **103**, 1593.
REDHEAD, P. A. 1958. Can. J. Phys. **36**, 255.
ROGERS, W. A., BURITZ, R. S., and ALPERT, D. 1954. J. Appl. Phys. **25**, 863.

THE SELF-CONSISTENT FIELD WITH EXCHANGE FOR NEON BY FERUT PROGRAM[1]

BEATRICE H. WORSLEY

ABSTRACT

A general program for the computation of atomic self-consistent fields with exchange has been prepared for the University of Toronto electronic digital computer, FERUT. It was developed by application to neutral neon, for which the results are given, and tested against the independently calculated results for Fe^{+14} and Fe^{+16}.

INTRODUCTION

The problem of defining atomic structures is a difficult one to reduce, even approximately, to practical terms. The usual treatment consists of applying the variational principle to the Schrödinger Hamiltonian, with an approximation to the wave function for the many-electron system in the form of a determinant of one-electron wave functions. The problem can then be reduced to the solution of a system of ordinary differential equations of the second order. These equations have been named after their discoverers, Hartree and Fock.

The Hartree–Fock equations are of the general form

$$P''(nl;r)+g(r)P(nl;r)+f(r) = 0, \tag{1}$$

for the set of functions $P(nl;r)$ defining the radial wave functions, there being one such function for each electron group in the configuration. The group is defined by the usual quantum numbers n and l. For each function $P(nl;r)$, the corresponding function $g(r)$ is known as the potential term, and it is in itself a function of all the wave functions in the set as well as of a Lagrange multiplier $\epsilon_{nl,nl}$ which defines the energy of the n, l electron group. For each function $P(nl;r)$ the corresponding function $f(r)$ is known as the exchange term, and this is also a function of all the wave functions in the set as well as of a set of Lagrange multipliers $\epsilon_{nl,n'l'}$ which define the exchange energies between electrons in the n, l group and electrons in all the other groups n', l'. Each solution $P(nl;r)$ is subject to two-point boundary as well as orthonormalizing conditions. The non-linear nature of the Hartree–Fock equations as well as the above-stated conditions renders them difficult to solve. The only known method is a tedious numerical process involving successive approximations developed by Hartree (1927). It is based on the principle that the field of the average electron distribution derived from the wave functions must be the same as the field used in evaluating these wave functions. The atomic field so determined is therefore known as the "self-consistent field" (S.C.F.). It is, except for ions with very few electrons, prob-

[1]Manuscript received October 24, 1957.
Contribution from the Computation Centre, McLennan Laboratory, University of Toronto, Toronto, Ontario.

ably the best theoretical description of atomic energy levels that can be obtained.

The importance of the one-electron atomic wave functions has long been recognized. Up to the end of the Second World War, calculations had been carried out by hand for most of the light atoms up to argon, and for several atoms in the first long period. Applications continue to be calculated by hand wherever the results are urgently needed, although each configuration may require from three months to over a year. An early attempt at mechanizing the process was made by Hartree (1934), applying a differential analyzer to Hg and Hg^{++}. This machine gave graphical results of low accuracy, and required considerable human intervention and ingenuity.

Recent interest in atomic structures arising in the fields of solid-state physics, crystallography, and astrophysics has coincided with the development of high-speed digital calculating machines. For these machines a program can be prepared once and for all, so that much of the tedium is removed from individual applications.

Such programs have been prepared independently for the EDSAC I Computer of the University of Cambridge by the author (Worsley 1952), by Douglas (Douglas *et al.* 1955; Douglas 1956*b*), by Ridley (1955), and by Froese (1957*a*); for the Manchester University Computer Mark II by Altmann (1955); for the IBM 650 Computer by Piper (1956), and by Treanor of the University of Buffalo; and, as described here, for the University of Toronto computer FERUT, by the author. Considerable variety has been shown in these programs in many particulars. These include such aspects as the extent of applicability, the amount of judgment coded into the program, the formulation of the equations for evaluating the potential and exchange terms as well as of the Hartree–Fock wave equation, the choice of independent variable, the selection of the intervals of integration, the technique for satisfying the conditions of orthonormality simultaneously with the boundary conditions in solving the wave equation, and finally such details as the numerical representation, scaling, and decimal-point location. Some programs have not allowed for the inclusion of the exchange terms, and are therefore of more limited application. However, they all follow the basic Hartree procedure described in such papers as Hartree and Hartree (1936). A concise summary of the problem and of the applications to that date has been published by Hartree (1948). Many more aspects of the entire subject of calculating atomic structures have more recently appeared in book form (Hartree 1957).

THE FERUT PROGRAM

The entire procedure for applying the FERUT S.C.F. program to a given configuration is illustrated in Fig. 1. To begin with, it is necessary to write out the detailed Hartree–Fock equation for each wave function in the set. This amounts to listing the set of coefficients which define the potential and exchange functions in terms of the wave functions. This information must be transcribed into input tapes which FERUT can interpret through the main S.C.F. program. These are termed *C* tapes. A tape for the main program

has been prepared once and for all. Then it is necessary to prepare a set of numerical estimates to the solution. For each wave function this amounts to preparing a tape containing the wave function tabulated at the intervals of integration, together with estimates of the starting value $[P(r)/r^{l+1}]_0$, $= A$ say, the potential energy $\epsilon_{nl,nl}$, and the set of exchange energies $\epsilon_{nl,n'l'}$. These are termed P tapes.

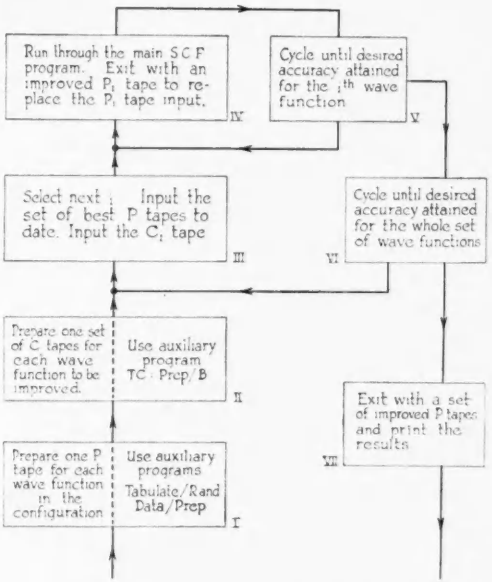

FIG. 1. Flow diagram for the FERUT S.C.F. process.

Auxiliary programs are provided to facilitate preparation of the C and P tapes. Also, since the S.C.F. process is essentially one of successive approximation, the time required to refine a given set of estimates to some prescribed degree is very greatly dependent on the accuracy of the initial estimates. Methods for obtaining them are summarized in the Hartree text (1957) and much work has been done in this direction on the EDSAC I and FERUT computers by Froese (1957*b*).

The sequence in which the wave functions to be improved are selected is left to the operator's judgment. It is usually best to refine the functions for the outer groups before disturbing the core. Also, it has been found that convergence is more rapid and direct for more highly ionized atoms.

In its basic form, the main S.C.F. program with exchange has been devised so as to deal with all atoms in neutral, excited, or ionized states with certain restrictions. The total number of wave functions is limited to 14, of points in the range of integration to 117, of terms in the potential function* to 8,

*Which are not of the form $2(2l+1)\,Y_0(nl, nl; \rho)$. Cf. p. 293.

of terms in the exchange function to 13, and of addends in each term of the exchange function to 5. Provision has been made for introducing certain variations into this basic form with ease. These include extension to more than 14 wave functions, neglect of exchange, selection of parameters to improve convergence, choice of a tractable approximation to ∞ for the upper bound to the independent variable, and introduction of short cuts when testing, without improvement, the accuracy of a given set of estimates.

The operations performed by a single run through the main S.C.F. program (boxes III to VI of Fig. 1) are illustrated in greater detail in Fig. 2. The subscript i is used to define the wave function and associated parameters

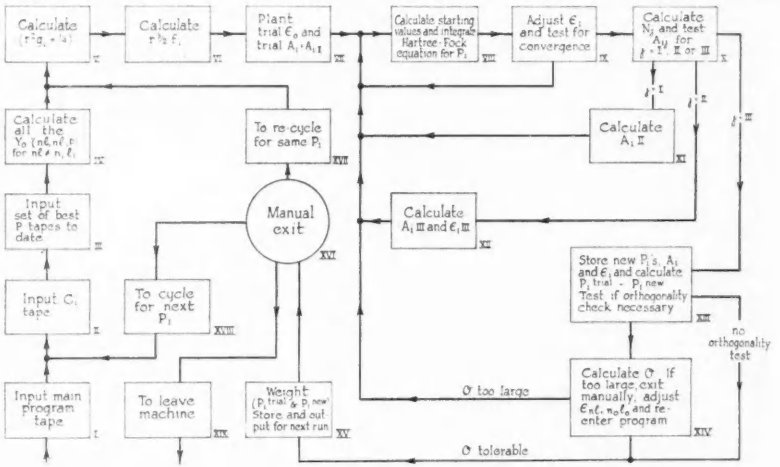

FIG. 2. Flow diagram of the main S.C.F. program.

under improvement. The subscript j defines stages in the A-improvement cycle within the main program. Also, in practice, it is usually necessary to test the orthogonality of the wave function being improved with one other wave function. The subscript 0 is used to define this latter function. The independent variable has been chosen as $\rho = \log_e cr$, where c and the interval $\delta\rho$ are constants which may be treated as parameters of the program.

With reference to Fig. 2, when tape input is complete (boxes I, II, and III), the program first calculates the potential function $g_i(\rho)$ and the exchange function $f_i(\rho)$ (boxes V and VI) for the wave function being improved. These functions are constructed out of functions $Y_k(n_1l_1, n_2l_2; \rho)$ which are in turn solutions of differential equations of the second order satisfying two-point boundary conditions and having functional coefficients dependent on pairs of wave functions, P_1 and P_2, in the configuration. The k's are small positive integers. The equations for Y_k have been reduced, by means of an auxiliary function Z_k, to a pair of first-order equations each having a one-point boundary condition, namely to

$$dZ_k/d\rho = rP_1P_2 - kZ_k, \tag{2}$$

where the integration is carried outwards from $Z_k(0) = 0$, and

$$dY_k/d\rho = (k+1)Y_k - (2k+1)Z_k, \tag{3}$$

where the integration is carried inwards from $Y_k(\infty) = Z_k(\infty)$. As a refinement, all the Y functions of the form $Y_0(nl, nl; \rho)$ for $nl \neq n_i l_i$ are constructed first and stored (box IV), so that they need not be recalculated in later recycling to improve the same wave function.

The Hartree–Fock equation is next solved for P_i, the wave function being improved (box VIII). This equation (1) has been rewritten in the form:

$$d^2(P_i r^{-1/2})/d\rho^2 = \{r^2(g_i + \epsilon_{nl,nl;i}) + 1/4\}(P_i r^{-1/2}) + r^{3/2} f_i, \tag{4}$$

where $\epsilon_{nl,nl;i}$ must be chosen so that $P_i(\rho) \to 0$ as $\rho \to \infty$, and A_i so that

$$\left\{\int_0^\infty r P_i^2 d\rho\right\}^{1/2} \equiv N \tag{5}$$

approaches unity.

The scheme for adjusting both ϵ_i and A_i will now be described (boxes VII, IX, X, XI, and XII). It has proved to be practicable and automatic, converging without operator intervention. It is well known that, if only an outwards integration is carried out, any solution of a Hartree–Fock equation diverges drastically to $\pm\infty$ after the asymptotic condition for large r has been satisfied. Also a value of ϵ, say ϵ^+, just above the true eigenvalue of (1) leads to a solution with $(n-l)$ nodes, whereas a value of ϵ, say ϵ^-, just below the true eigenvalue leads to a solution with $(n-l+1)$ nodes. The true solution has, of course, $(n-l)$ nodes. Only outwards integrating runs are employed in this program. The ϵ-adjustment to satisfy the condition $P(\rho) \to 0$ as $\rho \to \infty$, which takes place at the end of each run (box IX), is performed in two stages. In the first stage, the trial ϵ is adjusted by an increment of preassigned magnitude $\pm\Delta\epsilon$, the sign being selected by the program according as divergence takes place to $\mp\infty$. As soon as values of ϵ of each type, namely ϵ^+ and ϵ^-, are discovered, the second stage of the process begins. This is a binary or averaging process. The improved ϵ is taken to be $(\epsilon^+ + \epsilon^-)/2$. The two most recent values of ϵ^+ and ϵ^- are employed here, and their average is later used to replace ϵ^+ or ϵ^- according as it proves to be of the ϵ^+ or ϵ^- type. The stage II process continues until two successive values of ϵ differ by less than a preassigned amount ϵ_c. When this occurs, an integrating run is made with the most recent value of ϵ^-, and the resultant P is then used to evaluate $N = \{\int_0^\infty P^2 dr\}^{\frac{1}{2}}$. It was found that with solutions of the ϵ^- type, the best results were obtained when the outwards integration was carried out only as far as the $(n-l+1)$th node.* The trial values of P are used for the final values beyond this node, and checks are made that this approximation does not affect the accuracy of the orthonormalizing processes.

*It is likely that an ϵ^+ type solution would be equally satisfactory, provided that the outwards integration were carried out only to the point beyond the $(n-l)$th node at which the slope of $P(\rho)$ changed sign. However, this contingency was not so easy to detect automatically.

The A-adjustment is made by utilizing the close linear relationship which exists between good approximations to A, ϵ, and N. After the first adjustment of ϵ to determine the ϵ_{I} and N_{I} which correspond to the trial value of $A \equiv A_{\mathrm{I}}$, a new trial value for A, namely $A_{\mathrm{II}} = A_{\mathrm{I}}/N_{\mathrm{I}}$, is applied and the ϵ-adjustment process is repeated. Values ϵ_{II} and N_{II} are thus obtained. A_{III} and ϵ_{III} are then calculated from the formulae

$$A_{\mathrm{III}} = \{(N_{\mathrm{I}}-1)A_{\mathrm{II}}-(N_{\mathrm{II}}-1)A_{\mathrm{I}}\}/(N_{\mathrm{I}}-N_{\mathrm{II}})$$

and

$$\epsilon_{\mathrm{III}} = \{(N_{\mathrm{I}}-1)\epsilon_{\mathrm{II}}-(N_{\mathrm{II}}-1)\epsilon_{\mathrm{I}}\}/(N_{\mathrm{I}}-N_{\mathrm{II}}),$$

which assume that the relationships

$$\frac{A_{\mathrm{I}}}{N_{\mathrm{I}}} = \frac{A_{\mathrm{II}}}{N_{\mathrm{II}}} = \frac{A_{\mathrm{III}}}{N_{\mathrm{III}}}, \qquad \frac{\epsilon_{\mathrm{I}}}{N_{\mathrm{I}}} = \frac{\epsilon_{\mathrm{II}}}{N_{\mathrm{II}}} = \frac{\epsilon_{\mathrm{III}}}{N_{\mathrm{III}}}, \qquad \text{and } N_{\mathrm{III}} = 1$$

hold. By a third application of the ϵ-improvement process, this time with $\pm 1/100\Delta\epsilon$, the converged value of ϵ_{III} is determined. This value and A_{III} are used in the final run to determine P, and a check is made that N_{III} is equal to 1 to the desired degree of accuracy. Note that the resultant P function is never actually multiplied through by a normalizing factor.

When the program has thus selected values of A_i and ϵ_i, it calculates the corresponding value of P_i, storing this as the "new" wave function in standard P tape form (box XIII), and differencing it against the estimate of the function input. Wherever necessary, a check is also made that this new function is orthogonal to one other, say to P_0, i.e. that

$$\int_0^\infty r P_i^{\mathrm{new}} P_0 \, d\rho \equiv \mathcal{O} \tag{6}$$

tends to zero (box XIV). The operator must then decide whether or not to repeat the run with an improved estimate of the exchange energy $\epsilon_{n_i l_i, n_0 l_0}$. If not improving $\epsilon_{n_i l_i, n_0 l_0}$, the new wave function is next weighted with the trial wave function by some prescribed factor in a linear manner (box XV) and the resultant function stored and output as the improved estimate. The operator must then decide whether to recycle for the same wave function, starting now with the improved estimates of P_i, $\epsilon_{nl,n_i l_i}$, and A_i, or to proceed to improve the next wave function (boxes XVI to XIX).

NUMERICAL TECHNIQUES

Integrating routines were specially developed for FERUT with a view to speed and accuracy. To integrate equations (2), (3), (5), and (6) the following process (Hartree 1956) was found to yield 5 or 6 steps per second, meanwhile ensuring 5 or 6 significant decimal figures and remaining stable with increasing ρ:

To solve

$$dy/dx + ky = f(x)$$

introduce the integrating factor e^{kx}. This gives

$$de^{kx}y/dx = e^{kx}f(x).$$

Upon integrating from x_j to $x_{j+1} = x_j + \delta x$, one gets

$$y_{j+1} = y_j e^{-k\delta x} + e^{-k\delta x} \int_{x_j}^{x_{j+1}} e^{k(x-x_j)} f_j(x) dx.$$

By applying Simpson's rule to the integral in the latter equation, and by putting

$$f_{j+\frac{1}{2}} = (f_j + f_{j+1})/2 - (\delta^2 f_j + \delta^2 f_{j+1})/16 \qquad \text{and } \delta^2 f_j = f_{j+1} - 2f_j + f_{j-1},$$

the following formula* can be derived:

$$(7) \quad y_{j+1} = y_j e^{-k\delta x} - e^{-\frac{1}{2}k\delta x}\delta x f_{j+2}/24 + \{1/6 + 9e^{-\frac{1}{2}k\delta x}/24\}\delta x f_{j+1} + \{9e^{-\frac{1}{2}k\delta x}/24 + e^{-k\delta x}/6\}\delta x f_j - e^{-\frac{1}{2}k\delta x}\delta x f_{j-1}/24.$$

To integrate (1), which is of the type $y'' = Fy + G$, the Numerov formula (Numerov 1933) was applied in the form

$$(8) \quad y_{j+1} = \{2y_j - y_{j-1} + (\delta x)^2[5F_j y_j/6 + F_{j-1}y_{j-1}/12 + G_{j+1}/12 + 5G_j/6 + G_{j-1}/12]\} \div \{1 - (\delta x)^2 F_{j+1}/12\}.$$

Accuracy to five or six decimal figures was obtained without recourse to the refinement due to Olver (Hartree 1955). The speed is about two steps per second for the second-order equation.

Starting values for equation (4) are calculated by the main program from the approximating series for P and equation (4) itself. They also require the current value A_{ij}, and constants generated by an earlier part of the main program and by the auxiliary program TC : PREP/B. Finally, whenever the independent variable appears explicitly, it is generated by repeated multiplication.

CODING NOTES

In FERUT (Hume 1954) numbers are normally represented in binary form, each containing 40 bits and lying in absolute value between $+1/2$ and $-1/2$. Furthermore, all arithmetic operations hold the binary point fixed. It has therefore been necessary to code in alternative numerical representations and operations such as scaled, truncated, and floating point, at various stages of the calculation. Were it not for limitations of speed and storage capacity of the machine, floating point could have been used throughout. Assignment of storage space to the various parameters, functions, and intermediate results has also been complicated by the physical structure of

*Other methods investigated in this connection were:
(i) The Runge Kutta Process modified by Gill (1951), which was very slow (two steps per second) and required tabulation of auxiliary functions at the half-interval.
(ii) The Milne Process (1953), which developed a troublesome oscillating error as ρ increased.
(iii) A one-dimensional Liebmann process to solve the two-point equation for Y_k directly. This was much too slow, as of the order of 800 iterations were required over the entire range to obtain 4-decimal-figure convergence. Also convergence could take place to the wrong values when round-off errors were not kept to a minimum (Worsley 1952).

FERUT. The internal auxiliary magnetic drum store is of large capacity, holding the equivalent of over 16,000 standard numbers, or "words", but the high-speed store, which must share numbers as well as machine instructions, holds only 256. To allow as many as 117 points in the tabulation of ρ it was not feasible to take advantage of the matching technique (Douglas 1956*a*) for adjusting $\epsilon_{nl,nl}$ in the integration of (4).

All data, instructions, and intermediate results are stored on the magnetic drum at some stage of the calculation. Words are stored in tracks around the drum, each track containing 64 words. P tables require p tracks (p = number of wave functions in the set), C tables at most $3\frac{1}{2}$ tracks, machine instructions occupy $26\frac{1}{2}$ tracks,* and $(22+2m)$ tracks are required for intermediate data, where m = number of terms in the exchange function.

Several weeks are required to write out the wave equations, calculate estimates, prepare C and P tapes, and also to decide on the various runs necessary through the main program. However, the time to execute the main program on the machine is relatively short. One complete run to improve a specified wave function requires from 30 minutes to an hour, depending on the total number of functions in the system and the number of steps in the range of integration. If following up with an improvement run on the same wave function, about 10 minutes can be cut out of this time by by-passing read-in and evaluation of the unchanged $Y_0(nl, nl)$ functions. Also, if the value of N_I happens to be within a preassigned tolerance of unity, a by-pass occurs automatically to cut out the next two A-adjustment steps, thus saving a further 10 or 15 minutes. This latter is likely to occur eventually in the last one or two improvement cycles of each wave function. The main program is supplied with seven rescue points, so that in event of mechanical derail it is not necessary to restart the calculation at the beginning. Other console controls are coded in to facilitate such optional procedures as check printing, short cutting, and recycling.

RESULTS

The FERUT program results for neutral neon are presented, in atomic units, in Table I. The wave equations have been published in detail in the Hartree text (1957). The successive approximations were carried out until the maximum variations in the P's, A, and ϵ were 0.09, 0.001, and 0.01% respectively. The maximum errors in the normalizing and orthogonalizing constants were then 0.02 and 0.05% respectively. It was not found necessary to adjust the value of $\epsilon_{1s,2s}$ from its zero trial value. The results presented therefore satisfy the formulation to within two or three units in the least significant figure quoted. They differ by as much as 10% from the initial estimates, which were originally supplied by Prof. Hartree, and required some 15 hours of machine time, exclusive of check runs.

Some early hand calculations on neutral neon were published by Brown (1933). These are of the self-consistent type, the equations having been

*About 3400 machine instructions, since there are two instructions per word.

TABLE I

NORMALIZED RADIAL WAVE FUNCTIONS WITH EXCHANGE FOR NEON $(1s)^2(2s)^2(2p)^6$ CALCULATED WITH INDEPENDENT VARIABLE $\rho = \log_e 500r$, $\delta\rho = 0.1$

	$P(1s)$	$P(2s)$	$P(2p)$
$\epsilon_{nl,nl}$	65.55	3.866	1.705
$A = (P/r^{l+1})_0$	60.77	14.27	27.87

r	$P(1s)$	$P(2s)$	$P(2p)$
0.0020000	0.1191	0.0279	0.0000
22103	0.1313	0.0308	0.0001
24428	0.1448	0.0339	0.0001
26997	0.1596	0.0374	0.0001
29836	0.1759	0.0413	0.0002
0.0032974	0.1938	0.0455	0.0002
36442	0.2135	0.0501	0.0003
40275	0.2350	0.0551	0.0004
44511	0.2586	0.0607	0.0005
49192	0.2845	0.0668	0.0006
0.0054366	0.3128	0.0734	0.0007
60083	0.3437	0.0807	0.0009
66402	0.3775	0.0886	0.0011
73386	0.4143	0.0972	0.0014
81104	0.4544	0.1066	0.0017
0.0089634	0.4979	0.1168	0.0021
99061	0.5451	0.1279	0.0025
0.010948	0.5963	0.1398	0.0031
12099	0.6514	0.1527	0.0038
13372	0.7109	0.1666	0.0046
0.014778	0.7747	0.1815	0.0056
16332	0.8431	0.1974	0.0068
18050	0.9159	0.2144	0.0082
19948	0.9933	0.2323	0.0100
22046	1.0751	0.2512	0.0121
0.024365	1.1612	0.2710	0.0146
26927	1.2511	0.2916	0.0176
29759	1.3443	0.3128	0.0212
32889	1.4404	0.3344	0.0256
36348	1.5383	0.3561	0.0307
0.040171	1.6370	0.3777	0.0369
44396	1.7352	0.3986	0.0441
49065	1.8314	0.4185	0.0527
54225	1.9237	0.4366	0.0629
59928	2.0100	0.4523	0.0748
0.066231	2.0881	0.4647	0.0887
73196	2.1555	0.4730	0.1049
80895	2.2094	0.4762	0.1237
89402	2.2473	0.4731	0.1453
98805	2.2664	0.4626	0.1701
0.10920	2.2644	0.4435	0.1984
.12068	2.2391	0.4147	0.2303
.13337	2.1892	0.3750	0.2662
.14740	2.1137	0.3236	0.3060
.16290	2.0130	0.2597	0.3500
0.18003	1.8883	0.1831	0.3979
.19897	1.7421	0.0939	0.4495
.21989	1.5781	−0.0073	0.5043
.24302	1.4011	−0.1192	0.5616
.26858	1.2167	−0.2398	0.6206

TABLE I (*Concluded*)

NORMALIZED RADIAL WAVE FUNCTIONS WITH EXCHANGE FOR NEON $(1s)^2(2s)^2(2p)^6$ CALCULATED WITH INDEPENDENT VARIABLE $\rho = \log_e 500r$, $\delta\rho = 0.1$

	$P(1s)$	$P(2s)$	$P(2p)$
$\epsilon_{nl,nl}$	65.55	3.866	1.705
$A = (P/r^{l+1})_0$	60.77	14.27	27.87

r	$P(1s)$	$P(2s)$	$P(2p)$
0.29683	1.0313	−0.3661	0.6799
.32804	0.8513	−0.4948	0.7382
.36254	0.6825	−0.6216	0.7937
.40067	0.5301	−0.7419	0.8446
.44281	0.3977	−0.8508	0.8890
0.48938	0.2874	−0.9436	0.9249
.54085	0.1995	−1.0160	0.9506
.59773	0.1325	−1.0646	0.9646
.66060	0.0840	−1.0870	0.9657
.73007	0.0506	−1.0825	0.9535
0.80686	0.029	−1.0517	0.9280
.89172	0.014	−0.9969	0.8897
.98550	0.008	−0.9216	0.8398
1.0891	0.003	−0.8304	0.7799
1.2037	0.001	−0.7287	0.7122
1.3303		−0.622	0.6389
1.4702		−0.516	0.5624
1.6248		−0.414	0.4852
1.7957		−0.322	0.4096
1.9845		−0.242	0.3377
2.1933		−0.174	0.271
2.4239		−0.120	0.212
2.6789		−0.080	0.161
2.9606		−0.050	0.118
3.2720		−0.030	0.083
3.6161		−0.016	0.060
3.9964		−0.008	0.040
4.4167		−0.003	0.025
4.8812		−0.001	0.015
5.3946			0.009
5.9619			0.006
6.5889			0.004
7.2819			0.002
8.0477			0.001

modified to take account of the exchange between the $2p$ electrons only. The values of ϵ (in cm.$^{-1}$) compare with Brown's results as follows:

	$1s$	$2s$	$2p$
FERUT	65.55	3.866	1.705
Brown	65.68	2.75	1.5

The author's preliminary EDSAC I results (1952) were used by Seaton (1951) to calculate photoionization cross sections. The present results have been circulated in advance of publication for calculation of various other physical properties for comparison with experiment.

As an independent check on the program, test runs were made on Fe^{+14} and Fe^{+16}. Accuracy similar to that stated above for neon was achieved, and the results obtained on EDSAC I were confirmed to this extent (Froese 1957*a*). The program might be capable of producing greater numerical accuracy by repeated application, but it was not deemed worth while to try to produce results unjustified by the physical approximation. A typescript "Manual of operation of the S.C.F. program" (75 pp.) has been prepared as a guide to the use of the programs.

ACKNOWLEDGMENTS

This project was initiated by the Pure Physics Division of the National Research Council of Canada, and has been carried out at the Computation Centre of the University of Toronto with facilities extended by Professors W. H. Watson and C. C. Gotlieb. The program, under the guidance of Dr. G. Herzberg, has been directed by Prof. D. R. Hartree, who continues to act as consultant. The author is most grateful for Prof. Hartree's very kind interest and advice, as well as for helpful discussions with Drs. J. F. Hart and C. Froese and for technical assistance from Computation Centre Staff.

REFERENCES

ALTMANN, S. L. 1955. Proc. Phys. Soc. A, **68**, 987.
BROWN, F. W. 1933. Phys. Rev. **44**, 214.
DOUGLAS, A. S. 1956*a*. Proc. Cambridge Phil. Soc. **52**, 636.
——— 1956*b*. Proc. Cambridge Phil. Soc. **52**, 687.
DOUGLAS, A. S., HARTREE, D. R., and RUNCIMAN, W. A. 1955. Proc. Cambridge Phil. Soc. **51**, 486.
FROESE, C. 1957*a*. Proc. Cambridge Phil. Soc. **53**, Part I, 206.
——— 1957*b*. Proc. Roy. Soc. (London), A, **239**, 311.
GILL, S. 1951. Proc. Cambridge Phil. Soc. **47**, 96.
HARTREE, D. R. 1927. Proc. Cambridge Phil. Soc. **24**, 89 and 111.
——— 1934. Phys. Rev. **46**, 738.
——— 1948. Repts. Progr. in Phys. **11**, 113.
——— 1955. Numerical analysis (Clarendon Press, Oxford), §7.52.
——— 1956. Private communication.
——— 1957. The calculation of atomic structures (John Wiley & Sons, Inc., New York); Estimates, Chap. VII; equations for neon, p. 56.
HARTREE, D. R. and HARTREE, W. 1936. Proc. Roy. Soc. (London), A, **156**, 45.
HUME, J. N. P. 1954. Math. Tables and Other Aids to Computation, **8**, 30.
MILNE, W. E. 1953. Numerical solution of differential equations (John Wiley & Sons, Inc., New York), p. 64, Method VII.
NUMEROV, B. 1933. Publs. Observatory Central Astrophys. Russ. **2**, 188.
PIPER, W. W. 1956. Trans. A.I.E.E. **75**, Part I, 152.
RIDLEY, E. C. 1955. Proc. Cambridge Phil. Soc. **51**, 702.
SEATON, M. J. 1951. Proc. Roy. Soc. (London), A, **208**, 408.
WORSLEY, B. H. 1952. Ph.D. Dissertation, Univ. of Cambridge; S.C.F., Chap. V and Appendix II; Liebmann tests, Chap. VI; Neon results, p. 114.

A SURVEY OF THE MATHEMATICS AVAILABLE FOR DESCRIBING FRACTURE[1]

A. E. SCHEIDEGGER

ABSTRACT

An attempt is made to extend the mathematical finite strain theory of general rheological bodies to the inclusion of discontinuous displacements, i.e. to the description of fractures and related phenomena. A general analytical representation of discontinuities is given. A particularly simple type of discontinuity has been singled out for special investigation, i.e. "dislocations". The notion of "dislocation" is investigated from the standpoint of finite strain theory and several theorems are proved. Finally, the requirements for the establishment of a dynamic theory of fractures are outlined. It is shown that the mathematical theory cannot be carried further without additional physical investigations. The direction in which these have to be sought is indicated.

1. INTRODUCTION

The fracture of materials is a very common occurrence. Although humans have been breaking things since the inception of civilization, it is an unfortunate fact that the whole subject of fracture is very incompletely understood. There are quite a number of rule-of-thumb criteria of fracture—or better, of when a structure is supposed to be safe so as *not* to fracture—but the basic problem of describing the progress of a fracture surface in a given body under given external stresses and boundary conditions has not yet been solved. This, of course, is owing to the fact that the engineer is not particularly interested in exactly how a certain structure fails as long as he can develop criteria for making it safe. However, in other sciences, the fracture process itself is of utmost interest. Thus, the present physiography of the Earth's crust is the outcome of a giant deformation process in which fracture played a significant role. Similarly, earthquakes are certain to be the expression of a discontinuous displacement process within the Earth. If these subjects are to be more completely understood, it seems first necessary to obtain a thorough understanding of the fracture processes involved.

It is obvious that it would be a formidable undertaking to achieve a complete analytical formulation of the fracture problem. It is therefore proposed to investigate here, as a first step toward the final goal, at least the analytical means available to describe fractures in a proper, mathematical way. To the writer's knowledge, not even this has ever been done. In the course of the investigation, it becomes obvious that the theory can only be carried up to a point where it is seen that further *physical* investigations are necessary in order to further elucidate the fracture process. It is hoped that the present survey will indicate the direction in which these have to be undertaken.

In studying the mathematics of fracture, it becomes at once clear that it is necessary to invoke the formalism of *finite* strain theory. This is so because

[1]Manuscript received July 4, 1957.
Contribution from Imperial Oil Limited, 300 Ninth Avenue West, Calgary, Alberta.

the displacements, where fracture occurs, cannot be considered as infinitesimal. Unfortunately, this increases the mathematical difficulties tremendously.

A particular type of discontinuous displacement, which has been called *dislocations* (Volterra 1907; Love 1927, p. 221; Burgers 1939), has been singled out for special attention. Such dislocations have already been applied to the explanation of earthquakes (Housner 1953; Vvedenskaya 1956) and it seemed therefore indicated to give the proper formulation thereof in finite strain theory. There is some hope that such dislocations may describe fractures in some types of rheological bodies. Unfortunately, it can be shown that dislocations in *general* rheological bodies represent a rather restricted case of discontinuous displacement. In those cases where dislocations *can* be used to describe fracture, they effect a tremendous simplification of the mathematical formalism.

The mathematical framework arrived at in this paper clearly shows the difficulties involved in any proper description of fracture phenomena. However, there are no reasons other than tediousness why the proper experiments could not be performed and the proper mathematical models could not be constructed.

2. GENERAL THEORY OF DISCONTINUITIES

The treatment in the following pages is based upon an earlier summary of the writer (Scheidegger 1956), of the theory of finite displacements in rheological bodies. We therefore again describe the displacements by the co-ordinates as functions of the parameters:

$$x_i = x_i(\xi_\alpha, t), \tag{2.1}$$

where the x's represent the co-ordinates of any "point" ξ of the body. Let us assume that the parameters ξ_α are identical with the co-ordinates at time t_0 as this will simplify matters. Then, if x_i as a function of ξ_α is *discontinuous*, Eq. (2.1) describes a discontinuity in the body which has arisen in the time between t and t_0.

It appears from physical experience that discontinuities are distributed in sheets through the material. Thus, let

$$f(\xi_1', \xi_2', \xi_3', t) = 0 \tag{2.2}$$

describe a surface of discontinuity S. Equation (2.2) implies that the surface S may change its position in the body with the passing of time. As indicated in Eq. (2.2), an arbitrary point on the surface S will be denoted by ξ_α'.

The equation of the surface of discontinuity has been given in parameter space, because fracture sheets are usually fixed in the medium, except for possible extension with time. It would theoretically be possible to substitute (2.1) into (2.2) in order to obtain the equation of the surface S in co-ordinate space. However, because of the assumed discontinuity, (2.2) expressed in co-ordinate space would have multivalued solutions. It thus turns out that the parameter space is much more adapted to describe discontinuities than the co-ordinate space. In the writer's earlier paper, the formulas to transform

all dynamical quantities into parameter space have been put together. These formulas have to be used if certain quantities, in a particular problem, are not given in terms of the parameters.

The rim of a surface of discontinuity is a line that must obviously be closed in itself or begin and end on the boundary of the body. The discontinuity at the surface S can be described by giving the vector of "jump" X_i in x_i if one passes from one side of the surface to the other. The discontinuity is thus given as a vector field, defined on the surface S:

$$X_i = X_i(\xi_\alpha', t). \tag{2.3}$$

The vector of jump can be calculated if a circuit around the edge of the discontinuity is drawn, as follows:

$$X_i = \oint_{\substack{\xi_\alpha' \to \xi_\alpha' \\ \text{encircling rim}}} \frac{\partial x_i}{\partial \xi_\alpha} d\xi_\alpha. \tag{2.4}$$

For physical reasons, only such displacement fields are allowed where this integral does not depend on the circuit (but it will naturally depend on ξ_α').

Turning to the physical significance of the discontinuities discussed above, one notices that surfaces of discontinuity can describe, physically, various things. First of all, there is the possibility that they represent *fracture sheets*. The jump in displacement as one passes from one side of the surface of discontinuity to the other may represent the picture of a physical disruption of the material, i.e. of a fracture.

This is, however, not the *only* possibility. The discontinuity could be such that the material would have to penetrate itself in order to make the displacement possible. Physically, this corresponds to a case where a slice has been cut out of the body and the ends, then, have been pasted together.

An important special case is obtained if the vector of jump X_i is everywhere so behaved that its end point again lies on the surface of discontinuity; i.e. if the discontinuous displacement takes place entirely within that surface. This would correspond, physically, to a shear fracture.

3. DISLOCATIONS

A particular type of discontinuous displacement is called a "dislocation". Dislocations were encountered in the infinitesimal theory of elasticity as it was noted that Airy's stress function in multiply-connected regions could have many-valued solutions if one tried to calculate the displacements corresponding to a given continuous strain field. It has been shown later more generally that the displacements in the infinitesimal strain theory of elasticity of multiply-connected regions are, quite apart from the method using Airy's function, not necessarily one-valued although the strain components are. The proof, given by Love (1927, p. 222), was originally due to Cesàro. In order to restore one-valuedness of the displacement, one has to introduce surfaces of discontinuity (with regard to the displacement). Such discontinuities are called *dislocations*.

The surfaces of discontinuity are chosen in such a fashion that the body becomes singly-connected through them. It is thus evident that dislocations require the existence of non-evanescible circuits. In the limiting case, the multiple-connection of the body can be achieved by the assumption of singular lines upon which the strains are not continuous. These singular lines must either be closed in themselves or else begin and end on the external surface of the body. They are the rims of the surfaces of discontinuity.

In order to prove the fundamental theorems about dislocations one usually uses the formulas of infinitesimal elasticity theory. An inspection of Cesàro's proof, however, shows that it is based upon the compatibility relations only. Such compatibility relations obtain in various kinds of rheological theories and one would therefore expect that the notion of "dislocation" can be generalized for the finite strain theory of any type of rheological body. The particular assumptions made in elasticity theory may not be vital for the existence of dislocations.

Thus, let us again consider a rheological body whose displacement is described by means of parameters and co-ordinates:

$$x_i = x_i(\xi_\alpha, t). \tag{3.1}$$

The finite strain $\epsilon_{\alpha\beta}$ is defined as follows:

$$\epsilon_{\alpha\beta} = \tfrac{1}{2}(\kappa_{\alpha\beta} - \zeta_{\alpha\beta}), \tag{3.2}$$

where

$$\kappa_{\alpha\beta} = \frac{\partial x_i}{\partial \xi_\alpha}\frac{\partial x_i}{\partial \xi_\beta} \tag{3.3}$$

and $\zeta_{\alpha\beta}$ is the tensor of zero strain, which is a given and known tensor field (cf. Scheidegger 1956).

Generalizing now from the elasticity theory of dislocations, we shall try to calculate the "displacement", i.e. the co-ordinates x_i if the strains $\epsilon_{\alpha\beta}$ are given. We shall assume that the body is multiply-connected so that there exist non-evanescible circuits. In that case, we would expect "dislocations" to be possible. As mentioned earlier, the "hollows" causing the body to be multiply-connected can be contracted into singular lines upon which $\epsilon_{\alpha\beta}$ is no longer regular; the lines, then, become the rims of surfaces of discontinuity through which the body can again be made singly-connected. Dislocations found in the above manner are, by their characterization, physically allowable discontinuities of a rheological body, belonging to the class discussed in Section 2.

The condition that the $\epsilon_{\alpha\beta}$ be given continuous functions (except on the singular lines mentioned above) of the ξ's also implies the same for $\kappa_{\alpha\beta}$. It is more convenient to base the following calculations on $\kappa_{\alpha\beta}$ rather than on $\epsilon_{\alpha\beta}$. The problem, thus, is to calculate x_i from a given κ-field. The differential equation by which this has to be accomplished is (3.3).

Let us assume that we have found the co-ordinates at a point $A = (\xi_1, \xi_2, \xi_3)$.

Then, the co-ordinates at a point $B = (\xi_1'', \xi_2'', \xi_3'')$ are given by the following expressions containing a line integral:

$$x_i(\xi_\alpha'') = x_i(\xi_\alpha) + \int_A^B \frac{\partial x_i}{\partial \xi_\alpha} d\xi_\alpha = x_i(\xi_\alpha) + \int_A^B a_{i\alpha}\, d\xi_\alpha \tag{3.4}$$

with

$$a_{i\alpha} = \partial x_i / \partial \xi_\alpha \tag{3.5}$$

and

$$\kappa_{\alpha\beta} = a_{i\alpha} a_{i\beta}. \tag{3.6}$$

The basic problem in the present context is to decide what the conditions are that cause Eq. (3.4) to give a unique value for $x_i(\xi_\alpha'')$. Obviously, this expression contains two possible causes for multivaluedness: the path of integration and the expression of $a_{i\alpha}$ in terms of κ.

Let us consider first the question of the path of integration. Thus, let us assume that there exists a tensor field $a_{i\alpha}(\xi)$ which is single-valued and satisfies Eq. (3.6). Furthermore, let us consider two paths of integration and any surface bounded by those two paths. The condition that the line integral in Eq. (3.4) is the same along the two paths is that

$$a_{i\beta,\alpha} = a_{i\alpha,\beta} \tag{3.7}$$

must be satisfied everywhere on the surface bounded by the two paths. Here we have set for abbreviation:

$$a_{,\alpha} \equiv \partial a / \partial \xi_\alpha. \tag{3.8}$$

We can therefore state the result of the previous argument as follows: The displacement cannot depend on the path of integration if κ is so behaved that there exist single-valued solutions $a_{i\alpha}$ of Eq. (3.6) which satisfy Eq. (3.7). It must be assumed that not *all* imaginable κ-fields will be so behaved as to permit this, but only those that satisfy a certain "regularity-condition" which may be represented symbolically as follows:

$$R(\kappa) = 0. \tag{3.9}$$

For the further discussion it does not matter at all what the regularity condition (3.9) is, as long as we restrict ourselves to κ-fields that satisfy it.* Under such conditions, if the body is singly-connected so that all paths

*An idea of the form of the condition represented symbolically by Eq. (3.9) can be gained as follows. If the condition is satisfied, then the transformation $x = x(\xi)$ represents an actual displacement of a continuous medium. This can be described in such a fashion that, at the time $t = 0$, ξ is assumed to represent the Cartesian co-ordinates of the medium (assuming a certain origin and three orthogonal fundamental directions). However, at time t, the tensor $\kappa_{\alpha\beta}$ (3.3) can be regarded as representing a certain metric in a fictitious "strain space" (cf. Scheidegger 1956). This metric has been transformed, in the time 0 to t, from the above-mentioned Cartesian metric $\delta_{\alpha\beta}$ into the metric $\kappa_{\alpha\beta}$. The necessary and sufficient conditions that such a transformation $x = x(\xi)$ exists are (*a*) $\kappa_{\alpha\beta} = \kappa_{\beta\alpha}$ and is analytically regular (or else at least twice differentiable), (*b*) $\kappa_{\alpha\beta} d\xi_\alpha d\xi_\beta$ is a positive definite form, and (*c*) the Riemann–Christoffel curvature tensor R_{iklm} referring to κ as a metric is everywhere zero. The regularity condition (3.9) is equivalent to these three conditions.

can be continuously deformed into each other, then the co-ordinates x_i are univalent functions if the strains are everywhere regular; and there cannot be any "dislocations".

On the other hand, dislocations were *defined* as existing if the displacement turns out to be multivalued. It is obvious that this can only happen (if the strains are regular) if the body is multiply-connected, for then and only then cannot all paths be continuously deformed into each other. In other words, dislocations can be present only if there exist non-evanescible (also called non-reconcilable) circuits in the body. If there are no hollows in the body, then for dislocations to be possible, there must exist singular lines upon which the κ-field is singular so as not to satisfy the regularity condition (3.9). It is also immediately obvious that these singular lines must be either closed in themselves or begin and end on the boundaries of the body; for if this were not the case, non-evanescible circuits would obviously not be possible. Furthermore, it is also obvious that the line integral in (3.4) taken over a non-evanescible circuit around a particular singular line cannot depend on the circuit by which one returns to the same point. This defines the *strength* of a dislocation at that point.

In an actual body, displacements cannot of course be multivalued. In order to restore univaluedness, one has to introduce surfaces of discontinuity, bounded by the singular lines of the dislocations. For a particular dislocation, the surface of discontinuity can be any surface bounded by the singular lines. In a concrete case, of course, its position will be given by the physical conditions.

The results found above may therefore be summarized as follows:

(*a*) The defining characterization of a dislocation is the condition (i) that the finite strains are everywhere continuous and differentiable except on a singular line, and (ii) that the line integral in (3.4) around the singular line is different from zero.

(*b*) The singular line engendering a dislocation is either closed in itself or else begins and ends on the boundaries of the body.

(*c*) The line integral in (3.4) along any non-evanescible circuit around the singular line does not depend on the circuit.

(*d*) Single-valuedness of the displacement can be obtained if a surface is drawn, completely bounded by the singular line (or possibly extending to infinity or the boundary of the body), upon which the displacement "jumps". The displacement is continuous everywhere else.

(*e*) Dislocations form a special class of physically allowable discontinuities of a rheological body as they were generally discussed in Section 2.

Turning now to the physical significance of dislocations, we note that, theoretically, discontinuities of displacement can be entirely arbitrary. It would be advantageous if one could confine oneself to dislocations which are a particularly simple type of discontinuity. In fact, it is customary to do this in infinitesimal elasticity theory. The justification is that, across a discontinuity, the stress must be continuous (at least if inertia forces are neg-

lected). Since, in elasticity theory, the strains depend in a unique fashion on the stresses, this implies continuity of the strains also. Thus, the κ-field is continuous, a condition characteristic for dislocations.

In the finite strain theory of arbitrary rheological bodies, conditions are not so simple. Continuity of the stresses no longer implies continuity of the strains, not even in equilibrium problems. It is therefore undoubtedly true that discontinuities of the general type discussed in Section 2 are possible.

4. DYNAMICS OF DISCONTINUITIES

After having discussed the geometrical description of discontinuities, it seems proper to investigate what can be said about the dynamical conditions necessary for their physical formation.

Unfortunately, statements about the conditions for the formation of discontinuities have to remain very vague. This is in line with the fact that not too much is known about the physics of formation of fractures in materials in general.

Thus, let us assume that at time t_1 there is already a fracture surface present in the body

$$^1f(\xi_\alpha') = 0 \tag{4.1}$$

with boundary (expressed in parameter space)

$$\Xi_\alpha = {}^1\Xi_\alpha(\sigma), \tag{4.2}$$

where σ is the arc of the boundary (in parameter space). The jump vector at time t_1 is

$$X_i = {}^1X_i(\xi_\alpha'). \tag{4.3}$$

What one would like to know is the boundaries and jump vectors at a later time. What can be the conditions to determine this?

It has been mentioned that the fracture surface has a certain boundary. It will be necessary for physical reasons to assume that a fracture starts at a certain point ξ_α' in parameter space and that the boundary grows from that point and sweeps through a certain region of the body, thereby engendering the fracture surface. At the same time, the jump vectors may change on all points of the surface. That part of the fracture surface which has been engendered would not change its position in parameter space. A particularly important case will be the one where there is slippage along the fracture surface only, i.e. where there is complete "shear" fracture where no hollows are created inside the body. The condition for this is that the increment of the jump vector during an infinitesimal time dt is tangential to the fracture surface.

The problem is thus to find the following two functions of the parameters for the time t:

$$\Xi_\alpha = {}^t\Xi_\alpha(\sigma, t), \tag{4.4}$$

$$X_i = {}^tX_i(\xi_\alpha', t). \tag{4.5}$$

We have already pointed out earlier that, in general finite strain rheology, the problem of finding the displacements as functions of time and parameters is determined by three types of conditions: (i) the law of motion, (ii) the law of continuity, and (iii) the rheological condition. In the last, the whole strain history of the body may be involved. With the presence of discontinuities, the conditions at the latter must be added. There is thus (i) a condition for the stresses across the surface of discontinuity (e.g. whether there is friction present) from which, by means of the rheological equation, a condition for the strains can be deduced (which again may depend on the strain-history), (ii) a continuity condition for the displacements across the surface of discontinuity (e.g. stating whether the creation of cavities is allowed), and finally (iii) a condition for the spread of the rim. The latter again may depend on the whole strain history of the body.

Experiments available to date do not permit one to present even one case of a complete solution of the above problem. However, the above enumeration of the conditions required might well suggest the direction in which further efforts might be expended. Perhaps it will be found possible, for instance, to connect the spread of a shear crack with the stresses present near the edge; or, possibly, the spread of a tension crack may depend only on the type of singularity of stress present near the edge. Such relationships could be found either by making the appropriate experiments or, possibly, by studying the physics of molecular cohesion theoretically.

5. CONCLUSION

If we make a survey of the mathematical theory of discontinuous displacements as far as it can be set up to date, it is inevitable that we become aware of its incompleteness. There is no difficulty in formulating the geometry of the problem and of devising a general *scheme* of describing the dynamics, although this, too, does not seem to have been done heretofore. However, when it comes to formulating the "law of spreading" of a crack through a body, we note that the understanding of the underlying *physical* principles is missing. One can state the *types* of physical laws that are required for the mathematical theory, and this might be helpful for the further elucidation of the problem. The missing laws are the dynamical conditions for the spread, speed, direction of the edge of a crack as a function of the conditions prevailing in its neighborhood.

It might be argued that there is a large volume of literature on fracture and strength of materials (ably summarized, for example, by Orowan (1949)), but an inspection thereof shows that there are no instances, at least to the writer's knowledge, where there would be any such precise statements as are required for a mathematically complete formulation of a particular fracture problem. The closest to such a formulation may well be the Griffith (1920) theory of the spread of small tension cracks, in which the stresses at the tip of a crack have been calculated and a criterion has been formulated as to when the crack will spread. However, no information can be obtained as to the direction and speed of spreading of the crack during the next infinitesimal

time-interval. Perhaps it would be possible to extend the Griffith theory to provide this information for the case under consideration.

Another attack to obtain the required basic physical information might well be by means of experimentation. If one were to combine modern techniques of high-speed photography (see, e.g., Jones 1952) with those of experimental stress analysis (see, e.g., Hetenyi 1950), it would appear expectable that the dynamic conditions near the edge of a crack could be established for various typical cases.

Once the conditions at the edge of a crack can be formulated analytically, the problem of determining the spread of the crack through a body for given external conditions becomes a purely mathematical one. Even then, however, the solution of this problem is a very formidable undertaking. The problem is characterized by the fact that it contains a set of boundary conditions referring to a boundary which itself has to be determined by the solution. Such conditions are known as "floating boundary conditions"; they are notorious for the difficulties which they present if they occur in a problem. Nevertheless, it ought to be expected that solutions could be formed for a variety of typical cases.

ACKNOWLEDGMENTS

In conclusion, the writer wishes to thank Dr. E. Orowan of the Massachusetts Institute of Technology in Cambridge, Dr. J. A. Rottenberg of the Dominion Observatory in Ottawa, and Dr. M. S. Macphail of Carleton College in Ottawa for stimulating discussions about the subject matter of this paper. Their kind criticisms and comments proved to be invaluable.

REFERENCES

BURGERS, J. M. 1939. Proc. Koninkl. Ned. Akad. Wetenschap. **42**, 293.
GRIFFITH, A. A. 1920. Phil. Trans. Roy. Soc. London, Ser. A, **221**, 163.
HETENYI, M. 1950. Handbook of experimental stress analysis (John Wiley & Sons, Inc., New York).
HOUSNER, G. W. 1953. A dislocation theory of earthquakes, Calif. Inst. Technol. Rept. N6-onr-244.
JONES, G. A. 1952. High speed photography (Chapman and Hall, Ltd., London).
LOVE, A. E. H. 1927. A treatise on the mathematical theory of elasticity, 4th ed. (Cambridge University Press, London).
OROWAN, E. 1949. Repts. Progr. in Phys. **12**, 185.
SCHEIDEGGER, A. E. 1956. Can. J. Phys. **34**, 498.
VOLTERRA, V. 1907. Ann. école norm. supérieure Paris, **24**, 401.
VVEDENSKAYA, A. V. 1956. Izvest. Akad. Nauk S.S.S.R., Ser. Geofiz. 277.

ON THE SPIN–ORBIT INTERACTION IN DIATOMIC MOLECULES. I[1]

I. Kovács

ABSTRACT

The purpose of the present paper is to give further details of an investigation of the spin–orbit interaction in diatomic molecules. The first part of the paper deals with perturbations between states of odd multiplicity in a two-electron system. With the aid of the matrix elements which have been obtained, a comparison of the perturbations in the various components of a given state and in some cases a comparison of perturbations in two different states is possible. Also for certain cases it has been possible to establish relationships between the matrix elements which give the magnitude of the perturbations and experimentally measurable molecular constants of the perturbed states.

INTRODUCTION

The majority of the perturbations observable in the spectra of diatomic molecules—viz. those occurring between states of the same multiplicity—can be easily understood by taking into account the terms omitted at the separation of the wave equation with the aid of the perturbation method. As shown by many examples, however, perturbations can also occur between states of different multiplicity (Schmid and Gerö 1935; Kovács and Lagerqvist 1950; Lagerqvist, Nilheden, and Barrow 1952; Nilheden 1955) or, in other words, anomalous phenomena have been observed which can be explained only by the occurrence of such "intercombination" perturbations. The anomalous behavior of the $^4\Pi$ state of the O_2^+ molecule serves as an example for the latter (Budó and Kovács 1954). An exact discussion of the intercombination perturbation could be carried out if an exact relativistic form of the wave equation were known for a many-electron system. Lacking this, one can start from the form of the Dirac equation as extended to an atom with two electrons, and the occurrence of terms in the Hamiltonian operator which are due to the magnetic interaction between the orbital and spin momenta of the individual electrons can be assumed. Taking these terms into consideration, attempts have previously been made to explain the intercombination perturbations (Budó and Kovács 1938, 1939, 1950; Premaswarup 1954*a*, *b*). These investigations, however, with the exception of one (Budó and Kovács 1954), were of a fairly general character and thus were not adequate to draw conclusions concerning the magnitude of perturbing matrix elements for various electron configurations. The purpose of the present paper is to take into account individual electron configurations of two- and three-electron systems and to determine the values of matrix elements arising from the spin–orbit interaction. These matrix elements of various configurations are compared and related to the molecular constants known from the experimental data.

[1]Manuscript received July 29, 1957.
Contribution from the Department of Atomic Physics, Technical University, Budapest, Hungary.

In order to attain the aims set forth above, the spin–orbit operator, as well as a detailed form of the wave-function of the individual electron configurations, will be needed. The former has, as is well known, the following form:

$$(1)\quad \sum a_i(\mathbf{l}_i\mathbf{s}_i) = \sum a_i\left\{\frac{\hbar}{i}\frac{\partial}{\partial\varphi_i}s_{z_i}+\frac{1}{2}\left[e^{i\varphi_i}\left(f_i+ig_i\frac{\partial}{\partial\varphi_i}\right)(s_{x_i}-is_{y_i})\right.\right.$$
$$\left.\left.-e^{-i\varphi_i}\left(f_i-ig_i\frac{\partial}{\partial\varphi_i}\right)(s_{x_i}+is_{y_i})\right]\right\},$$

where φ_i is the azimuth angle of the ith electron around the z axis which lies along the axis of the molecule and s_{x_i}, s_{y_i}, s_{z_i} are the well-known Pauli operators. The operators f_i, g_i, and a_i are independent of φ_i and their form depends on the nature of the model applied.

To determine the electronic part of the wave-functions we shall start from the wave-functions of the individual electrons of the following form (Budó and Kovács 1954): $p_i e^{i\lambda_{ip}\varphi_i}\alpha_i$ and $p_i e^{i\lambda_{ip}\varphi_i}\beta_i$, where α_i and β_i are the wave-functions belonging to the $+\frac{1}{2}$ and $-\frac{1}{2}$ values of the spin quantum number σ_{ip}. The wave-functions independent of φ_i and corresponding to the state represented by the quantum numbers n_{ip}, l_{ip}, λ_{ip} of the ith electron are denoted by the symbol $p_i \equiv p_{n_{ip},l_{ip},\lambda_{ip}}$. Similarly, according to the quantum numbers n_{kq}, l_{kq}, λ_{kq} the wave-function $q_k \equiv q_{n_{kq},l_{kq},\lambda_{kq}}$ represents either for $k \neq i$ another state of another electron or for $k = i$ another state of the same electron.

Disregarding the mutual electrostatic interaction of the electrons, the wave-functions of the individual configurations can be given with the aid of the above-mentioned wave-functions in the form of determinants. These wave-functions of determinant form are in general the simultaneous eigenfunctions of the operators $L_z = \sum_i l_{z_i}$ and $S_z = \sum_i s_{z_i}$, whilst they are not eigenfunctions of the operators $S^2 = S_x^2+S_y^2+S_z^2$. It is, however, easy to form linear combinations of the above-mentioned eigenfunctions of determinant form which will be eigenfunctions of the operator S^2 with eigenvalues $S(S+1)$ determining the multiplicity of the respective terms.

TWO-ELECTRON SYSTEMS

1. Eigenfunctions

Assuming that all the electrons of a molecule, with the exception of two, are in closed shells, the states of the molecule might be characterized by the quantum numbers of these two valence electrons in the following manner: $(n_{ip}, l_{ip}, \lambda_{ip}, \sigma_{ip}; n_{kq}, l_{kq}, \lambda_{kq}, \sigma_{kq})$ or, since in many cases the writing in full of the principal and azimuthal quantum numbers is unnecessary, simply (λ_p, λ_q). In this case the state $(n_{ip}, l_{ip}, \lambda_{ip}, \sigma_{ip})$ has to be understood as a state in which the ith electron is in a state denoted by p, where $i = 1$ or 2, whilst $(n_{kq}, l_{kq}, \lambda_{kq}, \sigma_{kq})$ indicates that the kth electron is in a state denoted by q, where $k = 2$ or 1. The possible types of states of the molecule are given by the different possible positions of the λ's relative to one another. Further on, the simplest cases will be dealt with, where $|\lambda_p| = |\lambda_q| = \lambda$, or $|\lambda_p| = \lambda'$ and $|\lambda_q| = \lambda'+1$,

or $|\lambda_p| = \lambda'+1$ and $|\lambda_q| = \lambda'$. In the case of (λ, λ) it is well known that the following types of states are possible (Herzberg 1951): ${}^1\Sigma^\pm$, ${}^3\Sigma^\pm$, ${}^1(2\lambda)$, ${}^3(2\lambda)$, where for $\lambda = 0$ the terms Σ^- are lacking, whilst in the case of $(\lambda', \lambda'+1)$ and $(\lambda'+1, \lambda')$ the possible states are: ${}^1\Pi$, ${}^3\Pi$, ${}^1(2\lambda'+1)$, ${}^3(2\lambda'+1)$. If λ or $\lambda' = 0$, the terms (2λ) and $(2\lambda'+1)$ are not present, whilst if λ or $\lambda' = 1, 2, \ldots$ they signify Δ, $\Gamma \ldots$ or Φ, $H \ldots$ etc. types of states.

Further on, the cases occurring most frequently, viz. interaction between Σ and Π states, will be investigated. The electron part of the needed wave-functions assuming Hund's case (a) is, on the basis of the formulation mentioned above, the following:

$$\left.\begin{aligned}
\phi({}^1\Sigma^\pm_0) &= \phi({}^1\Sigma^\pm)(1/\sqrt{2})(\alpha_1\beta_2-\beta_1\alpha_2),\\
\phi({}^3\Sigma^\pm_{+1}) &= \phi({}^3\Sigma^\pm)\alpha_1\alpha_2,\\
\phi({}^3\Sigma^\pm_0) &= \phi({}^3\Sigma^\pm)(1/\sqrt{2})(\alpha_1\beta_2+\beta_1\alpha_2),\\
\phi({}^3\Sigma^\pm_{-1}) &= \phi({}^3\Sigma^\pm)\beta_1\beta_2,
\end{aligned}\right\} \tag{2}$$

where

$$\left.\begin{aligned}
\phi({}^1\Sigma^\pm) &= (1/2\pi)(p_1q_2 \pm p_2q_1)\begin{matrix}\cos\\ \sin\end{matrix}\lambda(\varphi_1-\varphi_2),\\
\phi({}^3\Sigma^\pm) &= (1/2\pi)(p_1q_2 \mp p_2q_1)\begin{matrix}\cos\\ \sin\end{matrix}\lambda(\varphi_1-\varphi_2)
\end{aligned}\right\} \tag{3}$$

for $\lambda \neq 0$. If $\lambda = 0$, the normalization factor will be $1/2\sqrt{2.}\pi$ instead of $1/2\pi$ and as a matter of course owing to the sine factor only the wave-functions corresponding to the upper signs differ from zero.

Similarly for Π states we obtain:

$$\left.\begin{aligned}
&\phi({}^1\Pi_{+1}) = \phi({}^1\Pi)(1/\sqrt{2})(\alpha_1\beta_2-\beta_1\alpha_2), \quad \phi({}^1\Pi'_{-1}) = \phi({}^1\Pi')(1/\sqrt{2})\\
&\qquad\qquad\qquad\qquad\qquad\qquad\qquad\qquad\qquad\qquad \times(\beta_1\alpha_2-\alpha_1\beta_2),\\
&\phi({}^3\Pi_{+2}) = \phi({}^3\Pi)\alpha_1\alpha_2, \qquad\qquad\qquad \phi({}^3\Pi'_{-2}) = \phi({}^3\Pi')\beta_1\beta_2,\\
&\phi({}^3\Pi_{+1}) = \phi({}^3\Pi)(1/\sqrt{2})(\alpha_1\beta_2+\beta_1\alpha_2), \quad \phi({}^3\Pi'_{-1}) = \phi({}^3\Pi')(1/\sqrt{2})\\
&\qquad\qquad\qquad\qquad\qquad\qquad\qquad\qquad\qquad\qquad \times(\beta_1\alpha_2+\alpha_1\beta_2),\\
&\phi({}^3\Pi_0) = \phi({}^3\Pi)\beta_1\beta_2, \qquad\qquad\qquad \phi({}^3\Pi'_0) = \phi({}^3\Pi')\alpha_1\alpha_2,
\end{aligned}\right\} \tag{4}$$

where

$$\left.\begin{aligned}
\phi({}^{2\mp1}\Pi) &= (1/2\sqrt{2.}\pi)(p_1q_2e^{-i[\lambda'(\varphi_1-\varphi_2)-\varphi_2]} \pm p_2q_1e^{+i[\lambda'(\varphi_1-\varphi_2)+\varphi_1]}),\\
\phi({}^{2\mp1}\Pi') &= (1/2\sqrt{2.}\pi)(p_1q_2e^{+i[\lambda'(\varphi_1-\varphi_2)-\varphi_2]} \mp p_2q_1e^{-i[\lambda'(\varphi_1-\varphi_2)+\varphi_1]})
\end{aligned}\right\} \tag{5}$$

for configuration $(\lambda', \lambda'+1)$ and

$$\left.\begin{aligned}
\phi({}^{2\mp1}\Pi) &= (1/2\sqrt{2.}\pi)(p_1q_2e^{+i[\lambda'(\varphi_1-\varphi_2)+\varphi_1]} \pm p_2q_1e^{-i[\lambda'(\varphi_1-\varphi_2)-\varphi_2]}),\\
\phi({}^{2\mp1}\Pi') &= (1/2\sqrt{2.}\pi)(p_1q_2e^{-i[\lambda'(\varphi_1-\varphi_2)+\varphi_1]} \pm p_2q_1e^{+i[\lambda'(\varphi_1-\varphi_2)-\varphi_2]})
\end{aligned}\right\} \tag{6}$$

for configuration $(\lambda'+1, \lambda')$.

Taking into account that the energies corresponding to the two possible positions of the resultant Ω relative to the axis of the molecule ($+\Omega$ and $-\Omega$) are degenerate and completing the above-mentioned wave-functions by the

part arising from the rotations and vibrations of nuclei, the new wave-functions will be the following:

$$
(7)\qquad
\begin{cases}
\psi(^1\Sigma^{\pm}_0) = \phi(^1\Sigma^{\pm}_0)R_{n,v}\,u_{J,0}, \\
\psi(^3\Sigma^{\pm}_1) = (1/\sqrt{2})[\phi(^3\Sigma^{\pm}_{+1})u_{J,+1}+\phi(^3\Sigma^{\pm}_{-1})u_{J,-1}]R_{n,v}, \\
\psi(^3\Sigma^{\pm}_1)' = (1/\sqrt{2})[\phi(^3\Sigma^{\pm}_{+1})u_{J,+1}-\phi(^3\Sigma^{\pm}_{-1})u_{J,-1}]R_{n,v}, \\
\psi(^3\Sigma^{\pm}_0) = \phi(^3\Sigma^{\pm}_0)R_{n,v}\,u_{J,0}, \\
\psi(^1\Pi^{\pm}_1) = (1/\sqrt{2})[\phi(^1\Pi_{+1})u_{J,+1}\pm\phi(^1\Pi'_{-1})u_{J,-1}]R_{n,v}, \\
\psi(^3\Pi^{\pm}_\Omega) = (1/\sqrt{2})[\phi(^3\Pi_{+\Omega})u_{J,+\Omega}\pm\phi(^3\Pi'_{-\Omega})u_{J,-\Omega}]R_{n,v},
\end{cases}
$$

where $R_{n,v}(\rho)$, $u_{J,\Omega}$, and v are the vibrational and rotational wave-functions and the vibrational quantum number of the molecule, respectively, and n designates all the principal quantum numbers of the electrons.

Since for Σ states the approximation obtained from Hund's case (a) has only a theoretical meaning, whilst for Π states case (b) is a limiting case as important as case (a), it seems advisable to use the wave-functions of case (b) for the states considered above. These wave-functions are given as the linear combinations of the earlier ones where the coefficients of the linear combinations can be easily determined by taking into account, by the perturbation method, the terms omitted at the separation of the wave-equation. Hence

$$
(8)\qquad
\begin{cases}
\psi(^1\Sigma^{\pm}_J) = \psi(^1\Sigma^{\pm}_0), \\
\psi(^3\Sigma^{\pm}_{J+1}) = -\sqrt{\dfrac{J+1}{2J+1}}\,\psi(^3\Sigma^{\pm}_0)-\sqrt{\dfrac{J}{2J+1}}\,\psi(^3\Sigma^{\pm}_1) \approx -\dfrac{1}{\sqrt{2}}[\psi(^3\Sigma^{\pm}_0) \\
\qquad\qquad +\psi(^3\Sigma^{\pm}_1)], \\
\psi(^3\Sigma^{\pm}_J) = \psi(^3\Sigma^{\pm}_1)', \\
\psi(^3\Sigma^{\pm}_{J-1}) = \sqrt{\dfrac{J}{2J+1}}\,\psi(^3\Sigma^{\pm}_0)-\sqrt{\dfrac{J+1}{2J+1}}\,\psi(^3\Sigma^{\pm}_1) \approx \dfrac{1}{\sqrt{2}}[\psi(^3\Sigma^{\pm}_0) \\
\qquad\qquad -\psi(^3\Sigma^{\pm}_1)], \\
\psi(^1\Pi^{\pm}_J) = \psi(^1\Pi^{\pm}_1), \\
\psi(^3\Pi^{\pm}_{J+1}) = \sqrt{\dfrac{J(J-1)}{2(2J+1)(J+1)}}\,\psi(^3\Pi^{\pm}_2)+\sqrt{\dfrac{J(J+2)}{(2J+1)(J+1)}}\,\psi(^3\Pi^{\pm}_1) \\
\qquad +\sqrt{\dfrac{J+2}{2(2J+1)}}\,\psi(^3\Pi^{\pm}_0) \approx \dfrac{1}{2}\psi(^3\Pi^{\pm}_2)+\dfrac{1}{\sqrt{2}}\psi(^3\Pi^{\pm}_1)+\dfrac{1}{2}\psi(^3\Pi^{\pm}_0), \\
\psi(^3\Pi^{\pm}_J) = -\sqrt{\dfrac{(J+2)(J-1)}{2(J+1)J}}\,\psi(^3\Pi^{\pm}_2)-\sqrt{\dfrac{1}{J(J+1)}}\,\psi(^3\Pi^{\pm}_1) \\
\qquad\qquad +\dfrac{1}{\sqrt{2}}\psi(^3\Pi^{\pm}_0) \approx -\dfrac{1}{\sqrt{2}}\psi(^3\Pi^{\pm}_2)+\dfrac{1}{\sqrt{2}}\psi(^3\Pi^{\pm}_0), \\
\psi(^3\Pi^{\pm}_{J-1}) = \sqrt{\dfrac{(J+1)(J+2)}{2(2J+1)J}}\,\psi(^3\Pi^{\pm}_2)-\sqrt{\dfrac{(J-1)(J+1)}{(2J+1)J}}\,\psi(^3\Pi^{\pm}_1) \\
\qquad +\sqrt{\dfrac{J-1}{2(2J+1)}}\,\psi(^3\Pi^{\pm}_0) \approx \dfrac{1}{2}\psi(^3\Pi^{\pm}_2)-\dfrac{1}{\sqrt{2}}\,\psi(^3\Pi^{\pm}_1)+\dfrac{1}{2}\psi(^3\Pi^{\pm}_0),
\end{cases}
$$

where the wave-functions of the left-hand side are characterized by the quantum number K as is usual in case (b). In those expressions, however, where the matrix elements between the terms of case (a) appear independent of the rotational quantum number J, the wave-functions of (8) should be taken in the simpler approximate form on the right-hand side.

The perturbation matrix elements appearing between individual terms can be easily computed with the aid of the wave-functions obtained above and the operator (1).

2. Perturbations $\Delta\Lambda = 0$

Primarily those cases will be dealt with where the terms perturbing each other belong to the same value of the resultant orbital angular momentum, viz. $\Delta\Lambda = 0$. In such perturbations only the first member of the operator (1) yields non-vanishing matrix elements.

(a) *Perturbation* $^1\Sigma$—$^3\Sigma$

It can easily be verified that between terms of the same symmetry in a first approximation there is no interaction (see Fig. 1), thus

$$(9)^2 \qquad H(^1\Sigma_J^{\pm}\ ^3\Sigma_{J+1}^{\pm}) = H(^1\Sigma_J^{\pm}\ ^3\Sigma_J^{\pm}) = H(^1\Sigma_J^{\pm}\ ^3\Sigma_{J-1}^{\pm}) = 0.$$

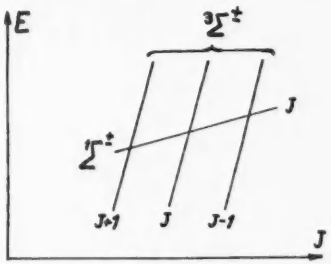

FIG. 1.

Between terms of different symmetry we find the following matrix elements (see Fig. 2):

$$(10) \quad \begin{cases} H(^3\Sigma_{J+1}^{\pm}\ ^1\Sigma_J^{\mp}) = -H(^3\Sigma_{J-1}^{\pm}\ ^1\Sigma_J^{\mp}) = \mp(i/2\sqrt{2})\lambda(a_p+a_q), \\ H(^3\Sigma_J^{\pm}\ ^1\Sigma_J^{\mp}) = 0. \end{cases}$$

The magnitude of the constants a_p and a_q will be dealt with later in the discussion of the selection rules. As is seen from (10), due to a $^1\Sigma^-$ (or $^1\Sigma^+$) state, perturbations of the same magnitude, and independent of J, will appear on the $K = J+1$ and $K = J-1$ components of the $^3\Sigma^+$ (or $^3\Sigma^-$) state. The order of magnitude of the perturbation might be corresponding to the values of the matrix elements appearing for heterogeneous perturbations of the same multiplicity.

[2]The perturbations discussed in this paper are everywhere of the first order of magnitude. Therefore in some cases it might happen that here between certain components no interaction exists in spite of results cited (Budó and Kovács 1938, 1939, 1950; Premaswarup 1954*a*, *b*). These interactions are, however, in every case only second-order effects.

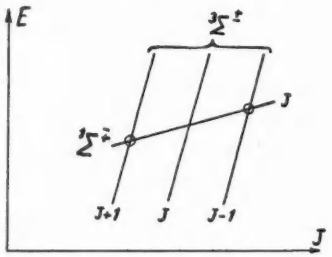

FIG. 2.

(*b*) *Perturbation* $^1\Pi$—$^3\Pi$

Owing to the fact that in several cases for a $^3\Pi$ state, at smaller rotational quantum numbers, Hund's case (*a*) is a better approximation whilst for higher quantum numbers Hund's case (*b*) is better, here both limiting cases are considered. As a matter of fact the best approximation would be obtained by an intermediate case; however, the formulae are fairly confused in this region.

(1) $^1\Pi$—$^3\Pi(a)$.—

$$(11)\quad H(^1\Pi_1^{\pm}\,{}^3\Pi_1^{\pm}) = -\tfrac{1}{2}[(\lambda'+1)a_q+\lambda' a_p], \qquad H(^1\Pi_1^{\pm}\,{}^3\Pi_2^{\pm}) = H(^1\Pi_1\,{}^3\Pi_0^{\pm}) = 0$$

(see Fig. 3).

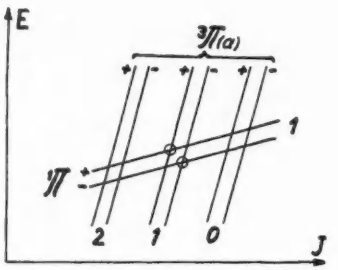

FIG. 3.

(2) $^1\Pi$—$^3\Pi(b)$.—

$$(12)\quad \begin{cases} H(^1\Pi_J^{\pm}\,{}^3\Pi_{J+1}^{\pm}) = -H(^1\Pi_J^{\pm}\,{}^3\Pi_{J-1}^{\pm}) = -(1/2\sqrt{2})[(\lambda'+1)a_q+\lambda' a_p], \\ H(^1\Pi_J^{\pm}\,{}^3\Pi_J^{\pm}) = 0 \end{cases}$$

(see Fig. 4).

(*c*) *Perturbation* $^1\Sigma$—$^1\Sigma^*$

In case of $^1\Sigma$ terms of the same symmetry (thus $^1\Sigma^{\pm}$—$^1\Sigma^{\pm *}$), operator (1) does not supply interaction matrix elements. The electrostatic interaction and certain terms omitted at the separation of the wave-equation do, however, give matrix elements independent of J, which sometimes might be very

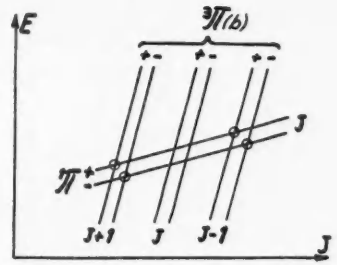

FIG. 4.

large (Gerö and Schmid 1943). Between terms of different symmetry, thus between $^1\Sigma^{\pm}$—$^1\Sigma^{\mp *}$, no interaction exists according to the aforesaid operators.

(*d*) *Perturbation* $^3\Sigma$—$^3\Sigma^*$

Between components of $^3\Sigma$ states of the same symmetry belonging to the same K the above-mentioned interactions similarly yield matrix elements independent of J, whilst owing to the operator (1) the perturbation between $\Delta K = 0, \pm 2$ components can be regarded as a second-order effect.

On the other hand between $^3\Sigma$ states of different symmetry (thus $^3\Sigma^{\pm}$—$^3\Sigma^{\mp}$) the operator (1) gives matrix elements of the first order of magnitude:

$$(13)\quad \begin{cases} H(^3\Sigma^{\pm}_{J+1}\,{}^3\Sigma^{\mp}_{J}) = H(^3\Sigma^{\pm}_{J}\,{}^3\Sigma^{\mp}_{J+1}) = H(^3\Sigma^{\pm}_{J}\,{}^3\Sigma^{\mp}_{J-1}) \\ \qquad\qquad = H(^3\Sigma^{\pm}_{J-1}\,{}^3\Sigma^{\mp}_{J}) = \pm(i/2\sqrt{2})\lambda(a_p - a_q) \end{cases}$$

(see Fig. 5), whilst the other matrix elements are zero.

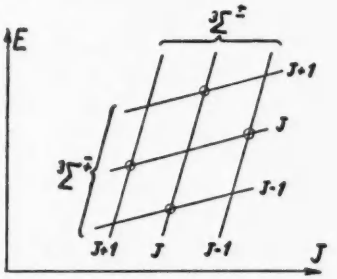

FIG. 5.

(*e*) *Perturbation* $^1\Pi$—$^1\Pi^*$

Operator (1) does not give matrix elements in this case, the perturbation being due only to the above-mentioned electrostatic interaction and to the terms omitted in the separation of the wave-equation. The matrix element is similarly independent of the rotational quantum number J.

(*f*) *Perturbation* $^3\Pi$—$^3\Pi^*$

Operator (1) and the above-mentioned operators give perturbations accord-

ing to the selection rule $\Delta\Omega = 0$ if both terms $^3\Pi$ belong to Hund's case (a), or according to $\Delta K = 0, \pm 1$ if both terms belong to case (b).

3. Selection Rules and the Values of the Constants a_p and a_q for Perturbations $\Delta\Lambda = 0$

The perturbations dealt with previously do not occur in each possible case, but only if certain selection rules are satisfied. Such a selection rule, according to which operator (1) yields interactions only between Σ states of different symmetry, has already been established. Other rules may be found by examining the expressions of the a_p and a_q constants occurring in each perturbation. Thus

$$(14)\quad \begin{cases} a_p = \int R^*_{n,v}(\rho) \int p^*_{n_{ip}, l_{ip}, \lambda_{ip}} a_i p_{n'_{ip}, l'_{ip}, \lambda_{ip}} d\tau_i \left(\int q^*_{n_{kq}, l_{kq}, \lambda_{kq}} q_{n'_{kq}, l'_{kq}, \lambda_{kq}} d\tau_k\right) \\ \qquad\qquad \times R_{n',v'}(\rho) d\rho, \\ a_q = \int R^*_{n,v}(\rho) \int q^*_{n_{kq}, l_{kq}, \lambda_{kq}} a_k q_{n'_{kq}, l'_{kq}, \lambda_{kq}} d\tau_k \left(\int p^*_{n_{ip}, l_{ip}, \lambda_{ip}} p_{n'_{ip}, l'_{ip}, \lambda_{ip}} d\tau_i\right) \\ \qquad\qquad \times R_{n',v'}(\rho) d\rho. \end{cases}$$

Those matrix elements from which these constants are derived, owing to the integrations carried out over the spin coordinates, are diagonal in σ_{ip} and σ_{kq}, thus $\Delta\sigma_{ip} = \Delta\sigma_{kq} = 0$; also these expressions, owing to the integration already carried out over φ_i and φ_k, are diagonal in λ_{ip} and λ_{kq}, hence $\Delta\lambda_{ip} = \Delta\lambda_{kq} = 0$. This means that even if every other selection rule were satisfied, perturbations can take place only between Σ terms belonging to the same electron configuration of the same λ; e.g. if both Σ states belong to the configurations (π, π) or (δ, δ) and so on. (Assuming a configuration (σ, σ) only $^1\Sigma^+$ and $^3\Sigma^+$ states will exist and according to the selection rules already mentioned no perturbation occurs between these.) In case of Π states, perturbations occur only if both Π terms belong to the configuration (σ, π) or (π, δ) or (π, σ) and so on.

Thus conclusions may be drawn concerning the electron configuration of the perturbing term from the occurrence or absence of the perturbations.

Taking into account some assumptions dealt with in detail in Section 5, further separations might be carried out and accordingly it can be readily seen that a_p and a_q have to be diagonal in l_{ip} and l_{kq}.

Finally owing to the orthogonality of the functions q and p, a_p has to be diagonal in n_{kq} and a_q has to be diagonal even in n_{ip}. This statement yields the result that the values of the bracketed integral in the expressions of a_p and a_q, owing to the normalization of the wave-functions, are unity.

According to the assumptions described in Section 5, the functions p and q as well as the coupling constant a do not depend on the internuclear distance ρ; hence (14) might be written simply in the following form:

$$(15)\quad \begin{cases} a_p = a(n_{ip}, n'_{ip}) \int R^*_{n,v}(\rho) R_{n',v'}(\rho) d\rho, \\ a_q = a(n_{kq}, n'_{kq}) \int R^*_{n,v}(\rho) R_{n',v'}(\rho) d\rho, \end{cases}$$

where

$$(15a)\quad \begin{aligned} a(n_{ip}, n'_{ip}) &= \int p^*_{n_{ip}, l_{ip}, \lambda_{ip}} a_i p_{n'_{ip}, l'_{ip}, \lambda_{ip}} d\tau_i, \\ a(n_{kq}, n'_{kq}) &= \int q^*_{n_{kq}, l_{kq}, \lambda_{kq}} a_k q_{n'_{kq}, l'_{kq}, \lambda_{kq}} d\tau_k \end{aligned}$$

and $i = 1, 2$, $k = 2, 1$.

If $\Delta n_{ip} \neq 0$, then according to (14) $a_q = 0$ and if at the same time $\Delta n_{kq} \neq 0$, then also $a_p = 0$. This means that in such cases no interaction at all exists between the two states since both constants vanish.

If one of the requirements $\Delta n_{ip} = 0$ and $\Delta n_{kq} = 0$ is satisfied one of the two constants differs from zero. In such cases the value of the remaining constant can only with difficulty be related to the multiplet splitting constants, which can be determined experimentally. Fortunately in general these states are energetically far from one another; therefore a perturbation with intersection between them will seldom occur.

For $\Delta n_{ip} = 0$ and at the same time $\Delta n_{kq} = 0$, viz. $\Delta n = 0$, the functions $p_{n_{ip}, l_{ip}, \lambda_{ip}}$, $p_{n'_{ip}, l'_{ip}, \lambda_{ip}}$, and $q_{n_{kq}, l_{kq}, \lambda_{kq}}$, $q_{n'_{kq}, l'_{kq}, \lambda_{kq}}$, which occur before and after a_i and a_k respectively in the wave-function of the two terms perturbing each other in equation (14), will also be the same. Under certain circumstances these constants can be related to the multiplet splitting constants $A_{^3\Pi}$ of the $^3\Pi$ term originating from the same electron configuration.

In case of equivalent electrons all of the quantum numbers n_{ip}, l_{ip}, λ_{ip} agree with the values n_{kq}, l_{kq}, λ_{kq} and the two electrons might differ only in the orientations of the λ's or σ's. In such cases evidently $p_{n_{ip}, l_{ip}, \lambda_{ip}} = q_{n_{iq}, l_{iq}, \lambda_{iq}}$ and $p_{n_{kp}, l_{kp}, \lambda_{kp}} = q_{n_{kq}, l_{kq}, \lambda_{kq}}$ and thus $a_p = a_q = a$. From the wave-functions (2) and (3) it follows at once that for a configuration λ^2 with $\lambda = 0$ only a term $^1\Sigma^+$ can exist, whilst with $\lambda \neq 0$ only the terms $^1\Sigma^+$, $^3\Sigma^-$, and $^1(2\lambda)$ can exist. In order to normalize the wave-functions occurring in equations (3) in the case of equivalent electrons they should be divided by $\sqrt{2}$. According to the present selection rules an interaction can only exist between $^1\Sigma^+$ and $^3\Sigma^-$ states belonging to the same configuration λ^2

$$H(^3\Sigma^-_{J+1}\ ^1\Sigma^+_J) = -H(^3\Sigma^-_{J-1}\ ^1\Sigma^+_J) = +(i/\sqrt{2})\lambda a. \tag{16}$$

If $\lambda_{kq} = \lambda_{ip} + 1$, but $n_{ip} = n_{kq}$ and $l_{ip} = l_{kq}$, then the above-mentioned equation will hold also in (5) and (6) so that in this case also $a_p = a_q = a$.

$$\begin{cases} H(^1\Pi^\pm_1\ ^3\Pi^\pm_1) = \tfrac{1}{2}(2\lambda+1)a \\ H(^1\Pi^\pm_J\ ^3\Pi^\pm_{J+1}) = -H(^1\Pi^\pm_J\ ^3\Pi^\pm_{J-1}) = -\dfrac{2\lambda+1}{2\sqrt{2}}\,a \end{cases} \tag{17}$$

Summing up the foregoing briefly, for $\Delta\Lambda \neq 0$ in Hund's case (a) the following holds:

$$H[(n_{ip}, l_{ip}, \lambda_{ip}, \sigma_{ip}; n_{kq}, l_{kq}, \lambda_{kq}, \sigma_{kq}; n, v, \Lambda, \Sigma); (n'_{ip}, l'_{ip}, \lambda'_{ip}, \sigma'_{ip}; n'_{kq}, l'_{kq}, \lambda'_{kq}, \sigma'_{kq}; n', v', \Lambda', \Sigma')] \neq 0 \tag{18}$$

for $\Delta n_{ip} = 0$ or $\Delta n_{kq} = 0$, $\Delta l_{ip} = \Delta l_{kq} = 0$, $\Delta\lambda_{ip} = \Delta\lambda_{kq} = 0$, $\Delta\sigma_{ip} = \Delta\sigma_{kq} = 0$, $\Delta\Lambda = \Delta\Sigma = 0$.

According to what has been said, in Hund's case (b) instead of the selection rule $\Delta\Sigma = 0$ the rule $\Delta K = \pm 1$ will hold.

4. Perturbations $\Delta\Lambda = \pm 1$

For $\Delta\Lambda = \pm 1$, the part inside of the angular brackets of operator (1) supplies the perturbation matrix elements. Here the following cases are possible:

(*a*) *Perturbation* $^1\Sigma$—$^3\Pi$

As above, for the two limiting cases of $^3\Pi$ states, perturbing matrix elements are also given here:

(1) $^1\Sigma^{\pm}$—$^3\Pi(a)$.—

$$H(^1\Sigma_0^{\pm}\ ^3\Pi_0^{\pm}) = (-i)^{\Sigma}|\xi|, \tag{19a}$$

where the exponent Σ is equal to 0 or 1, according to whether we are dealing with a $^1\Sigma^+$ or a $^1\Sigma^-$ state (see Fig. 6). The constant is expanded further in Section 5. Here it should be noted that the upper and lower signs on the Σ

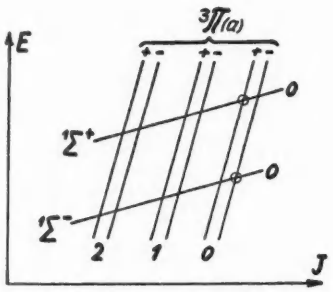

FIG. 6.

and Π symbols are to be taken in the same order and hence no interaction exists between $^1\Sigma_0^+$ and $^3\Pi_0^-$ states or between $^1\Sigma_0^-$ and $^3\Pi_0^+$ states.

(2) $^1\Sigma^{\pm}$—$^3\Pi(b)$.—

$$\begin{cases} H(^1\Sigma_J^{\pm}\ ^3\Pi_{J+1}^{\pm}) = H(^1\Sigma_J^{\pm}\ ^3\Pi_{J-1}^{\pm}) = \dfrac{(-i)^{\Sigma}}{2}|\xi|, \\ H(^1\Sigma_J^{\pm}\ ^3\Pi_J^{\pm}) = \dfrac{(-i)^{\Sigma}}{\sqrt{2}}|\xi| \end{cases} \tag{19b}$$

(see Fig. 7).

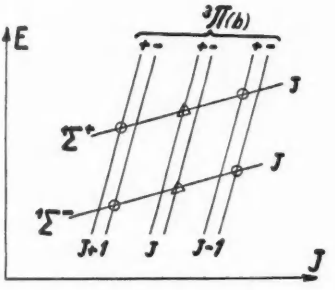

FIG. 7.

(*b*) *Perturbation* $^3\Sigma$—$^1\Pi$

$$\left.\begin{aligned} H(^3\Sigma^{\pm}_{J+1}\,{}^1\Pi^{\mp}_J) = H(^3\Sigma^{\pm}_{J-1}\,{}^1\Pi^{\mp}_J) &= \frac{(-i)^{\Sigma}}{2}\,|\xi|\,, \\ H(^3\Sigma^{\pm}_J\,{}^1\Pi^{\pm}_J) &= -\frac{(-i)^{\Sigma}}{\sqrt{2}}\,|\xi| \end{aligned}\right\} \tag{20}$$

(see Fig. 8).

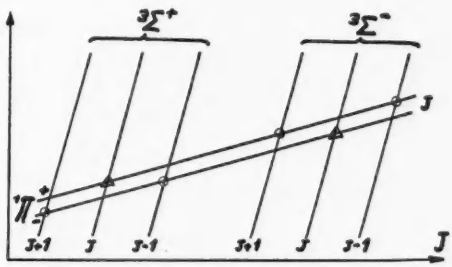

FIG. 8.

(*c*) *Perturbation* $^1\Sigma$—$^1\Pi$

Since this perturbation has been dealt with by several authors already, this case is now mentioned only for the sake of completeness. Operator (1) does not supply matrix elements but they are supplied only by the terms omitted at the separation of the wave-equation. It is known that these matrix elements are as follows:

$$H(^1\Sigma^{\pm}_0\,{}^1\Pi^{\pm}_1) = -(-i)^{\Sigma}2\eta\sqrt{2J(J+1)}\,. \tag{21}$$

The terms omitted at the separation of the wave-equation will supply matrix elements also for the case of the selection rules $\Delta\Omega = \pm 1$ or more explicitly in our case even for $\Delta\Lambda = \pm 1$ and $\Delta\Sigma = 0$, which depend to a large extent on the rotational quantum number J. A more detailed consideration of constant η occurring there will be given in Section 5.

(*d*) $^3\Sigma$—$^3\Pi$ *Perturbation*

Taking into account the interactions discussed above, then for a $^3\Sigma$—$^3\Pi$ perturbation, operator (1) as well as the terms omitted at the separation of the wave-equations will give perturbing matrix elements. Since in general the terms supplied by the two operators might be of the same order of magnitude, they should be taken into account simultaneously. In the earlier papers (Hebb 1936), operator (1) was more or less replaced by operator $A(\mathbf{L}.\mathbf{S})$. In the computation of terms diagonal in Λ and Σ these operators are equivalent but for non-diagonal elements (Λ, Σ; $\Lambda\pm1$, $\Sigma\mp1$); however, the two operators will give the same value of the matrix elements only if owing to the configuration neither of the two states perturbing each other will have intercombination interactions with other states. A decision as to the correct operator can easily be made. For intercombination, perturbations cannot be

interpreted by the interaction $A(\mathbf{L}.\mathbf{S})$ and since their occurrence has been observed experimentally it is evident that the behavior of a molecule may be described more exactly by operator (1) than by the operator $A(\mathbf{L}.\mathbf{S})$. Thus results supplied by operator (1) are to be accepted as correct.

(1) *Perturbation* $^3\Sigma$—$^3\Pi(a)$.—

$$
\begin{aligned}
H(^3\Sigma^{\pm}_{J+1}\,{}^3\Pi^{\mp}_{2}) &= (-i)^{\Sigma}2\sqrt{\frac{J}{2J+1}}\eta\,\sqrt{(J-1)(J+2)} \\
&\approx (-i)^{\Sigma}\eta\sqrt{2(J-1)(J+2)}\,, \\
H(^3\Sigma^{\pm}_{J+1}\,{}^3\Pi^{\mp}_{1}) &= (-i)^{\Sigma}\sqrt{2}\sqrt{\frac{J}{2J+1}}\,[\tfrac{1}{2}\xi+2\eta(J+2)] \\
&\approx (-i)^{\Sigma}[\tfrac{1}{2}\xi+2\eta(J+2)]\,, \\
H(^3\Sigma^{\pm}_{J+1}\,{}^3\Pi^{\mp}_{0}) &= (-i)^{\Sigma}\sqrt{\frac{J+1}{2J+1}}[\xi+2\eta(J+2)] \\
&\approx \frac{(-i)^{\Sigma}}{\sqrt{2}}[\xi+2\eta(J+2)]\,,
\end{aligned}
$$

(22)

$$
\begin{aligned}
H(^3\Sigma^{\pm}_{J}\,{}^3\Pi^{\pm}_{2}) &= -(-i)^{\Sigma}2\eta\sqrt{(J-1)(J+2)}\,, \\
H(^3\Sigma^{\pm}_{J}\,{}^3\Pi^{\pm}_{1}) &= -(-i)^{\Sigma}\sqrt{2}.(\tfrac{1}{2}\xi+2\eta), \\
H(^3\Sigma^{\pm}_{J}\,{}^3\Pi^{\pm}_{0}) &= (-i)^{\Sigma}2\eta\sqrt{J(J+1)}\,,
\end{aligned}
$$

$$
\begin{aligned}
H(^3\Sigma^{\pm}_{J-1}\,{}^3\Pi^{\mp}_{2}) &= (-i)^{\Sigma}2\sqrt{\frac{J+1}{2J+1}}\eta\,\sqrt{(J-1)(J+2)} \\
&\approx (-i)^{\Sigma}\eta\sqrt{2(J-1)(J+2)}, \\
H(^3\Sigma^{\pm}_{J-1}\,{}^3\Pi^{\mp}_{1}) &= (-i)^{\Sigma}\sqrt{2}.\sqrt{\frac{J+1}{2J+1}}\,[\tfrac{1}{2}\xi-2\eta(J-1)] \\
&\approx (-i)^{\Sigma}[\tfrac{1}{2}\xi-2\eta(J-1)], \\
H(^3\Sigma^{\pm}_{J-1}\,{}^3\Pi^{\mp}_{0}) &= -(-i)^{\Sigma}\sqrt{\frac{J}{2J+1}}\,[\xi-2\eta(J-1)] \\
&\approx -(-i)^{\Sigma}[\xi-2\eta(J-1)]\,.
\end{aligned}
$$

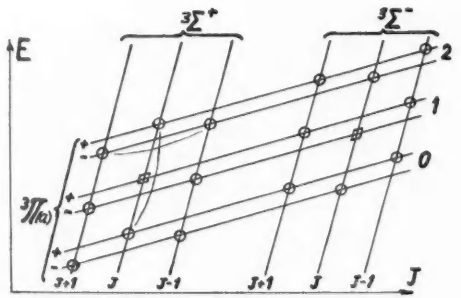

FIG. 9.

As can be seen from (22), here only a single matrix-element is independent of the rotational quantum number J, i.e. $H(^3\Sigma_J^+\ ^3\Pi_1^\pm)$. Of the others

$$H(^3\Sigma_{J+1}^\pm\ ^3\Pi_2^\mp) \text{ and } H(^3\Sigma_{J-1}^\pm\ ^3\Pi_2^\mp)$$

as well as $H(^3\Sigma_J^\pm\ ^3\Pi_2^\pm)$ and $H(^3\Sigma_J^\pm\ ^3\Pi_0^\pm)$ for the same J are approximately equal to one another and vary proportionately to J. (In Fig. 9, these are connected by a thin line.) Since one of the states, $^3\Sigma$, belongs to case (b) whilst the other, $^3\Pi$, to case (a), no selection rule exists and at each intersection perturbations will appear.

(2) *Perturbation* $^3\Sigma$—$^3\Pi(b)$.—

$$
\left|\begin{array}{l}
H(^3\Sigma_{J+1}^\pm\ ^3\Pi_{J+1}^\mp) = (-i)^\Sigma\sqrt{\dfrac{J+2}{2(J+1)}}\,[\xi+4\eta(J+1)] \\
\qquad\qquad\qquad\qquad \approx \dfrac{(-i)^\Sigma}{\sqrt{2}}[\xi+4\eta\sqrt{(J+1)(J+2)}] \\
H(^3\Sigma_{J+1}^\pm\ ^3\Pi_J^\mp) = (-i)^\Sigma\dfrac{J}{\sqrt{2(2J+1)(J+1)}}\,\xi \approx \dfrac{(-i)^\Sigma}{2}\,\xi \\
H(^3\Sigma_{J+1}^\pm\ ^3\Pi_{J-1}^\mp) = 0 \\
H(^3\Sigma_J^\pm\ ^3\Pi_{J+1}^\pm) = -(-i)^\Sigma\sqrt{\dfrac{J(J+2)}{2(2J+1)(J+1)}}\,\xi \approx -\dfrac{(-i)^\Sigma}{2}\,\xi \\
H(^3\Sigma_J^\pm\ ^3\Pi_J^\pm) = (-i)^\Sigma[\sqrt{2J(J+1)}\,2\eta+\dfrac{\xi}{\sqrt{2J(J+1)}} \\
\qquad\qquad\qquad\qquad \approx (-i)^\Sigma 2\eta\sqrt{2J(J+1)} \\
H(^3\Sigma_J^\pm\ ^3\Pi_{J-1}^\pm) = (-i)^\Sigma\sqrt{\dfrac{(J-1)(J+1)}{2(2J+1)J}}\,\xi \approx \dfrac{(-i)^\Sigma}{2}\,\xi \\
H(^3\Sigma_{J-1}^\pm\ ^3\Pi_{J+1}^\mp = 0 \\
H(^3\Sigma_{J-1}^\pm\ ^3\Pi_J^\mp) = -(-i)^\Sigma\dfrac{J+1}{\sqrt{2(2J+1)J}}\,\xi \approx -\dfrac{(-i)^\Sigma}{2}\,\xi \\
H(^3\Sigma_{J-1}^\pm\ ^3\Pi_{J-1}^\mp) = -(-i)^\Sigma\sqrt{\dfrac{J-1}{2J}}\,[\xi-4\eta J] \\
\qquad\qquad\qquad\qquad \approx -\dfrac{(-i)^\Sigma}{\sqrt{2}}\,[\xi-4\eta\sqrt{(J-1)J}]
\end{array}\right. \qquad (23)
$$

According to (23) matrix elements corresponding to $\Delta K = \pm 2$ are zero. Those corresponding to $\Delta K = \pm 1$ are constant and approximately equal to one another (in Fig. 10 these are connected by a thin line), whilst the elements corresponding to $\Delta K = 0$ depend to a large extent on J and are the largest ones.

This can be seen by noting that logically in the ideal case (a) $\eta = 0$, whilst in case (b) in (23) $\xi = 0$, since in (8) the coefficients of linear combinations

of the $^3\Pi$ wave-functions are calculated similarly in the two limiting cases. On the other hand, we are of the opinion that (22) and (23), in the forms given, will provide a better approximation to the ideal limiting cases, in case (*a*) for a small J and in case (*b*) for a large J.

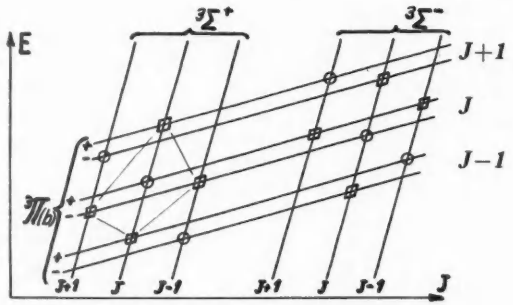

FIG. 10.

(3) *The Λ-type splitting of the* $^3\Pi$ *state in the limiting cases.*—As is well known, the Λ-type splittings observed in Π states are due to the perturbations by the more distant Σ states (Hebb 1936). According to what has been said in Sections (*a*) and (*d*) perturbations might be caused in $^3\Pi$ states by $^1\Sigma$ and $^3\Sigma$ states.[3] The $^1\Sigma^-$ and $^3\Sigma^+$ states on one side of the $^3\Pi$ state (energetically above or below it) and those $^1\Sigma^+$ and $^3\Sigma^-$ states lying on the other side of it will give rise to a shifting in the same direction. Taking into account all these interactions the following expression is obtained for the Λ-doubling:

$$h\Delta\nu(^3\Pi_i) = (-1)^{J+1} \sum_k \frac{|H(^3\Pi_i^+ \, \Sigma_k)|^2 - |H(^3\Pi_i^- \, \Sigma_k)|^2}{h\nu(^3\Pi_i \, \Sigma_k)}, \tag{24}$$

where $i = 2, 1, 0$ in Hund's case (*a*) and $i = J+1, J, J-1$ in Hund's case (*b*), whilst k is the index of the summation over each perturbing term $^1\Sigma^+$, $^1\Sigma^-$, $^3\Sigma^+$, $^3\Sigma^-$. On the basis of Sections (*a*) and (*d*) expressions can be given for both Hund's case (*a*) and case (*b*) coupling which hold rigorously not only for the two ideal limiting cases, but also hold well into the intermediate coupling range in their behavior with respect to variation with J.

These expressions, in case (*a*), are the following:

$$\begin{aligned} h\Delta\nu(^3\Pi_2) &= 0, \\ h\Delta\nu(^3\Pi_1) &= C_2 J(J+1), \\ h\Delta\nu(^3\Pi_0) &= C_0 + 2C_1 + 2C_2 \end{aligned} \tag{25}$$

[3]In case of two-electron systems $^3\Sigma$ terms do not exist.

and in the neighborhood of case (*b*),

$$(26)\qquad \begin{cases} h\Delta\nu(^3\Pi_{J+1}) = \frac{1}{2}C_0\frac{J+2}{2J+1} + C_1(J+2) + C_2(J+1)(J+2), \\ h\Delta\nu(^3\Pi_J) = \frac{1}{2}C_0 - C_1 - C_2J(J+1), \\ h\Delta\nu(^3\Pi_{J-1}) = \frac{1}{2}C_0\frac{J-1}{2J+1} - C_1(J-1) + C_2(J-1)J, \end{cases}$$

where

$$(26a)\qquad C_0 = \sum_k \frac{(-1)^\Sigma|\xi(^3\Pi\ ^3\Sigma_k)|^2}{h\nu(^3\Pi\ ^3\Sigma_k)} - \sum_k \frac{(-1)^\Sigma|\xi(^3\Pi\ ^1\Sigma_k)|^2}{h\nu(^3\Pi\ ^1\Sigma_k)},$$

$$C_1 = 4\sum_k \frac{(-1)^\Sigma|\xi(^3\Pi\ ^3\Sigma_k)\eta(^3\Pi\ ^3\Sigma_k)|}{h\nu(^3\Pi\ ^3\Sigma_k)}, \qquad C_2 = 8\sum_k \frac{(-1)^\Sigma|\eta(^3\Pi\ ^3\Sigma_k)|^2}{h\nu(^3\Pi\ ^3\Sigma_k)}.$$

From selection rules dealt with in Section 5, it can be seen over how many and what type of Σ terms the summation should be carried out.[4]

Concerning the application of (26) we note, for instance, that it gives a fairly good approximation for the Λ-doubling of the $B^3\Pi$ state of the N_2 molecule even for $J = 30$ (Hebb 1936) ($\Delta\nu(^3\Pi_{J+1}) = 0.98$ cm^{-1} instead of 1.18 cm^{-1}, $\Delta\nu(^3\Pi_J) = 0.89$ cm^{-1} instead of 0.86 cm^{-1}, $\Delta\nu(^3\Pi_{J-1}) = 0.65$ cm^{-1} instead of 0.48 cm^{-1}) in spite of the fact that at this quantum number the splitting term $h\Delta\nu = C_2K(K+1)$ (which is entirely valid in ideal case (*b*)) in (26) is much less important than the terms with coefficient C_0. For higher rotational quantum numbers the approximation is even better.

5. Selection Rules and the Values of the ξ and η Constants for Perturbations $\Delta\Lambda = \pm 1$

As before, a closer examination of the constants ξ and η leads to selection rules. The values of these constants are the following:

$$(27a)\quad \xi[(\lambda,\lambda)(\lambda\pm1,\lambda)] = \frac{1}{2\sqrt{2}}\int R^*_{n,v}(\rho)\int p^*_{n_{ip},l_{ip},\lambda}a_i[f_i+(1\pm\lambda)g_i] \times p_{n'_{ip},l'_{ip},\lambda\pm1}d\tau_i\int q^*_{n_{kq},l_{kq},\lambda}q_{n'_{kq},l_{kq},\lambda}d\tau_k R_{n',v'}(\rho)d\rho$$

or

$$(27b)\quad \xi[(\lambda,\lambda)(\lambda,\lambda\pm1)] = \frac{1}{2\sqrt{2}}\int R^*_{n,v}(\rho)\int q^*_{n_{kq},l_{kq},\lambda}a_k[f_k+(1\pm\lambda)g_k] \times q_{n'_{kq},l'_{kq},\lambda\pm1}d\tau_k\int p^*_{n_{ip},l_{ip},\lambda}p_{n'_{ip},l'_{ip},\lambda}d\tau_i R_{n',v'}(\rho)d\rho,$$

and two similar expressions for η except that the term $B = h^2/8\pi^2\mu\rho^2$ appears instead of a_i and a_k. This term does not depend on the integration coordinates τ_i and τ_k, but only on the internuclear distance ρ.

In the matrix elements where ξ given by (27*a*) occurs, since the integration is carried out over the spin coordinates, $\sigma'_{ip} = \sigma_{ip}\mp1$ and $\sigma'_{kq} = \sigma_{kq}$, while where ξ from (27*b*) occurs, $\sigma'_{ip} = \sigma_{ip}$ and $\sigma'_{kq} = \sigma_{kq}\mp1$, and finally in matrix

[4]For a more accurate discussion of C_0, the term arising from the spin–spin interaction should also be taken into consideration.

elements where η occurs, everywhere $\sigma'_{ip} = \sigma_{ip}$ and $\sigma'_{kq} = \sigma_{kq}$. In the integrations carried out previously over φ_i and φ_k a closer examination of the constants leads to the fact that their value differs from zero only if in (27*a*) and the corresponding expression of η, $\lambda'_{ip} = \lambda_{ip} \pm 1$ and $\lambda'_{kq} = \lambda_{kq}$ whilst in (27*b*) and the corresponding expression for η, $\lambda'_{ip} = \lambda_{ip}$ and $\lambda'_{kq} = \lambda_{kq} \pm 1$. Since in this investigation one of the terms is a Σ term, it follows that $|\lambda_{ip}| = |\lambda_{kq}| = \lambda \neq 0$. If $\lambda = 0$, then each constant has to be multiplied by $\sqrt{2}$. These selection rules expressed by the resultant orbital and spin quantum numbers of the molecule give the well-known selection rules, namely, for the ξ constant, $\Delta\Lambda = \pm 1$ and $\Delta\Sigma = \mp 1$, that is $\Delta\Omega = 0$, while for the η constant, $\Delta\Lambda = \pm 1$ and $\Delta\Sigma = 0$ (or $\Delta\Omega = \pm 1$).

Assuming a special model for the molecule, simple expressions for the constants ξ and η can be obtained. Considering the two nuclei of the molecule united in the mass center (the so-called united atom approximation) let us take this united nucleus as the center of the coordinate system. With this model the following equations will hold:

$$f_i = \hbar\, \partial/\partial\vartheta_i, \qquad g_i = \hbar \cot \vartheta_i, \tag{28}$$

where ϑ_i is the polar angle of the ith electron and where the orbital angular-momenta l_i and l_k of the two electrons are being referred to the origin. The wave-functions of the individual electrons might be thus written:

$$p_{n_{ip},\, l_{ip},\lambda_{ip}}(r_i, \vartheta_i) = L_{n_{ip},\, l_{ip}}(r_i)\Theta_{l_{ip},\lambda_{ip}}(\vartheta_i), \tag{29}$$

$$q_{n_{kq},\, l_{kq},\lambda_{kq}}(r_k, \vartheta_k) = L_{n_{kq},\, l_{kq}}(r_k)\Theta_{l_{kq},\lambda_{kq}}(\vartheta_k), \tag{30}$$

where the functions $\Theta_{l\lambda}(\vartheta)$ in which we are particularly interested are the terms of the derivatives of the Legendre polynomials. Using these, the expressions of ξ and η have the following form:

$$\xi[(\lambda, \lambda)(\lambda\pm 1, \lambda)] = (1/2\sqrt{2})[a(f+(1\pm\lambda)g)]_p \int R^*_{n,v}(\rho)R_{n',v'}(\rho)d\rho, \tag{31a}$$

$$\xi[(\lambda, \lambda)(\lambda, \lambda\pm 1)] = (1/2\sqrt{2})[a(f+(1\pm\lambda)g)]_q \int R^*_{n,v}(\rho)R_{n',v'}(\rho)d\rho, \tag{31b}$$

$$\eta[(\lambda, \lambda)(\lambda\pm 1, \lambda)] = (1/2\sqrt{2})[f+(1\pm\lambda)g]_p \int R^*_{n,v}(\rho)B(\rho)R_{n',v'}(\rho)d\rho, \tag{32a}$$

$$\eta[(\lambda, \lambda)(\lambda, \lambda\pm 1)] = (1/2\sqrt{2})[f+(1\pm\lambda)g]_q \int R^*_{n,v}(\rho)B(\rho)R_{n',v'}(\rho)d\rho. \tag{32b}$$

After integrating the orthogonal and normalized functions q and p for equations (31*a*) and (32*a*) values differing from zero will be obtained only if $\Delta n_{kq} = 0$ and $\Delta l_{kq} = 0$, respectively, and for equations (31*b*) and (32*b*) only if $\Delta n_{ip} = 0$ and $\Delta l_{ip} = 0$. Moreover:

$$[a(f+(1\pm\lambda)g)]_p = \int p^*_{n_{ip},\, l_{ip},\lambda}(r_i, \vartheta_i)a(r_i)[f_i+(1\pm\lambda)g_i] \times p_{n'_{ip},\, l'_{ip},\lambda\pm 1}(r_i, \vartheta_i)\sin\vartheta_i\, d\vartheta_i\, r_i^2 dr_i, \tag{33}$$

and a similar expression will also hold for $[a(f+(1\pm\lambda)g)]_q$. If we replace the values of p and q with those obtained from (30), we obtain the following (Condon and Shortley 1953):

$$[a(f+(1\pm\lambda)g)]_p = \mp a(n_{ip}, n'_{ip})\sqrt{l_p(l_p+1)-\lambda(\lambda\pm 1)}\,, \tag{34a}$$

$$[a(f+(1\pm\lambda)g)]_q = \mp a(n_{kq}, n'_{kq})\sqrt{l_q(l_q+1)-\lambda(\lambda\pm 1)}\,, \tag{34b}$$

where

$$a(n_{ip}, n'_{ip}) = \int L^*_{n_{ip}, l_{ip}}(r_i) a(r_i) L_{n'_{ip}, l'_{ip}}(r_i) r_i^2 dr_i \,, \tag{35a}$$

$$a(n_{kq}, n'_{kq}) = \int L^*_{n_{kq}, l_{kq}}(r_k) a(r_k) L_{n'_{kq}, l'_{kq}}(r_k) r_k^2 dr_k \,. \tag{35b}$$

Owing to the fact that the integrations are carried out over ϑ, further selection rules occur as follows: in (35*a*), (34*a*), (31*a*), and (32*a*), quite apart from what has been said previously, $\Delta l_{ip} = 0$ and further in (35*b*), (34*b*), (31*b*), and (32*b*), $\Delta l_{kq} = 0$.

If $\Delta n_{ip} \neq 0$ *and* $\Delta n_{kq} \neq 0$ hold simultaneously, then according to this model no interaction exists, since the expressions (31) and (32) are (owing to the orthogonality of the functions $L(r)$) zero. If $\Delta n_{ip} \neq 0$ and $\Delta n_{kq} = 0$, then expressions (31*b*) and (32*b*) are zero, while if $\Delta n_{ip} = 0$ and $\Delta n_{kq} \neq 0$ expressions (31*a*) and (32*a*) are zero. This means (assuming for instance that the Σ state belongs to a (π, π) configuration), in the first case, that the terms in question can interact only with Π states belonging to $(\delta\pi)$ and $(\sigma\pi)$ configurations whilst, in the second case only, they can interact only with Π states belonging to $(\pi\delta)$ and $(\pi\sigma)$ configurations.

For $\Delta n_{ip} = 0$ and $\Delta n_{kq} = 0$, i.e. $\Delta n = 0$, the expressions for ξ and η take the following forms:

$$\xi[(\lambda, \lambda)(\lambda \pm 1, \lambda)] = \mp \frac{1}{2\sqrt{2}} a_p \sqrt{l_p(l_p+1) - \lambda(\lambda \pm 1)} \,, \tag{36a}$$

$$\xi[(\lambda, \lambda)(\lambda, \lambda \pm 1)] = \mp \frac{1}{2\sqrt{2}} a_q \sqrt{l_q(l_q+1) - \lambda(\lambda \pm 1)} \,, \tag{36b}$$

$$\eta[(\lambda, \lambda)(\lambda \pm 1, \lambda)] = \mp \frac{1}{2\sqrt{2}} B_{\Sigma\Pi} \sqrt{l_p(l_p+1) - \lambda(\lambda \pm 1)} \,, \tag{37a}$$

$$\eta[(\lambda, \lambda)(\lambda, \lambda \pm 1)] = \mp \frac{1}{2\sqrt{2}} B_{\Sigma\Pi} \sqrt{l_q(l_q+1) - \lambda(\lambda \pm 1)} \,, \tag{37b}$$

where

$$\begin{cases} a_p &= a(n_{ip}, n_{ip}) \int R^*_{n,v}(\rho) R_{n',v'}(\rho) d\rho, \\ a_q &= a(n_{kq}, n_{kq}) \int R^*_{n,v}(\rho) R_{n',v'}(\rho) d\rho, \\ B_{\Sigma\Pi} &= \int R^*_{n,v}(\rho) B(\rho) R_{n',v'}(\rho) d\rho. \end{cases} \tag{38}$$

The constants a_p and a_q appearing here will have the same meaning as in (15) if there $n_{ip} = n'_{ip}$ and $n_{kq} = n'_{kq}$. Concerning the constant $B_{\Sigma\Pi}$, it can be said that it cannot be larger than the larger of the rotational constants of the Σ and Π states perturbing each other.

If the Σ states belong to equivalent electrons, then $a_p = a_q = 0$ and furthermore $l_p = l_q$ and thus the two expressions (*a*) and (*b*) for ξ and η are everywhere equal to one another. At the same time the constants should be multiplied by $\sqrt{2}$. This means for instance that for a Σ state belonging to a (π, π) configuration it makes no difference whether the perturbing Π state belongs to a (σ, π) or a (π, σ) configuration.

Summing up what has been said above, for $\Delta\Lambda = \pm 1$, then in Hund's

case (*a*) for the matrix elements given by operator (1) the following relation will hold (namely for those containing the constant ξ):

$$(39)\quad H[(n_{ip}, l_{ip}, \lambda_{ip}, \sigma_{ip}; n_{kq}, l_{kq}, \lambda_{kq}, \sigma_{kq}; n, v, \Lambda, \Sigma); (n'_{ip}, l'_{ip}, \lambda'_{ip}, \sigma'_{ip}; n'_{kq}, l'_{kq}, \lambda'_{kq}, \sigma'_{kq}; n', v', \Lambda', \Sigma')] \neq 0$$

for $\Delta n_{ip} = 0$ *or* $\Delta n_{kq} = 0$; furthermore $\Delta l_{ip} = \Delta l_{kq} = 0$, and at the same time either (1) $\Delta\lambda_{ip} = \pm 1$ and $\Delta\lambda_{kq} = 0$ or (2) $\Delta\lambda_{ip} = 0$ and $\Delta\lambda_{kq} = \pm 1$, viz. $\Delta\Lambda = \pm 1$ together with either (1) $\Delta\sigma_{ip} = \mp 1$ and $\Delta\sigma_{kq} = 0$ or (2) $\Delta\sigma_{ip} = 0$ and $\Delta\sigma_{kq} = \mp 1$ (i.e. $\Delta\Sigma = \mp 1$), then as in (18) the selection rule $\Delta\Omega = 0$ is also valid here.

In Hund's case (*b*) instead of selection rule $\Delta\Sigma = \mp 1$, $\Delta K = 0, \pm 1$ becomes valid.

For matrix elements depending on the rotational quantum number J which arise from the terms omitted at the separation of the wave-equation in Hund's case (*a*) (namely for those containing constant η) the same selection rules are valid, with the difference that in case (*a*) we always have $\Delta\sigma_{ip} = \Delta\sigma_{kq} = 0$, i.e. $\Delta\Sigma = 0$ and hence $\Delta\Omega = \pm 1$, whilst in Hund's case (*b*) instead of $\Delta\Sigma = 0$ the rule $\Delta K = \pm 1$ will be valid.

To summarize the above, we present a table (Table I) from which it can be readily seen which states belonging to what kind of electron configurations can interact with each other.

TABLE I

Electron configuration	Terms of molecules	Electron configuration
$\sigma\ \sigma$	$^1\Sigma^+$, $^3\Sigma^+$	$\sigma\ \sigma$
$\sigma\ \pi$	$^1\Pi$, $^3\Pi$	$\pi\ \sigma$
$\pi\ \pi$	$^1\Sigma^+$, $^3\Sigma^+$, $^1\Sigma^-$, $^3\Sigma^-$, $^1\Delta$, $^3\Delta$	$\pi\ \pi$
$\pi\ \delta$	$^1\Pi$, $^3\Pi$, $^1\phi$, $^3\phi$	$\delta\ \pi$
$\delta\ \delta$	$^1\Sigma^+$, $^3\Sigma^+$, $^1\Sigma^-$, $^3\Sigma^-$, $^1\Gamma$, $^3\Gamma$	$\delta\ \delta$

The operator (1), as well as those arising from the terms omitted at the separation of the wave-equation and depending on rotational coordinates, allows for perturbations only between such terms (if permitted by the other selection rules) as are to be found in the same or directly neighboring rows of Table I. The other rules are that $\Delta\Lambda = 0, \pm 1$ and between the Σ states the $+ \leftrightarrow -$ rules. No perturbations can appear between states belonging to different columns; thus for instance the Π states belonging to (σ, π) and (π, σ) configurations do not perturb one another, neither do those belonging to (π, δ) and (δ, π) and so on.

6. Relations between Matrix Elements and the Constants of Molecules

Calculating the diagonal elements of operators (1) and $A(\mathbf{L}.\mathbf{S})$ and equating them we obtain a relationship between the experimentally determinable multiplet splitting constant $A_{^3\Pi}$ of the term $^3\Pi$ and the constants a:

$$(40a)\qquad A_{^3\Pi} = \tfrac{1}{2}[(\lambda'+1)\bar{a}_p - \lambda'\bar{a}_q].$$

If apart from λ' the other quantum numbers of the two electrons agree, i.e. $\bar{a}_p = \bar{a}_q = a$, then:

$$A_{^3\Pi} = \tfrac{1}{2}a. \tag{40b}$$

Here the vibrational wave-functions play no roles, since the wave-functions of the same state occur on both sides of the operator.

Relations between $\bar{a}_p$ and a_p, and further between $\bar{a}_q$ and a_q, appearing in (40*a*) and (38) might be given for $\Delta n_{ip} = \Delta n_{kq} = 0$, that is if terms belonging to the same electron configurations are perturbing each other. In such cases the relation is supplied by (38) where $a(n_{ip}, n_{ip}) = \bar{a}_p$ and $a(n_{kq}, n_{kq}) = a_q$. In spite of the fact that in $R_{n,v}(\rho)$ and $R_{n,v'}(\rho)$ all the principal quantum number n of the electrons is the same, the two functions belong in general to two different sets of orthogonal functions. As a result, owing to the different values of the vibrational quantum numbers, the integral is in general not zero, but according to the magnitude of the "overlapping" region, it has some value less than unity.

If, however, the potential curves of the two states perturbing each other lie in such a manner that the vibrational wave-functions of the two interacting states have practically no overlapping regions (i.e. if the difference between equilibrium internuclear distances is very large) then the value of the above-mentioned integral will be very small and, between the two terms, no observable perturbation occurs, not even in a case where every selection rule is satisfied.

On the basis of what has been said, it can be stated that for the constants occurring in the matrix elements between the different components of two states perturbing each other the relations previously described will hold without question, and these perturbations might be compared with one another. On the other hand if two different perturbations are compared, for instance the ($^1\Sigma$ $^3\Sigma$) and ($^1\Pi$ $^3\Pi$) perturbations or the ($^1\Sigma$ $^3\Pi$) and ($^3\Sigma$ $^1\Pi$) perturbations, and if the constants appearing in these perturbations are to be expressed by the multiplet splitting constant (Budó and Kovács 1954), then, even if the electron part of the constants occurring in these is the same, it can be done only if the position of the potential curves is known and adequate values for the integrals of the vibrational wave-functions are taken into consideration.

The second part of the paper will deal with the perturbations between terms of even multiplicity in a three-electron system.

ACKNOWLEDGMENTS

I express my grateful thanks to Dr. A. E. Douglas, Ottawa, for having revised the translation and to Professor Budó, Szeged, for his valuable remarks made concerning the work.

REFERENCES

BUDÓ, A. and KOVÁCS, I. 1938. Z. Physik, **109**, 393.
——— 1939. Z. Physik, **111**, 633.
——— 1950. Acta Phys. Acad. Sci. Hung. **1**, 84.
——— 1954. Acta Phys. Acad. Sci. Hung. **4**, 273.
CONDON, E. U. and SHORTLEY, G. H. 1953. The theory of atomic spectra (Cambridge University Press), p. 53.

GERÖ, L. and SCHMID, R. 1943. Z. Physik, **121**, 459.
HEBB, M. H. 1936. Phys. Rev. **49**, 610.
HERZBERG, G. 1951. Molecular spectra and molecular structure, Vol. I, Spectra of diatomic molecules (D. van Nostrand Co., Inc., Princeton, N.J.), p. 335.
KOVÁCS, I. and LAGERQVIST, A. 1950. Arkiv Fysik, **2**, 411.
LAGERQVIST, A., NILHEDEN, G., and BARROW, R. F. 1952. Proc. Phys. Soc. A, **65**, 419.
NILHEDEN, G. 1955. Arkiv Fysik, **10**, 19.
PREMASWARUP, D. 1954*a*. Indian J. Phys. **28**, 256.
——— 1954*b*. Indian J. Phys. **28**, 581.
SCHMID, R. and GERÖ, L. 1935. Z. Physik, **93**, 656.

ON THE SPIN–ORBIT INTERACTION IN DIATOMIC MOLECULES. II[1]

I. Kovács

ABSTRACT

This paper deals with perturbations between states of even multiplicity in a three-electron system. With the aid of the matrix elements which have been obtained, a comparison of the perturbations in the various components of a given state and in some cases a comparison of perturbations in two different states is possible. Also for certain cases it has been possible to establish relationships between the matrix elements which give the magnitude of the perturbations and experimentally measurable molecular constants of the perturbed states.

The first part of this investigation (Kovács 1958) dealt with the various perturbations between states of odd multiplicity of a two-electron system taking into consideration the spin–orbit interactions. The present paper treats the perturbations between states of even multiplicity in a three-electron system.

1. EIGENFUNCTIONS

If the electrons of the molecule (with the exception of three) form closed shells, the states of the molecule can be characterized by the quantum numbers of the three electrons in question in the following manner: $(n_{ip}, l_{ip}, \lambda_{ip}, \sigma_{ip}; n_{kq}, l_{kq}, \lambda_{kq}, \sigma_{kq}; n_{lr}, l_{lr}, \lambda_{lr}, \sigma_{lr})$ or briefly: $(\lambda_p, \lambda_q, \lambda_r)$. The notations p, q, r signify that the ith electron is in a state denoted by p, the kth in a state denoted by q, and the lth in a state denoted by the index r, where (i, k, l) can take up every possible permutation of the indices 1, 2, 3. Since here we intend primarily to deal with interactions between the Σ and Π states, we will deal with only two of the many possible electron configurations, and the wave-functions of these two only will be considered. These will be $(\lambda, \lambda, \sigma)$ and $(\lambda', \lambda', \pi)$; this means in both cases $|\lambda_p| = |\lambda_q|$ and in the first case $\lambda_r = 0$, whilst in the second, $\lambda_r = 1$. As is well known in the case of a $(\lambda, \lambda, \sigma)$ configuration the following states are possible: $^2\Sigma^{\pm}$, $^2\Sigma^{*\pm}$, $^4\Sigma^{\pm}$, $^2(2\lambda)$, $^2(2\lambda)^*$, $^4(2\lambda)$, where for $\lambda = 0$ the Σ^- states are lacking whilst in the case $(\lambda', \lambda', \pi)$, the possible states are: $^2\Pi^{(1)}$, $^2\Pi^{*(1)}$, $^2\Pi^{(2)}$, $^2\Pi^{*(2)}$, $^2(2\lambda'-1)$, $^2(2\lambda'-1)^*$, $^4\Pi^{(1)}$, $^4\Pi^{(2)}$, $^4(2\lambda'-1)$, $^2(2\lambda'+1)$, $^2(2\lambda'+1)^*$, $^4(2\lambda'+1)$. If $\lambda = 0$ or $\lambda' = 0$ the terms 2λ or $2\lambda'-1$ and $2\lambda'+1$ states are not present whilst if $\lambda = 1, 2 \ldots$ the symbols (2λ) denote Δ, $\Gamma, \ldots$ states in case of $\lambda' = 1, 2 \ldots$, the symbols $(2\lambda'-1)$ denote Π, $\phi, \ldots$ states, and finally the symbols $(2\lambda'+1)$ denote the $\phi, \ldots$ states. The states designated by the sign * arise from the various possible orientations of the spin momenta of individual electrons, whilst the states distinguished by bracketed numbers above on the right-hand side arise

[1]Manuscript received September 17, 1957.
Contribution from the Department of Atomic Physics, Technical University, Budapest, Hungary.

from the different orientations of the λ's. It follows from the latter that for $\lambda = 0$ in case of a (σ, σ, π) configuration the $^2\Pi^{(1)}$ and $^2\Pi^{(2)}$ states as well as the further ones distinguished by $^{(1)}$ and $^{(2)}$ coincide; thus in such cases only $^2\Pi$, $^2\Pi^*$, and $^4\Pi$ states are present. If $\lambda' = 1$, altogether six $^2\Pi$ and three $^4\Pi$ states occur, since in such cases the configurations $(2\lambda'-1)$ give also Π states. In every other case four $^2\Pi$ and two $^4\Pi$ states occur.

The electronic part of the wave-functions of the Σ and Π states resulting from the above electron configurations can be given in Hund's case (*a*) according to the method described in I. For the $^2\Sigma^\pm$ states of the $(\lambda, \lambda, \sigma)$ configuration they will be

$$\begin{aligned}
\phi(^2\Sigma^\pm_{+\frac{1}{2}}) &= (1/\sqrt{6})\{\phi_1(^2\Sigma^\pm)(\alpha_1\beta_2-\beta_1\alpha_2)\alpha_3-\phi_2(^2\Sigma^\pm)(\alpha_1\beta_3-\beta_1\alpha_3)\alpha_2 \\
&\qquad +\phi_3(^2\Sigma^\pm)(\alpha_2\beta_3-\beta_2\alpha_3)\alpha_1\}, \qquad (1)\\
\phi(^2\Sigma^\pm_{-\frac{1}{2}}) &= (1/\sqrt{6})\{\phi_1(^2\Sigma^\pm)(\beta_1\alpha_2-\alpha_1\beta_2)\beta_3-\phi_2(^2\Sigma^\pm)(\beta_1\alpha_3-\alpha_1\beta_3)\beta_2 \\
&\qquad +\phi_3(^2\Sigma^\pm)(\beta_2\alpha_3-\alpha_2\beta_3)\beta_1\},
\end{aligned}$$

where

$$\begin{aligned}
\phi_1(^2\Sigma^\pm) &= (1/\sqrt{8\pi^3})\,[p_1q_2 \pm p_2q_1]r_3 \begin{matrix}\cos\\ \sin\end{matrix} \lambda(\varphi_1-\varphi_2), \\
\phi_2(^2\Sigma^\pm) &= (1/\sqrt{8\pi^3})\,[p_1q_3 \pm p_3q_1]r_2 \begin{matrix}\cos\\ \sin\end{matrix} \lambda(\varphi_1-\varphi_3), \qquad (1a)\\
\phi_3(^2\Sigma^\pm) &= (1/\sqrt{8\pi^3})\,[p_2q_3 \pm p_3q_2]r_1 \begin{matrix}\cos\\ \sin\end{matrix} \lambda(\varphi_2-\varphi_3),
\end{aligned}$$

and for $^2\Sigma^{*\pm}$ states

$$\begin{aligned}
\phi(^2\Sigma^{*\pm}_{+\frac{1}{2}}) &= (1/\sqrt{18})\{\phi_1(^2\Sigma^{*\pm})(\beta_1\alpha_2\alpha_3+\alpha_1\beta_2\alpha_3-2\alpha_1\alpha_2\beta_3) \\
&\qquad -\phi_2(^2\Sigma^{*\pm})(\beta_1\alpha_2\alpha_3-2\alpha_1\beta_2\alpha_3+\alpha_1\alpha_2\beta_3) \\
&\qquad +\phi_3(^2\Sigma^{*\pm})(-2\beta_1\alpha_2\alpha_3+\alpha_1\beta_2\alpha_3+\alpha_1\alpha_2\beta_3)\}, \qquad (2)\\
\phi(^2\Sigma^{*\pm}_{-\frac{1}{2}}) &= (1/\sqrt{18})\{\phi_1(^2\Sigma^{*\pm})(\alpha_1\beta_2\beta_3+\beta_1\alpha_2\beta_3-2\beta_1\beta_2\alpha_3) \\
&\qquad -\phi_2(^2\Sigma^{*\pm})(\alpha_1\beta_2\beta_3-2\beta_1\alpha_2\beta_3+\beta_1\beta_2\alpha_3) \\
&\qquad +\phi_3(^2\Sigma^{*\pm})(-2\alpha_1\beta_2\beta_3+\beta_1\alpha_2\beta_3+\beta_1\beta_2\alpha_3)\},
\end{aligned}$$

where all of the functions $\phi_1(^2\Sigma^{*\pm})$, $\phi_2(^2\Sigma^{*\pm})$, $\phi_3(^2\Sigma^{*\pm})$ correspond to the functions occurring in (1*a*) with the difference that the signs ∓ occurring there have to be changed to ∓ signs.

For the wave-functions of $^4\Sigma$ states we obtain

$$\begin{aligned}
\phi(^4\Sigma^\pm_{+3/2}) &= \phi(^4\Sigma^\pm)\alpha_1\alpha_2\alpha_3, \\
\phi(^4\Sigma^\pm_{+\frac{1}{2}}) &= (1/\sqrt{3})\phi(^4\Sigma^\pm)(\alpha_1\alpha_2\beta_3+\alpha_1\beta_2\alpha_3+\beta_1\alpha_2\alpha_3), \qquad (3)\\
\phi(^4\Sigma^\pm_{-\frac{1}{2}}) &= (1/\sqrt{3})\phi(^4\Sigma^\pm)(\alpha_1\beta_2\beta_3+\beta_1\alpha_2\beta_3+\beta_1\beta_2\alpha_3), \\
\phi(^4\Sigma^\pm_{-3/2}) &= \phi(^4\Sigma^\pm)\beta_1\beta_2\beta_3,
\end{aligned}$$

where

$$\phi(^4\Sigma^\pm) = (1/\sqrt{3})[\phi_1(^2\Sigma^{*\pm})-\phi_2(^2\Sigma^{*\pm})+\phi_3(^2\Sigma^{*\pm})]. \qquad (3a)$$

If $\lambda = 0$ in equation (1*a*) and (3*a*) the normalization factor will be $1/4\sqrt{\pi^3}$ instead of $1/\sqrt{8\pi^3}$ and in such cases only the expressions having the "cos" factor will differ from zero, i.e. the Σ^- states are lacking.

For the $^2\Pi^{(1)}$, $^2\Pi^{(2)}$, and $^2(2\lambda'-1)$ states of $(\lambda', \lambda', \pi)$ configuration the forms of the wave-functions formally correspond to those of functions (1) with the difference that in place of the expressions $\phi_1(^2\Sigma^\pm)$, $\phi_2(^2\Sigma^\pm)$, $\phi_3(^2\Sigma^\pm)$ for $^2\Pi_{+3/2}$ and $^2\Pi_{+\frac{1}{2}}$ states the functions $\phi_{i1}(^2\Pi^+)$, $\phi_{i2}(^2\Pi^+)$, $\phi_{i3}(^2\Pi^+)$ and for $^2\Pi'_{-\frac{1}{2}}$ and $^2\Pi'_{-3/2}$ states the functions $\phi_{i1}(^2\Pi^-)$, $\phi_{i2}(^2\Pi^-)$, $\phi_{i3}(^2\Pi^-)$ are to be written, where i can be equal to 1, 2, 3 corresponding to $^2\Pi^{(1)}$, $^2\Pi^{(2)}$, and $^2(2\lambda'-1)$ states. The form of the above-mentioned functions is the following:

$$
\begin{aligned}
\phi_{11}(^2\Pi^\pm) &= (1/4\sqrt{\pi^3})[p_2q_3e^{\pm i\lambda'(\varphi_2-\varphi_3)}+q_2p_3e^{\mp i\lambda'(\varphi_2-\varphi_3)}]r_1e^{\pm i\varphi_1},\\
\phi_{12}(^2\Pi^\pm) &= (1/4\sqrt{\pi^3})[p_1q_3e^{\pm i\lambda'(\varphi_1-\varphi_3)}+q_1p_3e^{\mp i\lambda'(\varphi_1-\varphi_3)}]r_2e^{\pm i\varphi_2},\\
\phi_{13}(^2\Pi^\pm) &= (1/4\sqrt{\pi^3})[p_1q_2e^{\pm i\lambda'(\varphi_1-\varphi_2)}+q_1p_2e^{\mp i\lambda'(\varphi_1-\varphi_2)}]r_3e^{\pm i\varphi_3}.
\end{aligned}
\tag{4a}
$$

The $\phi_{21}(^2\Pi^\pm)$, $\phi_{22}(^2\Pi^\pm)$, $\phi_{32}(^2\Pi^\pm)$ functions can be obtained from the foregoing if we write $-\lambda'$ instead of λ'. For a $(\lambda', \lambda', \pi)$ configuration the functions $i = 3$ will be the functions of the Π state for $\lambda' = 1$. Thus

$$
\begin{aligned}
\phi_{31}(^2\Pi^\pm) &= (1/4\sqrt{\pi^3})[p_2q_3+q_2p_3]r_1e^{\pm i(\varphi_2+\varphi_3-\varphi_1)},\\
\phi_{32}(^2\Pi^\pm) &= (1/4\sqrt{\pi^3})[p_1q_3+q_1p_3]r_2e^{\pm i(\varphi_1+\varphi_3-\varphi_2)},\\
\phi_{33}(^2\Pi^\pm) &= (1/4\sqrt{\pi^3})[p_1q_2+q_1p_2]r_3e^{\pm i(\varphi_1+\varphi_2-\varphi_3)}.
\end{aligned}
\tag{4b}
$$

The wave-functions of the $^2\Pi^{*(1)}$, $^2\Pi^{*(2)}$, and $^2(2\lambda'-1)^*$ states can be obtained from the formulae (2) if for $^2\Pi^*_{+3/2}$ and $^2\Pi^*_{+\frac{1}{2}}$ the functions $\phi_1(^2\Sigma^{*\pm})$, $\phi_2(^2\Sigma^{*\pm})$, $\phi_3(^2\Sigma^{*\pm})$ are replaced by $\phi_{i1}(^2\Pi^{*+})$, $\phi_{i2}(^2\Pi^{*+})$, $\phi_{i3}(^2\Pi^{*+})$ and for $^2\Pi^{*\prime}_{-\frac{1}{2}}$ and $^2\Pi^{*\prime}_{-3/2}$ by $\phi_{i1}(^2\Pi^{*-})$, $\phi_{i2}(^2\Pi^{*-})$, $\phi_{i3}(^2\Pi^{*-})$ functions where i can be 1, 2, 3 corresponding to the $^2\Pi^{*(1)}$, $^2\Pi^{*(2)}$, and $^2(2\lambda'-1)^*$ states. These latter functions can be obtained from (4a) and (4b) if we put within the bracket (but not in the exponent) the $-$ sign instead of a $+$ sign.

Finally the wave-functions of the $^4\Pi$ states obtained are from (3) if for $^4\Pi_{+5/2}$, $^4\Pi_{+3/2}$, $^4\Pi_{+\frac{1}{2}}$, $^4\Pi_{-\frac{1}{2}}$ the $\phi(^4\Sigma^\pm)$ functions are replaced by $\phi_i(^4\Pi^+)$ whilst for $^4\Pi'_{+\frac{1}{2}}$, $^4\Pi'_{-\frac{1}{2}}$, $^4\Pi'_{-3/2}$, $^4\Pi'_{-5/2}$ they are replaced by $\phi_i(^4\Pi^-)$ functions, where

$$
\phi_i(^4\Pi^\pm) = (1/\sqrt{3})[\phi_{i1}(^2\Pi^{*\pm})-\phi_{i2}(^2\Pi^{*\pm})+\phi_{i3}(^2\Pi^{*\pm})].
\tag{4c}
$$

Taking into account the two possible orientations of the resultant Ω relative to the axis of the molecule as well as the vibrations and rotations of the nuclei, the complete wave-functions for Hund's case (a) will be the following:

$$
\begin{aligned}
\psi(\Sigma^\pm_\Omega) &= (1/\sqrt{2})[\phi(\Sigma^\pm_{+\Omega})u_{J,+\Omega}+\phi(\Sigma^\pm_{-\Omega})u_{J,-\Omega}]R_{n,v},\\
\psi(\Sigma^\pm_\Omega)' &= (1/\sqrt{2})[\phi(\Sigma^\pm_{+\Omega})u_{J,+\Omega}-\phi(\Sigma^\pm_{-\Omega})u_{J,-\Omega}]R_{n,v},
\end{aligned}
\tag{5a}
$$

where for $^2\Sigma$ states Ω is equal to $1/2$ and for $^4\Sigma$ states it is equal to $3/2$ or $1/2$. Also

$$
\psi(\Pi^\pm_\Omega) = (1/\sqrt{2})[\phi(\Pi^+_{+\Omega})u_{J,+\Omega}\pm\phi(\Pi^-_{-\Omega})u_{J,-\Omega}]R_{n,v},
\tag{5b}
$$

where for $^2\Pi$ states Ω is equal to $3/2$, $1/2$ and for $^4\Pi$ states $5/2$, $3/2$, $1/2$, $-1/2$.

Further the eigenfunctions for Hund's case (b) are

$$
\begin{aligned}
\psi(^2\Sigma^\pm_{J+\frac{1}{2}}) &= \psi(^2\Sigma^\pm_{\frac{1}{2}})',\\
\psi(^2\Sigma^\pm_{J-\frac{1}{2}}) &= \psi(^2\Sigma^\pm_{\frac{1}{2}});
\end{aligned}
\tag{6a}
$$

$$
\begin{aligned}
\psi(^4\Sigma^{\pm}_{J+3/2}) &= -\frac{1}{2}\Big[\sqrt{\frac{J-\frac{1}{2}}{J+1}}\,\psi(^4\Sigma^{\pm}_{3/2}) + \sqrt{\frac{3(J+3/2)}{J+1}}\,\psi(^4\Sigma^{\pm}_{\frac{1}{2}})\Big] \\
&\approx -\tfrac{1}{2}\,\psi(^4\Sigma^{\pm}_{3/2}) - \tfrac{1}{2}\sqrt{3}\,\psi(^4\Sigma^{\pm}_{\frac{1}{2}}), \\
\psi(^4\Sigma^{\pm}_{J+\frac{1}{2}}) &= -\frac{1}{2}\Big[\sqrt{\frac{3(J-\frac{1}{2})}{J}}\,\psi(^4\Sigma^{\pm}_{3/2})' + \sqrt{\frac{J+3/2}{J}}\,\psi(^4\Sigma^{\pm}_{\frac{1}{2}})'\Big] \\
&\approx -\tfrac{1}{2}\sqrt{3}\,\psi(^4\Sigma^{\pm}_{3/2})' - \tfrac{1}{2}\psi(^4\Sigma^{\pm}_{\frac{1}{2}}), \\
\psi(^4\Sigma^{\pm}_{J-\frac{1}{2}}) &= -\frac{1}{2}\Big[\sqrt{\frac{3(J+3/2)}{J+1}}\,\psi(^4\Sigma^{\pm}_{3/2}) - \sqrt{\frac{J-\frac{1}{2}}{J+1}}\,\psi(^4\Sigma^{\pm}_{\frac{1}{2}})\Big] \\
&\approx -\tfrac{1}{2}\sqrt{3}\,\psi(^4\Sigma^{\pm}_{3/2}) + \tfrac{1}{2}\,\psi(^4\Sigma^{\pm}_{\frac{1}{2}}), \\
\psi(^4\Sigma^{\pm}_{J-3/2}) &= -\frac{1}{2}\Big[\sqrt{\frac{J+3/2}{J}}\,\psi(^4\Sigma^{\pm}_{3/2})' - \sqrt{\frac{3(J-1/2)}{J+1}}\,\psi(^4\Sigma^{\pm}_{\frac{1}{2}})'\Big] \\
&\approx -\tfrac{1}{2}\psi(^4\Sigma^{\pm}_{3/2})' + \tfrac{1}{2}\sqrt{3}\,\psi(^4\Sigma^{\pm}_{\frac{1}{2}})';
\end{aligned}
\tag{6b}
$$

$$
\begin{aligned}
\psi(^2\Pi^{\pm}_{J+\frac{1}{2}}) &= \sqrt{\frac{J-\frac{1}{2}}{2(J+\frac{1}{2})}}\,\psi(^2\Pi^{\pm}_{3/2}) - \sqrt{\frac{J+3/2}{2(J+\frac{1}{2})}}\,\psi(^2\Pi^{\pm}_{\frac{1}{2}}) \\
&\approx (1/\sqrt{2})\,[\psi(^2\Pi^{\pm}_{3/2}) - \psi(^2\Pi^{\pm}_{\frac{1}{2}})], \\
\psi(^2\Pi^{\pm}_{J-\frac{1}{2}}) &= \sqrt{\frac{J+3/2}{2(J+\frac{1}{2})}}\,\psi(^2\Pi^{\pm}_{3/2}) + \sqrt{\frac{J-\frac{1}{2}}{2(J+\frac{1}{2})}}\,\psi(^2\Pi^{\pm}_{\frac{1}{2}}) \\
&\approx (1/\sqrt{2})\,[\psi(^2\Pi^{\pm}_{3/2}) + \psi(^2\Pi^{\pm}_{\frac{1}{2}})];
\end{aligned}
\tag{6c}
$$

$$
\begin{aligned}
\psi(^4\Pi^{\pm}_{J+3/2}) &= -\frac{1}{\sqrt{8}}\Big[\sqrt{\frac{(J-3/2)(J-\frac{1}{2})}{(J+1)(J+3/2)}}\,\psi(^4\Pi^{\pm}_{5/2}) \\
&\quad + \sqrt{\frac{3(J-\frac{1}{2})(J+5/2)}{(J+1)(J+3/2)}}\,\psi(^4\Pi^{\pm}_{3/2}) + \sqrt{\frac{3(J+5/2)}{J+1}}\,\psi(^4\Pi^{\pm}_{\frac{1}{2}}) \\
&\quad + \sqrt{\frac{J+5/2}{J+1}}\,\psi(^4\Pi^{\pm}_{-\frac{1}{2}})\Big] \\
&\approx -1/\sqrt{8}[\psi(^4\Pi^{\pm}_{5/2}) + \sqrt{3}\psi(^4\Pi^{\pm}_{3/2}) + \sqrt{3}\psi(^4\Pi^{\pm}_{\frac{1}{2}}) + \psi(^4\Pi^{\pm}_{-\frac{1}{2}})], \\
\psi(^4\Pi^{\pm}_{J+\frac{1}{2}}) &= \frac{1}{\sqrt{8}}\Big[-\sqrt{\frac{3(J-3/2)(J-\frac{1}{2})(J+5/2)}{J(J+\frac{1}{2})(J+3/2)}}\,\psi(^4\Pi^{\pm}_{5/2}) \\
&\quad - \sqrt{\frac{(J+9/2)^2(J-\frac{1}{2})}{J(J+\frac{1}{2})(J+3/2)}}\,\psi(^4\Pi^{\pm}_{3/2}) + \sqrt{\frac{(J-3/2)^2}{J(J+\frac{1}{2})}}\,\psi(^4\Pi^{\pm}_{\frac{1}{2}}) \\
&\quad + \sqrt{\frac{3(J+\frac{1}{2})}{J}}\,\psi(^4\Pi^{\pm}_{-\frac{1}{2}})\Big] \approx \frac{1}{\sqrt{8}}\,[-\sqrt{3}\psi(^4\Pi^{\pm}_{5/2}) - \psi(^4\Pi^{\pm}_{3/2}) \\
&\quad + \psi(^4\Pi^{\pm}_{\frac{1}{2}}) + \sqrt{3}\,\psi(^4\Pi^{\pm}_{-\frac{1}{2}})], \\
\psi(^4\Pi^{\pm}_{J-\frac{1}{2}}) &= \frac{1}{\sqrt{8}}\Big[-\sqrt{\frac{3(J-3/2)(J+3/2)(J+5/2)}{(J+1)(J-\frac{1}{2})(J+\frac{1}{2})}}\,\psi(^4\Pi^{\pm}_{5/2}) \\
&\quad + \sqrt{\frac{(J-7/2)^2(J+3/2)}{(J+1)(J-\frac{1}{2})(J+\frac{1}{2})}}\,\psi(^4\Pi^{\pm}_{3/2}) + \sqrt{\frac{(J+5/2)^2}{(J+1)(J+\frac{1}{2})}}\,\psi(^4\Pi^{\pm}_{\frac{1}{2}}) \\
&\quad - \sqrt{\frac{3(J+\frac{1}{2})}{J+1}}\,\psi(^4\Pi^{\pm}_{-\frac{1}{2}})\Big] \approx \frac{1}{\sqrt{8}}[-\sqrt{3}\,\psi(^4\Pi^{\pm}_{5/2}) \\
&\quad + \psi(^4\Pi^{\pm}_{3/2}) + \psi(^4\Pi^{\pm}_{\frac{1}{2}}) - \sqrt{3}\,\psi(^4\Pi^{\pm}_{-\frac{1}{2}})],
\end{aligned}
\tag{6d}
$$

$$\psi(^4\Pi^{\pm}_{J-3/2}) = \frac{1}{\sqrt{8}}\Big[-\sqrt{\frac{(J+3/2)(J-5/2)}{J(J-\frac{3}{2})}}\,\psi(^4\Pi^{\pm}_{5/2}) + \sqrt{\frac{3(J-3/2)(J+3/2)}{J(J-\frac{1}{2})}}\,\psi(^4\Pi^{\pm}_{3/2}) - \sqrt{\frac{3(J-\frac{1}{2})}{J}}\,\psi(^4\Pi^{\pm}_{\frac{1}{2}}) + \sqrt{\frac{J-3/2}{J}}\,\psi(^4\Pi^{\pm}_{-\frac{1}{2}})\Big]$$

$$\approx \frac{1}{\sqrt{8}}[-\psi(^4\Pi^{\pm}_{5/2}) + \sqrt{3}\,\psi(^4\Pi^{\pm}_{3/2}) - \sqrt{3}\,\psi(^4\Pi^{\pm}_{\frac{1}{2}}) + \psi(^4\Pi^{\pm}_{-\frac{1}{2}})].$$

In case (a) and in case (b) the same formulae will hold for doublet states denoted by * except that on the right-hand side everywhere the eigenfunctions denoted by * are to be written. For the perturbations $\Delta\Lambda = 0$ it seems adequate in Hund's case (b) to use the simpler approximate formulae of the right-hand side.

Using the above wave-functions as well as the operator equation (1) of Part I some perturbation matrix elements can be computed.

2. PERTURBATIONS $\Delta\Lambda = 0$

For $\Delta\Lambda = 0$, i.e. in case of perturbations between Σ states or Π states, only the first term of operator I(1) supplies non-vanishing matrix elements.

(a) $^2\Sigma$—$^4\Sigma$ *Perturbation*

Between Σ states of the same symmetry but different multiplicity there is no perturbation (in other words at most only second-order effects can occur). Thus for each component in the first approximation we have

$$H(^2\Sigma^{\pm}\,{}^4\Sigma^{\pm}) = 0. \tag{7}$$

For Σ states of different symmetry a different matrix element applies according to whether the wave-functions (1) or (2) are used for the $^2\Sigma$ state. The following expressions are obtained for the non-vanishing matrix elements:

$$\sqrt{3}\,H(^2\Sigma^{\pm}_{J+\frac{1}{2}}\,{}^4\Sigma^{\mp}_{J+3/2}) = -H(^2\Sigma^{\pm}_{J+\frac{1}{2}}\,{}^4\Sigma^{\mp}_{J-\frac{1}{2}}) = H(^2\Sigma^{\pm}_{J-\frac{1}{2}}\,{}^4\Sigma^{\mp}_{J+\frac{1}{2}}) = -\sqrt{3}\,H(^2\Sigma^{\pm}_{J-\frac{1}{2}}\,{}^4\Sigma^{\mp}_{J-3/2}) = \pm\tfrac{1}{2}i\sqrt{3/2}\,\tau, \tag{8}$$

where in case of wave-functions (1),

$$\tau(^2\Sigma^{\pm}\,{}^4\Sigma^{\mp}) = \lambda(a_p + a_q), \tag{9a}$$

whilst in case of wave-functions (2),

$$\tau(^2\Sigma^{*\pm}\,{}^4\Sigma^{\mp}) = (1/\sqrt{3})\,\lambda(a_p - a_q) \tag{9b}$$

(see Fig. 1). The a_p and a_q constants have similar meaning as in Part I and they will be dealt with later in the discussion of the selection rules. Since both states belong to Hund's case (b), the matrix elements connecting levels that violate the selection rule $\Delta K = \pm 1$ are zero.

(b) $^2\Sigma$—$^2\Sigma'$ *Perturbation*

Between $^2\Sigma$ states of the same symmetry the electrostatic interaction and certain terms neglected at the separation of the wave equation supply a matrix element independent of the rotational quantum number J according to the selection rule $\Delta K = 0$.

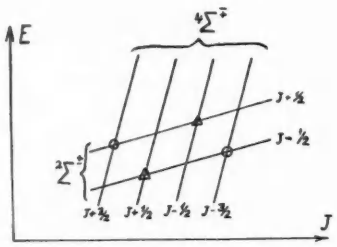

FIG. 1.

Between $^2\Sigma$ states of different symmetry the operator I(1) gives matrix elements of first order of magnitude; these are

$$H(^2\Sigma^{\pm}_{J+\frac{1}{2}}\ {}^2\Sigma'^{\mp}_{J-\frac{1}{2}}) = H(^2\Sigma^{\pm}_{J-\frac{1}{2}}\ {}^2\Sigma'^{\mp}_{J+\frac{1}{2}}) = \mp(i/2\sqrt{3})\tau \tag{10}$$

(see Fig. 2), where, according to whether we use the wave-functions (1) and (2) for a $(\lambda, \lambda, \sigma)$ configuration, the value of τ will be

$$\begin{aligned} &\tau(^2\Sigma^{\pm}\ {}^2\Sigma^{\mp}) = 0, \qquad \tau(^2\Sigma^{\pm}\ {}^2\Sigma^{*\mp}) = \lambda(a_p+a_q), \\ &\qquad\qquad \tau(^2\Sigma^{*\pm}\ {}^2\Sigma^{*\mp}) = (1/\sqrt{3})\lambda(a_p-a_q). \end{aligned} \tag{11}$$

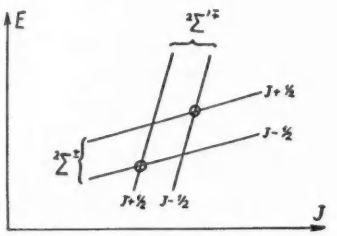

FIG. 2.

Hence the $^2\Sigma^+$ or $^2\Sigma^-$ states corresponding to the wave-functions (1) can perturb only the $^2\Sigma^{*-}$ or $^2\Sigma^{*+}$ states corresponding to the wave-function (2), whilst $^2\Sigma^{*+}$ or $^2\Sigma^{*-}$ states can interact with each other as well as with $^2\Sigma^-$ or $^2\Sigma^+$ states. The selection rule $\Delta K = \pm 1$ holds throughout. The selection rule relative to the Σ states belonging to electron configurations of different λ's will be dealt with in the following section.

(c) $^4\Sigma$—$^4\Sigma'$ *Perturbation*

Between $^4\Sigma$ states of the same symmetry the perturbation terms previously mentioned in case of $^2\Sigma$ states give matrix elements independent of the rotational quantum number J according to the selection rules $\Delta K = 0$. Between components with $\Delta K = \pm 2$ only second-order effects occur.

For different symmetries I(1) gives the following matrix elements:

$$2H(^4\Sigma^{\pm}_{J+3/2}\ {}^4\Sigma^{\mp}_{J+\frac{1}{2}}) = \sqrt{3}\,H(^4\Sigma^{\pm}_{J+\frac{1}{2}}\ {}^4\Sigma^{\mp}_{J-\frac{1}{2}}) = 2H(^4\Sigma^{\pm}_{J-\frac{1}{2}}\ {}^4\Sigma^{\mp}_{J-3/2}) = \pm i\tau \tag{12}$$

(see Fig. 3), where

$$\tau(^4\Sigma^+, {}^4\Sigma^-) = (1/\sqrt{3})\lambda(a_p - a_q). \tag{13}$$

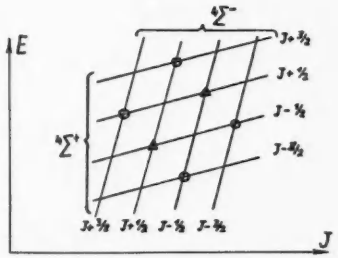

FIG. 3.

In Fig. 3 perturbations of the same magnitude are denoted by the same sign. Within the selection rule $\Delta K = \pm 1$ the operator I(1) allows for an interaction only between $^4\Sigma^+$ and $^4\Sigma^-$ states belonging to the $(\lambda, \lambda, \sigma)$ configuration of the same λ.

(*d*) $^2\Pi$—$^4\Pi$ *Perturbation*

Here various cases must be distinguished, on the one hand owing to the different $^2\Pi$ and $^4\Pi$ wave-functions belonging to the $(\lambda', \lambda', \pi)$ configuration, and on the other hand owing to the fact that $^2\Pi$ and $^4\Pi$ states can occur in either Hund's case (*a*) or (*b*). Therefore the perturbations are first investigated in general according to the various Hund's limiting cases, and later expressions of the matrix elements are given for special cases.

(1) $^2\Pi(a)$—$^4\Pi(a)$ *perturbation.*—In this case for both the $^2\Pi(a)$ state and the $^4\Pi(a)$ state the wave-functions (5*b*) must be used. Thus we obtain:

$$H(^2\Pi^{\pm}_{3/2}\ {}^4\Pi^{\pm}_{3/2}) = -H(^2\Pi^{\pm}_{\frac{1}{2}}\ {}^4\Pi^{\pm}_{\frac{1}{2}}) = (1/\sqrt{6})\,\tau \tag{14}$$

(see Fig. 4). For these perturbations the selection rule $\Delta\Omega = 0$ is characteristic since both states contributing to the perturbations belong to Hund's case (*a*).

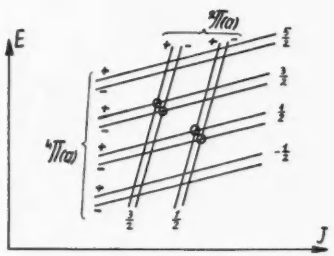

FIG. 4.

(2) $^2\Pi(b)$—$^4\Pi(a)$ *perturbation.*—In this case using the simplified form of the wave-function (6*c*) for $^2\Pi(b)$ states and the wave-functions (5*b*) for the $^4\Pi(a)$ states we obtain (see Fig. 5):

$$(15)\quad H(^2\Pi^{\pm}_{J+\frac{1}{2}}\,{}^4\Pi^{\pm}_{3/2}) = H(^2\Pi^{\pm}_{J+\frac{1}{2}}\,{}^4\Pi^{\pm}_{\frac{1}{2}}) = H(^2\Pi^{\pm}_{J-\frac{1}{2}}\,{}^4\Pi^{\pm}_{3/2}) = -H(^2\Pi^{\pm}_{J-\frac{1}{2}}\,{}^4\Pi^{\pm}_{\frac{1}{2}}) = (1/2\sqrt{3})\tau.$$

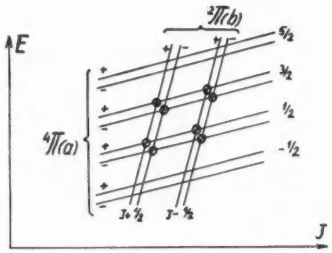

FIG. 5.

(3) $^2\Pi(a)$—$^4\Pi(b)$ *perturbation.*—Here we take the wave-functions (5*b*) for the $^2\Pi(a)$ states and the simplified form of (6*d*) for the $^4\Pi(b)$ states (see Fig. 6):

$$(16)\quad H(^2\Pi^{\pm}_{3/2}\,{}^4\Pi^{\pm}_{J+3/2}) = \sqrt{3}\,H(^2\Pi^{\pm}_{3/2}\,{}^4\Pi^{\pm}_{J+\frac{1}{2}}) = -\sqrt{3}\,H(^2\Pi^{\pm}_{3/2}\,{}^4\Pi^{\pm}_{J-\frac{1}{2}}) = -H(^2\Pi^{\pm}_{3/2}\,{}^4\Pi^{\pm}_{J-3/2}) = H(^2\Pi^{\pm}_{\frac{1}{2}}\,{}^4\Pi^{\pm}_{J+3/2}) = -\sqrt{3}\,H(^2\Pi^{\pm}_{\frac{1}{2}}\,{}^4\Pi^{\pm}_{J+\frac{1}{2}}) = -\sqrt{3}\,H(^2\Pi^{\pm}_{\frac{1}{2}}\,{}^4\Pi^{\pm}_{J-\frac{1}{2}}) = H(^2\Pi^{\pm}_{\frac{1}{2}}\,{}^4\Pi^{\pm}_{J-3/2}) = -\tfrac{1}{4}\tau.$$

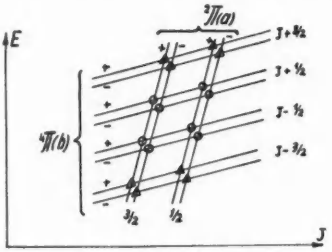

FIG. 6.

(4) $^2\Pi(b)$—$^4\Pi(b)$ *perturbation.*—Here we use the wave-functions (6*c*) for the $^2\Pi(b)$ states whilst the simplified form of the wave-functions (6*d*) is used for the $^4\Pi(b)$ state and we obtain (see Fig. 7):

$$(17)\quad H(^2\Pi^{\pm}_{J+\frac{1}{2}}\,{}^4\Pi^{\pm}_{J+3/2}) = -\sqrt{3}\,H(^2\Pi^{\pm}_{J+\frac{1}{2}}\,{}^4\Pi^{\pm}_{J-\frac{1}{2}}) = \sqrt{3}\,H(^2\Pi^{\pm}_{J-\frac{1}{2}}\,{}^4\Pi^{\pm}_{J+\frac{1}{2}}) = -H(^2\Pi^{\pm}_{J-\frac{1}{2}}\,{}^4\Pi^{\pm}_{J-3/2}) = -(1/2\sqrt{2})\tau.$$

Since in this case both states belong to Hund's case (*b*) the selection rule $\Delta K = \pm 1$ will hold.

It may be noted if the $^4\Pi$ state belongs to Hund's case (a) only the two middle components will be perturbed, while if the $^4\Pi$ state belongs to Hund's

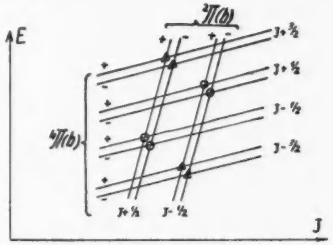

FIG. 7.

case (b) the two middle and the two extreme components will suffer *different* perturbations. Consequently if the $^2\Pi$ state does not intersect the $^4\Pi$ state, the two middle components will be continuously displaced relative to the two extreme components. On account of this displacement the $^4\Pi$ term formula will not be exactly valid. This is the case for the $^4\Pi$ state of the O_2^+ molecule (Budó and Kovács 1954).

(5) *The value of the τ constant in different cases.*—As we have seen for the $(\lambda', \lambda', \pi)$ configuration, four $^2\Pi$ and two $^4\Pi$ states and for $\lambda' = 1$, six $^2\Pi$ and three $^4\Pi$ states arise. Not all of these $^2\Pi$ and $^4\Pi$ states interact with every other one. One can see that

$$\tau(^2\Pi^{(i)}, {}^4\Pi^{(k)}) = \tau(^2\Pi^{*(i)}, {}^4\Pi^{(k)}) = 0 \tag{18}$$

unless $i = k$. This means that in several cases even between $^2\Pi$ and $^4\Pi$ states belonging to the same electron configuration no perturbations will exist. When $i = k$, the value of τ can be different for the various interactions:

$$\begin{aligned} \tau(^2\Pi^{(1)}, {}^4\Pi^{(1)}) &= -\tau(^2\Pi^{(2)}, {}^4\Pi^{(2)}) = \lambda'(a_p+a_q), \\ \tau(^2\Pi^{*(1)}, {}^4\Pi^{(1)}) &= (1/\sqrt{3})[2a_r-\lambda'(a_p-a_q)], \\ \tau(^2\Pi^{*(2)}, {}^4\Pi^{(2)}) &= (1/\sqrt{3})[2a_r+\lambda'(a_p-a_q)], \end{aligned} \tag{19a}$$

whilst for $\lambda' = 1$, the following is added to these:

$$\tau(^2\Pi^{(3)}, {}^4\Pi^{(3)}) = a_p-a_q, \qquad \tau(^2\Pi^{*(3)}, {}^4\Pi^{(3)}) = -(1/\sqrt{3})[2a_r+a_p+a_q], \tag{19b}$$

where the meaning of a_r is analogous to the values of a_p and a_q and its detailed form will be given in the next section.

(*e*) $^2\Pi$—$^2\Pi'$ *and* $^4\Pi$—$^4\Pi'$ *Perturbations*

For $^2\Pi$—$^2\Pi'$ and $^4\Pi$—$^4\Pi'$ perturbations if both states belong to Hund's case (a), the electrostatic interaction and the terms neglected at the separation of the wave equation as well as the operator $I(1)$ give matrix elements independent of the rotational quantum number according to the selection rule $\Delta\Omega = 0$. If both states belong to Hund's case (b) then in the matrix elements

corresponding to the selection rule $\Delta K = 0$, terms occur that are independent of J and have values determined by the electrostatic interaction and the certain terms neglected at the separation of the wave equation, whilst the perturbations between the components $\Delta K = \pm 1$ are given by the elements of operator I(1).

3. THE VALUES OF THE CONSTANTS a_p, a_q, AND a_r AND THE SELECTION RULES FOR PERTURBATIONS $\Delta\Lambda = 0$

In addition to the selection rules already mentioned, by a more detailed consideration of the constants further selection rules can be obtained. The constants a are given by

$$(21)\quad a_r = \int R^*_{n,v}(\rho) \int r^*_{n_{lr},l_{lr},\lambda_{lr}} a_l\, r_{n'_{lr},l'_{lr},\lambda_{lr}} d\tau_l \int p^*_{n_{ip},l_{ip},\lambda} p_{n'_{ip},l'_{ip},\lambda} d\tau_i \times \int q^*_{n_{kq},l_{kq},\lambda} q_{n'_{kq},l'_{kq},\lambda} d\tau_k\, R_{n',v'}(\rho) d\rho,$$

while for a_p and a_q the expressions I(14) will hold if the integral

$$\int r^*_{n_{lr},l_{lr},\lambda_{lr}}\, r_{n'_{lr},l'_{lr},\lambda_{lr}}\, d\tau_l$$

is added. These expressions, similar to the previous ones, are diagonal in λ and according to the assumptions of Section 1.5 are diagonal in l as well; hence $\Delta\lambda = \Delta\lambda_{lr} = 0$, $\Delta l_{ip} = \Delta l_{kq} = \Delta l_{lr} = 0$. This means that in this case also an interaction can occur only between Σ states belonging to the same $(\lambda, \lambda, \sigma)$ configuration and between π states belonging to the same $(\lambda', \lambda', \pi)$ configuration. Thus a large number of the possible perturbations is excluded.

According to the previous assumptions the expressions for a_r, a_p, a_q can be written in an even simpler form:

$$(22)\quad \begin{aligned} a_p &= a(n_{ip}, n'_{ip}) \int R^*_{n,v}\, R_{n',v'} d\rho, \\ a_q &= a(n_{kq}, n'_{kq}) \int R^*_{n,v}\, R_{n',v'} d\rho, \\ a_r &= a(n_{lr}, n'_{lr}) \int R^*_{n,v}\, R_{n',v'} d\rho, \end{aligned}$$

where each constant is diagonal in the other two principal quantum numbers not written out.

More explicitly, the situation with regard to the principal quantum numbers is the following: If two states are examined in which the principal quantum numbers of all the three electrons or only of two electrons differ, then each of the constants a_p, a_q, and a_r will be zero and between such states operator I(1) does not give rise to perturbations. If two states differ only in the principal quantum numbers of one electron, two cases are possible: (1) $\Delta n_{lr} \neq 0$ and $\Delta n_{ip} = \Delta n_{kq} = 0$ and thus $a_r \neq 0$, $a_p = a_q = 0$. In this case operator I(1) supplies no perturbing matrix elements between Σ states, because in these only the constants a_p and a_q occur. (2) $\Delta n_{lr} = 0$ and $\Delta n_{ip} = 0$, $\Delta n_{kq} \neq 0$ or $\Delta n_{ip} \neq 0$, $\Delta n_{kq} = 0$, thus $a_r = 0$ and moreover $a_p = 0$, $a_q \neq 0$ or $a_p \neq 0$, $a_q = 0$. In such cases every perturbation dealt with until now is possible, with the restriction that in the matrix elements one of the constants is always zero. Finally if the principal quantum numbers of all the three electrons are equal in the two states, i.e. if the states belong to the same electron configuration, we have $\Delta n_{ip} = \Delta n_{kq} = \Delta n_{lr} = 0$, and therefore $a_p \neq 0$, $a_q \neq 0$,

$a_r \neq 0$, hence the relations given in the previous sections are fully valid. Only in this case can a relationship be established between the matrix elements and the multiplet splitting constants $A_{^2\Pi}$ and $A_{^4\Pi}$. For a (σ, σ, σ) configuration only $^2\Sigma^+$, $^2\Sigma^{*+}$, $^4\Sigma^+$ states are possible. According to operator I(1) these Σ states cannot interact, since in such a configuration no Σ^- state exists.

If in a $(\lambda, \lambda, \sigma)$ configuration with $\lambda \neq 0$ two electrons are equivalent, only $^2\Sigma^+$, $^2\Sigma^{*-}$, $^4\Sigma^-$ states exist. Among these, according to (1), (2), and (3), states of different symmetry can interact and in this case $a_p = a_q$. A perturbation can also occur between the above states and states belonging to another $(\lambda, \lambda, \sigma)$ configuration which differ from the previous ones only in that $\Delta n_{ip} \neq 0$ or $\Delta n_{kq} \neq 0$, whereas if $\Delta n_{lr} \neq 0$, then $a_p = a_q = 0$ and each matrix element would be zero.

If $\lambda = 0$ and the two σ electrons are equivalent, then only one $^2\Sigma^+$ state arises and according to I(1) this state cannot interact with other Σ states.

If in a $(\lambda', \lambda', \pi)$ configuration the two electrons are equivalent, only one $^2\Pi$, one $^2\Pi^*$, and one $^4\Pi$ state arise assuming that $\lambda' > 1$. For $\lambda' = 1$ a further $^2\Pi^{(3)}$ state is added to these, whilst for $\lambda' = 0$, only one $^2\Pi$ state exists.

Between states of the same configuration and $\lambda' > 1$ the perturbations dealt with previously are possible with the variation that everywhere $a_p = a_q$. In the case of perturbations between states of different configurations if the principal quantum number of the Π electron varies, i.e. if $\Delta n_{lr} \neq 0$, and therefore $a_p = a_q = 0$, an intercombination perturbation can occur only between $^2\Pi^*$ (but not $^2\Pi$) and $^4\Pi$ states. If only the principal quantum number of one of the λ' electrons differs, i.e. $\Delta n_{ip} \neq 0$, or $\Delta n_{kq} \neq 0$, and therefore $a_r = a_q = 0$ or $a_r = a_p = 0$, each of the perturbations which have been dealt with can occur but two constants are always zero. Since for $\lambda' = 0$ there is only one $^2\Pi$ state, this state cannot interact with any $^4\Pi$ state.

Summarizing what has been said before for $\Delta\Lambda = 0$ in Hund's case (a) operator I(1) gives matrix elements:

$$(23)\quad H[(n_{ip}, l_{ip}, \lambda_{ip}, \sigma_{ip}; n_{kq}, l_{kq}, \lambda_{kq}, \sigma_{kq}; n_{lr}, l_{lr}, \lambda_{lr}, \sigma_{lr}; n, v, \Lambda, \Sigma) \times (n'_{ip}, l'_{ip}, \lambda'_{ip}, \sigma'_{ip}; n'_{kq}, l'_{kq}, \lambda'_{kq}, \sigma'_{kq}; n'_{lr}, l'_{lr}, \lambda'_{lr}, \sigma'_{lr}; n', v', \Lambda', \Sigma')] \neq 0$$

if among Δn_{ip}, Δn_{kq}, Δn_{lr} at least two are zero, $\Delta l_{ip} = \Delta l_{kq} = \Delta l_{lr} = 0$, $\Delta\lambda_{ip} = \Delta\lambda_{kq} = \Delta\lambda_{lr} = 0$, i.e. $\Delta\Lambda = 0$ and $\Delta\sigma_{ip} = \Delta\sigma_{kq} = \Delta\sigma_{lr} = 0$, i.e. $\Delta\Sigma = 0$.

In Hund's case (b) instead of $\Delta\Sigma = 0$, the relation $\Delta K = \pm 1$ holds. (For states of the same K, i.e. $\Delta K = 0$, only the electrostatic interaction and certain terms neglected at the separation of the wave equation give matrix elements, whilst operator I(1) does not give any.)

4. $\Delta\Lambda = \pm 1$ PERTURBATIONS

In these cases the bracketed part of operator I(1) supplies the perturbing matrix elements. Here the following cases can occur:

(a) $^2\Sigma$—$^4\Pi$ *Perturbation*

(1) $^2\Sigma^\pm$—$^4\Pi(a)$.—If the $^4\Pi$ state belongs to Hund's case (a),

$$(24)\quad \sqrt{3}\,H(^2\Sigma^\pm_{J+\frac{1}{2}}\,{}^4\Pi^\pm_{\frac{1}{2}}) = H(^2\Sigma^\pm_{J+\frac{1}{2}}\,{}^4\Pi^\pm_{-\frac{1}{2}}) = \sqrt{3}\,H(^2\Sigma^\pm_{J-\frac{1}{2}}\,{}^4\Pi^\mp_{\frac{1}{2}}) = -H(^2\Sigma^\pm_{J-\frac{1}{2}}\,{}^4\Pi^\mp_{-\frac{1}{2}}) = -i^\Sigma\sqrt{2/3}\,\xi$$

(see Fig. 8), where the Σ exponent is 0 or 1 according to whether we are dealing with a $^2\Sigma^+$ or a $^2\Sigma^-$ state. The value of the constant ξ appearing here as well as later on will be dealt with below:

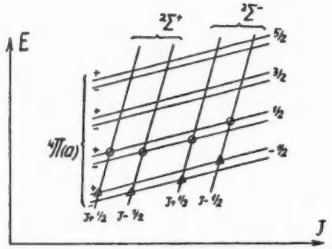

FIG. 8.

(2) $^2\Sigma^\pm$—$^4\Pi(b)$.—If the $^4\Pi$ state belongs to Hund's case (b),

$$(25)\quad 2H(^2\Sigma^\pm_{J+\frac{1}{2}}\ ^4\Pi^\pm_{J+3/2}) = -\sqrt{3}\,H(^2\Sigma^\pm_{J+\frac{1}{2}}\ ^4\Pi^\pm_{J+\frac{1}{2}}) = 2\sqrt{3}\,H(^2\Sigma^\pm_{J-\frac{1}{2}}\ ^4\Pi^\pm_{J-\frac{1}{2}}) = 2\sqrt{3}\,H(^2\Sigma^\pm_{J-\frac{1}{2}}\ ^4\Pi^\mp_{J+\frac{1}{2}}) = -\sqrt{3}\,H(^2\Sigma^\pm_{J-\frac{1}{2}}\ ^4\Pi^\mp_{J-\frac{1}{2}}) = 2H(^2\Sigma^\pm_{J-\frac{1}{2}}\ ^4\Pi^\mp_{J-3/2}) = i^\Sigma(2/\sqrt{3})\xi$$

(see Fig. 9). Here as in the following figures the perturbations of the same order of magnitude are denoted everywhere by the same sign. Since both states are in case (b) the selection rule $\Delta K = 0, \pm 1$ will hold.

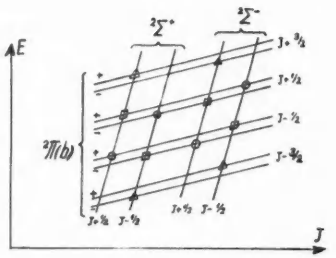

FIG. 9.

(b) $^4\Sigma$—$^2\Pi$ *Perturbation*

Here again two cases can be distinguished:

(1) $^4\Sigma^\pm$—$^2\Pi(a)$.—

$$(26)\quad \sqrt{3}H(^4\Sigma^\pm_{J-3/2}\ ^2\Pi^\pm_{3/2}) = \sqrt{3}H(^4\Sigma^\pm_{J-3/2}\ ^2\Pi^\pm_{\frac{1}{2}}) = H(^4\Sigma^\pm_{J+\frac{1}{2}}\ ^2\Pi^\pm_{3/2}) = -3H(^4\Sigma^\pm_{J+\frac{1}{2}}\ ^2\Pi^\pm_{\frac{1}{2}}) = H(^4\Sigma^\pm_{J-\frac{1}{2}}\ ^2\Pi^\mp_{3/2}) = 3H(^4\Sigma^\pm_{J-\frac{1}{2}}\ ^2\Pi^\mp_{\frac{1}{2}}) = \sqrt{3}H(^4\Sigma^\pm_{J+3/2}\ ^2\Pi^\mp_{3/2}) = -\sqrt{3}H(^4\Sigma^\pm_{J+3/2}\ ^2\Pi^\mp_{\frac{1}{2}}) = -(i^\Sigma/\sqrt{2})\xi$$

(see Fig. 10).

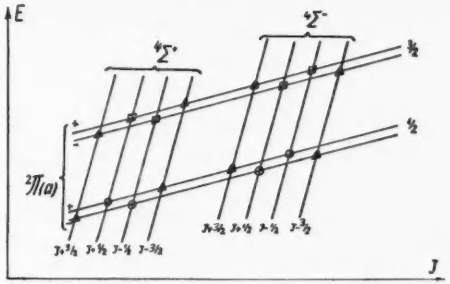

FIG. 10.

(2) $^4\Sigma^+$—$^2\Pi(b)$.—

$$(27)\quad 2H(^4\Sigma^{\pm}_{J-3/2}\,{}^2\Pi^{\pm}_{J-\frac{1}{2}}) = 2\sqrt{3}H(^4\Sigma^{\pm}_{J+\frac{1}{2}}\,{}^2\Pi^{\pm}_{J-\frac{1}{2}}) = \sqrt{3}H(^4\Sigma^{\pm}_{J+\frac{1}{2}}\,{}^2\Pi^{\pm}_{J+\frac{1}{2}})$$
$$= \sqrt{3}H(^4\Sigma^{\pm}_{J-\frac{1}{2}}\,{}^2\Pi^{\mp}_{J-\frac{1}{2}}) = 2\sqrt{3}H(^4\Sigma^{\pm}_{J-\frac{1}{2}}\,{}^2\Pi^{\mp}_{J+\frac{1}{2}}) = 2H(^4\Sigma^{\pm}_{J+3/2}\,{}^2\Pi^{\mp}_{J+\frac{1}{2}})$$
$$= -i^{\Sigma}(2/\sqrt{3})\xi$$

(see Fig. 11).

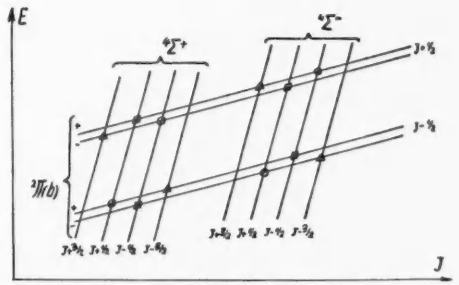

FIG. 11.

(*c*) $^2\Sigma$—$^2\Pi$ *Perturbation*

Between Σ and Π states of the same multiplicity the operator I(1) gives matrix elements independent of J, whilst the terms neglected at the separation of the wave equation give elements depending on J. Operator I(1) can supply terms non-diagonal in Λ and Σ unlike operator $A(LS)$, as can be seen in detail in the next section.

(1) $^2\Sigma^{\pm}$—$^2\Pi(a)$.—

$$H(^2\Sigma^{\pm}_{J+\frac{1}{2}}\,{}^2\Pi^{\pm}_{3/2}) = H(^2\Sigma^{\pm}_{J-\frac{1}{2}}\,{}^2\Pi^{\mp}_{3/2}) = -i^{\Sigma}2\eta\sqrt{(J-\tfrac{1}{2})(J+3/2)}\,,$$
$$(28)\quad H(^2\Sigma^{\pm}_{J+\frac{1}{2}}\,{}^2\Pi^{\pm}_{\frac{1}{2}}) = i^{\Sigma}[\xi+2\eta(J+3/2)],$$
$$H(^2\Sigma^{\pm}_{J-\frac{1}{2}}\,{}^2\Pi^{\mp}_{\frac{1}{2}}) = i^{\Sigma}[\xi-2\eta(J-1/2)]$$

(see Fig. 12). The value of the constant η will be dealt with in the following section.

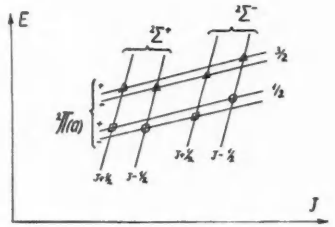

FIG. 12.

(2) $^2\Sigma^{\pm}$—$^2\Pi(b)$.—

$$H(^2\Sigma^{\pm}_{J+\frac{1}{2}}\ ^2\Pi^{\pm}_{J+\frac{1}{2}}) = -\frac{i^{\Sigma}}{\sqrt{2}}\sqrt{\frac{J+3/2}{J+1/2}}\,[\xi+4\eta(J+\tfrac{1}{2})]$$

$$\approx -\frac{i^{\Sigma}}{\sqrt{2}}\,[\xi+4\eta\sqrt{(J+1/2)(J+3/2)}]$$

(29)
$$H(^2\Sigma^{\pm}_{J+\frac{1}{2}}\ ^2\Pi^{\pm}_{J-\frac{1}{2}}) = \frac{i^{\Sigma}}{\sqrt{2}}\sqrt{\frac{J-\frac{1}{2}}{J+\frac{1}{2}}}\,\xi \approx \frac{i^{\Sigma}}{\sqrt{2}}\,\xi$$

$$H(^2\Sigma^{\pm}_{J-\frac{1}{2}}\ ^2\Pi^{\mp}_{J+\frac{1}{2}}) = \frac{i^{\Sigma}}{\sqrt{2}}\sqrt{\frac{J+3/2}{J+1/2}}\,\xi \approx \frac{i^{\Sigma}}{\sqrt{2}}\,\xi$$

$$H(^2\Sigma^{\pm}_{J-\frac{1}{2}}\ ^2\Pi^{\mp}_{J-\frac{1}{2}}) = -\frac{i^{\Sigma}}{\sqrt{2}}\sqrt{\frac{J-\frac{1}{2}}{J+\frac{1}{2}}}\,[\xi-4\eta(J+\tfrac{1}{2})]$$

$$\approx -\frac{i^{\Sigma}}{\sqrt{2}}\,[\xi-4\eta\sqrt{(J-1/2)(J+1/2)}]$$

(see Fig. 13). For perturbations with $\Delta K = 0$ the matrix elements depend on J whilst for perturbations with $\Delta K = \pm 1$ they are independent of J and have approximately the same order of magnitude.

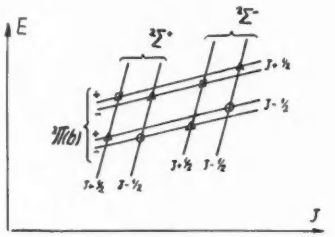

FIG. 13.

(3) *The Λ-type splitting of the* $^2\Pi$ *state in the limiting cases.*—$^2\Pi$ states can be perturbed by $^2\Sigma$ and $^4\Sigma$ states. As can be seen from eqs. (26) and (27) the

$^4\Sigma$ states, owing to the equality of the corresponding matrix elements, cannot cause the splitting of the $^2\Pi$ rotational levels of + and − symmetry. Thus the Λ-type doubling in $^2\Pi$ states can be caused only by the more distant $^2\Sigma$ states. Applying the general formula described in I(24), formulae which can be used in the two ideal limiting cases and even in the neighborhood of them can be given as follows:

In Hund's case (*a*)

$$\begin{aligned} h\Delta\nu(^2\Pi_{3/2}) &= 0, \\ h\Delta\nu(^2\Pi_{\frac{1}{2}}) &= 2(C_1+C_2)(J+\tfrac{1}{2}), \end{aligned} \tag{30}$$

whilst in the neighborhood of case (*b*)

$$\begin{aligned} h\Delta\nu(^2\Pi_{J+\frac{1}{2}}) &= C_1(J+3/2)+C_2(J+\tfrac{1}{2})(J+3/2), \\ h\Delta\nu(^2\Pi_{J-\frac{1}{2}}) &= C_1(J-\tfrac{1}{2})-C_2(J-\tfrac{1}{2})(J+\tfrac{1}{2}), \end{aligned} \tag{31}$$

where C_1 and C_2 are identical with the expressions given in I(26*a*) with the difference that doublet terms are to be written everywhere instead of triplet.

(*d*) $^4\Sigma$—$^4\Pi$ *Perturbation*

For this perturbation special attention has to be paid to the elements of operator I(1) that are non-diagonal in Λ and Σ. For the configurations under consideration, operator I(1) supplies only a third of the contribution supplied by operator $A(L.S)$. Here smaller values are obtained owing to the fact that $^4\Sigma$ as well as $^4\Pi$ states are in intercombination interaction with other states and the remaining two thirds of the interaction is consumed there. (For details see the next section.)

(1) $^4\Sigma^{\pm}$—$^4\Pi(a)$.—

$$H(^4\Sigma^{\pm}_{J+3/2}\,{}^4\Pi^{\mp}_{5/2}) = i^{\Sigma}\eta\sqrt{\frac{(J+5/2)(J-3/2)(J-\frac{1}{2})}{J+1}} \approx i^{\Sigma}\eta\sqrt{(J+5/2)(J-3/2)}$$

$$H(^4\Sigma^{\pm}_{J+3/2}\,{}^4\Pi^{\mp}_{3/2}) = \frac{i^{\Sigma}}{2\sqrt{3}}\sqrt{\frac{J-\frac{1}{2}}{J+1}}\,[\xi+6\eta(J+5/2)] \approx \frac{i^{\Sigma}}{2\sqrt{3}}\,[\xi+6\eta(J+5/2)]$$

$$H(^4\Sigma^{\pm}_{J+3/2}\,{}^4\Pi^{\mp}_{+\frac{1}{2}}) = \frac{i^{\Sigma}}{\sqrt{3}}\sqrt{\frac{J+3/2}{J+1}}\,[\xi+3\eta(J+5/2)] \approx \frac{i^{\Sigma}}{\sqrt{3}}\,[\xi+3\eta(J+5/2)]$$

$$H(^4\Sigma^{\pm}_{J+3/2}\,{}^4\Pi^{\mp}_{-\frac{1}{2}}) = \frac{i^{\Sigma}}{2}\sqrt{\frac{J+3/2}{J+1}}\,[\xi+2\eta(J+5/2)] \approx \frac{i^{\Sigma}}{2}\,[\xi+2\eta(J+5/2)]$$

$$H(^4\Sigma^{\pm}_{J+\frac{1}{2}}\,{}^4\Pi^{\pm}_{5/2}) = i^{\Sigma}\eta\sqrt{\frac{3(J+5/2)(J-3/2)(J-\frac{1}{2})}{J}} \approx i^{\Sigma}\eta\sqrt{3(J+5/2)(J-3/2)}$$

$$H({}^4\Sigma^{\pm}_{J+\frac{1}{2}}\,{}^4\Pi^{\pm}_{3/2}) = \frac{i^{\Sigma}}{2}\sqrt{\frac{J-\frac{1}{2}}{J}}\,[\xi+2\eta(J+9/2)] \approx \frac{i^{\Sigma}}{2}\,[\xi+2\eta(J+9/2)]$$

$$H({}^4\Sigma^{\pm}_{J+\frac{1}{2}}\,{}^4\Pi^{\pm}_{\frac{1}{2}}) = \frac{i^{\Sigma}}{3}\sqrt{\frac{J+3/2}{J}}\,[\xi-3\eta(J-3/2)] \approx \frac{i^{\Sigma}}{3}\,[\xi-3\eta(J-3/2)]$$

$$H({}^4\Sigma^{\pm}_{J+\frac{1}{2}}\,{}^4\Pi^{\pm}_{-\frac{1}{2}}) = \frac{i^{\Sigma}}{2\sqrt{3}}\sqrt{\frac{J+3/2}{J}}\,[\xi+6\eta(J+\tfrac{1}{2})] \approx -\frac{i^{\Sigma}}{2\sqrt{3}}\,[\xi+6\eta(J+\tfrac{1}{2})]$$

$$(32)\quad H({}^4\Sigma^{\pm}_{J-\frac{1}{2}}\,{}^4\Pi^{\mp}_{5/2}) = i^{\Sigma}\eta\sqrt{\frac{3(J+5/2)(J+3/2)(J-3/2)}{J+1}} \approx i^{\Sigma}\eta\sqrt{3(J+5/2)(J-3/2)}$$

$$H({}^4\Sigma^{\pm}_{J-\frac{1}{2}}\,{}^4\Pi^{\mp}_{3/2}) = \frac{i^{\Sigma}}{2}\sqrt{\frac{J+3/2}{J+1}}\,[\xi-2\eta(J-7/2)] \approx \frac{i^{\Sigma}}{2}\,[\xi-2\eta(J-7/2)]$$

$$H({}^4\Sigma^{\pm}_{J-\frac{1}{2}}\,{}^4\Pi^{\mp}_{\frac{1}{2}}) = -\frac{i^{\Sigma}}{3}\sqrt{\frac{J-\frac{1}{2}}{J+1}}\,[\xi+3\eta(J+5/2)] \approx -\frac{i^{\Sigma}}{3}\,[\xi+3\eta(J+5/2)]$$

$$H({}^4\Sigma^{\pm}_{J-\frac{1}{2}}\,{}^4\Pi^{\mp}_{-\frac{1}{2}}) = -\frac{i^{\Sigma}}{2\sqrt{3}}\sqrt{\frac{J-\frac{1}{2}}{J+1}}\,[\xi-6\eta(J+\tfrac{1}{2})] \approx -\frac{i^{\Sigma}}{2\sqrt{3}}\,[\xi-6\eta(J+\tfrac{1}{2})]$$

$$H({}^4\Sigma^{\pm}_{J-3/2}\,{}^4\Pi^{\pm}_{5/2}) = i^{\Sigma}\eta\sqrt{\frac{(J+5/2)(J+3/2)(J-3/2)}{J}} \approx i^{\Sigma}\eta\sqrt{(J+5/2)(J-3/2)}$$

$$H({}^4\Sigma^{\pm}_{J-3/2}\,{}^4\Pi^{\pm}_{3/2}) = \frac{i^{\Sigma}}{2\sqrt{3}}\sqrt{\frac{J+3/2}{J}}\,[\xi-6\eta(J-3/2)] \approx \frac{i^{\Sigma}}{2\sqrt{3}}\,[\xi-6\eta(J-3/2)]$$

$$H({}^4\Sigma^{\pm}_{J-3/2}\,{}^4\Pi^{\pm}_{\frac{1}{2}}) = -\frac{i^{\Sigma}}{\sqrt{3}}\sqrt{\frac{J-\frac{1}{2}}{J}}\,[\xi-3\eta(J-3/2)] \approx -\frac{i^{\Sigma}}{\sqrt{3}}\,[\xi-3\eta(J-3/2)]$$

$$H({}^4\Sigma^{\pm}_{J-3/2}\,{}^4\Pi^{\pm}_{-\frac{1}{2}}) = \frac{i^{\Sigma}}{4}\sqrt{\frac{J-\frac{1}{2}}{J}}\,[\xi-2\eta(J-3/2)] \approx \frac{i^{\Sigma}}{2}\,[\xi-2\eta(J-3/2)]$$

(see Fig. 14). According to these operations each perturbation is possible

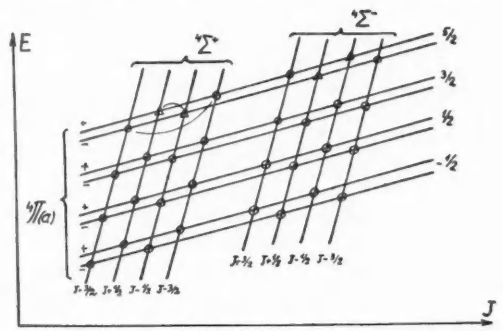

FIG. 14.

because the $^4\Sigma$ state belongs to case (b) and the $^4\Pi$ state to case (a). Every matrix element depends on J and those which are approximately the same are connected in the figure by a thin line.

(2) $^4\Sigma^{\pm}$—$^4\Pi(b)$.—

$$H(^4\Sigma^{\pm}_{J+3/2}\,{}^4\Pi^{\mp}_{J+3/2}) = -\frac{i^z}{\sqrt{2}}\sqrt{\frac{J+5/2}{J+3/2}}\,[\xi+4\eta(J+3/2)]$$
$$\approx -\frac{i^z}{\sqrt{2}}\,[\xi+4\eta\sqrt{(J+5/2)(J+3/2)}]$$

$$H(^4\Sigma^{\pm}_{J+3/2}\,{}^4\Pi^{\mp}_{J+\frac{1}{2}}) = \frac{i^z}{\sqrt{2}}\sqrt{\frac{J(J+\frac{1}{2})}{3(J+1)(J+3/2)}}\,\xi \approx \frac{i^z}{\sqrt{6}}\,\xi$$

$$H(^4\Sigma^{\pm}_{J+3/2}\,{}^4\Pi^{\mp}_{J-\frac{1}{2}}) = 0$$

$$H(^4\Sigma^{\pm}_{J+3/2}\,{}^4\Pi^{\mp}_{J-3/2}) = 0$$

$$H(^4\Sigma^{\pm}_{J+\frac{1}{2}}\,{}^4\Pi^{\pm}_{J+3/2}) = -\frac{i^z}{\sqrt{2}}\sqrt{\frac{J(J+5/2)}{3(J+1)(J+3/2)}}\,\xi \approx -\frac{i^z}{\sqrt{6}}\,\xi$$

$$H(^4\Sigma^{\pm}_{J+\frac{1}{2}}\,{}^4\Pi^{\pm}_{J+\frac{1}{2}}) = -\frac{i^z}{\sqrt{2}}\left[\frac{J+9/2}{\sqrt{(J+\frac{1}{2})(J+3/2)}}\,\frac{\xi}{3}+4\eta\sqrt{(J+\tfrac{1}{2})(J+3/2)}\right]$$
$$\approx -\frac{i^z}{\sqrt{2}}\left[\frac{\xi}{3}+4\eta\sqrt{(J+3/2)(J+\tfrac{1}{2})}\right]$$

$$H(^4\Sigma^{\pm}_{J+\frac{1}{2}}\,{}^4\Pi^{\pm}_{J-\frac{1}{2}}) = i^z\,\frac{\sqrt{2}}{3}\sqrt{\frac{(J+3/2)(J-\frac{1}{2})^3}{J(J+1)(J+\frac{1}{2})}}\,\xi \approx i^z\,\frac{\sqrt{2}}{3}\,\xi$$

(33) $H(^4\Sigma^{\pm}_{J+\frac{1}{2}}\,{}^4\Pi^{\pm}_{J-3/2}) = 0$

$$H(^4\Sigma^{\pm}_{J-\frac{1}{2}}\,{}^4\Pi^{\mp}_{J+3/2}) = 0$$

$$H(^4\Sigma^{\pm}_{J-\frac{1}{2}}\,{}^4\Pi^{\mp}_{J+\frac{1}{2}}) = -\,i^z\,\frac{\sqrt{2}}{3}\sqrt{\frac{(J-\frac{1}{2})(J+3/2)^2}{J(J+1)(J+\frac{1}{2})}}\,\xi \approx -\,i^z\,\frac{\sqrt{2}}{3}\,\xi$$

$$H(^4\Sigma^{\pm}_{J-\frac{1}{2}}\,{}^4\Pi^{\mp}_{J-\frac{1}{2}}) = \frac{i^z}{\sqrt{2}}\left[\frac{J-7/2}{\sqrt{(J-\frac{1}{2})(J+\frac{1}{2})}}\,\frac{\xi}{3}-4\eta\sqrt{(J+\tfrac{1}{2})(J-\tfrac{1}{2})}\right]$$
$$\approx \frac{i^z}{\sqrt{2}}\left[\frac{\xi}{3}-4\eta\sqrt{(J+\tfrac{1}{2})(J-\tfrac{1}{2})}\right]$$

$$H(^4\Sigma^{\pm}_{J-\frac{1}{2}}\,{}^4\Pi^{\mp}_{J-3/2}) = \frac{i^z}{\sqrt{2}}\sqrt{\frac{(J+1)(J-3/2)}{3J(J-\frac{1}{2})}}\,\xi \approx \frac{i^z}{\sqrt{6}}\,\xi$$

$$H(^4\Sigma^{\pm}_{J-3/2}\,{}^4\Pi^{\pm}_{J+3/2}) = 0$$

$$H(^4\Sigma^{\pm}_{J-3/2}\,{}^4\Pi^{\pm}_{J+\frac{1}{2}}) = 0$$

$$H(^4\Sigma^{\pm}_{J-3/2}\,{}^4\Pi^{\pm}_{J-\frac{1}{2}}) = -\frac{i^z}{\sqrt{2}}\sqrt{\frac{(J+1)(J+\frac{1}{2})}{3J(J-\frac{1}{2})}}\,\xi \approx -\frac{i^z}{\sqrt{6}}\,\xi$$

$$H(^4\Sigma^{\pm}_{J-3/2}\,{}^4\Pi^{\pm}_{J-3/2}) = \frac{i^z}{\sqrt{2}}\sqrt{\frac{J-3/2}{J-\frac{1}{2}}}\,[\xi-4\eta(J-\tfrac{1}{2})]$$
$$\approx \frac{i^z}{\sqrt{2}}\,[\xi-4\eta\sqrt{(J-\tfrac{1}{2})(J-3/2)}]$$

(see Fig. 15). According to the selection rules valid for case (*b*) the matrix elements $\Delta K = \pm 2, \pm 3$, are zero, the matrix elements $\Delta K = \pm 1$ are independent of J, and four of the six perturbations are approximately equal while the other two have a different value but are approximately equal to each other (in Fig. 15 these are connected by thin lines). The matrix elements $\Delta K = 0$ depend on J and differ from one another.

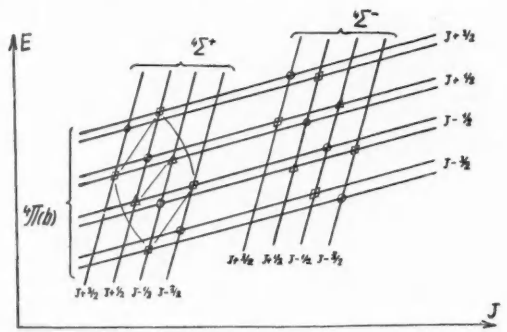

FIG. 15.

(3) *The Λ-type splitting of the* $^4\Pi$ *states in the limiting cases.*—According to what has been said in points (*a*) and (*d*) perturbations can be caused in a $^4\Pi$ state by $^2\Sigma^{\pm}$ and $^4\Sigma^{\pm}$ states. (In our model $^6\Sigma^{\pm}$ states do not occur.) The $^2\Sigma^-$ and $^4\Sigma^+$ states lying on one side of the $^4\Pi$ state and the $^2\Sigma^+$ and $^4\Sigma^-$ states lying on the other side will give rise to a shift in the same direction. Taking into consideration what has been said above according to I(24) as well as (24) and (32) for Hund's case (*a*) we obtain:

$$
\begin{aligned}
&h\Delta\nu(^4\Pi_{5/2}) = 0,\\
&h\Delta\nu(^4\Pi_{3/2}) = 0,\\
&h\Delta\nu(^4\Pi_{\frac{1}{2}}) = ((4/3)C_1 + 4C_2)(J+\tfrac{1}{2}),\\
&h\Delta\nu(^4\Pi_{-\frac{1}{2}}) = 0,
\end{aligned}
\tag{34}
$$

and in the neighborhood of Hund's case (*b*) according to (25) and (33):

$$
\begin{aligned}
h\Delta\nu(^4\Pi_{J+3/2}) &= \frac{1}{3}C_0\,\frac{J+5/2}{J+1} + C_1(J+5/2) + C_2(J+3/2)(J+5/2),\\
h\Delta\nu(^4\Pi_{J+\frac{1}{2}}) &= \frac{1}{3}C_0\,\frac{J-3/2}{J} - \tfrac{1}{3}C_1(J+9/2) - C_2(J+\tfrac{1}{2})(J+3/2),\\
h\Delta\nu(^4\Pi_{J-\frac{1}{2}}) &= \frac{1}{3}C_0\,\frac{J+5/2}{J+1} - \tfrac{1}{3}C_1(J-7/2) + C_2(J-\tfrac{1}{2})(J+\tfrac{1}{2}),\\
h\Delta\nu(^4\Pi_{J-3/2}) &= \frac{1}{3}C_0\,\frac{J-3/2}{J} + C_1(J-3/2) - C_2(J-3/2)(J-\tfrac{1}{2}),
\end{aligned}
\tag{35}
$$

where C_0, C_1, and C_2 correspond to the value given in I(26*a*) with the difference that the triplet and singlet notations should be replaced by the quartet and doublet notations.

As an example of equation (35) it may be mentioned for instance that for the Λ-type splitting of the $^4\Pi$ state of the O_2^+ molecule the difference between the experimental and the theoretical values at $J = 40$ (extrapolated) is small. [$\Delta\nu(^4\Pi_{J+3/2}) = 0.84$ cm.$^{-1}$ (theor.) and 0.56 cm.$^{-1}$ (exp.), $\Delta\nu(^4\Pi_{J+\frac{1}{2}}) = -0.33$ cm.$^{-1}$ (theor.) and -0.30 cm.$^{-1}$ (exp.), $\Delta\nu(^4\Pi_{J-\frac{1}{2}}) = 0.03$ cm.$^{-1}$ (theor.) and 0.02 cm.$^{-1}$ (exp.), $\Delta\nu(^4\Pi_{J-3/2}) = 0.04$ cm.$^{-1}$ (theor.) and 0.00 cm^{-1} (exp.) (Budó and Kovács 1944).]

5. SELECTION RULES AND THE VALUES OF THE CONSTANTS ξ AND η FOR ΔΛ = ±1 PERTURBATIONS

The values of the constants ξ and η occurring in $\Delta\Lambda = \pm 1$ perturbations are the following:

$$(36a)\qquad \xi[(\lambda\lambda\sigma)(\lambda\lambda\pi)] = \frac{1}{2\sqrt{2}}\int R^*_{n,v}(\rho)\int r^*_{nlr,\,l_{lr},0}\,a_l(f_l+g_l)r_{n'l_r,\,v'l_r,\pm1}\,d\tau_l$$
$$\times\int p^*_{n_{ip},\,l_{ip},\lambda}\,p_{n'_{ip},\,l'_{ip},\lambda}\,d\tau_i\int q^*_{n_{kq},\,l_{kq},\lambda}\,q_{n'_{kq},\,l'_{kq},\lambda}\,d\tau_k R_{n',v'}(\rho)d\rho,$$

$$(36b)\qquad \eta[(\lambda\lambda\sigma)(\lambda\lambda\pi)] = \frac{1}{2\sqrt{2}}\int R^*_{n,v}(\rho)\int r^*_{nlr,\,l_{lr},0}(f_l+g_l)r_{n'l_r,\,v'l_r,\pm1}d\tau_l$$
$$\times\int p^*_{n_{ip},\,l_{ip},\lambda}\,p_{n'_{ip},\,l'_{ip},\lambda}\,d\tau_i\int q^*_{n_{kq},\,l_{kq},\lambda}\,q_{n'_{kq},\,l_{kq},\lambda}\,d\tau_k B(\rho)R_{n',v'}(\rho)d\rho,$$

where $B = h^2/8\pi^2\mu\rho^2$ and μ is the reduced mass of the molecule.

For matrix elements containing ξ, owing to the integration carried out previously over the spin-coordinates, two of the spin quantum number pairs $(\sigma_{ip}, \sigma'_{ip})$, $(\sigma_{kq}, \sigma'_{kq})$, $(\sigma_{lr}, \sigma'_{lr})$ have to be always equal to one another, and where the two members of a pair are different from one another, the difference can only be ±1. For matrix elements in which the constant η occurs, all three pairs of spin quantum numbers have to be equal. As a result of the integrations over φ (as can also be seen from the expressions of the constants) one finds that $\Delta\lambda = 0$ and $\Delta\lambda_{lr} = \pm 1$. For $\lambda = 0$ the expressions (36*a*) and (36*b*) have to be multiplied by $\sqrt{2}$.

The preceding selection rules expressed by the resultant quantum numbers of the molecule are the well-known selection rules: for ξ $\Delta\Lambda = \pm 1$ and $\Delta\Sigma = \mp 1$, i.e. $\Delta\Omega = 0$, and for η $\Delta\Lambda = \pm 1$, $\Delta\Sigma = 0$, i.e. $\Delta\Omega = \pm 1$.

For the perturbations dealt with in Section 4 a more detailed examination of the integration over φ and the spin coordinates shows that not every perturbation from among those which satisfy the above general selection rules is possible. Thus in the case of perturbations between terms of different multiplicity the $^2\Sigma$ state described by the eigenfunction (1) cannot interact with any $^2\Pi$ state, hence $H(^2\Sigma, {}^4\Pi) = 0$; only between $^2\Sigma^*$ states having the eigenfunction (2) and $^4\Pi$ states is an interaction possible. Similarly between $^2\Pi$ and $^4\Sigma$ no interaction exists, i.e. $H(^2\Pi, {}^4\Sigma) = 0$, but there is interaction

between $^2\Pi^*$ and $^4\Sigma$ states. In the case of states of the same multiplicity no perturbation occurs between $^2\Sigma$ and $^2\Pi^*$ states nor between $^2\Sigma^*$ and $^2\Pi$ states, i.e. $H(^2\Sigma, {}^2\Pi^*) = H(^2\Sigma^*, {}^2\Pi) = 0$. This statement holds not only for matrix elements in which the ξ constant occurs but also for those in which the η constant occurs.

There is a difference between the ($^2\Sigma$, $^2\Pi$) and ($^2\Sigma^*$, $^2\Pi^*$) perturbations. For the matrix elements ($^2\Sigma$, $^2\Pi$) perturbations containing the constant ξ the operator I(1) gives the same values as the operator $A(LS)$ whilst in the case of perturbation ($^2\Sigma^*$, $^2\Pi^*$) as well as of ($^4\Sigma$, $^4\Pi$) a difference appears. More explicitly: $H(^2\Sigma^*, {}^2\Pi^*) = \frac{1}{3} H(^2\Sigma, {}^2\Pi)$. In general it can be stated that between two states of the same multiplicity which owing to configurational reasons are not in $\Delta\Lambda = \pm 1$ intercombination interaction with other states (for instance $^2\Sigma$ and $^2\Pi$) the operators I(1) and $A(LS)$ give the same matrix elements, whilst between two states of the same multiplicity which can be in $\Delta\Lambda = \pm 1$ intercombination interaction with other states (for instance $^2\Sigma^*$, $^2\Pi^*$ or $^4\Sigma$, $^4\Pi$, as well as from I the $^3\Sigma$, $^3\Pi$ states) smaller values are given by operator I(1) than by operator $A(LS)$. The $^2\Pi^{(3)}$ and $^4\Pi^{(3)}$ states occurring for $\lambda = 1$ cannot interact with any of the $^2\Sigma$, $^2\Sigma^*$, $^4\Sigma$ states.

If the assumptions of Section I.5 are introduced, additional selection rules can be obtained. For the non-vanishing elements we have $\Delta n_{ip} = \Delta n_{kq} = 0$, and $\Delta l_{ip} = \Delta l_{kq} = \Delta l_{lr} = 0$. In such cases the equations (36*a*) and (37*b*) can be written in even simpler forms

$$\xi[(\lambda\lambda\sigma)(\lambda\lambda\pi)] = \frac{1}{2\sqrt{2}}[a(f+g)]_r \int R^*_{n,v}(\rho) R_{n',v'}(\rho) d\rho, \tag{37a}$$

$$\eta[(\lambda\lambda\sigma)(\lambda\lambda\pi)] = \frac{1}{2\sqrt{2}}[f+g]_r \int R^*_{n,v}(\rho) B(\rho) R_{n',v'}(\rho) d\rho, \tag{37b}$$

where

$$[a(f+g)]_r = \int r^*_{nlr,\, llr,\, 0}(\bar{r}_l, \vartheta_l) a(\bar{r}_l)(f_l+g_l) r_{n'l'r,\, l'lr,\, \pm 1}(\bar{r}_l, \vartheta_l) \sin\vartheta_l \bar{r}_l^2 d\bar{r}_l d\vartheta_l. \tag{38}$$

Here the distance of the electron from the origin has been designated by $\bar{r}$ in order to distinguish it from the eigenfunction r.

If according to I(29) and I(30) in the r eigenfunction the two variables are separated, we find

$$[a(f+g)]_r = \mp a(n_{lr}, n'_{lr}) \sqrt{l_r(l_r+1)}, \tag{39}$$

where the expression $a(n_{lr}, n'_{lr})$ is analogous to those occurring in I(35).

As we have seen before for the principal quantum numbers only Δn_{lr} may differ from zero. If it is different from zero the constant $a(n_{lr}, n'_{lr})$ cannot be related to the multiplet constants. If however $\Delta n_{lr} = 0$, then the ξ and η constants will take the following form:

$$\begin{aligned} \xi[(\lambda\lambda\sigma)(\lambda\lambda\pi)] &= \mp \frac{1}{2\sqrt{2}} a_r \sqrt{l_r(l_r+1)}, \\ \eta[(\lambda\lambda\sigma)(\lambda\lambda\pi)] &= \mp \frac{1}{2\sqrt{2}} B_{\Sigma\Pi} \sqrt{l_r(l_r+1)}, \end{aligned} \tag{40}$$

where

$$a_r = a(n_{lr}, n_{lr}) \int R^*_{n,v}(\rho) R_{n,v}(\rho) d\rho, \tag{41a}$$

$$B_{\Sigma\Pi} = \int R^*_{n,v}(\rho) B(\rho) R_{n,v}(\rho) d\rho. \tag{41b}$$

Summarizing what has been said before for $\Delta\Lambda = \pm 1$ in Hund's case (a) operator I(1) gives

$$H[(n_{ip}, l_{ip}, \lambda, \sigma_{ip}; n_{kq}, l_{kq}, \lambda, \sigma_{kq}; n_{lr}, l_{lr}, 0, \sigma_{lr}; n, v, \Lambda, \Sigma)(n_{ip}, l_{ip}, \lambda, \sigma'_{ip}; n_{kq}, l_{kq}, \lambda, \sigma'_{kq}; n'_{lr}, l_{lr}, 1, \sigma'_{lr}; n', v', \Lambda \pm 1, \Sigma \mp 1)] \neq 0 \tag{42}$$

if for the principal quantum numbers $\Delta n_{ip} = \Delta n_{kq} = 0$ (Δn_{lr} may be zero but might also differ from it), and if $\Delta l_{ip} = \Delta l_{kq} = \Delta l_{lr} = 0$; $\Delta\lambda = 0$, $\Delta\lambda_{lr} = \pm 1$ that is $\Delta\Lambda = \pm 1$; furthermore from among $\Delta\sigma_{ip}$, $\Delta\sigma_{kq}$, $\Delta\sigma_{lr}$ two are always zero, whilst the third is equal to ± 1, that is $\Delta\Sigma = \mp 1$ and thus $\Delta\Omega = 0$.

In Hund's case (b) instead of the selection rule $\Delta\Sigma = \mp 1$ the selection rule $\Delta K = 0, \pm 1$ holds.

In Hund's case (a) for matrix elements depending on J and neglected at the separation of the wave equation the same selection rules are valid except that now $\Delta\sigma_{ip} = \Delta\sigma_{kq} = \Delta\sigma_{lr} = 0$, hence $\Delta\Sigma = 0$ and thus $\Delta\Omega = \pm 1$, whilst for Hund's case (b) selection rule $\Delta K = \pm 1$ takes the place of $\Delta\Sigma = 0$.

In Table I below the states between which perturbations can occur are indicated.

TABLE I

Electron config.	Molecular states
$\sigma\ \sigma\ \sigma$	$^2\Sigma^+$, $^2\Sigma^{*+}$, $^4\Sigma^+$
$\sigma\ \sigma\ \pi$	$^2\Pi_r^{(1)} = {}^2\Pi_r^{(2)}$, $^2\Pi_i^{*(1)} = {}^2\Pi_i^{*(2)}$, $^4\Pi_r^{(1)} = {}^4\Pi_r^{(2)}$
$\pi\ \pi\ \sigma$	$^2\Sigma^+$, $^2\Sigma^-$, $^2\Sigma^{*+}$, $^2\Sigma^{*-}$, $^4\Sigma^+$, $^4\Sigma^-$ . . .
$\pi\ \pi\ \pi$	$^2\Pi_r^{(1)}$, $^2\Pi_r^{(2)}$, $^2\Pi_i^{(3)}$, $^2\Pi^{*(1)}$, $^2\Pi^{*(2)}$, $^2\Pi_r^{*(3)}$, $^4\Pi^{(1)}$, $^4\Pi^{(2)}$, $^4\Pi^{(3)}$ . . .

The connecting lines in Table I connect states which can perturb one another except that perturbations between states in the same row are not indicated in order not to overcrowd the diagram. The (Σ and Π) states occurring here—with the exception of those indicated—cannot interact with (Π and Σ) states of another configuration. Thus an explanation is found for cases in which perturbations otherwise possible do not occur. For values $i = 1, 2$ the matrix elements $H(\Sigma, \Pi^{(i)})$ differ only in sign from each other.

If two electrons are equivalent, then Table I must be replaced by Table

II. The first two rows illustrate the case of one valence-electron, because two equivalent σ electrons form a closed shell in the molecule.

TABLE II

Electron config.	Molecular terms
$\sigma^2\,\sigma$	$^2\Sigma^+$
$\sigma^2\,\pi$	$^2\Pi_r^{(1)} = {}^2\Pi_r^{(2)}$
$\pi^2\,\sigma$	$^2\Sigma^+$, $^2\Sigma^{*-}$, $^4\Sigma^-$ . . .
$\pi^2\,\pi$	$^2\Pi_r^{(1)} = {}^2\Pi_r^{(2)}$, $^2\Pi_i^{(3)}$, $^2\Pi_i^{*(1)} = {}^2\Pi_i^{*(2)}$, $^4\Pi_r^{(1)} = {}^4\Pi_r^{(2)}$ . . .

6. RELATIONS BETWEEN THE MATRIX ELEMENTS AND THE CONSTANTS OF MOLECULES

If the diagonal elements of the operator $\mathrm{I}(1)$ and $A(LS)$ are calculated and equated, relations are obtained between the experimentally measurable multiplet splitting constants of $^2\Pi$ and $^4\Pi$ states and the constants a. Moreover with the knowledge of these the regular or inverted character of the $^2\Pi$ and $^4\Pi$ states can be established in certain cases. (The places where this can be done unambiguously are denoted in Tables I and II.)

$$A^{2\Pi(1)} = \bar{a}_r, \quad A^{2\Pi^*(1)} = \tfrac{1}{3}[-\bar{a}_r+2\lambda(\bar{a}_p-\bar{a}_q)], \quad A^{4\Pi(1)} = \tfrac{1}{3}[\bar{a}_r+\lambda(\bar{a}_p-\bar{a}_q)];$$

$$A^{2\Pi(2)} = \bar{a}_r, \quad A^{2\Pi^*(2)} = \tfrac{1}{3}[-\bar{a}_r-2\lambda(\bar{a}_p-\bar{a}_q)], \quad A^{4\Pi(2)} = \tfrac{1}{3}[\bar{a}_r-\lambda(\bar{a}_p-\bar{a}_q)];$$

$$A^{2\Pi(3)} = -\bar{a}_r, \quad A^{2\Pi^*(3)} = \tfrac{1}{3}[\bar{a}_r+2(\bar{a}_p+\bar{a}_q)], \quad A^{4\Pi(3)} = \tfrac{1}{3}[-\bar{a}_r+(\bar{a}_p+\bar{a}_q)]$$

where the values of $\bar{a}_p$, $\bar{a}_q$, and $\bar{a}_r$ correspond to the a constants on the right-hand side of (22) if there the principal quantum numbers distinguished by a prime are equal, similar to those without a prime. If two states for which $\Delta n_{ip} = \Delta n_{kq} = \Delta n_{lr} = 0$, i.e. states belonging to the same electron configuration, perturb each other, then the difference between the constants of the matrix elements and of (43) can arise only from the fact that in (43) the integral of the vibrational eigenfunctions has been assumed to give exactly unity, whilst the actual value of the integrals occurring in the matrix elements depends on the relative position of the potential curves of the two states.

In the case of two equivalent electrons $\bar{a}_p$ is equal to $\bar{a}_q$ and thus they do not occur in (43); in such cases for each II state it doubtless can be decided whether it is a regular or an inverted state.

ACKNOWLEDGMENTS

I express my grateful thanks to Dr. A. E. Douglas, Ottawa, for having revised the translation and to Dr. G. Herzberg, Ottawa, for his valuable remarks made concerning the work.

REFERENCES

BUDÓ, A. and KOVÁCS, I. 1954. Acta Phys. Acad. Sci. Hung. **4**, 273.
——— 1944. Physik. Z. **45**, 122.
KOVÁCS, I. 1958. Can. J. Phys. **36**, 309.

BAND STRUCTURE OF RHOMBOHEDRAL GRAPHITE[1]

R. R. HAERING[2]

ABSTRACT

The band structure of rhombohedral graphite has been investigated using the nearest-neighbor tight-binding approximation. The resulting behavior of the π-bands near the Fermi surface is more complex than in the case of the Bernal stacking. The two π-bands still touch, but the touching points no longer lie on the edges of a hexagonal prism in k-space. Instead, they lie on cylinders whose axes are the edges of the hexagonal prism. The radii of these cylinders are proportional to γ_1, the nearest "out-of-plane" exchange integral. The de Haas – Van Alphen effect in the rhombohedral structure may be expected to yield useful information about the magnitude of γ_1.

1. INTRODUCTION

The band structure of graphite has received a great deal of attention in the literature (Wallace 1947; Coulson and Taylor 1952; Lomer 1955; Slonczewski 1955; Slonczewski and Weiss 1955, 1957; Johnston 1955, 1956; Corbato 1956). Most of these investigations are extensions of the work of Wallace (1947), who used a nearest-neighbor tight-binding approximation based on the $2p_z$ orbitals. All of the above calculations assume that graphite crystallizes in the Bernal structure (Bernal 1924). In this structure, the carbon atoms within a single layer of graphite form a plane hexagonal lattice (assumed to be the xy plane), in which the atoms are separated by 1.42 Å. The layers are then placed on top of each other in a sequence which we may denote by 1–2–1–2 . . . , indicating that alternate layers have the same projections on the xy plane. The interlayer separation is 3.35 Å and the unit cell contains four carbon atoms.

The X-ray and electron diffraction spectra of graphite show a number of extra lines which cannot be attributed to the Bernal lattice. These extra lines were first observed in the electron diffraction spectrum by Finch and Wilman (1936), who explained them in terms of diffraction from very thin crystallites (thickness $\sim$4 unit cells). Taylor and Laidler (1940) and Lipson and Stokes (1942) also observed such reflections by X-ray diffraction. The sharpness of the X-ray lines suggested that one was dealing with much larger crystallites, so that the explanation of Finch and Wilman (1936) had to be rejected. Lipson and Stokes (1942) showed that the extra reflections were consistent with a rhombohedral structure of graphite, which differs from the Bernal structure in that the stacking sequence is 1–2–3–1–2–3 . . . . Line intensities suggested that graphite was a mixture of the two structures in the following ratio: 80% Bernal, 14% rhombohedral, 6% disordered. Lukesh (1950, 1951) found furthermore that the bond angles were not quite equal

[1]Manuscript received December 18, 1957.
Contribution from Department of Mathematical Physics, University of Birmingham, Birmingham, England.
[2]Holder of a National Research Council Postdoctoral Fellowship. Now at Department of Mathematical Physics, Birmingham, England.

and that impurities introduce a superstructure with a 15-ring periodicity which could also yield extra lines. However, his conclusions were tentative, and these points have not yet been settled conclusively.

All of the effects mentioned here may be important in a complete discussion of the band structure of graphite. Here, however, we shall be concerned only with the effect of the rhombohedral modification.

Hennig (1957) has pointed out that natural graphite is a mosaic combination of the 1–2–1–2 and the 1–2–3–1–2–3 structures, the latter comprising perhaps 5–10% of the total crystal. On heat treatment, the rhombohedral structure disappears almost completely. This finding is in accord with what one expects theoretically. The binary mixture of the two graphite phases may be treated in terms of a one-dimensional Ising model (Newell and Montrell 1953). An exact solution is possible, which yields the result that one of the two phases disappears almost completely as the temperature is raised. If the crystal is then quenched, a sample of nearly pure Bernal-type graphite is obtained. Hennig (1957) pointed out that it would be possible to make samples containing an appreciable fraction of the rhombohedral structure, so that the energy bands of this structure could be investigated. Since these bands depend on the same parameters as do those of the Bernal structure, one may expect to learn something about the numerical values of these parameters, particularly about the strength of the interplanar interaction.

In the next sections we will outline a nearest-neighbor tight-binding calculation based on the $2p_z$ orbitals, in a manner completely analogous to Wallace's calculation (1947) for the Bernal structure. More detailed investigations of the Bernal structure (Coulson and Taylor 1952; Lomer 1955; Slonczewski 1955; Slonczewski and Weiss 1955, 1957; Johnston 1955, 1956; Corbato 1956) have shown that the results of Wallace (1947) for two-dimensional graphite are unaffected by a more general treatment. However, for the three-dimensional structure, a more general treatment admits the possibility of "vertical" overlap of the π-bands, while in the Wallace treatment these bands touch, but do not overlap. The fault lies in the nearest-neighbor approximation. In this approximation, the vertical edges of the Brillouin zone are lines of constant energy, a condition not required by the crystal symmetry. A variation of energy along these edges results in the vertical overlap mentioned above. By analogy, we may anticipate the manner in which the band structure of rhombohedral graphite would change if the nearest-neighbor approximation were abandoned.

2. RHOMBOHEDRAL GRAPHITE STRUCTURE AND BRILLOUIN ZONE

The crystal structure of rhombohedral graphite is shown in Fig. 1. The interlayer spacing is $c = 3.37$ Å, and the spacing between similar atoms in the same plane is $a = 2.46$ Å. The unit cell for this structure contains only two atoms. The cell we choose is shown in Fig. 1. Relative to the cartesian coordinate system shown in Fig. 1, the primitive lattice vectors may be chosen to be:

$$\boldsymbol{\tau}_1 = \left(\frac{a\sqrt{3}}{2}, \frac{a}{2}, 0\right),$$

$$\boldsymbol{\tau}_2 = \left(\frac{a\sqrt{3}}{2}, -\frac{a}{2}, 0\right),$$

$$\boldsymbol{\tau}_3 = \left(\frac{a}{\sqrt{3}}, 0, c\right).$$

The volume of the unit cell is thus

$$V_c = |\boldsymbol{\tau}_1 \cdot (\boldsymbol{\tau}_2 \times \boldsymbol{\tau}_3)| = \tfrac{1}{2}a^2c\sqrt{3}.$$

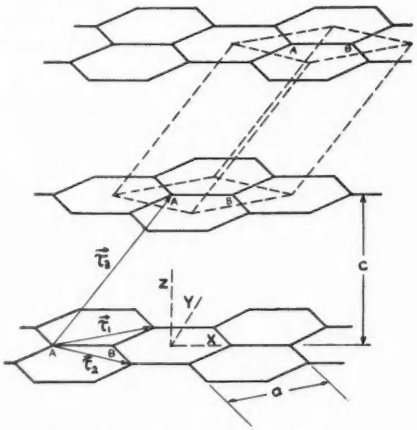

FIG. 1. Structure of rhombohedral graphite.

From the definition of the primitive vectors for the reciprocal lattice, viz.

$$\mathbf{b}_i \cdot \boldsymbol{\tau}_j = 2\pi\delta_{ij},$$

one easily finds:

$$\mathbf{b}_1 = 2\pi\left(\frac{1}{a\sqrt{3}}, \frac{1}{a}, -\frac{1}{3c}\right),$$

$$\mathbf{b}_2 = 2\pi\left(\frac{1}{a\sqrt{3}}, -\frac{1}{a}, -\frac{1}{3c}\right),$$

$$\mathbf{b}_3 = 2\pi\left(0, 0, \frac{1}{c}\right).$$

The volume of the first Brillouin zone is thus

$$V_{\mathrm{B.Z.}} = |\mathbf{b}_1 \cdot (\mathbf{b}_2 \times \mathbf{b}_3)| = 8\pi^3/V_c.$$

The surface of this zone is formed by the perpendicular bisecting planes of

the following set of vectors: $\pm\mathbf{b}_3$, $\pm\mathbf{b}_1$, $\pm\mathbf{b}_2$, $\pm(\mathbf{b}_1+\mathbf{b}_2+\mathbf{b}_3)$, $\pm(\mathbf{b}_1+\mathbf{b}_2)$, $\pm(\mathbf{b}_1+\mathbf{b}_3)$, $\pm(\mathbf{b}_2+\mathbf{b}_3)$. The resulting zone is shown in Fig. 2. The coordinates of the 24 corners of this zone are given in Table I. These corners are labelled 1 to 4 according to their k_z value. The six corners corresponding to a fixed

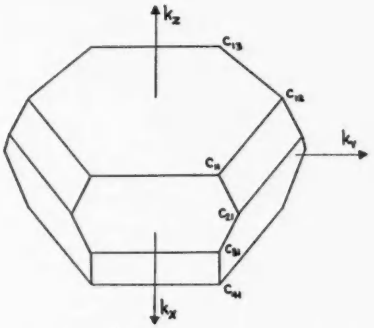

FIG. 2. Brillouin zone of rhombohedral graphite.

k_z value are counted 1 to 6 starting at the positive k_z-axis, and numbering counterclockwise. Thus, each corner has two labels; the first giving the k_z value to which it belongs, and the second giving its position relative to the k_z-axis. Some of the corners have been labelled in this manner in Fig. 2.

3. BAND STRUCTURE OF RHOMBOHEDRAL GRAPHITE

The object of a band-structure calculation is to give at least a qualitative description of the energy bands for the conduction electrons. By analogy with the Bernal structure, we may expect that the bands of interest in the rhombohedral structure are those formed by the $2p_z$ orbitals. We shall restrict our discussion to these orbitals, so that our problem will involve one electron per carbon atom and two atoms per unit cell. In particular, we shall be interested in knowing the shape of the energy surfaces near the highest energy in the first Brillouin zone, since this region corresponds to the Fermi surface. This may be seen as follows: The density of states in k-space is uniform and is given by

$$N(k)d^3k = (2V/8\pi^3)d^3k.$$

Here $V = NV_c$ is the volume of the crystal and N is the number of unit cells. The number of states in the first Brillouin zone is just $(2NV_c/8\pi^3)\times V_{\text{B.Z.}} = 2N$. Thus, there are $2N$ states in this zone, or one state per atom. It follows that at 0° K. the Brillouin zone will be just filled, so that the Fermi energy is the highest energy in this zone.

Following the usual tight-binding treatment, we choose an approximate Bloch function of the form

$$\psi = \phi_1+\lambda\phi_2, \tag{1}$$

TABLE I. COORDINATES OF THE BRILLOUIN ZONE CORNERS

Corner	k_x	k_y	k_z
C_{11}	$\frac{2\pi}{a\sqrt{3}}\left(1-\frac{a^2}{6c^2}\right)$	$\frac{2\pi}{3a}\left(1-\frac{a^2}{6c^2}\right)$	$\frac{\pi}{c}$
C_{12}	0	$\frac{4\pi}{3a}\left(1-\frac{a^2}{6c^2}\right)$	$\frac{\pi}{c}$
C_{13}	$-\frac{2\pi}{a\sqrt{3}}\left(1-\frac{a^2}{6c^2}\right)$	$\frac{2\pi}{3a}\left(1-\frac{a^2}{6c^2}\right)$	$\frac{\pi}{c}$
C_{14}	$-\frac{2\pi}{a\sqrt{3}}\left(1-\frac{a^2}{6c^2}\right)$	$-\frac{2\pi}{3a}\left(1-\frac{a^2}{6c^2}\right)$	$\frac{\pi}{c}$
C_{15}	0	$-\frac{4\pi}{3a}\left(1-\frac{a^2}{6c^2}\right)$	$\frac{\pi}{c}$
C_{16}	$\frac{2\pi}{a\sqrt{3}}\left(1-\frac{a^2}{6c^2}\right)$	$-\frac{2\pi}{3a}\left(1-\frac{a^2}{6c^2}\right)$	$\frac{\pi}{c}$
C_{31}	$\frac{2\pi}{a\sqrt{3}}\left(1+\frac{a^2}{6c^2}\right)$	$\frac{2\pi}{3a}\left(1-\frac{a^2}{6c^2}\right)$	$-\frac{\pi}{3c}$
C_{32}	$-\frac{\pi}{3a\sqrt{3}}\left(\frac{a^2}{c^2}\right)$	$\frac{4\pi}{3a}\left(1+\frac{a^2}{12c^2}\right)$	$-\frac{\pi}{3c}$
C_{33}	$-\frac{2\pi}{a\sqrt{3}}$	$\frac{2\pi}{3a}\left(1+\frac{a^2}{3c^2}\right)$	$-\frac{\pi}{3c}$
C_{34}	$-\frac{2\pi}{a\sqrt{3}}$	$-\frac{2\pi}{3a}\left(1+\frac{a^2}{3c^2}\right)$	$-\frac{\pi}{3c}$
C_{35}	$-\frac{\pi}{3a\sqrt{3}}\left(\frac{a^2}{c^2}\right)$	$-\frac{4\pi}{3a}\left(1+\frac{a^2}{12c^2}\right)$	$-\frac{\pi}{3c}$
C_{36}	$\frac{2\pi}{a\sqrt{3}}\left(1+\frac{a^2}{6c^2}\right)$	$-\frac{2\pi}{3a}\left(1-\frac{a^2}{6c^2}\right)$	$-\frac{\pi}{3c}$

Corner	k_x	k_y	k_z
C_{21}	$\frac{2\pi}{a\sqrt{3}}$	$\frac{2\pi}{3a}\left(1+\frac{a^2}{3c^2}\right)$	$\frac{\pi}{3c}$
C_{22}	$\frac{\pi}{3a\sqrt{3}}\left(\frac{a^2}{c^2}\right)$	$\frac{4\pi}{3a}\left(1+\frac{a^2}{12c^2}\right)$	$\frac{\pi}{3c}$
C_{23}	$-\frac{2\pi}{a\sqrt{3}}\left(1+\frac{a^2}{6c^2}\right)$	$\frac{2\pi}{3a}\left(1-\frac{a^2}{6c^2}\right)$	$\frac{\pi}{3c}$
C_{24}	$-\frac{2\pi}{a\sqrt{3}}\left(1+\frac{a^2}{6c^2}\right)$	$-\frac{2\pi}{3a}\left(1-\frac{a^2}{6c^2}\right)$	$\frac{\pi}{3c}$
C_{25}	$\frac{\pi}{3a\sqrt{3}}\left(\frac{a^2}{c^2}\right)$	$-\frac{4\pi}{3a}\left(1+\frac{a^2}{12c^2}\right)$	$\frac{\pi}{3c}$
C_{26}	$\frac{2\pi}{a\sqrt{3}}$	$-\frac{2\pi}{3a}\left(1+\frac{a^2}{3c^2}\right)$	$\frac{\pi}{3c}$
C_{41}	$\frac{2\pi}{a\sqrt{3}}\left(1-\frac{a^2}{6c^2}\right)$	$\frac{2\pi}{3a}\left(1-\frac{a^2}{6c^2}\right)$	$-\frac{\pi}{c}$
C_{42}	0	$\frac{4\pi}{3a}\left(1-\frac{a^2}{6c^2}\right)$	$-\frac{\pi}{c}$
C_{43}	$-\frac{2\pi}{a\sqrt{3}}\left(1-\frac{a^2}{6c^2}\right)$	$\frac{2\pi}{3a}\left(1-\frac{a^2}{6c^2}\right)$	$-\frac{\pi}{c}$
C_{44}	$-\frac{2\pi}{a\sqrt{3}}\left(1-\frac{a^2}{6c^2}\right)$	$-\frac{2\pi}{3a}\left(1-\frac{a^2}{6c^2}\right)$	$-\frac{\pi}{c}$
C_{45}	0	$-\frac{4\pi}{3a}\left(1-\frac{a^2}{6c^2}\right)$	$-\frac{\pi}{c}$
C_{46}	$\frac{2\pi}{a\sqrt{3}}\left(1-\frac{a^2}{6c^2}\right)$	$-\frac{2\pi}{3a}\left(1-\frac{a^2}{6c^2}\right)$	$-\frac{\pi}{c}$

where

$$\phi_1 = \sum_A \exp(i\mathbf{k}\cdot\mathbf{r}_A)\chi(\mathbf{r}-\mathbf{r}_A), \tag{2a}$$

$$\phi_2 = \sum_B \exp(i\mathbf{k}\cdot\mathbf{r}_B)\chi(\mathbf{r}-\mathbf{r}_B). \tag{2b}$$

In equations (2*a*) and (2*b*) the sums are over all A and B atoms, and $\chi(\mathbf{r}-\mathbf{r}_A)$ and $\chi(\mathbf{r}-\mathbf{r}_B)$ are $2p_z$ orbitals centered on A and B atoms respectively. We now substitute (1) into the Schrödinger equation

$$H\psi = E\psi. \tag{3}$$

Multiplying this equation in turn by ϕ_1^* and ϕ_2^* and integrating over all space, we find (if we neglect overlap of $2p_z$ orbitals centered on different atoms):

$$\begin{aligned} H_{11}+\lambda H_{12} &= NE, \\ H_{21}+\lambda H_{22} &= \lambda NE. \end{aligned} \tag{4}$$

In equation (4) we put:

$$H_{11} = H_{22} = \sum_{A,A'} \exp[i\mathbf{k}\cdot(\mathbf{r}_A-\mathbf{r}_{A'})] \int \chi^*(\mathbf{r}-\mathbf{r}_{A'})H\chi(\mathbf{r}-\mathbf{r}_A)d\tau, \tag{5a}$$

$$H_{12} = H_{21}^* = \sum_{A,B} \exp[i\mathbf{k}\cdot(\mathbf{r}_B-\mathbf{r}_A)] \int \chi^*(\mathbf{r}-\mathbf{r}_A)H\chi(\mathbf{r}-\mathbf{r}_B)d\tau. \tag{5b}$$

It should be pointed out that Wallace (1947) also used the relation $H_{11} = H_{22}$. Carter and Krumhansl (1953) have pointed out that, in the case of the Bernal structure, these energies are actually different by an amount of the order of γ_1, the nearest out-of-plane exchange integral. However, this observation does not apply to the rhombohedral structure, for which the relation $H_{11}=H_{22}$ is exact.

The energy resulting from equations (4), by elimination of λ, is

$$E = \frac{1}{N}H_{11} \pm \left| \frac{1}{N}H_{12} \right| . \tag{6}$$

We now perform the double sums involved in (5*a*) and (5*b*) by keeping only nearest and second-nearest neighbors in and out of the graphite planes. Consider, for instance, equation (5*a*). We fix the value of $\mathbf{r}_{A'}$ for the moment and perform the sum over A keeping only terms for which $(\mathbf{r}_A-\mathbf{r}_{A'})$ has one of the following values: 0; $\pm\boldsymbol{\tau}_1$, $\pm\boldsymbol{\tau}_2$, $\pm(\boldsymbol{\tau}_1-\boldsymbol{\tau}_2)$; $\pm\boldsymbol{\tau}_3$, $\pm(\boldsymbol{\tau}_3-\boldsymbol{\tau}_2)$, $\pm(\boldsymbol{\tau}_3-\boldsymbol{\tau}_1)$. The sum over A' then multiplies our result by N.

The various exchange integrals which occur in the above manner are listed in Table II. The notation corresponds exactly to that used by Wallace (1947). The various minus signs in Table II are convenient, in order that all γ's be positive. Keeping only the terms listed in Table II, one finds:

$$\begin{aligned} \frac{H_{11}}{N} = E_0 &- \gamma_0' \left\{ 2\cos(ak_y) + 4\cos\left(\frac{\sqrt{3}ak_x}{2}\right)\cos\left(\frac{ak_y}{2}\right) \right\} \\ &+ \gamma_1' \left\{ 2\cos\left(\frac{ak_z}{\sqrt{3}}+ck_z\right) + 4\cos\left(\frac{ak_y}{2}\right)\cos\left(\frac{ak_z}{2\sqrt{3}}-ck_z\right) \right\}, \end{aligned} \tag{7}$$

TABLE II

NEAREST AND NEXT NEAREST NEIGHBOR EXCHANGE INTEGRALS

$(\mathbf{r}_A-\mathbf{r}_{A'})$	$\int\chi^*(\mathbf{r}-\mathbf{r}_{A'})H\chi(\mathbf{r}-\mathbf{r}_A)d\tau$
0	E_0
$\pm\boldsymbol{\tau}_1,\ \pm\boldsymbol{\tau}_2,\ \pm(\boldsymbol{\tau}_1-\boldsymbol{\tau}_2)$	$-\gamma_0'$
$\pm\boldsymbol{\tau}_3,\ \pm(\boldsymbol{\tau}_3-\boldsymbol{\tau}_1),\ \pm(\boldsymbol{\tau}_3-\boldsymbol{\tau}_2)$	γ_1'
$(\mathbf{r}_B-\mathbf{r}_A)$	$\int\chi^*(\mathbf{r}-\mathbf{r}_A)H\chi(\mathbf{r}-\mathbf{r}_B)d\tau$
$\frac{1}{3}(\boldsymbol{\tau}_2-2\boldsymbol{\tau}_1)$, $\frac{1}{3}(\boldsymbol{\tau}_1+\boldsymbol{\tau}_2)$, $\frac{1}{3}(\boldsymbol{\tau}_1-2\boldsymbol{\tau}_2)$	$-\gamma_0$
$\frac{1}{3}(\boldsymbol{\tau}_1+\boldsymbol{\tau}_2)-\boldsymbol{\tau}_3$	γ_1
$\frac{1}{3}(\boldsymbol{\tau}_1-2\boldsymbol{\tau}_2)+\boldsymbol{\tau}_3$, $\frac{1}{3}(\boldsymbol{\tau}_2-2\boldsymbol{\tau}_1)+\boldsymbol{\tau}_3$, $-\frac{2}{3}(\boldsymbol{\tau}_1+\boldsymbol{\tau}_2)+\boldsymbol{\tau}_3$	γ_1'

$$(8)\quad \frac{H_{12}}{N} = -\gamma_0\left\{\exp\left(\frac{iak_x}{\sqrt{3}}\right)+2\exp\left(-\frac{iak_x}{2\sqrt{3}}\right)\cos\left(\frac{ak_y}{2}\right)\right\}$$
$$+\gamma_1'\left\{\exp\left(-\frac{iak_x}{\sqrt{3}}\right)+2\exp\left(\frac{iak_x}{2\sqrt{3}}\right)\cos\left(\frac{ak_y}{2}\right)\right\}+\gamma_1\exp(-ick_z).$$

The inclusion of the γ_1' term presents no difficulty, but greatly complicates the analytical form of the $E(k)$ relation. From now on, we shall ignore this term completely. It may be shown that the inclusion of this term would not alter our basic conclusions about the energy surfaces near the Fermi level. Equation (6) then becomes

$$(9)\quad E(\mathbf{k}) = E_0-\gamma_0'\left\{2\cos(ak_y)+4\cos\left(\frac{\sqrt{3}ak_x}{2}\right)\cos\left(\frac{ak_y}{2}\right)\right\}$$
$$\pm\left[\gamma_0^2\left\{1+4\cos^2\left(\frac{ak_y}{2}\right)+4\cos\left(\frac{ak_y}{2}\right)\cos\left(\frac{\sqrt{3}ak_x}{2}\right)\right\}\right.$$
$$\left.+\gamma_1^2-2\gamma_1\gamma_0\left\{\cos\left(\frac{ak_x}{\sqrt{3}}+ck_z\right)+2\cos\left(\frac{ak_y}{2}\right)\cos\left(\frac{ak_x}{2\sqrt{3}}-ck_z\right)\right\}\right]^{\frac{1}{2}}.$$

The minus sign applies to the inside of the first Brillouin zone (valence band). The energy at various points in the Brillouin zone may now be computed from equation (9). Consider, for example, the energy at the center of the zone, O. Putting $k_x = k_y = k_z = 0$, one easily finds:

$$E(O) = E_0-6\gamma_0'\pm[3\gamma_0-\gamma_1].$$

In a similar manner, the energy at each of the 24 zone corners is

$$E(C) = E_0+2.865\gamma_0'\pm[0.3375\gamma_0+\gamma_1].$$

We may also evaluate the energy at the center of each of the 14 faces of the Brillouin zone. Denoting these points by F_R, F_{RH}, F_{IH} depending on whether the face in question is a rectangle, a regular hexagon, or an irregular hexagon respectively, we find for the energies at these points:

$$E(F_R) = E_0+2\gamma_0'\pm[\gamma_0+\gamma_1] \qquad \text{(six faces)},$$
$$E(F_{RH}) = E_0-6\gamma_0'\pm[3\gamma_0+\gamma_1] \qquad \text{(two faces)},$$
$$E(F_{IH}) = E_0+2\gamma_0'\pm[\gamma_0-\gamma_1] \qquad \text{(six faces)}.$$

The significant feature of these results is that the two π-bands are separated by an energy of the order of γ_0. None of these points in k-space are of great interest, since they do not correspond to the highest valence band energy. This maximum energy is principally determined by the magnitude of H_{12}, which should be as small as possible. In order to discuss the $E(k)$ relation near the maximum valence band energy, it is convenient to introduce a volume in k-space which is bounded by a hexagonal cylinder whose height and volume are equal to the height and volume of the Brillouin zone shown in Fig. 2. The edges of this cylinder are given by:

$$\epsilon_1 = \left(\frac{2\pi}{a\sqrt{3}}, \frac{2\pi}{3a}, k_z\right), \qquad \epsilon_2 = \left(0, \frac{4\pi}{3a}, k_z\right),$$
$$\epsilon_3 = \left(\frac{-2\pi}{a\sqrt{3}}, \frac{2\pi}{3a}, k_z\right), \qquad \epsilon_4 = \left(\frac{-2\pi}{a\sqrt{3}}, \frac{-2\pi}{3a}, k_z\right),$$
$$\epsilon_5 = \left(0, \frac{-4\pi}{3a}, k_z\right), \qquad \epsilon_6 = \left(\frac{2\pi}{a\sqrt{3}}, \frac{-2\pi}{3a}, k_z\right).$$

From Table I it is easily seen that the actual Brillouin zone would go over into this hexagonal cylinder if all a^2/c^2 terms were neglected (i.e. in the limit $c \to \infty$). Let us now evaluate the $E(k)$ relation at the edges ϵ of this hexagonal cylinder. It is readily shown that the energy along these edges is independent of k_z and is given by

$$E(\epsilon) = E_0+3\gamma_0'\pm\gamma_1.$$

Since $\gamma_0 \gg \gamma_0', \gamma_1$, this is by far the highest V-band (and lowest C-band) energy found so far. However, there is still an energy gap between these bands equal to $2\gamma_1$. The question now arises whether there are any points in the Brillouin zone where the gap is zero (i.e. $H_{12} = 0$). An exact solution of the relation $H_{12} = 0$ shows that there are such points, and that they lie very near the edges ϵ of our hexagonal cylinder. We may therefore find these touching points by expanding the $E(k)$ relation about the edges ϵ. We put:

$$k_x = k_x^{\epsilon}+K_x, \qquad k_y = k_y^{\epsilon}+K_y, \qquad k_z = K_z.$$

Furthermore, we shall use the notation of McClure (1957) and put:

$$\tfrac{1}{2}\sqrt{3}a[K_x^2+K_y^2]^{\frac{1}{2}} = \tfrac{1}{2}\sqrt{3}a|K| = \sigma,$$
$$K_y/|K| = \sin\alpha, \qquad K_x/|K| = \cos\alpha, \qquad K_z c = \xi, \qquad \gamma_1/\gamma_0 = \beta.$$

Energy will be measured from the point $E_0+3\gamma_0'$, so that we put $E_0+3\gamma_0' = 0$. By expanding equation (9) in the indicated manner for each of the edges $\epsilon_i (i = 1, 2, \ldots 6)$, one finds:

$$(10a) \qquad E_{\epsilon_i}(\sigma, \alpha, \xi) = \pm\gamma_0[\sigma^2+\beta^2+2\beta\sigma\cos(\xi-\alpha+\phi_i)]^{\frac{1}{2}} \qquad (i = 1, 3, 5),$$

$$(10b) \qquad E_{\epsilon_i}(\sigma, \alpha, \xi) = \pm\gamma_0[\sigma^2+\beta^2+2\beta\sigma\cos(\xi+\alpha+\phi_i)]^{\frac{1}{2}} \qquad (i = 2, 4, 6).$$

In these relations, ϕ_i is a phase angle which is different at each edge: $\phi_1 = \pi/6$, $\phi_3 = 5\pi/6, \phi_5 = 3\pi/2; \phi_2 = -\pi/2, \phi_4 = -7\pi/6, \phi_6 = \pi/6$. It is easily verified that only that portion of our hexagonal cylinder for which

$$-\tfrac{1}{3}\pi \leqslant \xi \leqslant +\tfrac{1}{3}\pi$$

lies within the first Brillouin zone.

From equations (10*a*) and (10*b*), we see that the bands will actually touch near $\sigma = 0$, but only in special directions (fixed α). The condition for touching bands is

$$\sigma^2+\beta^2+2\beta\sigma\cos\theta = 0, \tag{11}$$

where θ is any one of the angles $\xi \pm \alpha + \phi_i$. Solving for σ, we find:

$$\sigma = -\beta e^{\pm i\theta}. \tag{12}$$

For a physical solution, we require that:

$$\sigma = \text{real}, \qquad \sigma \geqslant 0,$$

which implies that

$$\theta = \pi, \qquad \sigma = \beta. \tag{13}$$

For any ξ in the range $-\frac{1}{3}\pi \leqslant \xi \leqslant \frac{1}{3}\pi$ the bands touch at six points in the Brillouin zone. These touching points lie on six cylinders whose axes are the edges ϵ_i and whose radii are $\sigma = \beta$. The loci of these touching points are shown in Fig. 3.

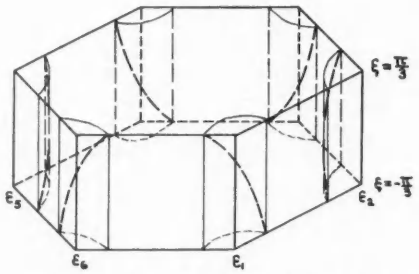

FIG. 3. Lines along which the two π-bands touch. The lines lie on cylinders $\sigma = \beta$, whose axes are the edges ϵ_i. (The drawing is not to scale.)

It may also be verified that the energy contours in a plane ξ = constant are circular about the touching point. If $\tilde{\sigma}$ is σ measured from the touching point instead of from an edge ϵ_i, one finds:

$$E_{\xi=\text{const}}(\tilde{\sigma}) = \pm\gamma_0\tilde{\sigma} = \pm\tfrac{1}{2}\sqrt{3}a\gamma_0|K-K_0|. \tag{14}$$

In equation (14), K_0 denotes the K corresponding to the touching point. Typical constant-energy contours for such a plane of constant ξ are shown in Fig. 4. The broken circles in Fig. 4 represent the cylinders $\sigma = \beta$. As ξ changes, the energy contours move along the broken lines (cf. Fig. 3).

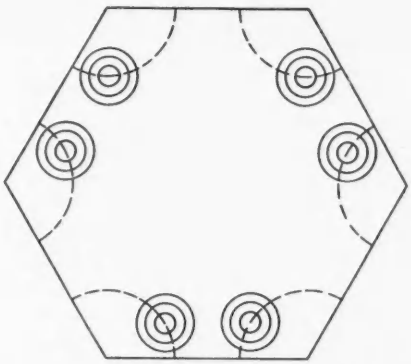

FIG. 4. Typical energy contours in a plane ξ = constant. Broken lines denote the cylinders $\sigma = \beta$. (The drawing is not to scale.)

4. DISCUSSION

The band structure of rhombohedral graphite which emerges from this simple calculation is surprisingly complex. The two π-bands still touch, as they do in two-dimensional graphite or in Bernal-type graphite in this approximation (Wallace 1947). However, the touching does not occur at points of special symmetry of the zone. In fact, one sees from equation (13) that it is the value of the exchange integral γ_1 and not any condition of symmetry which determines the location of the touching point. For a non-zero value of γ_1, the energy contours for energies near zero are highly warped cylinders, whose axes are the loci of the touching points (cf. Fig. 3). The warping becomes more and more severe as γ_1 is chosen larger and larger. For $\gamma_1 = 0$ the warping disappears and the energy contours are regular cylinders whose axes are the edges ϵ_i, as in the case of two-dimensional graphite. The energy surfaces for $E \gg \gamma_1$ also display only a slight warping.

It seems that the complexity of this band structure may furnish a useful criterion for the magnitude of γ_1. Consider first a sample of rhombohedral graphite for which $E_F \ll \gamma_1$. Let us see what we may expect to be the result of a de Haas – Van Alphen effect measurement in this case. The periods of the susceptibility fluctuations are a measure of the areas of cross-section of the constant energy surface $E = E_F$ and a plane perpendicular (in k-space) to the direction of the applied magnetic field. If the magnetic field is applied along the c-axis in graphite, one period will be observed in the de Haas – Van Alphen effect, since the six cross-sectional areas in question are all equal and correspond to circular disks (cf. equation (14)). However, if the magnetic field is tilted away from the c-axis, six different periods will result, because of the warping of the energy surfaces.

Consider next a sample for which $E_F \gg \gamma_1$. In this case, the warping of the surfaces is very much less severe, so that essentially one period (i.e. six very nearly equal periods) will result in the de Haas – Van Alphen effect, for any orientation of the magnetic field (the period will of course be a function

of the direction of the field, but for any direction, only one period is present). If we may assume that the relative magnitudes of E_F and γ_1 are the same for rhombohedral graphite as for Bernal-type graphite, then the case of $E_F \ll \gamma_1$ corresponds to the McClure model of graphite (McClure 1957), while the case of $E_F \gg \gamma_1$ corresponds to the model of Haering and Wallace (1957). Actually, the model of McClure (1957) involves holes as well as electrons, owing to the "vertical" overlap mentioned in Section 1. If such overlap were accounted for in the present calculation, we would expect that the loci of the touching points (cf. Fig. 3) would no longer be lines of constant energy. This alteration does not markedly affect the above argument, which is based solely on the warping of the surface. The presence of holes as well as electrons would however increase the number of distinct oscillations to be expected (but equally for all orientations of the field).

We conclude that a measurement of the de Haas – Van Alphen effect of rhombohedral graphite as a function of orientation of the magnetic field could yield in a convincing manner the relative magnitudes of E_F and γ_1.

ACKNOWLEDGMENTS

The author would like to thank Dr. G. Hennig, Dr. J. R. Schrieffer, and Professor R. E. Peierls for stimulating discussions. The financial assistance of the National Research Council in the form of a postdoctoral fellowship is gratefully acknowledged.

REFERENCES

BERNAL, J. D. 1924. Proc. Roy. Soc. (London), A, **106**, 749.
CARTER, J. L. and KRUMHANSL, J. A. 1953. J. Chem. Phys. **21**, 2238.
CORBATO, F. J. 1956. Quarterly Progress Report, Solid State and Molecular Theory Group, Mass. Inst. Technol., No. 21, p. 23.
COULSON, C. A. and TAYLOR, R. 1952. Proc. Phys. Soc. A, **65**, 815.
FINCH, G. I. and WILMAN, H. 1936. Proc. Roy. Soc. (London), A, **155**, 345.
HAERING, R. R. and WALLACE, P. R. 1957. J. Phys. Chem. Solids, **3**, 253.
HENNIG, G. 1957. Private communication.
JOHNSTON, D. F. 1955. Proc. Roy. Soc. (London), A, **227**, 349.
——— 1956. Proc. Roy. Soc. (London), A, **237**, 48.
LIPSON, H. and STOKES, A. R. 1942. Proc. Roy. Soc. (London), A, **181**, 101.
LOMER, W. M. 1955. Proc. Roy. Soc. (London), A, **227**, 330.
LUKESH, J. S. 1950. Phys. Rev. **80**, 226.
——— 1951. J. Chem. Phys. **19**, 383.
MCCLURE, J. W. 1957. Tech. Memorandum TM 253, National Carbon Research Labs., Parma, Ohio.
NEWELL, G. F. and MONTRELL, E. W. 1953. Revs. Modern Phys. **25**, 353.
SLONCZEWSKI, J. C. 1955. Ph.D. Thesis, Rutgers University, New Brunswick, N.J.
SLONCZEWSKI, J. C. and WEISS, P. R. 1955. Phys. Rev. **99**, 636.
——— 1957. Phys. Rev. (To be published).
TAYLOR, A. and LAIDLER, D. 1940. Nature, **146**, 130.
WALLACE, P. R. 1947. Phys. Rev. **71**, 622.

MECHANICAL STRENGTH OF ICE FROZEN FROM AN IMPURE MELT[1]

E. R. POUNDER

ABSTRACT

Ice frozen from a melt containing a small amount of a light alcohol, ketone, or ether is much weaker than normal ice, for a limited freezing exposure. The weakening effect is enhanced if the melt also contains traces of one or more of a variety of long-chain, organic substances, one of the most effective being sodium carboxymethyl cellulose. Inorganic salts, on the other hand, appear to be largely ineffective and may even cancel out the weakening action of the organic solvent. It is suggested that the organic additives are concentrated in the surface of the melt and remain as liquid layers between the ice crystals, thereby causing a large reduction in the shear strength of the ice sheet. Adsorption at the surface is discussed as a mechanism for concentrating organic substances in the surface layer and rejecting inorganic salts into the interior of the solution.

INTRODUCTION

When a solid is grown from a melt containing traces of impurities, it is well known that the crystal structure of the solid and its mechanical, electrical, and other physical properties may depend strongly on the nature and concentration of the impurities in the melt. In the case of ice, Truby (1955) has shown that one fluorine ion per 5×10^4 water molecules alters the microstructure of the ice drastically. Smith-Johannsen (1946) measured the adhesion of ice frozen on to a waxed aluminum plate from 10^{-3} molar solutions of various salts. He found values for the adhesion ranging from 4250 for distilled water through 1300 for magnesium chloride solution down to less than 100 for solutions of strontium chloride and other salts, values of adhesion being quoted in grams per square centimeter.

Moesveld (1934, 1937) showed that if minute quantities of certain organic materials having long carbon chains were added to the surface of still water as it was starting to freeze, the resulting ice consisted of largely non-coherent crystals so that the shear strength of the ice sheet was negligible. He reported that the most effective chemical additives were sodium and ammonium salts of stearic and alginic acids and mixtures of these salts.

Inorganic salts, particularly chlorides of calcium and sodium, have been used for many years to combat icing problems but since the useful property of these salts is the depression of the freezing point the quantities which must be employed are large. In addition, the corrosive properties of salt solutions (which need not be stressed to anyone driving a car in Montreal) virtually rule out their use in connection with aircraft. The use of organic additives offered possibilities of the need for smaller quantities of anti-icing material and freedom from corrosion problems, and this study was undertaken to confirm and if possible extend the investigation of Moesveld.

[1]Manuscript received October 24, 1957.
Contribution from the Ice Research Project, Department of Physics, McGill University, Montreal, Quebec.

METHOD

Numerous freezing tests were carried out in a commercial deep-freeze unit which could be set to temperatures in the range $-5°$ to $-30°$ C. The temperature in the box was measured with a resistance thermometer and it was found that the actual temperature varied within a range of about two degrees on either side of its mean value, as the refrigeration equipment cycled under the control of its thermostat. Freezing was carried out in glass or plastic tanks, insulated on the bottom and sides with 1 in. of a foamed plastic with a thermal conductivity $K = 0.25$ B.t.u./ft.^{2}/hr./° F./in. For the freezing times involved, this insulation ensured that heat transfer was virtually limited to the top surface of the water or ice, as in the freezing of natural bodies of water.

The normal procedure was as follows. The substance being tested was dissolved in water or in water and alcohol. The freezing tank was partially filled with distilled water and placed in the freezer to cool, the water being stirred frequently until it was at a uniform temperature below 4° C. but with no ice present. A quantity of the solution was then sprayed uniformly over the surface of the water from a plastic squeeze-bottle. Several polyethylene rings of 10 cm. internal diameter were placed in the tank, resting on the bottom and projecting slightly above the surface. The tank was then allowed to freeze for the desired exposure, usually from 40 to 100 degree-hours. The exposure was calculated as the product of ambient temperature in the freezer (degrees Celsius below zero) multiplied by the time the tank was left in the freezer after the solution was added.

When the tank was removed from the freezer, the disks of ice contained in the polyethylene rings could be removed easily from the tank and tested. The thickness of the disks ranged from about 5 mm. to 1.5 cm., depending on both the exposure and the nature of the additives used. Each disk was placed centrally on a padded ring stand with an internal diameter of 5 cm. A padded brass pin of area 10 cm.^{2} was placed on the center of the disk and loaded with a lever arrangement until the ice broke. The loading pressure for fracture of the ice (P_F) was used to compare samples. It is a satisfactory relative measure of strength, but is difficult to relate to the ultimate tensile and shear strengths. For any series of tests the degree-hours of freezing must, of course, be held constant. Despite the relatively large area of the loading pin relative to the ice sample, fracture patterns observed were typical of those found when a "point" load is applied to an infinite sheet of ice. Fig. 1 is a photograph of the assembled pieces of a disk which had been fractured. It will be noted that most of the breaks occur along radial lines. With some of the weaker ices, as the load increased the first crack was a rough circle centered about the point of application of the load. A small increase in load then resulted in complete failure, again along radial lines.

RESULTS

Initially, freezing tests were carried out using solutions of various chemicals in water only. The tests were of two types: volume tests in which the additive

PLATE I

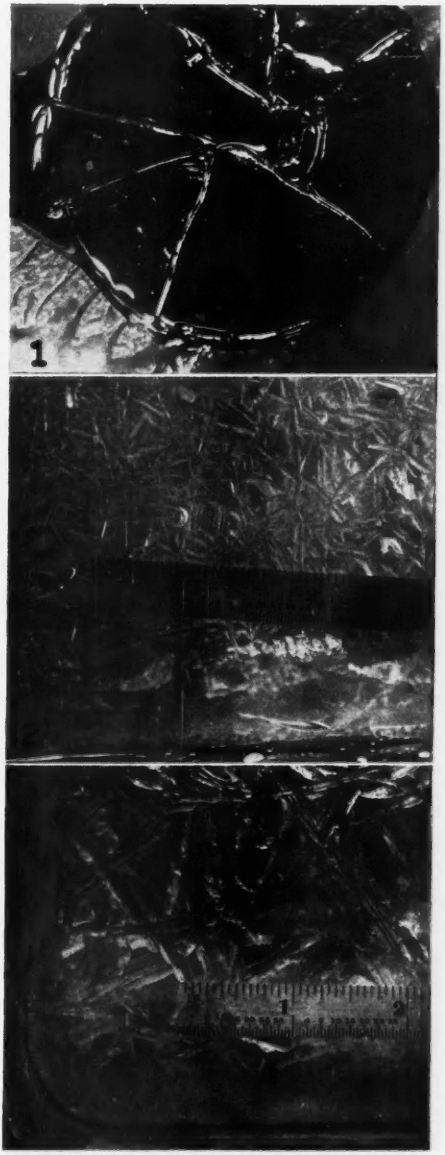

FIG. 1. Fracture pattern of a disk of ice loaded centrally.
FIG. 2. Lower surface of ice sheet containing alcohol and soluble starch.
FIG. 3. Lower surface of ice sheet containing alcohol, polyvinylmethyl ether, and sodium carboxymethyl cellulose.

was dispersed uniformly throughout the volume of the water before freezing, and "surface" tests in which a technique, described under *Method* above, was used to ensure a maximum concentration of the additive in the surface layer of the water. For a given quantity of additive, the surface tests were from two to five times as effective in reducing the strength of the ice, showing clearly that we are dealing with a surface phenomenon. Results were disappointing with water solutions, the resulting ice being at best only 30% weaker than pure ice. However, it was found that traces of alcohol (of the order of 5 milliliters of ethyl alcohol applied to a surface of 800 cm.^{2}), either by itself or in combination with other additives, gave extremely weak ice. In some cases the strength was less than 10% of that of normal ice.

Table I lists the results of a series of tests. One gram of each additive was dissolved in 75 ml. of water and 25 ml. of industrial ethyl alcohol. Twenty milliliters of the resulting solution was sprayed on a tank of surface area 800 cm.^{2} and containing 2.5 liters of distilled water. The concentration of additives was thus 2.5 g. of solid and 50 g. of ethyl alcohol per square meter of surface. In all cases the freezing exposure was 60 degree-hours at an ambient

TABLE I

FRACTURE LOADING PRESSURES OF IMPURE ICE

Additive in 25% alcohol solution	P_F	Average % deviation
Pure water (no alcohol)	1.000	9
20 ml. of 25% C_2H_5OH	0.263	18
20 ml. LiCl	0.139	15
20 ml. methyl cellulose	0.180	8
10 ml. sodium stearate + 10 ml. PVM	0.185	0
10 ml. PVM + 10 ml. D-235	0.185	16
20 ml. T-253	0.202	18
20 ml. PVM	0.211	17
20 ml. ethyl cellulose	0.221	12
10 ml. sodium stearate + 10 ml. D-235	0.224	6
10 ml. PVM + 10 ml. L-245	0.255	20
20 ml. soluble starch	0.262	5
10 ml. sodium stearate + 10 ml. agar–agar	0.275	6
10 ml. soluble starch + 10 ml. D-235	0.288	3
20 ml. sodium stearate	0.302	29
20 ml. agar–agar	0.325	29
10 ml. sodium stearate + 10 ml. sodium alginate	0.345	28

temperature of −25° C. This resulted in ice sheets of thickness 7 mm. for pure water and about 8 to 10 mm. for various additives. The first column of the table lists the additives used. The abbreviations D-235, L-245, and T-253 refer to grades of Carboxel, the trade name used by Chemical Developments of Canada, Ltd., for sodium carboxymethyl cellulose. PVM is an abbreviation for polyvinyl methyl ether. In the second column, the average value of P_F, the loading pressure for fracture, is listed after being normalized to unity for pure ice. Each figure is the average of from 2 to 10 measurements and the third column gives the average percentage deviation from this average value, as a measure of the reproducibility of the tests.

The appearance of the impure ice differs greatly from that of natural ice. Pure ice is clear and glassy with perfectly smooth top and bottom surfaces. The impure ice is opaque and the top surface slightly roughened, but the most striking difference is in the bottom surface, which is irregular and often covered with stalactites and ridges of clear ice, ranging in horizontal length up to an inch or more. The ridges show no preferred orientation in either vertical or horizontal planes. They sometimes form irregular polygons bounding empty spaces in the ice which extend almost to the top surface. Figs. 2 and 3 show two examples. Fig. 2 is a photograph of the lower surface of ice grown from a melt containing alcohol and soluble starch, whereas the additives in Fig. 3 were alcohol, PVM, and L-245. A polariscopic study of crystal sizes and orientations will be reported in a later paper.

All the additives listed in Table I are organic compounds with the exception of lithium chloride. The peculiar effect of the lithium chloride was discovered in a series of freezing tests carried out with a variety of inorganic salts as additives, both in aqueous and ethyl alcohol solutions. These tests were undertaken to see if there was any correlation between the reduction of adhesion reported by Smith-Johannsen (1946) and cohesive strength as measured here. No correlation was found. The concentration of the salts used (various chlorides, nitrates, and acetates) was 6.2 g. per square meter of surface, some five times greater than in the tests summarized in Table I. In aqueous solution, lithium chloride reduced the strength of the ice by some 20%, whereas the other salts had little effect, if anything usually increasing the strength slightly. Similar results were obtained with alcohol solutions. Lithium chloride reduced the strength sharply to about half of the strength obtained with alcohol as the only additive, whereas the other salts had little effect or increased the strength.

Other variables investigated were concentration of additives, variation of exposure for a fixed ambient temperature, variation of ambient temperature for a fixed exposure, and the effect of substituting various organic solvents for the alcohol.

To investigate the effect of concentration, equal weights of PVM and D-235 were dissolved in a mixture of 75% water and 25% ethyl alcohol (by volume) in the proportion of 1 g. of solids to 100 ml. of solvent. Varying amounts of this solution were added to distilled water and frozen for 60 degree-hours in each test. Fig. 4 shows the variation of fracture loading pressure with concentration, in milliliters of added solution. Curve A gives the results obtained when the additives were concentrated in the surface and Curve B when they were diluted uniformly throughout the volume of the freezing tank. The experimental spread of values is indicated by the lengths of the vertical lines.

Using the same stock solution described in the last paragraph, a series of surface tests were made for different exposures. Five milliliters of the solution was added to the water and the tank was allowed to freeze at an ambient temperature of $-25°$ C. Results are shown in Fig. 5. Curve A is a plot of relative fracture loading pressure vs. exposure, normalized so that unity gives

the strength of a sheet of ice formed from pure water in 60 degree-hours, and curve B shows the way in which ice thickness varies with time. Note that logarithmic scales have been used in this figure. Experimental spreads have

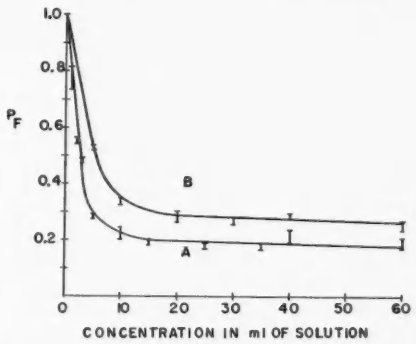

FIG. 4. Loading pressure for fracture as a function of concentration of additives. Curve A, surface concentration. Curve B, volume dilution.

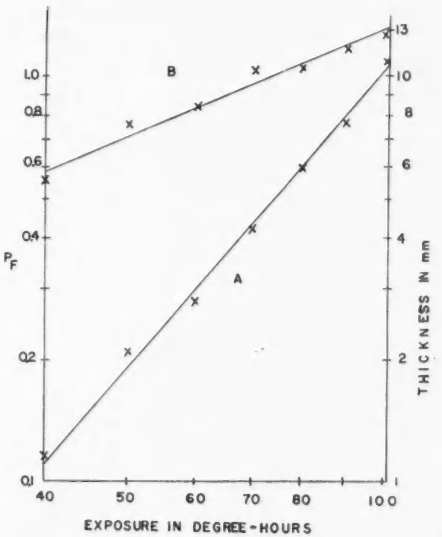

FIG. 5. Effect of freezing exposure. Curve A, fracture loading pressure. Curve B, thickness of ice sheet.

not been shown but are comparable with those in Fig. 4. Thickness could not be measured very accurately because of the unevenness of the lower surface of the ice sheets. If we let E stand for the exposure in degree-hours

and t for ice thickness, the data of Fig. 5 can be represented by the approximate equations

$$P_F = aE^{2.4}, \qquad t = bE^{0.82},$$

where a and b are constants. The simplest theoretical expression for the rate of ice thickening is $t \propto E^{0.5}$. An empirical equation frequently used is

$$(t^2 + \tfrac{1}{2}t) \propto E.$$

The index of 0.8 obtained here shows that this highly artificial ice thickens considerably more rapidly than ice frozen from pure water.

A series of tests was made in which both pure water and water containing additives were frozen for a fixed exposure but at various ambient temperatures. The results indicated a very slight reduction of strength as the ambient temperature was increased. The reduction was only slightly greater than the uncertainty of the experimental measurements so the only conclusion to be drawn is the fairly obvious one that exposure is the major factor in determining the strength of the ice sheet grown from a given melt.

Finally, a series of solutions was prepared in which 1 g. of D-435 (a grade of sodium carboxymethyl cellulose very similar to D-235) was dissolved in 75 ml. of distilled water and mixed with 25 ml. of various organic solvents. "Surface" freezing tests were then made with 25 ml. of the resulting solution added to 2.5 liters of distilled water and frozen for 45 degree-hours in a cold room at −15° C. Results are shown in Table II.

TABLE II

FRACTURE LOADING PRESSURE AND PROPERTIES OF LIQUID ADDITIVES

Additive	Relative P_F	Melting point in °C.	Boiling point in °C.	Specific gravity
Pure ice	1.000			
D-435 alone	0.750			
Methyl alcohol	0.062	−98	65	0.792
Ethyl alcohol	0.093	−114	78	0.789
Isopropyl alcohol	0.065	−90	82	0.785
n-Propyl alcohol	0.143	−127	97	0.804
Isobutyl alcohol	0.162	−108	108	0.802
Ethyl ether	0.168	−116	35	0.708
Isopropyl ether	0.475	−60	69	0.725
n-Butyl ether	0.647	−98	142	0.773
Acetone	0.114	−95	56	0.791
Methyl ethyl ketone	0.060	−87	80	0.805
n-Heptane	1.01	−91	98	0.684
Ethylene glycol	0.378	−16	198	1.113
Methylene chloride	0.374	−97	40	1.336

DISCUSSION

Any foreign matter dissolved in water reduces the freezing point of the solution below that of pure water. The reduction is proportional to the number of "particles" (molecules or ions) present per unit volume. For equal masses

of organic and inorganic materials, the latter usually produce much greater lowering of the freezing point because of, firstly, their normally much lower molecular weights and, secondly, their high degree of dissociation in aqueous solution. For the concentrations of additives used in this experiment the over-all lowering of the freezing point is, at most, a small fraction of a degree but, on a microscopic scale, if a mechanism exists for concentrating the additives then it is possible for pockets or layers of solution to exist whose freezing point is lower than the temperature of the surrounding ice.

It is a known property of ice that a growing crystal rejects impurities. Hence when two crystals grow towards each other the layer of liquid between them becomes a concentration layer for impurities. It is suggested that the reduction in strength of ice sheets observed in these experiments results from the presence of liquid layers separating crystals and permitting them to slide fairly readily with respect to each other. These intercrystalline layers must usually be of microscopic thickness, although occasionally regions develop in the ice sheet, below the thin surface crust, in which evidently the melt contains too high a concentration of additives to freeze. These pockets may be several millimeters across and can be seen in Fig. 3.

If this suggestion is valid we must look for an explanation of the ineffectiveness of inorganic salts relative to organic materials in weakening ice. A mechanism for concentrating organic impurities in the surface and inorganic impurities in the body of the solution is known to exist. Adam (1941) discusses adsorption on liquid surfaces and points out that "organic substances with more than two carbon atoms for each soluble group in the molecule usually show marked positive adsorption", i.e. tend to concentrate in the surface layer. Inorganic salts usually show negative adsorption. Adsorption phenomena are explained in terms of strength of intermolecular forces. Aqueous solutions of inorganic salts have a surface tension greater than that of water so the forces of attraction on the salt molecules or ions must be greater than those on the water molecules. Hence intermolecular forces tend to draw the salt into the interior. An illustration is the freezing of salt water. When normal sea water of salinity 35 parts per thousand is frozen the resulting ice has a salinity of only about 4 parts per thousand.

Organic compounds usually lower the surface tension and hence are concentrated in the surface. The technique of applying the additives in the "surface" tests tended to enhance this concentration. The water was cooled to its maximum density before adding the solution, which in most cases had a density less than that of the water. This is probably part of the explanation for the effectiveness of alcohol as an additive. In addition, because of its low freezing point the alcohol must aid greatly in the formation of the intercrystalline liquid layers. The tests summarized in Table II were undertaken to try to sharpen the understanding of the role of the alcohol. Tests were made using two or more members of the homologous series of alcohols, ethers, and ketones plus a few assorted organic solvents. A few conclusions can be drawn. The liquid organic additive should be soluble in water—*n*-heptane, which is virtually insoluble in water, had no weakening effect at all and the

ethers, which have limited solubility, were the least effective class of the solvents tried. The alcohols and ketones appear to be of the same order of effectiveness in weakening ice. Within a homologous series, there is a definite decrease in strength reduction of ice as one goes to higher members of the series. The reversal of this generalization for the two ketones is probably caused by the high vapor pressure of acetone, which may well evaporate in large part before the ice sheet forms to trap it. Isopropyl alcohol appears to behave anomalously, and the large difference obtained with the iso and normal forms of this alcohol is interesting. In this connection it is worth mentioning that the number of samples of ice tested in preparing Table II was small (in most cases only two for each solvent) and that the general experience in the experiments reported in this paper is one of poor reproducibility. Samples prepared, frozen, and tested under apparently identical conditions sometimes show deviations of up to 50% in the results. Individual results in Table II might thus be modified if more extensive testing is done, but it is felt that the trends indicated are reliable.

These experiments were supported by the Defence Research Board of Canada through D.D.P. contracts C.69-10-157 and C.69-700102. The assistance of P. Protopapas and F. G. J. Perey in performing some of the measurements is gratefully acknowledged. Mr. H. O. Stahl, formerly of Chemical Developments of Canada, Ltd., kindly suggested and supplied some of the chemicals used.

REFERENCES

ADAM, N. K. 1941. The physics and chemistry of surfaces, 3rd ed. (Oxford University Press, London), p. 106 et seq.

MOESVELD, A. L. T. 1934. Chem. Weekblad, **31**, 170.

——— 1937. Canadian Patent No. 367,852.

SMITH-JOHANNSEN, R. 1946. Report 5539 of General Electric Co. to USAAF (Contract W33-038AC-9151), p. 149.

TRUBY, F. K. 1955. J. Appl. Phys. **26**, 1416.

NOTE ON THE FORCED AND DAMPED OSCILLATOR IN QUANTUM MECHANICS[1]

EDWARD H. KERNER

ABSTRACT

The wave equations for the forced, damped, and forced and damped oscillators are solved in closed form for an arbitrary forcing function; the solutions produced being in one-to-one correspondence with the stationary states of the unforced, undamped Hamiltonian H_0. The quantal motion is closely connected with the classical: for the forced oscillator the probability density is that of H_0 but moves as a whole with the classical motion; for the forced and damped oscillator this motion is accompanied by a contraction progressing eventually into a delta function at the classical position. Transition probabilities between states of H_0 are computed in the case of forced motion and depend solely on the classically acquired energy of the oscillator at any time. The transition probability vanishes strictly only when this energy has a value falling at the roots of a Laguerre polynomial associated with the transition. The classical dipole radiation emitted by a disturbed oscillator is, when the damping force is identified with the force of radiation damping, that of the classical oscillator: a shifted and broadened line.

INTRODUCTION

The customary development of perturbation theory for time-varying perturbations ordinarily leaves unanswered the question of the long-time behavior of the perturbed system. Even supposing a perturbation calculation to be carried out to any desired order of accuracy, there remains the serious problem of the convergence of the calculation, about which little seems to be understood. We should like here to sketch the rigorous solution of the quantum motion of an oscillator exposed to an arbitrary time-varying external force. Special though the oscillator is, one may hope from a full knowledge of a simple problem to learn something of the nature of the answers to the more general questions posed above, or perhaps to replace these questions by more relevant ones. It will appear below, for example, that the effect of a perturbing force is intimately related to the corresponding classical motion, and it is not at all clear that discussing the perturbation in terms of transition probabilities between unperturbed states is in general very illuminating.

Additionally it will be pointed out how the motion of the damped and simultaneously forced and damped oscillator may be solved. We shall have altogether a little isomorphism of the simple classical motions that are so instructive and their equally simple quantal counterparts. Our object will be principally mathematical for the present, namely to demonstrate techniques for managing the wave equation; in another report it is planned to work out illustrative examples and physical consequences in greater detail.

[1]Manuscript received October 17, 1957.
Contribution from the Physics Department, University of Buffalo, Buffalo, New York, U.S.A.

FORCED OSCILLATOR

For the Newtonian motion of an oscillator subject to an external force $F(t)$ we have

$$m\ddot{x}_0+kx_0 = F(t), \tag{1}$$

and for the quantum motion,

$$-\frac{\hbar^2}{2m}\frac{\partial^2\psi}{\partial x^2}+[\tfrac{1}{2}kx^2-xF(t)]\psi = i\hbar\frac{\partial\psi}{\partial t}. \tag{2}$$

We may construct solutions to (2) that are in one-to-one correspondence with the unforced stationary solutions ($F = 0$) as follows. Write $\psi = \chi\exp[xg(t)]$ and then $\chi = \phi(x-u(t), t)$, where g and u are to be determined. The Schrödinger equation transforms* into

$$-\frac{\hbar^2}{2m}\frac{\partial^2\phi}{\partial\xi^2}+\left(i\hbar\dot{u}-\frac{\hbar^2}{m}g\right)\frac{\partial\phi}{\partial\xi} + \left\{\tfrac{1}{2}k\xi^2+\xi(ku-F-i\hbar\dot{g})+\left(\tfrac{1}{2}ku^2-Fu-i\hbar u\dot{g}-\frac{\hbar^2}{2m}g^2\right)\right\}\phi = i\hbar\frac{\partial\phi}{\partial t},$$

where $\xi = x-u(t)$. Choosing now g and u so that the coefficients of $\partial\phi/\partial\xi$ and $\xi\phi$ vanish,

$$-m\dot{u} = i\hbar g,$$

$$ku-F-i\hbar\dot{g} = 0 \quad \text{or} \quad m\ddot{u}+ku = F, \tag{3}$$

one is left with

$$-\frac{\hbar^2}{2m}\frac{\partial^2\phi}{\partial\xi^2}+[\tfrac{1}{2}k\xi^2+\delta(t)]\phi = i\hbar\frac{\partial\phi}{\partial t}, \tag{4}$$

$$\delta(t) = \tfrac{1}{2}ku^2-Fu-i\hbar u\dot{g}-\frac{\hbar^2}{2m}g^2$$

$$= \tfrac{1}{2}m\dot{u}^2-\tfrac{1}{2}ku^2.$$

Thence, ξ and t variables being separable,

$$\phi = N_n\exp\left\{-\frac{i}{\hbar}\int[\delta(t)+E_n]dt\right\}\exp(-\tfrac{1}{2}\alpha^2\xi^2)H_n(\alpha\xi),$$

$$\alpha^4 = mk/\hbar^2, \qquad E_n = (n+\tfrac{1}{2})\hbar\omega_0 \quad (\omega_0 = [k/m]^{\frac{1}{2}}),$$

$$H_n = n\text{th Hermite polynomial}, \qquad N_n^2 = \alpha/\pi^{\frac{1}{2}}2^n n!$$

In words, a class of solutions of equation (2) is that formed from the stationary states of the unforced problem, with x replaced by ξ and with a phase $\exp(-i/\hbar)(\int\delta dt+xg)$; by equation (3) ξ is nothing other than $x-x_0(t)$, and by (4) δ is the classical Lagrangian for the unforced motion written as a function in time of classical forced position and velocity.

*An alternative route for transformation is via contact transformation of the classical Hamiltonian.

Conventionally we may suppose an initial state $\psi(x, 0)$ that coincides with one of the eigenfunctions $v_m(x)$ of the unforced Hamiltonian. Then if the classical motion (1) be restricted to the initial conditions $x_0(0) = 0 = \dot{x}_0(0)$, $\psi(x, t)$ is

$$(5) \quad \psi_m(x, t) = N_m \exp\left(\frac{i}{\hbar} p_0(t)x\right)\exp\left(-\frac{i}{\hbar}\int_0^t (\delta+E_n)dt\right) \times \exp\{-\tfrac{1}{2}\alpha^2[x-x_0(t)]^2\}H_m(\alpha[x-x_0(t)]),$$

p_0 denoting classical momentum $m\dot{x}_0(t)$. Plainly these eigenfunctions form a complete set at any time t and a superposition of them can represent an arbitrarily specified wave function at any time. Though $i\hbar\dot{\psi} = H(t)\psi$ can possess no "true" stationary states, it is clear that in some suitable $\xi(x, t)$-space it may do so.

The meaning of the ξ-stationary states is at once visible: $\bar{x}(t)$ is just $x_0(t)$: the probability density

$$|\psi_m|^2 = N_m{}^2 \exp\{-\alpha^2[x-x_0(t)]^2\}H_m{}^2(\alpha[x-x_0(t)])$$

dances a classical dance centered at the instantaneous classical position $x_0(t)$, moving *in toto* classically. This generalizes the well-known "oscillating wave-packet" solution of the unforced problem.

The computation of the transition probability

$$P_{mn} = \left|\int_{-\infty}^{\infty} \psi_m(x, t)\, v_n{}^*(x)dx\right|^2,$$

giving the probability that at time t the oscillator is in the unperturbed state v_n if initially it was in the state v_m, is readily performed using the generating function for the Hermite polynomials. The result is

$$P_{mn} = \frac{\mu!}{\nu!}\, e^{-\epsilon_0}\, \epsilon_0{}^{\nu-\mu}|L_\nu^{\nu-\mu}(\epsilon_0)|^2,$$

where

$$\epsilon_0(t) = \frac{\text{classical energy, } \tfrac{1}{2}m\dot{x}_0{}^2+\tfrac{1}{2}kx_0{}^2}{\text{quantum energy, } \hbar\omega_0}$$

and ν is the greater, μ the lesser of m, n; $L_\nu^{\nu-\mu}$ denotes the associated Laguerre polynomial. There follows the rigorous selection rule that the transition probability vanishes only when the classically accumulated energy of the oscillator in units of $\hbar\omega_0$ falls at a zero of the appropriate Laguerre polynomial. The discussion of several interesting illustrative examples will be taken up at a later time.

DAMPING

For the linearly damped motion of a particle in a field of force $V(\mathbf{r})$ the Newtonian equation

$$m\ddot{\mathbf{r}}+\gamma\dot{\mathbf{r}} = -\nabla V(\mathbf{r})$$

may be cast into Lagrangian form by means of

$$L = \exp(\lambda t)(\tfrac{1}{2}m\dot{\mathbf{r}}^2 - V(\mathbf{r})), \qquad \lambda \equiv \gamma/m.$$

A brief quantum-mechanical discussion of the damped oscillator was given first by Kanai (1948). Havas (1956, 1957) has considered quite generally the theory of multipliers, such as $\exp(\lambda t)$ above, that allow a Lagrangian formulation of a broad class of Newtonian problems not otherwise fitting into the Lagrange–Hamilton scheme of mechanics; and he has emphasized the impossibility or else ambiguity (due to the multiplicity of possible integrating factors) of proceeding to quantization by the usual rules.* Although the meaning of doing so is not altogether clear at this point, we shall in the conventional way quantize the damped motion described by L and show that physically reasonable results are consequent.

By the customary route, the Hamiltonian implied by L is

$$H = \frac{\mathbf{p}^2}{2m}\exp(-\lambda t) + V(\mathbf{r})\exp(\lambda t), \qquad \mathbf{p} = m\dot{\mathbf{r}}\exp(\lambda t), \tag{6}$$

and is neither the energy nor any constant of the motion, but is just the generator of motion. To place H in a more familiar light, make the contact transformation

$$\mathbf{r} = \exp(-\tfrac{1}{2}\lambda t)\mathbf{R}, \qquad \mathbf{p} = \exp(\tfrac{1}{2}\lambda t)\mathbf{P},$$

giving the new Hamiltonian

$$G = \frac{\mathbf{P}^2}{2m} + \tfrac{1}{2}\lambda\mathbf{R}\cdot\mathbf{P} + \exp(\lambda t)\,V(\exp(-\tfrac{1}{2}\lambda t)\mathbf{R}),$$

in which the whole burden of time dependence is in the potential-energy term. When V is homogeneous of the second degree, the V term is $V(\mathbf{R})$, and G, being free of t, is a constant of the motion and is an energy though not *the* energy. For the one-dimensional oscillator, for example,

$$G = \frac{P^2}{2m} + \tfrac{1}{2}\lambda RP + \tfrac{1}{2}kR^2. \tag{7}$$

The further transformation in this case generated by the generating function

$$F(R, \Pi) = \frac{\lambda}{4m\omega^2}\Pi^2 + \frac{\omega_0}{\omega}R\Pi$$

gives a new Hamiltonian

$$\Gamma = \frac{\Pi^2}{2m} + \tfrac{1}{2}KX^2 \tag{8}$$

in the new momentum $\Pi = (\omega/\omega_0)P$ and conjugate coordinate $X = (\lambda/2m\omega\omega_0)P + (\omega_0/\omega)R$, where ω_0 is the undamped frequency $(k/m)^{\frac{1}{2}}$, ω the damped frequency $(K/m)^{\frac{1}{2}} = (k/m - \lambda^2/4)^{\frac{1}{2}}$.

It is interesting to see here that the Gibbs statistical mechanics is applicable to ensembles of weakly coupled damped oscillators, just as for the undamped ones; for in the phase space (Π_t, X_t) Liouville's theorem holds and Γ is conserved. Hence, for example, in a microcanonical ensemble mean values for

*I am indebted to Dr. Havas for correspondence on this matter.

any quantity of interest may be found, in a parallel with the usual computations; and in a canonical ensemble, with a "heat" bath of damped oscillators, there is a modulus of the distribution playing a role analogous to temperature and telling the preferred direction of flow of Γ between ensembles with different moduli. There is, in short, a kind of thermodynamics of macroscopic systems damped in their microscopic coordinates.

Turning now to quantization we have that, as a fundamental proposition stemming from the commutation rules, $\mathbf{p}$ may be represented as $-i\hbar\nabla$, and that, because only of the meaning of the Hamiltonian as generator of the motion, the Schrödinger wave function is controlled by $i\hbar\dot{\psi} = H\psi$, with H as in (6). That ψ retains its meaning of positional probability amplitude is indicated by maintenance of probability conservation (since H is Hermitian) and of the validity of Ehrenfest's theorem, to the effect that the quantal mean position is Newtonian.

For the oscillator, either by direct transformation of the wave equation or by use of the transformed Hamiltonians (7) or (8), the states corresponding to the undamped ones come out to be

$$\psi_n = \exp\left\{\left(-\frac{i}{\hbar}\epsilon_n+\tfrac{1}{4}\lambda\right)t-\left(\frac{im\lambda}{4\hbar}+\tfrac{1}{2}\beta^2\right)x^2\exp(\lambda t)\right\} H_n(\beta x\exp(\tfrac{1}{2}\lambda t)),$$

where the ϵ_n are eigenvalues of Γ, $\hbar\omega(n+\frac{1}{2})$, and $\beta^4 = mK/\hbar^2$ $(K > 0)$. The factor $\exp(\frac{1}{4}\lambda t)$ guarantees the time-independent normalization of ψ_n. These are stationary states in R-space: a measurement of G for them is certain to give the value ϵ_n. So to speak the moving states are stationary with respect to the moving Hamiltonian G. The position–momentum uncertainty product is $\Delta x\Delta p = \hbar(\omega_0/\omega)(n+\frac{1}{2})$ while the mean energy $(\frac{1}{2}m\dot{x}^2+\frac{1}{2}kx^2)$ becomes $\hbar\omega_0(\omega_0/\omega)(n+\frac{1}{2})\exp(-\lambda t)$. Altogether the quantum motion, like the classical, winds down (or up, for increasing t), $|\psi_n|^2$ shrinking eventually into a delta function. So long as quantum mechanics is linked to classical mechanics via Ehrenfest's theorem such a result is inevitable; the ground state of the *un*damped oscillator can not in the course of time be the favored one, as it might at first sight be expected to be.

SIMULTANEOUS FORCING AND DAMPING

The forced and damped oscillator, controlled classically by

$$m\ddot{x}_0+\gamma\dot{x}_0+kx_0 = F(t), \tag{9}$$

has the Hamiltonian

$$H = \frac{p^2}{2m}\exp(-\lambda t)+(\tfrac{1}{2}kx^2-xF)\exp(\lambda t)$$

with Hamiltonian equations equivalent to (9).

The Schrödinger equation becomes

$$-\frac{\hbar^2}{2m}\exp(-\lambda t)\frac{\partial^2\psi}{\partial x^2}+(\tfrac{1}{2}kx^2-xF)\exp(\lambda t)\psi = i\hbar\frac{\partial\psi}{\partial t}.$$

First put $\zeta = x\exp(\frac{1}{2}\lambda t)$ and $\psi = U(\zeta, t)$; then with $U = V\exp[-(im/4\hbar)\zeta^2]$, the transformed wave equation is

$$-\frac{\hbar^2}{2m}\frac{\partial^2 V}{\partial\zeta^2}+[\tfrac{1}{2}K\zeta^2+\tfrac{1}{4}i\hbar\lambda-F\exp(\tfrac{1}{2}\lambda t)\zeta]V = i\hbar\frac{\partial V}{\partial t},$$

with K as previously defined. From this point on, with the problem reduced to an equivalent forced and undamped oscillator problem in ζ-space, we proceed as before, placing $V = W\exp[\zeta f(t)]$ and $W = S(\zeta-w(t), t)$ to give (η being $\zeta-w(t)$)

$$-\frac{\hbar^2}{2m}\frac{\partial^2 S}{\partial\eta^2}+[\tfrac{1}{2}K\eta^2+\Delta(t)]S = i\hbar\frac{\partial S}{\partial t},$$

provided f, w satisfy

$$-m\dot{w} = i\hbar f,$$

$$Kw-F\exp(\tfrac{1}{2}\lambda t)-i\hbar\dot{f} = 0 \qquad \text{or} \qquad m\ddot{w}+Kw = F\exp(\tfrac{1}{2}\lambda t), \tag{10}$$

and Δ is

$$\Delta = \tfrac{1}{4}i\hbar\lambda+\tfrac{1}{2}m\dot{w}^2-\tfrac{1}{2}Kw^2.$$

Finally, for $K > 0$,

$$S = \exp\left(-\frac{i}{\hbar}\int(\Delta+\epsilon_n)dt\right)\exp(-\tfrac{1}{2}\beta^2\eta^2)H_n(\beta\eta).$$

For $K < 0$ (no oscillation at all classically in the damped but unforced motion) S is of continuum type. By (9) and (10) we identify

$$w(t) = x_0(t)\exp(\tfrac{1}{2}\lambda t),$$

$$\Delta(t) = L_0+\tfrac{1}{2}m\lambda x_0\dot{x}_0\exp(\lambda t)+\tfrac{1}{4}i\hbar\lambda,$$

where L_0 represents the classical Lagrangian for the damped but unforced motion as a function in time of the damped and forced position and velocity.

Altogether, for the ψ_n that are in correspondence with the v_n, we get

$$\psi_n = \exp\left(-\frac{i}{\hbar}\{\int\Delta dt+\epsilon_n t+\tfrac{1}{4}m\lambda x^2\exp(\lambda t)-x[p_0+\tfrac{1}{2}\lambda m x_0\exp(\lambda t)]\}\right)$$
$$\times\exp\{-\tfrac{1}{2}\beta^2[x-x_0(t)]^2\exp(\lambda t)\}H_n(\beta[x-x_0(t)]\exp(\tfrac{1}{2}\lambda t)),$$

where p_0 is $m\dot{x}_0\exp(\lambda t)$, the momentum conjugate to x_0. The probability density again moves as a whole in the classical rhythm, simultaneously deforming by a scale change $\exp(\frac{1}{2}\lambda t)$ in the x-scale. Asymptotically for $t \gg \lambda^{-1}$, $|\psi_n|^2$ becomes a delta function centered at $x_0(t)$: for sufficiently long times the classical and quantal motions coincide. This does not, formally, contravene the uncertainty principle, for, as a calculation shows, the momentum becomes wholly indeterminate in this limit. On the other hand we recognize the gradual transition into the classical regime by the disappearance of $\hbar$ from the commutation rule

$$x(m\dot{x})-(m\dot{x})x = i\hbar\exp(-\lambda t)$$

connecting position and *mechanical* momentum $m\dot{x}$.

Suppose the damped oscillator is hit by any transitory disturbing force F, $F(t) \simeq 0$ $(t > T)$. The oscillator motion subsequent to time T decays classically according to

$$x_{0T} = x_0(T) \exp(-\tfrac{1}{2}\lambda t) \cos \omega t.$$

If the oscillator is charged with charge e, we may interpret $-\gamma\dot{x}$ as the approximate force of radiation damping, and may examine the Maxwell fields emanating from the quantal charge–current distribution (Schrödinger 1926). The charge density $e|\psi_n|^2$ has a dipole moment ex_{0T}; an observer in the radiation zone will see a dipole line centered at ω with a width λ; that is, he will see the classical result of a shifted and broadened line. Quite generally, in fact, the dipole field will be the same as that calculated classically. In the case that the oscillator is damped but not forced the quasi-stationary states ψ_n give a nearly static charge distribution having no dipole or other odd moments. What radiation there is is confined mainly to the induction field; so the oscillator as it damps out creates variable fields predominantly in its immediate neighborhood, i.e. is surrounded by a "virtual" field of varying energy content, one that can affect closely approaching particles but not distant ones.

ACKNOWLEDGMENT

I am obliged to Mr. A. Flax for several stimulating discussions.

REFERENCES

HAVAS, P. 1956. Bull. Am. Phys. Soc. **1**, 337.
——— 1957. Nuovo cimento, Suppl. No. 3, 363.
KANAI, E. 1948. Progr. Theoret. Phys. **3**, 440.
SCHRÖDINGER, E. 1926. Ann. Physik, **81**, 134.

AN INTERPRETATION OF THE LOW-LYING EXCITED STATES OF Mg^{25} AND Al^{25} [1]

A. E. Litherland, H. McManus, E. B. Paul,[2]
D. A. Bromley, and H. E. Gove

ABSTRACT

A description of the experimental results obtained for Mg^{25} and Al^{25} is given based upon the assumption that the excited nuclear states are rotational states. In Mg^{25} and Al^{25} members of four rotational bands can be identified. The band based on the ground state can be assigned $K = 5/2$ whilst the three excited-state bands, two positive parity and one negative parity, can be assigned $K = 1/2$. The dipole γ-ray transitions between the $K = 1/2$ bands and the ground state $K = 5/2$ band are forbidden on the rotational model and it is a salient feature of the γ-ray cascading in Mg^{25} and Al^{25} that the ground-state transitions are always amongst the weakest transitions from excited states assigned to $K = 1/2$ bands. Besides giving a quantitative account of the γ-ray decay of the excited states the rotational model also predicts the number and type of the bands observed. The experimental values of the $Mg^{24}(d, p)Mg^{25}$ deuteron stripping reduced widths can also be approximately predicted by the model.

I. INTRODUCTION

The low-lying excited states of the nuclei Mg^{25} and Al^{25} have recently been studied extensively and a large body of information gathered. This information comprises evidence from proton and neutron capture γ-ray studies (Ager-Hanssen *et al.* 1956; Campion and Bartholomew 1957; Bromley *et al.* 1957; Craig 1956; Endt and Braams 1957; Green *et al.* 1955; Litherland *et al.* 1956; Varma and Jack 1956); deuteron stripping and proton scattering (Endt and Braams 1957); inelastic proton scattering by Gove *et al.* (1956–57); and beta-decay measurements by Maeder and Stahelin (1955) and Gove *et al.* (1956–57).

The experiments on $Mg^{24}(p, \gamma)Al^{25}$ described by Litherland *et al.* (1956) first suggested that the excited states of Al^{25} could be described in terms of overlapping bands of states having some of the characteristics of rotational states and a brief description of the states of Al^{25} as rotational states was given. It is the object of Section II of this paper to apply the rotational description to the states of Mg^{25} and Al^{25} in more detail and of Section III to make a comparison of some of the properties of Mg^{25} and Al^{25} with those calculated from the eigenfunctions, for a nucleon in a spheroidal potential, determined by Nilsson (1955).

The success of the description for Mg^{25} and Al^{25} has resulted in its extension to neighboring nuclei. Attempts to do this have been made recently by Paul (1956) for F^{19}, Sheline (1956–57) for Al^{28}, and Bromley *et al.* (1957) for Si^{29}. Though in each case there is less evidence than in the case of Mg^{25} and Al^{25} the success obtained seems to justify further experiments to test the interpretations.

[1]Manuscript received November 12, 1957.
Contribution from Physics Division, Atomic Energy of Canada Limited, Chalk River, Ontario.
Issued as A.E.C.L. No. 548.
[2]Now at Physics Division, A.E.R.E., Harwell, England.

II. ROTATIONAL DESCRIPTION OF THE STATES IN Mg^{25} AND Al^{25}

1. The Sequences of States

A summary of the experimental results on the γ-ray cascading in Al^{25} is shown in Fig. 1* and a separation of the low-lying states of Al^{25} into bands of rotational states is shown in Fig. 2. The evidence for this separation has

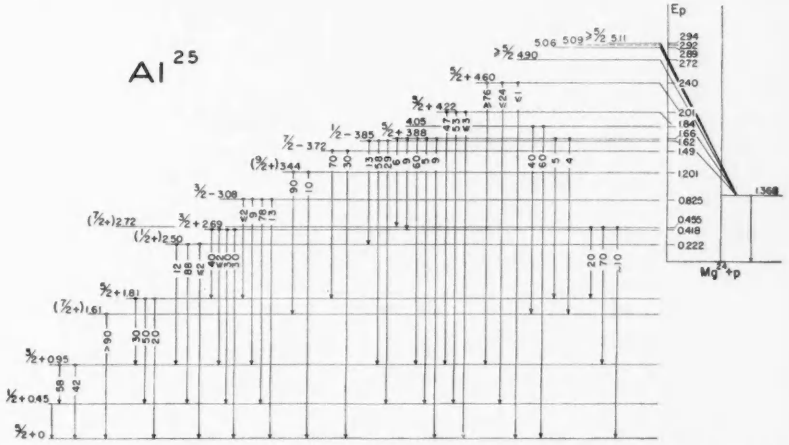

FIG. 1. A summary of the decay scheme showing all states in Al^{25} which were studied and their spins and parities where they could be established. The principal gamma transitions from each state are shown with the measured branching ratios. The energy of the excited state is given in Mev.

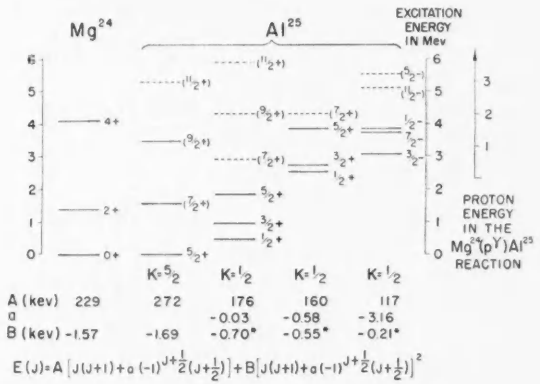

FIG. 2. The decomposition of the low-lying states in Al^{25} into bands of rotational states with the parameters used to fit the bands. Equations 1, 2, and 3 given in the text are used. The values of B marked with an asterisk show that the same vibrational parameters were used as for the sequence of states in Mg^{24}.

*Where the energies shown in Fig. 1 differ from those on subsequent figures the energies in Fig. 1 are to be regarded as more accurate values.

been discussed by Litherland *et al.* (1956) and consists mainly of total angular momentum and de-excitation γ-ray branching-ratio determinations. The states shown as dashed lines are predicted on the basis of the listed parameters and Equation 2. Evidence for the predicted 7/2+ state near 2.80 Mev. has recently been obtained by Bromley *et al.* (1957). Fig. 3 shows a summary of the present knowledge of the excited states of the mirror pair Mg^{25} and Al^{25}. Some of the details of this figure have been discussed recently by Gove and Litherland (1957).

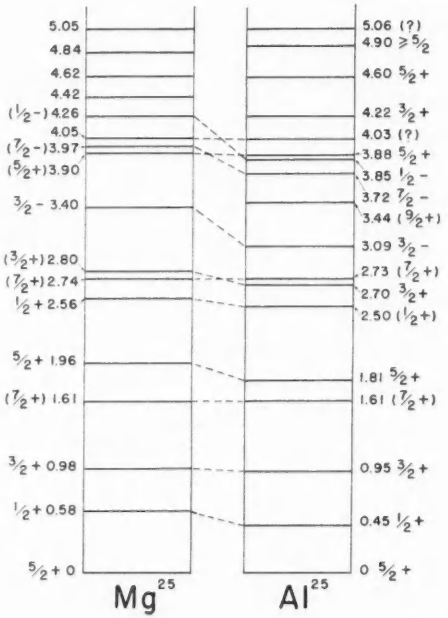

FIG. 3. A comparison of the mirror pair of nuclei Mg^{25} and Al^{25}.

In describing the states of Al^{25} as rotational states, the concepts developed by Bohr (1954) and Bohr and Mottelson (1953) are used. They considered the model of a nucleus of stable spheroidal shape capable of executing collective rotations about an axis perpendicular to the axis of symmetry.* It has been shown by Bohr (1954) that such rotations, for the case of an even–even nucleus, have an energy spectrum given by

$$E(J) = A[J(J+1)], \tag{1}$$

where J is the total angular-momentum quantum number of the nucleus and

*The nuclei in the region of $A = 25$ may be considered to be prolate spheroids since the electric quadrupole moments of Na^{23} and Al^{27} are positive.

A is constant for each band and is equal to $\hbar^2/2I$; I is the effective moment of inertia of the nucleus undergoing collective rotations.

For some time Mg^{24} has been known to exhibit the 0+, 2+, 4+ sequence of spins and also to have approximately the correct energy-state spacing given by Equation 1. The small discrepancy may be attributed to a vibration–rotation interaction term (cf. Fig. 2). Bohr and Mottelson (1955) also give the expected energy spectrum for an even–odd nucleus:

$$(2) \qquad E(J) = A[J(J+1)+\delta_{K,1/2}a(-1)^{J+1/2}(J+1/2)] + B[J(J+1)+\delta_{K,1/2}a(-1)^{J+1/2}(J+1/2)]^2.$$

Fig. 4 shows a plot of Equation 2 as a function of a for various values of J with $K = 1/2$ and $B = 0$. Using Fig. 4 the order and relative spacing of the

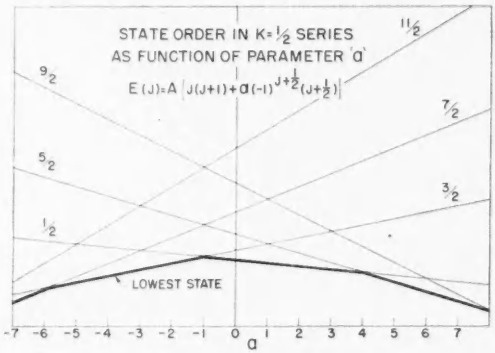

FIG. 4. The order of the excited states for a rotational band with $\Omega = 1/2$ is displayed as a function of the parameter a. For $a = 0$ the order of the states is given by $J(J+1)$. For $a = -3.5$ the order of the excited states is 3/2, 7/2, 1/2, which is the order observed for the negative-parity band in Al^{25}.

rotational states can be obtained for various values of a. In Equation 2, B is the vibration–rotation interaction parameter. a is a parameter which is relevant only to the $K = 1/2$ bands and is a result of the assumption of reflection symmetry of the nuclear shape and the coupling of the particle motion to the rotation. a, which is often referred to as the decoupling parameter, is given by Equation 3 (Bohr 1954):

$$(3) \qquad a = \sum_j (-1)^{j-1/2}(j+1/2)C_j^2.$$

In Equation 3, j is the total angular-momentum quantum number of the odd nucleon in a spheroidal nucleus. K is the projection of the total nuclear angular momentum J onto the axis of symmetry of the spheroid. The parity of the wave function is a good quantum number, but, because of the absence of spherical symmetry, j is not a good quantum number. However the projection of j along the axis of symmetry of the spheroidal potential is a good quantum number (Bohr and Mottelson 1955). This last quantum number is usually

called Ω. The single-particle wave function in a spheroidal potential χ_Ω can then be expressed in terms of a sum of single-particle wave functions for a spherical potential ψ_j:

$$\chi_\Omega = \sum_j C_j \psi_j. \tag{4}$$

The C_j coefficients are normalized so that $\sum_j C_j^2 = 1$ and the square of the coefficient C_j is then the probability that the single nucleon has total angular-momentum quantum number j.

The system of a spheroidal nucleus plus a single nucleon has a good quantum number J together with M, the projection of J upon some axis fixed in space, and K, the projection of J upon the axis of symmetry of the spheroid. K is equal to Ω in the absence of beta and gamma vibrations, which is usually the case for low-lying states. The wave function for such a system has been given by Bohr and Mottelson (1953).

K and Ω are, however, good quantum numbers only in the absence of what has been called 'rotation-particle coupling' or RPC (Kerman 1956). The rotations of the spheroidal nucleus perturb the nucleon motion very little provided the frequency of rotation of the nucleus is much smaller than the frequency associated with the nucleon motion. The latter frequency is related to the excitation energy of the single nucleon, and the former frequency is related to the energy separation of the rotational states. Thus if the rotational bands due to different single-nucleon excitations overlap, then perturbations of the bands are to be expected. However, the RPC in first order couples together only bands of the same parity and whose K's differ by one or zero (Kerman 1956). It is probably due to this that Mg^{25} and Al^{25} show rotational bands so clearly amongst their low-lying states since the two principal strongly overlapping bands have $\Delta K = 2$. Other nearby nuclei such as Na^{23}, which might be expected to show rotational spectra, have neighboring bands which differ in K by only one unit. Consequently Na^{23} would be expected to show perturbed bands. This point is discussed briefly in Appendix A.

In the case of the $K = 1/2$ bands in Mg^{25} and Al^{25}, the effect of the RPC is to modify the value of the parameters A and a obtained from the bands. Until further members of the bands are located the values shown in Fig. 2 should be treated with some caution, though, as will be discussed later, the mutual perturbing effect of the two positive parity $K = 1/2$ bands is probably small.

The decoupling parameters a obtained from the bands with $K = 1/2$ are intimately related to the state of the odd nucleon in the spheroidal nucleus (cf. Equation 3). The case of the anomalous state order of the negative-parity $K = 1/2$ band in Al^{25} (Fig. 2) is particularly interesting since it has a value of $a = -3.16$ which is close to the limiting value of $a = -4.00$ obtained by making $C_{7/2}^2 = 1$; Fig. 4 shows the order of the states for these values of the decoupling parameter. This suggests that the band can be described fairly well by an $f_{7/2}$ particle in a rotating spheroidal nucleus. Moszkowski (1955) has shown that for a nucleus in the vicinity of $A = 25$ with the shape of a

prolate spheroid there would be a low-lying single-nucleon state with $\Omega = 1/2$ which originated from the $1f_{7/2}$ shell. The deviation from spherical symmetry of the nucleus results in the $1f_{7/2}$ state being split into states with $\Omega = 1/2$, $3/2$, $5/2$, and $7/2$ with the $\Omega = 1/2$ state lying lowest for a prolate nucleus. The anomalous order of the low negative-parity states of Al^{25} can thus be well described by the rotational equation 2. From Equation 3 alone no conclusions can be reached concerning the origin of the even-parity $K = 1/2$ bands other than that various mixtures of $j = 1/2$, $3/2$, $5/2$ are allowed by the observed values of a. The evaluation by Nilsson (1955) of the single-particle wave functions for a spheroidal potential permits the calculation to be made of the values of a. This will be discussed later.

2. The Moments of Inertia Obtained from the Bands

The moments of inertia of the bands shown in Fig. 2 show that there is an appreciable difference between the various bands, with the moments of inertia for the $K = 1/2$ bands being significantly higher than the values for the $K = 0$ and $K = 5/2$ bands. The difference in moment of inertia between even–even nuclei and even–odd nuclei has been discussed in some detail by Bohr and Mottelson (1955) and by Kerman (1956).

The values of the moments of inertia are approximately equal to the values for the rotation of a spherical rigid nucleus. For a spherical nucleus with mass number 25 and $R_0 = 4.1 \times 10^{-13}$ cm., the parameter $A = \hbar^2/2I$ shown in Fig. 2 is 128 kev., which is quite close to the values for the $K = 1/2$ bands. If the nucleus is considered to be a spheroid of constant density, then for mass number 25 the moment of inertia for rigid rotation about one of the minor axes is given to first order by the following equation:

$$\hbar^2/2I_{\text{rigid}} = 128(1-0.3\delta) \text{ kev.} \tag{5}$$

If the nuclear distortion parameter δ, which is approximately equal to $\Delta R/R_0$ where R_0 is the mean nuclear radius and ΔR is the difference between the semi-major and semi-minor axes of the spheroidal nucleus, is obtained from the quadrupole moment of the neighboring nucleus Al^{27}, the value of $\hbar^2/2I_{\text{rigid}}$ is changed very little from the value for a spherical nucleus since $\delta \sim 0.3$. The situation for mass number 25 can be compared with the well-studied rotational spectra in heavier elements. There the moments of inertia deduced from the spacing of the nuclear states lie roughly between a third and a quarter of the values for rigid rotation. The significance of this fact has been discussed at length by Bohr and Mottelson (1955).

3. Particle Widths in Mg^{25} and Al^{25}

The C_j coefficients in the case of Mg^{25} and Al^{25} have a readily appreciated physical significance. The square of a C_j coefficient is proportional to the nucleon reduced width for the addition of a nucleon of angular momentum j to the ground state of Mg^{24} as shown in Equation 7.

The general expression for the stripping reduced width for rotational states has been given by Yoshida (1954) and by Satchler (1955) and a modified form of these expressions is given by Equation 6:

$$\theta^2 = \frac{2(2J_i+1)}{2J_f+1}(\theta_0)^2 \sum_j |C_j|^2 (J_i j K_i \Omega | J_f K_f)^2. \tag{6}$$

In Equation 6, (J_i, K_i) and (J_f, K_f) are the angular momenta and their projections along the axis of symmetry of the nucleus for the initial and final states, while $(j\Omega)$ are the corresponding quantities for the added nucleon. The quantity $(\theta_0)^2$ is dimensionless and expresses how well the nuclear wave function for $A+1$ particles can be split up into the product of a wave function for A particles and the wave function for a single nucleon. $(\theta_0)^2$ is assumed to be unity (independent-particle model) for the purposes of this paper.

Equation 6 reduces to Equation 7 when $J_i = 0$:

$$\theta_{J_f}{}^2 = \frac{2}{2J_f+1}|C_{J_f}|^2. \tag{7}$$

From this equation a sum rule for reduced widths obtained from stripping reactions and elastic proton scattering on a zero-spin nucleus follows:

$$\sum_{J_f} |C_{J_f}|^2 = 1 = \sum_{J_f} \theta_{J_f}{}^2 \frac{(2J_f+1)}{2}. \tag{8}$$

In equation 8 the sum is taken over all states belonging to one particular band.

In order to compare the nucleon reduced widths with theory, calculations of the C_j coefficients must be made using some model. Section III.3 of this paper contains such a comparison. It is, however, possible to use Equation 8 without making detailed calculations once the rotational bands have been identified. Table I shows some examples of the sum rule. The neutron capture probabilities Λ quoted by Holt and Marsham (1953) and by Hinds *et al.*

TABLE I

EXAMPLES OF THE REDUCED WIDTH SUM RULE

(1)		(2)	(3)
5	Mg^{25}	15.4	5/2+
9		17.3	1/2+
11		~12.5	1/2+
14		≳39	1/2−
9	Si^{29}	14.7	1/2+
8		16.9	3/2+
10		19	7/2−

(1) Nilsson orbit number.
(2) The sum of the Λ in arbitrary units for the various bands.
(3) The Ω value and parity of the band.

(private communication) are proportional to $\theta_{J_f}{}^2(2J_f+1)$. Apart from the high value for orbit number 14,* there is good agreement for the nuclei Mg^{25}

*The high value for the summation in the case of the negative-parity band is probably due to the use of the peak cross section of the angular distribution as a measure of the reduced stripping width. Any contribution from compound-nucleus formation would tend to make the reduced width smaller. Since the $l = 3$ angular distribution was measured only from 0° to 60°, this effect cannot be estimated.

and Si^{29}.* The possibility of rotational states in Si^{29} has been discussed recently by Bromley *et al.* (1957), who make the orbit number identifications. An application of Equation 6 to the higher members of the rotational bands is given in Appendix C. In Appendix D the application of Equation 6 to some stripping reduced widths in the *d*-shell is discussed briefly.

4. Gamma-Ray Transition Widths

The γ-ray decay within a rotational band of states is characterized by the enhancement of the $E2$ radiation and the subsequent effective competition with the $M1$ radiation also present. Enhanced $E2$ transition widths have now been measured for a large number of medium and heavy nuclei and their association with rotational groups of states established in many cases (Alder *et al.* 1956). In the case of Mg^{25} and Al^{25} there are no lifetime measurements of the rotational states and there is no evidence from Coulomb excitation so that the enhancement of the $E2$ transitions within a rotational band cannot be established.

In the case of Mg^{24} however electron scattering measurements by Helm (1956) have permitted an estimate of the lifetime of the first excited state of Mg^{24} to be made. The results of Helm (1956) for Mg^{24}, Si^{28}, S^{32} together with those of Devons *et al.* (1956) for Ne^{20}, for the lifetimes and ratios of the measured lifetime to the Weisskopf $E2$ unit (Wilkinson 1956), are shown in Table II. In all cases there is enhancement of the $E2$ lifetime over the single-particle estimate. Using the measured lifetime for Mg^{24} it is possible

TABLE II

$E2$ TRANSITION WIDTHS FOR SOME EVEN–EVEN NUCLEI WITH $20 < A < 32$

	(1)	(2)	(3)
Ne^{20}	7.6±3.3	0.82	11.1±5
Mg^{24}	19	0.34	10.8
Si^{28}	6	1.1	6.2
S^{32}	1.6	4.0	5.7

(1) Lifetime of the first excited state in units of 10^{-13} seconds.
(2) Transition width in millielectron volts.
(3) Ratio of experimental transition width to the Weisskopf estimate (Wilkinson 1956).

to calculate the intrinsic quadrupole moment of Mg^{24}. The value of $Q_0 = 0.43$ barns is very close to the value obtained by Gugelot and Rickey (1956) who deduced a value of $Q_0 = 0.45$ barns from the elastic scattering of 40 Mev. α-particles from Mg^{24}. It is also close to the values obtainable, assuming strong coupling, from the measured quadrupole moments of Na^{23} and Al^{27} of 0.55 and 0.41 barns respectively.

It seems likely from some of the properties of neighboring nuclei that $E2$

Note added in proof.*—The recent studies on the $Mg^{25}(p, d)Mg^{24}$ reaction by Bennett (Bull. Am. Phys. Soc., Ser. 2, **26, 1958) are relevant here. The reduced neutron widths for the formation of the first three states in Mg^{24} have been interpreted successfully by Blair (Bull. Am. Phys. Soc., Ser. 2, **26**, 1958) within the collective model framework.

transitions in Mg^{25} and Al^{25} would also be enhanced. Though at present this cannot be demonstrated from the absolute transition widths the ratios of the reduced $M1$ to reduced $E2$ transition widths when expressed in terms of Weisskopf units show that either the $E2$ transition widths are enhanced or the $M1$ transition widths are inhibited. This point is illustrated in Fig. 5 for the two identified bands exhibiting $E2$ crossover and cascade transitions.

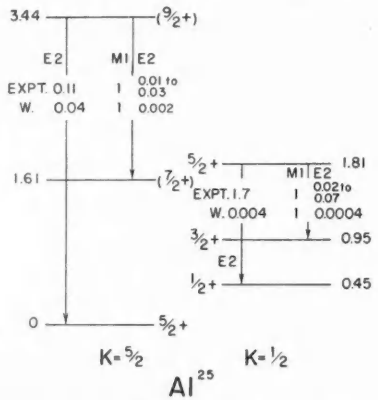

FIG. 5. The experimental $M1$–$E2$ ratios within the two lowest bands in Al^{25} are compared with the ratios of the corresponding Weisskopf (W) units. The $M1$ transition widths have been taken as unity for purposes of this comparison.

The prominent $E2$ crossover transitions to the first excited state from the fourth excited state of Mg^{25} and Al^{25} observed by Litherland *et al.* (1956) and Gove *et al.* (1956) were pieces of evidence which led to the rotational interpretation of the excited states of Mg^{25} and Al^{25}.

The rotational model makes definite predictions concerning the ratios of the reduced $E2$ transition widths (Alaga *et al.* 1955). There are two cases in Al^{25} where such a comparison can be made. These two cases are shown in Fig. 6 where the results of Litherland *et al.* (1956) have been used. Although the measured ratios with their errors include the theoretical ratios it is clear that more accurate measurements would be worth making.

For dipole radiation between rotational bands the quantum number K must change by 0 or ± 1. If K changes by more than one unit the transition is said to be K-forbidden (Alaga *et al.* 1955). The operation of the K-selection rule in Al^{25} was another piece of evidence that led to the rotational interpretation of the states. It was found by Litherland *et al.* (1956) that transitions to the ground state of Al^{25} were in general weak compared with the cascading radiations even though nearly all the radiations were dipole in nature.* Fig. 7

*The strong inhibition of the ground-state transitions from the states at 4.22 Mev. and 4.60 Mev. is striking. However, it is difficult to attribute this inhibition to a K-selection rule since the most likely K value for each state would be 3/2. A possible explanation of the inhibition is discussed in Appendix B.

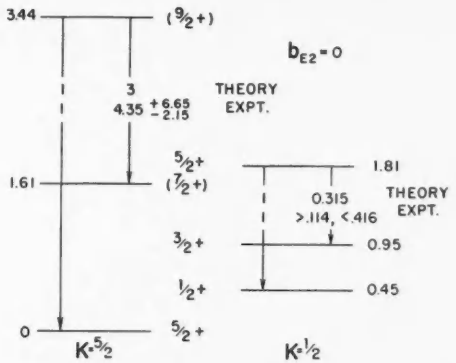

FIG. 6. The experimental ratios of the reduced $E2$ transition widths within the two lowest bands in Al^{25} are compared with the ratios calculated on the rotational model. The $E2$ crossover widths have been taken as unity for purposes of this comparison.

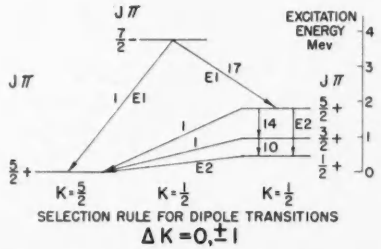

FIG. 7. Branching ratios in the decay scheme of the state in Al^{25} at 3.72 Mev. with the reduced transition probabilities for the electric dipole and magnetic dipole transitions shown in such a manner that K-forbidden transitions have the value unity.

shows the decay scheme of the $7/2-$, $K = 1/2$ state to the lower states in Al^{25} together with the reduced γ-ray transition widths. The operation of the K-selection rule is demonstrated quite clearly. The transitions in Mg^{25} and Al^{25} show many examples of the K-selection rule, and these are listed in Table III. The numbers in the table are the ratios of the reduced dipole transition widths between the excited states, listed horizontally and vertically, to the reduced transition width for the ground-state dipole transition. The energies are in Mev. The branching ratio of the 3.40 Mev. state in Mg^{25} is from the $Mg^{24}(n, \gamma)$ reaction measured by Campion and Bartholomew (1957). Quadrupole mixing has not been allowed for, since in most measured cases it has been shown to be small (Litherland *et al.* 1956). The values shown in parentheses are preliminary values (Bromley *et al.* 1957).

Violation of the selection rule is due to K not being a perfectly good quantum number, and this is a partial reflection of the presence of a vibration–rotation interaction and of the admixture of the bands with another band or bands which differ in their K by 0 or ± 1. Such a perturbing band would be the

TABLE III

EXAMPLES OF K-FORBIDDEN TRANSITIONS IN Al^{25} AND Mg^{25}

Al^{25}

	0.95	1.81	2.70	3.09	3.72	3.88
0.45	9.5		1.73	9.6		
0.95		13.9	<0.24	2.07		15.4
1.81			37.5	<2.16	17.3	(6.5)
2.70						(63)

Mg^{25}

	0.98	1.96	2.80	3.40
0.58	14.1			8.7
0.98		8.0		

expected, but hitherto unobserved, band with $K = 3/2$ based upon the $d_{3/2}$ single-nucleon orbit. The degree of violation of the K-selection rule varies considerably and this may be partly due to the variations of the magnitudes of the allowed dipole reduced widths among themselves, as discussed below.

It is possible using the equations given by Alaga *et al.* (1955) to give some account of the variations of the ratios of the reduced-dipole transition widths. For transitions from members of one band of rotational states to another band it is possible to form ratios which can be compared with theory. There is only one parameter b available to fit several ratios. Fig. 8 shows the experimental ratios compared with the theoretical ratios for the $M1$ transitions between the band based on the 2.51 Mev. state in Al^{25} and the band based on the first excited state of Al^{25} at 0.45 Mev. Fig. 9 shows the experimental ratios for the $E1$ transitions between the negative-parity band and the band based on the first excited state at 0.45 Mev. Although the fit to the experi-

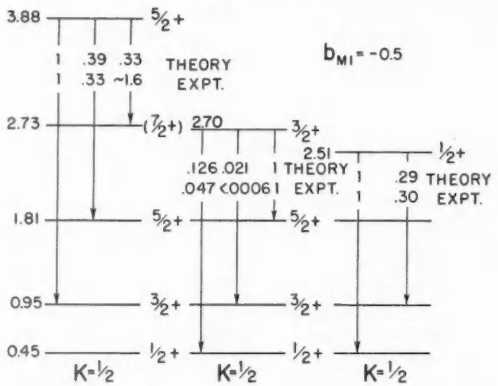

FIG. 8. The experimental ratios of the $M1$ transition widths from one band to another are compared with the theoretical ratios for $b_{M1} = -0.5$. The strongest $M1$ transition width from each state is taken to be unity for this comparison.

mental ratios is not perfect there is enough qualitative agreement to justify the hope that if all the perturbing effects, discussed briefly in Section III.4

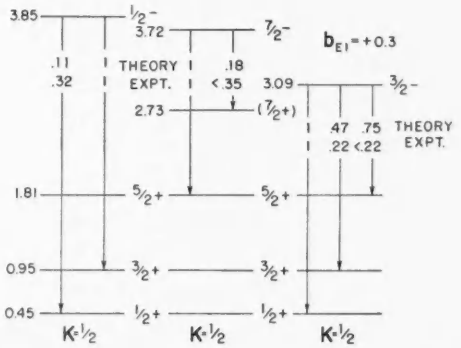

FIG. 9. The experimental ratios of the $E1$ transition widths from one band to another are compared with the theoretical ratios for $b_{E1} = +0.3$. The strongest $E1$ transition width from each state is taken to be unity for this comparison.

of this paper, are taken into account the agreement would be improved. The large variations in the ratios also illustrate one of the reasons why Table III of K-forbidden transitions contains such apparent large variations in the degree of K-forbiddenness.

5. Beta Decay of Al^{25} and Na^{25}

The beta decay of the nuclei Al^{25} and Na^{25} has been studied, and several points of interest emerge. In the positron decay of Al^{25} there is, besides a transition to the ground state of Mg^{25} with a log ft value of 3.5, a transition to the state at 1.61 Mev. with a log ft value lying between 4.7 and 5.6 (Maeder and Stahelin 1955). Possible values of the spin and parity of the 1.61 Mev. state in Mg^{25} and Al^{25} have been discussed by Gove *et al.* (1956–1957) and by Litherland *et al.* (1956) and the conclusion reached that an assignment of $7/2+$, with a K of $5/2$, is the most reasonable. This is in agreement with the allowed log ft value. As the ground state of Al^{25} is $5/2+$, transitions to the state in Mg^{25} at 0.98 Mev. $(3/2+)$ would also be allowed ($\Delta J = 1$), as well as those to the 1.96 Mev. state $(5/2+)$ ($\Delta J = 0$). These transitions have not been observed and in the case of the transition to the 0.98 Mev. state in Mg^{25} there is a lower limit to the log ft value of 4.9 obtained by Stribel (1956). The measurements, though consistent with the K-forbiddenness of the transition to the 0.98 state, are clearly inadequate to yield any quantitative idea of the degree of K-forbiddenness.

An accurate measurement of the positron branching to the 1.61 Mev. state in Al^{25} is of importance because the log ft value can be calculated if the rotational character of the states is assumed (Bohr and Mottelson 1953; Nilsson 1955). The value of log ft calculated is 4.24, which is smaller than the experimental lower limit. The uncertainty of the experimental log ft value

is almost entirely due to the difficulty of estimating the contribution of Al^{26} to the positron annihilation quanta in the decay of Al^{25} studied by Maeder and Stahelin (1955).

The beta decay of Na^{25} is quite different from that of Al^{25} as transitions with very similar *ft* values are observed to the ground state (5/2+), second excited state (3/2+), and third excited state (7/2+) (Gove *et al.* 1956–57). As the ground state and third excited state have $K = 5/2$ and the second excited state has $K = 1/2$, the most likely spin, parity, and K quantum number for Na^{25} are (5/2+ 3/2), which is anomalous, since one might expect the ground-state properties of Na^{25} to resemble those of Na^{23}. However, as discussed in Appendix A, the states of Na^{23}, if they can be described as rotational states, are anomalous in that respect and require the introduction of RPC to describe their order. It is possible that in the case of Na^{25} the 5/2+ first excited state has crossed over the 3/2+, owing to the RPC, to become the ground state (cf. Fig. 19). This conjecture implies that the state would be of mixed $K = 3/2, 5/2$, which would make transitions to the states of $K = 1/2$ allowed by the K-selection rule. A low-lying state of $J = 3/2+$ would then be expected for Na^{25}.

The foregoing discussion results in the conclusion that a satisfactory qualitative description of the spectra of Mg^{25} and Al^{25} can be obtained by the simple extension of the model of a single nucleon in a spherical potential to the model of a single nucleon strongly coupled to a rotating spheroidal potential. The eigenvalues and eigenfunctions for a nucleon in a fixed spheroidal potential have been calculated by Nilsson (1955), and the application of these calculations to Mg^{25} and Al^{25} will now be discussed.

III. COMPARISON OF THE EXPERIMENTAL DATA FOR Mg^{25} AND Al^{25} WITH THE CALCULATIONS OF NILSSON

1. The Energy States in a Spheroidal Well

The calculation of the energy states in a static spheroidal potential has been carried out by Moszkowski (1955), Nilsson (1955), and Gottfried (1956). The calculations of Nilsson are most suitable for our purpose as they include the calculations of the eigenfunctions for the region of $A = 25$. Fig. 10 shows the energy states of the model in the vicinity of $A = 25$ obtained by extending Nilsson's calculations of the energy of an individual particle in a spheroidal potential to larger values of η. For this purpose Nilsson's equation (C3) has been rewritten as follows:

$$(9) \qquad \frac{E_j}{3/4.\hbar\mathring{\omega}_0} = (N_j+3/2)(1-1/3.\epsilon^2-2/27.\epsilon^3)^{-1/3}+\kappa r_j(\epsilon)-\frac{1}{3\hbar\mathring{\omega}_0}\langle U_j\rangle,$$

where the following relationships between ϵ, η, and δ were employed:

$$(10) \qquad \kappa\eta = \epsilon[1-1/3.\epsilon^2-2/27.\epsilon^3]^{-1/3}$$

and

$$(11) \qquad \epsilon = 3\left[\frac{\sqrt{(1+2/3.\delta)}-\sqrt{(1-4/3.\delta)}}{\sqrt{(1-4/3.\delta)}+2\sqrt{(1+2/3.\delta)}}\right].$$

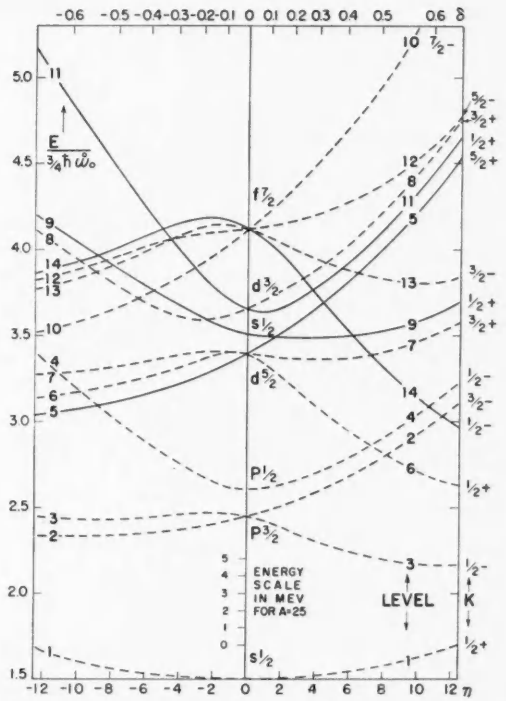

FIG. 10. The energy of states in a spheroidal potential taken in part from the paper "Binding states of individual nucleons in strongly deformed nuclei" by Nilsson (1955). The orbit numbers are those given by Nilsson. Orbits 5, 9, 11, 14 are those identified in Mg^{25} and Al^{25}.

The value κ, which measures the strength of the spin–orbit coupling, used in calculating the curves for Fig. 10 was 0.08. This appears to be a better value for light nuclei than 0.05 and, in this connection it is probably worth noting that the $d_{5/2}$–$d_{3/2}$ splitting of 5.08 Mev. in O^{17} would require $\kappa = 0.13$. In view of the uncertainty of the value of κ to use for $A = 25$, all subsequent graphs are given as functions of η since it is then straightforward to consider the variation of the strength of the spin–orbit interaction.

The value of η used in the subsequent comparisons varies from approximately $+3$ to $+5$. There is no reason *a priori* for expecting η to be a constant for each rotational band and the fact that different values of η give better agreement between theory and experiment in the subsequent comparisons probably implies that neglected effects, such as RPC, are significant.

2. Sequences of States for Mg^{25} and Al^{25}

Two protons and two neutrons are allowed for each orbit, so that, considering Mg^{24} to be a prolate spheroid with $0 < \eta < 6$ as indicated by the magnitude and sign of the neighboring quadrupole moments, orbit numbers

1, 2, 3, 4, 6, and 7 (see Fig. 10) are filled. The value of δ depends upon the strength of the spin–orbit interaction through Equations 10 and 11.

The next four orbits available are numbers 5, 9, 11, and 8, with number 14 being the lowest negative-parity orbit. Of these orbits all but the $\Omega = 3/2$, number 8 orbit can be identified amongst the low-lying states of Mg^{25} and Al^{25} (cf. Fig. 2). Orbit number 5 can be identified with the ground-state band ($\Omega = 5/2$) and orbit number 9 with the $\Omega = 1/2$ band based on the first excited state at 0.58 Mev. in Mg^{25} and 0.45 Mev. in Al^{25}. The next two $\Omega = 1/2$ orbits identified in Mg^{25} and Al^{25} can be identified with orbits number 11 and 14. The latter is based on the $1f_{7/2}$ orbit in a spherical potential. There is no clear indication at present for the band based on orbit number 8 ($\Omega = 3/2$). However, the region above 4 Mev. excitation where the lowest member of this band might be located is not known quite so well as the region below. In the case of Mg^{25}, magnetic analysis of charged-particle reactions indicates a number of unidentified states in the region of 4 Mev. excitation (Endt and Braams 1957), and in the case of Al^{25} the region above 4 Mev. excitation is complicated by the onset of inelastic scattering in the $Mg^{24}+p$ reaction. It is therefore possible that the $\Omega = 3/2$ band might be found if the less well known regions of Mg^{25} and Al^{25} were searched.*

The order of the bands number 5 and 9 in Mg^{25} and Al^{25} depends sensitively on the prolateness of the spheroid, and the close proximity of the first $\Omega = 1/2$ band to the $\Omega = 5/2$ ground-state band suggests that the parameter η in the case of Mg^{25} and Al^{25} is approximately $+2.0$. However if the individual-particle energies of Fig. 10 are summed for the 25 particles the potential-energy curves, as a function of η, can be calculated and the equilibrium distortion estimated. The results of the calculation are shown in Fig. 11. On the left-hand side of the figure the normal configurations are plotted in which 24 particles fill the orbits number 1, 2, 3, 4, 6, and 7 (Nilsson's notation shown in Fig. 10) and the odd particle is placed in orbit 5, 8, 9, 11, or 14. In the right half of Fig. 11, potential plots for states of core excitation are shown; in each case one of the four particles is removed from orbit 7 and paired with the odd particle in the upper state. No contribution for differences in pairing energy has been included. The results indicate an equilibrium value of $\eta \sim 4.5$ but do not reproduce the sequence of the observed bands in Al^{25}.† However the potential-energy plots do indicate that orbit 14 is expected to play an important role among the low states of Al^{25}, a result which is not immediately apparent from Fig. 10. Also the calculations show that the so-called 'excited-core' states can be expected among the higher excited states; their exact position being in doubt because of pairing-energy uncertainties. A tentative identification of two members of the band based upon the lowest of the

*If the $3/2+$ state in Al^{25} at 4.22 Mev. excitation were the first state of the $K = 3/2$ band, then the low reduced proton width of this state found by Mooring *et al.* (1951) would be in disagreement with the rotational interpretation of the states of Al^{25}. The reduced elastic proton width of the $3/2+$, $K = 3/2$ state can be calculated from Fig. 13(ϵ) and Equation 6, assuming no K admixtures and no inelastic scattering, and is approximately the single-particle width. A possible explanation for the low reduced proton width is given in Appendix B.

†The value of $\eta = +4.5$ corresponds to a distortion parameter $\delta = +0.23$ for $\kappa = 0.05$ and $\delta = +0.36$ for $\kappa = 0.08$. In Section 3 it was pointed out that for nuclei in the region Na^{23} to Al^{27} the electric quadrupole moments indicate $\delta \sim 0.3$.

excited-core configurations of Fig. 11 is given in Appendix B. While these calculations are not quite consistent among themselves it is noteworthy that this very simple model is in more than qualitative agreement with this very complicated nucleus.

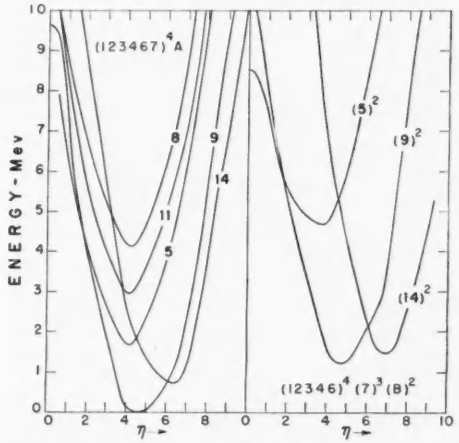

FIG. 11. The potential-energy plots obtained from Nilsson (1955) for Mg^{25} and Al^{25} are shown for several of the possible configurations.

Having assigned orbit numbers to the various bands, it is a straightforward matter to calculate the values of the parameters a. Fig. 12 shows the results as a function of η for the orbit numbers 9, 11, and 14. The experimental values

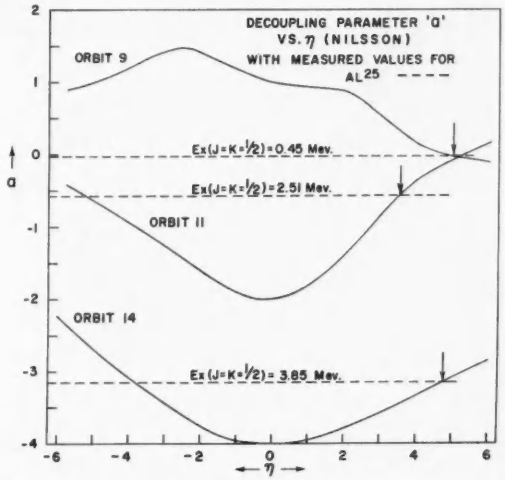

FIG. 12. The decoupling parameter a is shown as a function of the parameter η for the Nilsson orbits numbers 9, 11, and 14.

of a, obtained from the observed order of the energy states, are also shown. These comparisons indicate values of η in the vicinity of $+4$, which is approximately the same as the value obtained from Fig. 11. Until other members of the $K = 1/2$ bands are identified it would be premature to speculate upon the indicated differences of η from band to band.

3. Particle Widths in Al^{25} and Mg^{25}

It is also a straightforward matter to calculate the values of C_j^2 for each orbit, and these are presented graphically in Fig. 13. The graphs show some common pronounced characteristics. At $\eta = 0$ one of the C_j^2's becomes

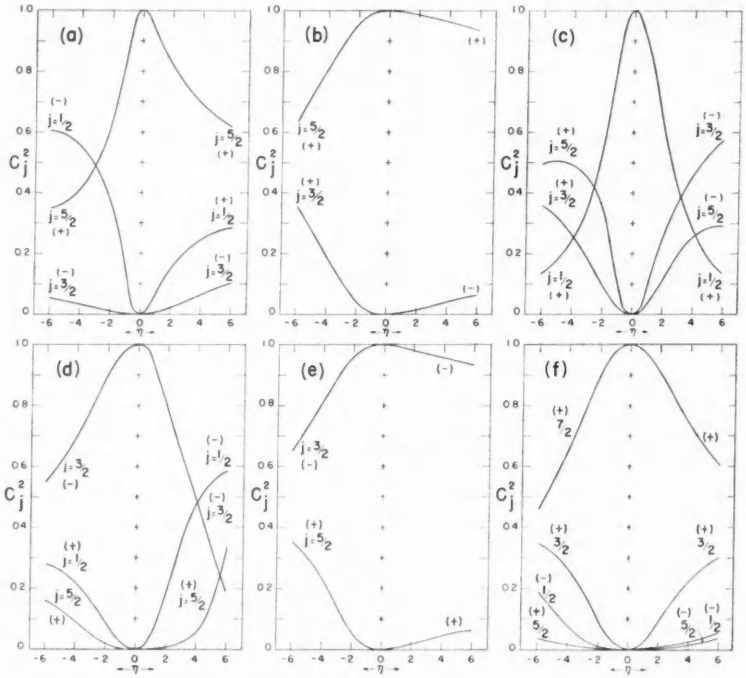

FIG. 13. Graphs of C_j^2 versus η.
(*a*) Nilsson orbit number 6 based on the $1d_{5/2}$ shell. $\Omega = 1/2$.
(*b*) Orbit number 7 based on the $1d_{5/2}$ shell. $\Omega = 3/2$.
(*c*) Orbit number 9 based on the $2s_{1/2}$ shell. $\Omega = 1/2$.
(*d*) Orbit number 11 based on the $1d_{3/2}$ shell. $\Omega = 1/2$.
(*e*) Orbit number 8 based on the $1d_{3/2}$ shell. $\Omega = 3/2$.
(*f*) Orbit number 14 based on the $1f_{7/2}$ shell. $\Omega = 1/2$.
The positive and negative signs give the signs of the C_j's.

unity. This C_j^2 is the one for which the j value is equal to that of the parent orbit in a spherical potential. As the prolateness or oblateness of the spheroidal potential becomes more pronounced, coefficients with other values of j increase whilst the coefficient whose value was originally unity decreases. The relation between the stripping reduced width and the C_j^2 is given by Equation 7.

Table IV shows a comparison of the relative reduced widths for the $Mg^{24}(d, p)Mg^{25}$ reaction compared to the values of C_j^2 for $\eta = 3$; Table V shows the comparison of the reduced proton-scattering widths* for $Mg^{24}(p, p)$ obtained by Koester (1952) with the C_j^2 for $\eta = +3$ and $+6$; the comparisons in Tables IV and V show that, although the agreement is fairly good, there are some obvious discrepancies.

TABLE IV

THE RELATIVE REDUCED STRIPPING WIDTHS FOR $Mg^{24}(d, p)Mg^{25}$ ARE COMPARED WITH THE VALUES OF THE COEFFICIENTS $|C_j|^2$

(1)	(2)	(3)	(4)	(5)
0	2	5/2+	15.4	1
0.582	0	1/2+	5.8	0.44
0.976	2	(3/2+)	6.0	0.36
1.612	—	(7/2+)	—	0
1.957	2	(5/2+)	5.5	0.20
2.565	0	1/2+	2.2	0.35
2.742	—	(7/2+)		0
2.806	2	(3/2+)	10.3	0.64
3.405	1	(3/2−)	11.2	0.16
3.899	—	(5/2+)	?	0.01
3.972	3	(7/2−)	25	0.82

(1) Energy of excited state in Mev. (Endt and Braams 1957).
(2) l-value of stripping pattern.
(3) Spin and parity of excited state. The values in parentheses have been obtained by comparison with Al^{25}, the mirror nucleus.
(4) A from Holt and Marsham (1953) and Hinds *et al.*
(5) $|C_j|^2$ for $\eta = +3$ obtained from Nilsson (1955).

TABLE V

THE REDUCED WIDTHS FOR THE SCATTERING OF PROTONS BY Mg^{24} ARE COMPARED WITH THE VALUES OF $|C_j|^2$

(1)	(2)	(3)	(4)	(5)
3.09	3/2−	0.54	0.16	0.30
3.72	7/2−	0.99	0.82	0.60
3.85	1/2−	0.21	0.015	0.06
3.88	5/2+	0.006	0.01	0.30
?	5/2−	?	0.005	0.04

(1) Energy of excited state of Al^{25}.
(2) Spin and parity (Koester 1952; Litherland *et al.* 1956).
(3) Ratio of the reduced width to $\hbar^2/\mu a$ multiplied by $\frac{1}{2}(2J+1)$, where μ is the reduced mass and a is the interaction radius assumed: $a = 5.05\times10^{-13}$ cm. (Koester 1952).
(4) $|C_j|^2$ for $\eta = +3$.
(5) $|C_j|^2$ for $\eta = +6$.

The agreement between theory and experiment in Tables IV and V can be improved by varying the parameter η independently for each band. Also the agreement could possibly be improved by varying the parameters assumed

*The reduced width for the 7/2− state is smaller by a factor 3/4 than the value quoted by Koester since he assumed 5/2− when calculating the reduced width.

by Nilsson for the spheroidal potential and by introducing RPC. Such attempts to improve the agreement would scarcely be justified in view of the difficulty in obtaining the reduced widths from the stripping angular distributions. The neutron capture probabilities Λ have been used because many of the results from the (d, p) and (d, n) reactions in the region $A = 25$ were analyzed using the Born approximation theory of Bhatia *et al.* (1952). If the theory of Butler (1951) is used the reduced widths show a systematic deviation from the reduced widths obtained from the theory of Bhatia *et al.* (Hinds *et al.* private communication). Until the derivation of reduced widths from stripping reactions is made more precise it would be premature to speculate upon the discrepancies between the calculated reduced widths and the reduced widths derived from the experimental results. The use of Equation 8 also has surprising success first of all in the case of Table I and later in Table V. In Table V the sum of the reduced widths equals 1.74 instead of the theoretically expected value of 1. This is reasonable agreement considering that the experimental value depends quite sensitively on the assumed radius of the interaction.

The agreement between theory and experiment in Tables I, IV, and V indicates that the further study of stripping reactions leading to rotational states both in light and heavier nuclei would be profitable.

4. Gamma-Ray Transition Widths

The usefulness of the concept of K-forbiddenness in describing the γ-ray transitions in Mg^{25} and Al^{25} has been discussed in Section 5, and the results for Mg^{25} and Al^{25} are given in Table III.

Before discussing the results of the calculations of the b and G^2 coefficients, it is worth estimating to what extent such calculations can be relied upon. Using the relations given by Kerman (1956), it is possible to estimate the mixing of the various rotational states. The parameters which describe the mixing of the Al^{25} states in the first $K = 1/2$ band (based on the first excited state at 0.45 Mev.) with those in the second $K = 1/2$ band (based on the 2.51 Mev. state) are given in Table VI. The notation employed in Table VI is as follows: the perturbed wave function for the lower band can be expressed as

$$\phi_J = a\psi_J{}^L + b\psi_J{}^U,$$

TABLE VI

THE MIXING AMPLITUDE, OF THE BAND ($K = 1/2$) BASED ON THE 2.51 MEV. STATE IN Al^{25} IN THE WAVE FUNCTION OF THE BAND ($K = 1/2$) BASED ON THE 0.45 MEV. STATE, IS SHOWN AS A FUNCTION OF THE J VALUE OF THE STATE

J	a	b
1/2	0.99	−0.13
3/2	0.97	−0.24
5/2	0.95	−0.31
7/2	0.92	−0.39

where $a^2+b^2 = 1$ and $\psi_J{}^L$ is the unperturbed wave function for the lower band and $\psi_J{}^U$ is the unperturbed wave function for the upper band. J is the angular-momentum quantum number of the state.

The values of a and b, together with the observed degree of K-forbiddenness, indicate that the comparison of theory with experiment in the case of γ-ray transitions is likely to be much less satisfactory than in the case of reduced particle widths unless an extensive calculation is made which takes into account the RPC. Such a calculation has been made for W^{183} by Kerman (1956).

The calculations of b and G^2 coefficients were carried out for Al^{25} assuming that the RPC was negligible. The formulae for dipole transitions used in the calculations have been given by Nilsson (1955). The results of such calculations, though encouraging, show that there is much room for improvement.

In Figs. 8 and 9 the branching ratios of a number of $M1$ and $E1$ transitions have been compared with the theoretical expressions of Alaga *et al.* (1955) to obtain empirical values of b_{M1} and b_{E1}. A good fit to the branching ratios was obtained by a single value of the parameter b in each case. The Nilsson eigenfunctions permit these to be calculated *a priori*; the results of such calculations are shown in Fig. 14. All the $E1$ transitions considered involve transitions between rotational levels based on Nilsson's orbit number 14 to ones based on orbit number 9, and for positive values of the parameter η,

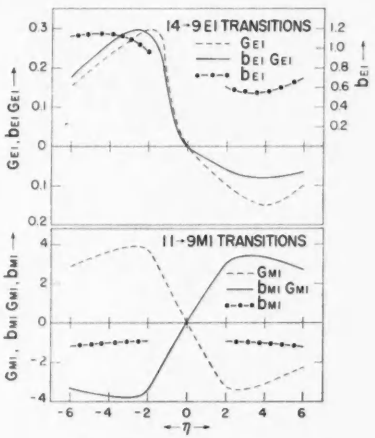

FIG. 14. The calculated values of G_{E1}, $b_{E1}G_{E1}$, b_{E1} and G_{M1}, $b_{M1}G_{M1}$, b_{M1} are shown as a function of η.

$b_{E1} \sim +0.6$. This is to be compared with the empirical value of $+0.3$. Similarly, for the $M1$ transitions involving Nilsson's number 11 to number 9 orbits, the empirical value of $b_{M1} = -0.5$ is to be compared to the theoretical value of -1.0 obtained from Fig. 14.

An empirical value can also be obtained for G_{E1}^2 and G_{M1}^2 from the measured absolute transition probabilities. The values are $G_{E1}^2\,(14 \rightarrow 9) = 0.13$ and $G_{M1}^2\,(11 \rightarrow 9) = 2.5$. They can be compared to the theoretical values given in Fig. 14, about 0.023 and 11.2 respectively, which is good agreement for absolute gamma transition probabilities. The b and G^2 coefficients are derived from all the measured transitions between different rotational bands which are not K-forbidden.

Transitions within rotational bands are of considerable interest since it is here that enhanced $E2$ transitions would be expected. It has been shown by McManus and Sharp that, in addition to the single-particle contribution to the $E2$ transition probability given by Nilsson, an additional and, for values of the parameter $\eta > 0.05$, considerably greater contribution of a collective nature occurs for transitions within a rotational band. This collective $E2$ transition is essentially negligible for transitions between different bands. The complete expression for $E2$ transition widths provided by McManus and Sharp has been quoted by Bromley *et al.* (1957) and has been employed in the discussion to follow.

The results for transitions within the rotational band based on Nilsson's level 9 are shown in Fig. 15. The theoretical branching ratio $\Gamma_{E2}^a/(\Gamma_{M1}^b + \Gamma_{E2}^b)$ for the 2.73 and 1.81 Mev. states is plotted as a function of the distortion parameter η. In both cases the experimental ratio is greater than unity. For the 1.81 Mev. state, the calculated $M1$ transition probability vanishes at values of η near ± 4 causing the ratio to be very large at these values. Agree-

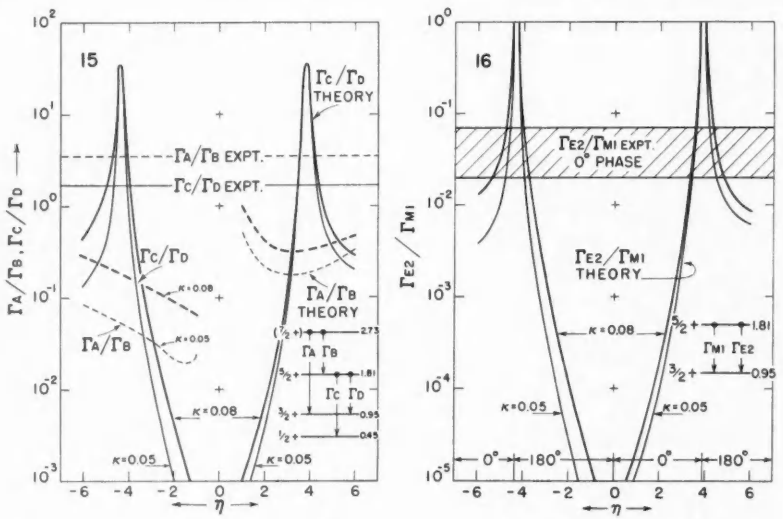

FIG. 15. The experimental γ-ray branching ratios within the band based on the first excited state of Al^{25} are compared with theory.

FIG. 16. The experimental $E2/M1$ ratio for the transition from the state at 1.81 Mev. to the state at 0.95 Mev. in Al^{25} is compared with theory.

ment with experiment occurs for $\eta = +3.4$ and $+4.4$. The agreement is not as good for the branching of the 2.73 Mev. state since the observed value is about 10 times greater than predicted.

The measured $E2$–$M1$ mixture in the transition between the 1.81 and 0.95 Mev. states is compared with theory in Fig. 16 and again good agreement is obtained both for the intensity ratio and phase with a distortion parameter $\eta \sim 3.5$.

Similar comparisons for transitions within the rotational band based on Nilsson's orbit 5 are shown in Figs. 17 and 18. Here, however, the measured branching for the 3.44 Mev. state is considerably larger than the predicted value while the measured phase for the $E2$–$M1$ mixture in the $3.44 \rightarrow 1.61$ Mev. transition is opposite to the predicted value.

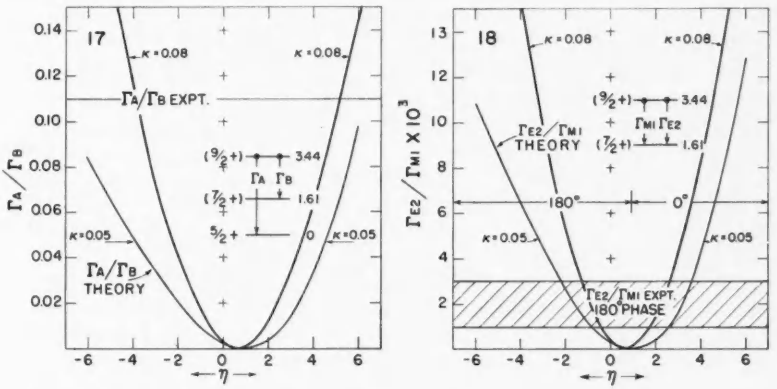

FIG. 17. The experimental γ-ray branching ratio of the 3.44 Mev. state in Al^{25} is compared with theory.

FIG. 18. The experimental $E2/M1$ ratio for the transition from the state at 3.44 Mev. to the state at 1.61 Mev. in Al^{25} is compared with theory.

The disagreement between some of the experimental results and the calculations based upon Nilsson's eigenfunctions possibly reflects the inaccuracy of the assumption that RPC is negligible (cf. Table VI). It is also possible that better agreement could be obtained by a limited variation of the parameters assumed by Nilsson for the nuclear potential. Such detailed calculations would be of value, particularly if further members of the rotational bands are found.

IV. CONCLUSIONS

It has been demonstrated that the strong-coupling wave function is a good approximation for the nuclei Mg^{25} and Al^{25}. The evidence in favor of the strong-coupling wave function is as follows:

(1) The appearance of well-defined rotational bands each of which has a sequence of states with the energy separation characteristic of rotational states.

(2) The nucleon widths for the excited states are in good agreement with the sum rule.

(3) The γ-ray decay of the excited states exhibits the phenomenon of K-forbiddenness.

(4) A good fit to the ratios of the reduced dipole widths can be obtained using only two parameters b_{E1} and b_{M1}, one for the electric dipole transitions and one for the magnetic dipole transitions.

The single-nucleon part of the strong-coupling wave function has been calculated by Nilsson (1955) using a specific spheroidal potential. Using these wave functions the decoupling parameters a, the gamma-ray branching ratios, and the nucleon reduced widths have been evaluated. Comparison of these with the results of experiment led to the following conclusions:

(1) Although the bands observed for Mg^{25} and Al^{25} are predicted by the model, the order of the two lowest bands is inverted and one of the expected bands is missing.

(2) The calculated decoupling parameters, for $\eta \sim 4$, for the three $K = 1/2$ bands are in good agreement with the experimental values.

(3) The equilibrium distortion of Mg^{25} and Al^{25} is predicted to lie between $\eta = 4$ and $\eta = 6$.

(4) No good over-all fit to the reduced nucleon widths is possible. However the best agreement is obtained for $\eta \sim 3$.

(5) The calculated values for the parameters b_{E1} and b_{M1} are in fair agreement with experiment.

(6) The branching ratios within the lowest bands are only in approximate agreement with experiment.

The evidence presented here would seem to indicate that the rotational model has real significance for this region of atomic number. Although the Nilsson model of a single nucleon in a deformed potential fails to give quantitative agreement with all the experimental data, this failure is not surprising in view of the relative simplicity of the model. Preliminary calculations by Elliott (1957) indicate that there may be a rather close connection between the shell model and the collective model and, if this is so, it provides some theoretical justification for applying the collective model to nuclei in regions between closed shells where calculations using the intermediate coupling shell model are prohibitively tedious.

The authors wish to record their indebtedness to Professor A. Bohr, Dr. B. R. Mottelson, Dr. S. G. Nilsson, Dr. A. K. Kerman, and Dr. K. Gottfried for several stimulating discussions and communications.

APPENDIX A. PERTURBED BANDS IN Na^{23}

Reference to Fig. 10 indicates that Na^{23} is expected to have $K = 3/2$ and $K = 5/2$ for its first two bands. Such bands, if separated by the order of 1 Mev., would be expected to interact strongly, and in fact the perturbed order of the states of Na^{23}, from the point of view of the rotational model, can be explained in this way. Fig. 19 shows a possible fit to the lower states of Na^{23} together with the assumed parameters. The nucleus Ne^{23} would,

however, be expected to show the same sort of band structure as Mg^{25} and Al^{25} amongst its low-lying states. This is because the odd nucleon in Ne^{23} is the fifth neutron after the closed shell at O^{16}, which is the case for Mg^{25} (fifth neutron) and Al^{25} (fifth proton). There is at the moment no evidence

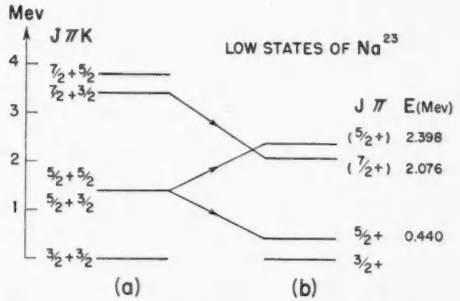

FIG. 19. A possible description of the low-lying states in Na^{23} based upon the two rotational bands $K = 3/2$ and $K = 5/2$ with the rotation-particle-coupling RPC parameter $A_K = 440$ kev. and the parameters $\hbar^2/2I = 283$ kev. and 340 kev. respectively. (*a*) shows the unperturbed overlapping bands ($A_K = 0$) and (*b*) shows the perturbed band ($A_K = 440$ kev.).

for rotational-like bands in Ne^{23}, but the measurement of the angular distributions from the stripping reaction $Ne^{22}(d, p)Ne^{23}$ by Burrows *et al.* (1956) to the ground and first excited states shows prominent $l = 2$ and $l = 0$ patterns respectively, which is similar to the $Mg^{24}(d, p)Mg^{25}$ reaction studied by Holt and Marsham (1953). This is to be contrasted with $Ne^{20}(d, p)Ne^{21}$, where the angular distributions show isotropy for the ground-state transition and an $l = 2$ pattern for the first-excited-state transition (Burrows *et al.* 1956).

APPENDIX B. STATES OF CORE EXCITATION IN Al^{25}

As mentioned in Section 5, the strong inhibition of the ground-state transitions from the states in Al^{25} at 4.22 and 4.60 Mev. requires some discussion, which can be based upon Figs. 10 and 11. The first states in Al^{25} of core excitation, contrasted with states arising from the excitation of the odd proton, should involve the excitation of a nucleon from orbit number 7 to orbit number 5 or 9 which are close together. In either case the unpaired proton in orbit number 7 might generate a $K = 3/2$ band. The possibility gives a plausible explanation for the small reduced proton widths for the states at 4.22 and 4.60 Mev. Also if the two excited nucleons are considered to be in the orbit number 9 dipole, γ-ray transitions to the ground state are two-particle transitions whereas transitions to the band based on the first excited state are single-particle transitions which are K-allowed. The potential-energy curves of Fig. 11 support this assignment. If the two nucleons are in orbit number 5 the ground-state transitions would be expected to be strongest. It may not be coincidental that the separation 380 kev. of the 3/2+ and 5/2+ states is close to the values for the separations of the ground and first excited states of Ne^{21} and Na^{23} (347 kev. and 440 kev. respectively) which

can be interpreted as a perturbed $3/2+$, $5/2+$ pair (cf. Fig. 19). The first state in Mg^{24} which is not a member of the ground-state band is the $2+$ state at 4.23 Mev. The prominent $l = 0$ stripping pattern for this state observed in the $Na^{23}(d, n)Mg^{24}$ reaction strongly suggests that the parents of the 4.22 Mev. and 4.60 Mev. states in Al^{25} are members of a band based upon the 4.23 Mev. state in Mg^{24}. Evidence for such a band has been obtained by Newton (1954); the $Na^{23}(d, n)Mg^{24}$ reaction is discussed briefly in Appendix D.

APPENDIX C. PROTON WIDTHS FOR THE UNBOUND ROTATIONAL STATES IN Al^{25}

Equation 6 enables the calculation of reduced widths for the emission of protons from rotational states in Al^{25} to the first excited state of Mg^{24}. Since no inelastic scattering from the rotational states belonging to the first four observed bands in Al^{25} has been observed, the calculations can only serve as a guide to future experiments to locate the missing members of the bands.

Consider, for example, the missing $9/2+K = 1/2$ state belonging to the band based on the first excited state of Al^{25}. If this state occurs near the expected bombarding energy of 1.7 Mev. then it can be shown, using the tables for barrier penetrability given by Gove (1957), that the inelastic d-wave proton width is approximately 25 millivolts. The inelastic proton width increases rapidly with energy because of the proximity of the inelastic threshold and at 2.0 Mev. bombarding energy becomes 13 ev. As in each case the g-wave elastic proton width is expected to be smaller than the inelastic proton width the resonance would be difficult to detect. This conclusion probably applies to the higher spin members of the rotational bands in Al^{25}. In addition to the barrier effect the reduced formation width in each case is expected to be very low because the distance of the $1g$ and $1h$ from the $1d$ and $1f$ shells results in small admixing. The protons emitted to the first excited state of Mg^{24} can however be p, d, or f protons with large reduced widths.

Equation 6 also shows another way of testing the goodness of the K-quantum number since the Clebsch-Gordan coefficient vanishes unless $K_i + \Omega = K_f$. A state whose $(J\pi K)$ values are $(3/2 + 3/2)$ for example cannot break up into an s-wave proton plus Mg^{24} in its first excited state since the above equality is violated. If however there was an admixture of $K = 1/2$ in the state, s-wave protons could be emitted.

APPENDIX D. DEUTERON STRIPPING AND THE ROTATIONAL MODEL NEAR $A = 25$

Recent studies of the (d, n) and (d, p) reactions by Calvert *et al.* (1955) and Holt and Marsham (1953*a*, *b*) have yielded information concerning nucleon widths in the vicinity of $A = 25$. The $Na^{23}(d, n)Mg^{24}$ reaction is of particular interest because of the rotational spectrum of Mg^{24}. The stripping patterns allowed by conservation of angular momentum for the $0+$, $2+$, and $4+$ states are $l = 2$, $l = 0$ and $l = 2$, and $l = 2$ respectively. However, if the rotational model gives a good description of Mg^{24} Equation 6 and Fig. 13 can be used to determine the reduced widths as a function of distortion. Unfortunately the low yield of neutrons to the low-lying states of Mg^{24}

prevented a determination of the reduced widths (Calvert *et al.* 1955). However it is possible to make some qualitative statements concerning the relation of the results to the rotational model. No marked stripping pattern for the first excited state of Mg^{24} was observed in spite of the fact that an $l = 0$ transition is allowed from the conservation of angular momentum. Since $l = 0$ patterns even with small proton capture probabilities can be observed by the (d, n) reaction,* this implies that the addition of an s-wave proton to Na^{23} to form the first excited state of Mg^{24} is strongly inhibited by some selection rule. The rotational model provides such an inhibition because since $K_i = 3/2$ and $K_f = 0$, the addition of s-wave protons, $\Omega = 1/2$, is forbidden.

Fig. 13(b) also shows that the proton capture probability to the ground state of Mg^{24} is very small for prolate distortions whereas the proton capture probability for the first excited state is near the maximum value possible. For a distortion $\eta = +4$ the ratio of the proton capture probabilities to the two states is approximately 20. The differential cross section at 0° for the ground-state neutron group is a factor of five smaller than that for the first excited state, which is possibly a lower limit to the ratio of the proton capture probabilities in view of the uncertainties introduced by compound-nucleus and other effects (cf. footnote to Section 4). The remeasurement with improved statistics of the proton-capture probabilities for the two lowest states of Mg^{24} from the $Na^{23}(d, n)Mg^{24}$ reactions would be of considerable interest.

The angular distribution of the sum of the neutron groups to the second and third excited states (unresolved) of Mg^{24} shows a prominent $l = 0$ stripping pattern together with a possible $l = 2$ pattern. The $l = 0$ pattern must be associated with the 2+ state at 4.23 Mev. and the large proton capture probability implies that a rather simple description of the state is possible.† A description based upon Fig. 10 would be that the unpaired proton of Na^{23} in orbit number 7 pairs with a proton in orbit number 9 to produce a state with $J = 2+$ and with $K = 2$. This state is then the base state for a rotational band. Evidence for the second member of this band $J = 3+$ has been given by Newton (1954). A possible connection of this band with Al^{25} has been considered in Appendix B.

The $Mg^{25}(d, p)Mg^{26}$ studied by Holt and Marsham also is of interest since the target nucleus is well described by the rotational model. Comparatively little is known about the properties of Mg^{26}. The first excited state is most probably 2+ and the excited states do not suggest a rotational structure as in the case of Mg^{24}. The angular distribution of the protons leading to the first excited state of Mg^{26} shows a mixed $l = 0$ and $l = 2$ pattern. The reduced neutron capture probability is 20 times smaller for the addition of an $l = 0$ neutron to Mg^{25} to form Mg^{26} in its first excited state than for the addition of an $l = 2$ neutron. This observation is quite consistent with the rotational model since the first excited state of Mg^{26} would be expected to be 2+ with $K = 0$. The inhibited $l = 0$ patterns for the Mg^{24} and Mg^{26} excited states

*The prominent $l = 0$ deuteron stripping pattern for neutrons leaving Si^{28} in its first excited state has a proton capture probability a factor of 10 times smaller than the observed ground state $l = 2$ pattern (Calvert *et al.* 1955).

†The $l = 2$ component could be from either or both of the 2+ or the 4+ member of the doublet.

could also be explained on the basis of nearly pure j–j coupling. Both nuclei are then in the $d_{5/2}$ shell which would imply no $l = 0$ transitions to states which are described by a number of $d_{5/2}$ particles. On the rotational picture the appearance of an $l = 0$ component to the angular distribution implies a small admixture of other K-values to the predominantly $K = 0$ first excited state. It is not possible to correlate further the appearance of forbidden stripping patterns with the deviation from a rotational spectrum until more experimental evidence is available.

REFERENCES

AGER-HANSSEN, H., LONSJO, O. M., and NORDHAGEN, R. 1956. Phys. Rev. **101**, 1779.
ALAGA, G., ALDER, K., BOHR, A., and MOTTELSON, B. R. 1955. Kgl. Danske Videnskab. Selskab, Mat.-fys. Medd. **29**, No. 9.
ALDER, K., BOHR, A., HUUS, T., MOTTELSON, B., and WINTHER, A. 1956. Revs. Modern Phys. **28**, 432.
BHATIA, A. B., HWANG, K., HUBY, R., and NEWNS, H. C. 1952. Phil. Mag., Ser. 7, **43**, 485.
BOHR, A. 1954. Rotational states of atomic nuclei (Munksgaards Forlag, Copenhagen).
BOHR, A. and MOTTELSON, B. R. 1953. Kgl. Danske Videnskab. Selskab, Mat.-fys. Medd. **27**, No. 16.
——— 1955. Kgl. Danske Videnskab. Selskab, Mat.-fys. Medd. **30**, No. 1.
BROMLEY, D. A., GOVE, H. E., and LITHERLAND, A. E. 1957. Can. J. Phys. **35**, 1057.
BROMLEY, D. A., GOVE, H. E., LITHERLAND, A. E., and ALMQVIST, E. 1957. Bull. Am. Phys. Soc. **2**, No. 4.
BURROWS, H. B., GREEN, T. S., HINDS, S., and MIDDLETON, R. 1956. Proc. Phys. Soc. (London), A, **69**, 310.
BUTLER, S. T. 1951. Proc. Roy. Soc. (London), A, **208**, 559.
CALVERT, J. M., JAFFE, A. A., LITHERLAND, A. E., and MASLIN, E. E. 1955. Proc. Phys. Soc. (London), A, **68**, 1008.
CAMPION, P. J. and BARTHOLOMEW, G. A. 1957. Can. J. Phys. **35**, 1361.
CRAIG, D. S. 1956. Phys. Rev. **101**, 1479.
DEVONS, S., MANNING, G., and TOWLE, J. H. 1956. Proc. Phys. Soc. (London), A, **69**, 173.
ELLIOTT, J. P. 1957. Pittsburgh Conference on Nuclear Structure (unpublished).
ENDT, P. M. and BRAAMS, C. M. 1957. Revs. Modern Phys. **29**, 683.
GOTTFRIED, K. 1956. Phys. Rev. **103**, 1017.
GOVE, H. E. 1957. Resonance Reactions—Experimental, Atomic Energy of Canada Limited, Chalk River Project, PD-287 (unpublished).
GOVE, H. E., BARTHOLOMEW, G. A., PAUL, E. B., and LITHERLAND, A. E. 1956–57. Nuclear Phys. **2**, 132.
GOVE, H. E. and LITHERLAND, A. E. 1957. Phys. Rev. **107**, 1458.
GREEN, L. L., SINGH, J. J., and WILLMOTT, J. C. 1955. Phil. Mag., Ser. 7, **46**, 982.
GUGELOT, P. C. and RICKEY, M. 1956. Phys. Rev. **101**, 1613.
HELM, R. H. 1956. Phys. Rev. **104**, 1471.
HINDS, S., MIDDELTON, R., and PARRY, G. 1957. Private communication.
HOLT, J. R. and MARSHAM, T. N. 1953*a*. Proc. Phys. Soc. (London), A, **56**, 258.
——— 1953*b*. Proc. Phys. Soc. (London), A, **56**, 467.
KERMAN, A. K. 1956. Kgl. Danske Videnskab. Selskab, Mat.-fys. Medd. **30**, No. 15.
KOESTER, L. J. 1952. Phys. Rev. **85**, 643.
LITHERLAND, A. E., PAUL, E. B., BARTHOLOMEW, G. A., and GOVE, H. E. 1956. Phys. Rev. **102**, 208.
MAEDER, D. and STAHELIN, P. 1955. Helv. Phys. Acta, **28**, 193.
MOORING, F. P., KOESTER, L. J., GOLDBERG, E., SAXON, D., and KAUFMANN, S. G. 1951. Phys. Rev. **84**, 703.
MOSZKOWSKI, S. A. 1955. Phys. Rev. **99**, 803.
NEWTON, J. O. 1954. Phys. Rev. **96**, 241; and private communication.
NILSSON, S. G. 1955. Kgl. Danske Videnskab. Selskab, Mat.-fys. Medd. **29**, No. 16.
PAUL, E. B. 1956. Physica, **22**, 1140.
——— 1957. Phil. Mag., Ser. 8, **2**, 311.
SATCHLER, G. R. 1955. Phys. Rev. **97**, 1416.
SHELINE, R. K. 1956–57. Nuclear Phys. **2**, 382.
STRIBEL, T. 1956. Z. Naturforsch. **11a**, 166.
VARMA, J. and JACK, W. 1956. Physica, **22**, 1139.
WILKINSON, D. H. 1956. Phil. Mag., Ser. 8, **1**, 127.
YOSHIDA, S. 1954. Progr. Theoret. Phys. (Kyoto), **12**, 141.

LETTERS TO THE EDITOR

Under this heading brief reports of important discoveries in physics may be published. These reports should not exceed 600 words and, for any issue, should be submitted not later than six weeks previous to the first day of the month of issue. No proof will be sent to the authors.

The Influence of Paramagnetic Resonance Saturation on the Faraday Effect

The Faraday effect (the rotation of the plane of polarization of light passing through a material in a magnetic field) is very large, in general, in paramagnetic salts. The rotation of the plane of polarization is proportional to the magnetic moment of the salt, and for a single crystal of neodymium-ethylsulphate the maximum rotation corresponding to complete magnetization is about 114° per mm. of path length for green mercury light ($\lambda = 5461$ Å) propagated along the optic axis (Becquerel *et al.* 1938). When the crystal is exposed to microwave radiation of the frequency which causes paramagnetic resonance, and the microwave power is sufficient to cause appreciable saturation of the resonance, the magnetic moment is reduced and the Faraday rotation should also be reduced. This effect was predicted by Kastler (1951) and a theory of this effect has been developed by Opechowski (1953).

We have observed this effect in a single crystal of neodymium-ethylsulphate. The crystal was mounted with the optic axis parallel to the external d-c. magnetic field, in a TE_{101} rectangular cavity, with two holes, about 2 mm. in diameter, in the large faces to let the light through. Microwave power at 9060 Mc./sec. from a 2K39 klystron was fed into the cavity, which was critically coupled to the microwave transmission line and had an unloaded Q of about 9000. The cavity was immersed in liquid helium at about 1.5° K. The light, from a mercury lamp, was filtered to leave only the green line ($\lambda = 5461$ Å). It was then passed through a nicol prism polarizer, through the hollow poles of the electromagnet, through the cavity, out through the magnet, and finally through a nicol prism analyzer. The emergent light was condensed onto the cathode of a photomultiplier (1P21), and the anode current was taken as a measure of the light passing through the system. The light passed along the optic axis of the neodymium-ethylsulphate crystal, and the path length was 1.6 mm. The ends of the crystal were cut perpendicular to the optic axis and polished. The analyzer was rotated until the photomultiplier current was a minimum, and the Faraday rotation was read off from a scale on the analyzer housing.

The results are shown in Fig. 1. The angle of rotation of the plane of polarization is plotted as a function of magnetic field for four cases: no microwave power, full microwave power,

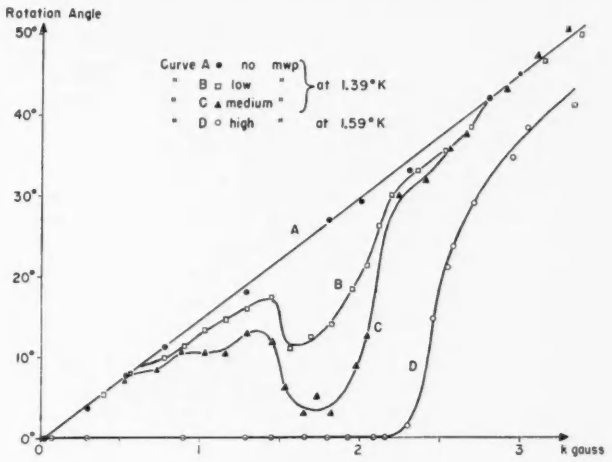

FIG. 1.

medium power, and a low value of power. The power levels have not been determined. These investigations are being continued and will be reported at a later date.

The financial support of the National Research Council of Canada and of the President's Research Fund of U. B. C. is gratefully acknowledged.

BECQUEREL, J., DE HAAS, A., and VAN DEN HANDEL, J. 1938. Physica, **5**, 753.
KASTLER, A. 1951. Compt. rend. **232**, 953.
OPECHOWSKI, W. 1953. Revs. Modern Phys. **25**, 264.

RECEIVED DECEMBER 23, 1957.
DEPARTMENT OF PHYSICS,
UNIVERSITY OF BRITISH COLUMBIA,
VANCOUVER, B.C.

J. M. DANIELS
H. WESEMEYER

אין אין

CANADIAN JOURNAL OF PHYSICS

Notes to Contributors

Manuscripts

(i) General. Manuscripts, in English or French, should be typewritten, double spaced, on paper 8½×11 in. **The original and one copy are to be submitted.** Tables and captions for the figures should be placed at the end of the manuscript. Every sheet of the manuscript should be numbered.

Style, arrangement, spelling, and abbreviations should conform to the usage of recent numbers of this journal. Names of all simple compounds, rather than their formulas, should be used in the text. Greek letters or unusual signs should be written plainly or explained by marginal notes. Superscripts and subscripts must be legible and carefully placed.

Manuscripts and illustrations should be carefully checked before they are submitted. Authors will be charged for unnecessary deviations from the usual format and for changes made in the proof that are considered excessive or unnecessary.

(ii) Abstract. An abstract of not more than about 200 words, indicating the scope of the work and the principal findings, is required, except in Notes.

(iii) References. References should be listed **alphabetically by authors' names,** unnumbered, and typed after the text. The form of the citations should be that used in current issues of this journal; in references to papers in periodicals, titles should not be given and only initial page numbers are required. The names of periodicals should be abbreviated in the form given in the most recent *List of Periodicals Abstracted by Chemical Abstracts.* All citations should be checked with the original articles and each one referred to in the text by the authors' names and the year.

(iv) Tables. Tables should be numbered in roman numerals and each table referred to in the text. Titles should always be given but should be brief; column headings should be brief and descriptive matter in the tables confined to a minimum. Vertical rules should not be used. Numerous small tables should be avoided.

Illustrations

(i) General. All figures (including each figure of the plates) should be numbered consecutively from 1 up, in arabic numerals, and each figure referred to in the text. The author's name, title of the paper, and figure number should be written in the lower left corner of the sheets on which the illustrations appear. Captions should not be written on the illustrations (see Manuscripts (i)).

(ii) Line Drawings. Drawings should be carefully made with India ink on white drawing paper, blue tracing linen, or co-ordinate paper ruled in blue only; any co-ordinate lines that are to appear in the reproduction should be ruled in black ink. Paper ruled in green, yellow, or red should not be used. All lines should be of sufficient thickness to reproduce well. Decimal points, periods, and stippled dots should be solid black circles large enough to be reduced if necessary. Letters and numerals should be neatly made, preferably with a stencil (**do NOT use typewriting**) and be of such size that the smallest lettering will be not less than 1 mm. high when reproduced in a cut 3 in. wide.

Many drawings are made too large; originals should not be more than 2 or 3 times the size of the desired reproduction. Whenever possible two or more drawings should be grouped to reduce the number of cuts required. In such groups of drawings, or in large drawings, full use of the space available should be made; the ratio of height to width should conform to that of a journal page (4¾×7½ in.), but allowance must be made for the captions.

The original drawings and one set of clear copies (e.g. small photographs) are to be submitted.

(iii) Photographs. Prints should be made on glossy paper, with strong contrasts. They should be trimmed so that essential features only are shown and mounted carefully, with rubber cement, on white cardboard, with no space between them. In mounting, full use of the space available should be made to reduce the number of cuts required (see Illustrations (ii)). Photographs or groups of photographs should not be more than 2 or 3 times the size of the desired reproduction.

Photographs are to be submitted in duplicate; if they are to be reproduced in groups one set should be mounted, the duplicate set unmounted.

Reprints

A total of 50 reprints of each paper, without covers, are supplied free. Additional reprints, with or without covers, may be purchased at the time of publication.

Charges for reprints are based on the number of printed pages, which may be calculated approximately by multiplying by 0.6 the number of manuscript pages (double-spaced typewritten sheets, 8½×11 in.) and including the space occupied by illustrations. An additional charge is made for illustrations that appear as coated inserts. Prices and instructions for ordinary reprints are sent out with the galley proof.

Any reprints required in addition to those requested on the author's reprint requisition form must be ordered officially as soon as the paper has been accepted for publication.

Contents

Page

The Townsend discharge in a coaxial diode with axial magnetic field—*P. A. Redhead* - 255

Operation of an inverted-magnetron gauge in the pressure range 10^{-3} to 10^{-12} mm. Hg—*J. P. Hobson and P. A. Redhead* - - - - - - - - - - 271

The self-consistent field with exchange for neon by Ferut program—*Beatrice H. Worsley* - 289

A survey of the mathematics available for describing fracture—*A. E. Scheidegger* - 300

On the spin–orbit interaction in diatomic molecules. I—*I. Kovács* - - - - 309

On the spin–orbit interaction in diatomic molecules. II—*I. Kovács* - - - 329

Band structure of rhombohedral graphite—*R. R. Haering* - - - - - - 352

Mechanical strength of ice frozen from an impure melt—*E. R. Pounder* - - 363

Note on the forced and damped oscillator in quantum mechanics—*Edward H. Kerner* - 371

An interpretation of the low-lying excited states of Mg^{25} and Al^{25}—*A. E. Litherland, H. McManus, E. B. Paul, D. A. Bromley, and H. E. Gove* - - - - 378

Letters to the Editor:

The influence of paramagnetic resonance saturation on the Faraday effect —*J. M. Daniels and H. Wesemeyer* - - - - - - - - - - - 405

Printed in Canada *by* University of Toronto Press